

**Behaviour of elliptical concrete-filled steel tube (CFT)
columns under axial compression load**

Norwati Jamaluddin

Submitted in accordance with the requirements for the degree of
Doctor of Philosophy

The University of Leeds
School of Civil Engineering

October, 2011

*The candidate confirms that the work submitted is her own and that
appropriate credit has been given where reference has been made to the
work of others.*

*This copy has been supplied on the understanding that it is copyright
material and that no quotation from the thesis may be published without
proper acknowledgement.*

Acknowledgements

This thesis would not have been possible without the help from both of my supervisors, Professor D.Lam and Dr J.Ye. It has been an honour for me to work under their supervision. They have made available their support in a number of ways, and have guided and supported me from the initial stages through to the final.

I wish to express my great appreciation to Dr. X.Dai and to the laboratory staff, Marvin, Steve, Pete and Paul, for all their help and technical input. The authors greatly acknowledge this help. Special thanks also go to Mick Marsden for his guidance during my lab works.

I would also like to thank my sponsors, The Ministry of Malaysian Higher Education and The Universiti Tun Hussein Onn, for awarding me with the PhD scholarship, as well as to the Tata Steel Europe (formerly known as Corus) and Drax Power Station, both of which have provided the research specimens. These supports have been greatly appreciated.

I am indebted to many of my colleagues and friends for their support; Rafidah, Azzura, Suhaila, Noridah, Julia Idaly and Murni.

From the depth of my heart I wish to express my uninhibited gratitude for my beloved husband, Nizam, and both my sons, Danish and Firas. There are no words to describe my feeling towards them. They have been my inspiration and kept me motivated during my difficult time.

Last, but certainly not least, my parents who continue to support me; love you both. Thank you so much.

Abstract

This thesis describes a research of the behaviour of the elliptical CFT columns under axial loading. The most substantial part of this research is experimental works conducted on twenty-seven specimens including the hollow stub columns as references. Parameters such as slenderness ratio, uni-axial compressive strength of concrete infill and the aspect ratio were considered to investigate their influence on the behaviour on these columns. The results presented are the first member buckling tests on elliptical CFT columns. Key results from the tests have been presented and discussed. Parallel with the experimental works, numerical analyses were carried out and verified with the experimental results. Parametric studies were performed following the validation of the numerical models.

As there is no design guidance seems to be available in any standard, thus this research provides a review of the existing design standards of Eurocode 4 (EC4) and American Specifications (AISC). The design expressions from these current design provisions for circular, square and rectangular concrete-filled tubes design strengths were used to predict the capacities of elliptical CFT columns. The influences of concrete enhancement, steel reduction due to biaxial effects and column slenderness were all incorporated in design rules of EC4. Based on the experimental, numerical findings the evaluations were made on the design rules of the codes. This investigation was aimed at providing reliable design guidelines for practising engineers to employ the elliptical concrete-infill columns in the construction industry.

Contents

Acknowledgements	ii
Abstract	iii
Contents	iv
Figures	viii
Tables	xii
Chapter 1 Introduction	1
1.1 Background.....	1
1.2 Concrete-filled Tube (CFT) Composite Column.....	3
1.2.1 Functional principle.....	3
1.2.2 Composite Column Materials.....	5
1.3 Research Significance.....	6
1.4 Thesis Aims and Objectives.....	7
1.5 Research Scope.....	8
1.6 Dissertation Structure.....	10
Chapter 2 Literature Review	12
2.1 Introduction.....	12
2.2 Behaviour of CFT Column.....	13
2.2.1 Confinement.....	16
2.2.2 Axial Buckling.....	18
2.2.2.1 Local Buckling.....	19
2.2.2.2 Overall Buckling.....	20
2.2.3 Modes of Failure.....	21
2.2.4 Creep and Shrinkage.....	22
2.3 Composite Column Materials and Structure.....	23
2.3.1 Concrete Infill.....	23
2.3.2 Steel.....	25
2.4 Finite Element Model.....	26
2.4.1 Element Types.....	26
2.4.2 Materials modelling.....	27
2.4.3 Geometrical Imperfection.....	34
2.4.4 Concrete-steel tube interface.....	35
2.5 Elliptical steel section.....	36

2.5.1 Experimental works on elliptical tube	36
2.5.2 Numerical works on elliptical steel sections	40
Chapter 3 Self-Compacting Concrete.....	43
3.1 Introduction	43
3.2 SCC Characteristics.....	44
3.3 Self Compatibility Mechanism	45
3.4 SCC Constituent Materials	47
3.4.1 Additions	48
3.4.2 Admixture.....	48
3.5 Test Methods	49
3.6 SCC Mix Design Approach.....	53
3.7 Mixing Procedure	55
3.8 Concrete Tests.....	58
3.8.1 Fresh Concrete Tests	58
3.8.2 Hardened Concrete Properties	62
3.9 Trial concrete mixing	62
3.9.1 Fresh concrete tests results.....	63
3.9.2 Hardened concrete testing.....	65
Chapter 4 Experimental Studies	71
4.1 General	71
4.2 Experimental Programme.....	72
4.2.1 Properties of Ellipse.....	72
4.2.2 Instrumentation	73
4.2.3 Columns' Set-up and Test Procedure.....	76
4.2.4 Column Labelling and Dimension	83
4.2.5 Column Supports	87
4.2.6 Testing Procedure	88
4.3 Casting of Composite Column.....	90
4.4 Material Properties Tests	91
4.4.1 Steel	91
4.4.2 Concrete infill	92
4.5 Initial out-of-straightness	93
Chapter 5 Experimental Results	95
5.1 Introduction	95
5.2 Material Properties	95

5.2.1	Concrete Properties	95
5.2.2	Steel Tube Properties	99
5.3	Experimental Results of Stub Tests	100
5.3.1	Observation on the Short Columns Tests	100
5.3.2	Axial Load-Shortening Relationship of Short Columns	104
5.3.3	Stub Columns Failure Modes.....	106
5.4	Experimental Results of Long Column Tests	109
5.4.1	Observation on Series II columns	109
5.4.2	Observation on Series III Columns	115
5.4.3	Observation on Series IV Columns.....	119
5.4.4	Strain Characteristics.....	123
5.4.5	Failure Modes of Long Columns	126
Chapter 6	Numerical Modelling.....	131
6.1	Introduction to the Finite Element model	131
6.2	Description of the Finite Element model.....	132
6.2.1	Boundary conditions and load application	135
6.2.2	Members contact	136
6.2.3	Elements types and meshes density	138
6.2.4	Imperfection and Residual Stress	140
6.3	Material properties	142
6.3.1	Steel section	142
6.3.2	Concrete material	142
6.4	FEM Verification.....	150
6.4.1	Introduction	150
6.4.2	Validation of Stub Columns.....	151
6.4.3	Validation of Long Columns.....	158
6.5	Parametric Study.....	169
Chapter 7	Analysis and Discussion.....	173
7.1	Introduction	173
7.2	Stub Columns.....	173
7.2.1	Strength Enhancement Index, SI	177
7.3	Long Columns	179
7.3.1	Slenderness.....	183
7.3.2	Ductility Index, DI and Stiffness	188
7.4	Design Codes.....	189

7.4.1 Euro-code 4 (BS EN 1994-1-1:2004).....	190
7.4.2 AISC 360-05.....	193
7.4.3 Design Capacities.....	195
7.4.3.1 Member strength of short columns.....	195
7.4.3.2 Member strength of long columns.....	197
7.4.4 Summary of Evaluation on Design Codes.....	205
Chapter 8 Conclusion	211
8.1 Concluding Remarks.....	211
8.2 Suggestion for Future Research	216

Figures

Figure 1.1: Typical cross-section of composite columns.....	3
Figure 2.1: Concrete material model used by Schneider (1998)	28
Figure 2.2: Equivalent stress-strain curves by Ellobody and Young (2006)	30
Figure 2.3: Comparison of average contact stresses in columns with EHS and CHS	33
Figure 2.4: Stress- strain curves concrete properties of elliptical CFT stub columns proposed by Dai and Lam	34
Figure 3.1: Slump Flow Test (Ambedkar, 2008).....	49
Figure 3.2: Typical L-Box test (Ambedkar, 2008).....	50
Figure 3.3: Typical J-Ring test (Ambedkar, 2008).....	51
Figure 3.4: Typical sieve segregation resistance test (SCCEPG, 2005).....	52
Figure 3.5: Sand and coarse aggregate are mixed first.....	56
Figure 3.6: The mixer is covered with plastic.....	57
Figure 3.7: Superplasticizer is mixed with water.....	58
Figure 3.8: Slump flow test and T500.....	60
Figure 3.9: Sieve Segregation Test.....	61
Figure 3.10: Spread of SCC fresh concrete for trial mixing.....	63
Figure 3.11: Cubes and cylinder concrete.....	66
Figure 3.12: Present of some air voids in the concrete cubes.....	66
Figure 3.13: Curing of concrete cubes and cylinder.....	67
Figure 3.14: Concrete cube after failure.....	67
Figure 3.15: Concrete strength development for $f_{cu} = 30 \text{ N/mm}^2$	68
Figure 3.16: Density test equipment.....	69

Figure 3.17: Concrete cube was weighted	69
Figure 3.18: Concrete cube has to be fully submerged	69
Figure 4.1: Definition of ellipse	72
Figure 4.2: Location of LVDTs for axial shortening measurement.....	74
Figure 4.3: Instrumentation of columns	75
Figure 4.4: Long columns test setup.	83
Figure 4.5: Buckling length of long column.....	85
Figure 4.6: Groove plate and steel ball.....	87
Figure 4.7: Test arrangement for elliptical composite columns	89
Figure 4.8: Preparation of long tube for concrete casting.....	90
Figure 4.9: Coupon tests	92
Figure 4.10: Preparation for specimens of hardened concrete properties tests.....	93
Figure 4.11: Imperfection measurement using feeler gauges	94
Figure 5.1: Stress-strain relation of unconfined concrete cylinders	98
Figure 5.2: Failure pattern of cube and cylinder tests.....	99
Figure 5.3: Coupon tests results	100
Figure 5.4: Load-axial shortening relationship of stub columns.....	105
Figure 5.5: Typical failure modes of elliptical hollow column	107
Figure 5.6: Typical failure modes of elliptical stub composite columns	108
Figure 5.7: Concrete failure of C100 concrete strength in stub CFT columns	109
Figure 5.8: Load-lateral displacement series II.....	111
Figure 5.9: Load-mid-height vertical strain of series II.....	114

Figure 5.10: Load-horizontal displacement series III	117
Figure 5.11: Vertical strains characteristics at mid-height of series III.....	118
Figure 5.12: Load-horizontal displacement series IV.....	121
Figure 5.13: Mid-height vertical strain characteristics of series IV columns	122
Figure 5.15: Load versus axial strain at middle length of CFT column	126
Figure 5.16: The removal of steel enveloped	130
Figure 6.1: Typical FE model of stub columns	133
Figure 6.2: Typical FE model of long columns	133
Figure 6.3: Boundary condition for stub columns	135
Figure 6.4: Three-dimensional finite element mesh for steel tube and concrete core.....	140
Figure 6.5: Equivalent stress-strain curve of concrete by Hu et al	146
Figure 6.6: Schematic representation of the stress-strain relation	149
Figure 6.7: Load-axial shortening curves of stub CFT columns with 150x75x4 mm tube size.....	154
Figure 6.8: Load-axial shortening curves of stub CFT columns with 200x100x5 mm tube size.....	155
Figure 6.9: Comparison of failure mode observed in stub FE model.....	157
Figure 6.10: Typical deformation of long column FE model	161
Figure 6.11: Comparison between test and FE models of Series II columns	164

Figure 6.12: Comparison between test and FE models of Series III columns	166
Figure 6.13: Comparison between test and FE models of Series IV columns	168
Figure 6.14: Column strength and concrete cube strength relationships obtained from parametric study.	172
Figure 7.1: Strength and nominal ratio versus D/t ratio of stub columns ...	179
Figure 7.2: Measured load versus vertical deformation of elliptical columns with various compressive concrete strength and slenderness	182
Figure 7.3: Stress-strain relationship curves of long columns	183
Figure 7.4: Load-mid height lateral displacement relationship with various columns' slenderness	187
Figure 7.5: Ratio between experimental ultimate load, numerical results and codes provision.....	200
Figure 7.6: Ratio of measured strength and predicted strength from codes against slenderness.....	206
Figure 7.7: SCC infill versus conventional concrete infill	207
Figure 7.8: Ratio of measured strength and predicted strength from codes against concrete cylinder strength	208
Figure 7.9: Normalised experimental results and buckling curves	210
Figure 7.10: Normalised FE results and buckling curves	210

Tables

Table 2.1: Shape effect on ultimate strength CFT columns.....	39
Table 3.1: GMT test results indication	52
Table 3.2: Fresh concrete tests requirements	54
Table 3.3: Mix design proportion of SCC.....	55
Table 3.4: Proposed criteria for used test methods by Brite EuRam (2000)	64
Table 3.5: Fresh concrete tests results for trial mix.....	65
Table 3.6: Density of cubes concrete	69
Table 4.1: Summary of dimension and columns' properties.....	86
Table 5.1: Material properties.....	97
Table 5.2: Summary of experimental results of stub and long columns	103
Table 6.1: Comparison of maximum loads	157
Table 6.2: Comparison of ultimate strength obtained from experiments and predicted by FE models.....	160
Table 6.3: Parametric studies for flexural buckling	171
Table 7.1: Analysis of experimental results of stub columns	175
Table 7.2: Analysis of long columns results	185
Table 7.3: Calculated strength comparison for stub CFT columns.....	197
Table 7.4: Comparison of the design codes with experimental and FE models	201
Table 7. 5: Comparison of the design codes with parametric study	203

Chapter 1

Introduction

1.1 Background

The composite structure of steel-concrete columns is not new to the construction industry. The columns have been used for over 100 years with the concrete material was initially used as insulation that was required to fulfil the fire-rating requirement.

In the case of its early application, the contribution of composite action, which is in the structure, was not taken into consideration. The composite action exists when two different materials are joined together so strongly that, from a structural perspective, together, they are able to act as a single unit. Owing to the composite action, the composite member is stiffer and stronger than the sum of the individual members. However, these structural benefits were only established in the middle of the 20th century when the increment of stiffness and strength were observed in another type of composite structure namely encased composite beam (Vrcelj and Uy, 2002). In 1948, British Standard has taken into account the increase of stiffness due to the concrete encasement in the design application (Grauers, 1993).

Composite columns possess many significant advantages over conventional reinforced concrete and steel structures. Its growing usage in the case of structural and architectural applications is predominantly owing to the

significant advantages of the structure, such as high load-carrying capacity owing to the blend of properties of differing materials in the structure. Steel is the most versatile traditional construction material and well known to provide high reliability in terms of its consistent quality and full efficiency when placed under tension whereas concrete is efficient in compression.

The composite structures are commonly used when the conventional structure is unable to develop sufficient resistance associated with design loading or in the case where more specialised applications were needed (Nethercot, 2004). This form of structure can be utilised in different configurations; whether the steel structure is used externally, known as concrete-filled tube column or the steel section is encased in the concrete material. Concrete-filled tubes column, hereafter referred to as CFT, is being increasingly used as a structural element, especially in seismic zones, as it offers a number of significant advantages. The structure exploits the characteristics and overall configuration of the structure elements; steel offers high tensile strength, ductility and construction speed, whereas concrete provides high compressive strength, stiffness and cost reduction. Another notable advantage associated with the use of composite columns is construction cost saving, as the steel tube can serve as a formwork to the concrete core. With the concrete-filled column profile, the steel frame can be erected after filling in the concrete material, without waiting for the concrete to harden provides the advantage of saving both time and cost.

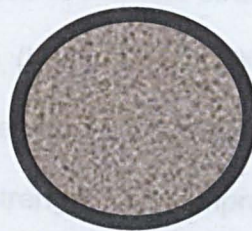
1.2 Concrete-filled Tube (CFT) Composite Column

1.2.1 Functional principle

CFT composite columns can be introduced in various forms. The hollow steel tubes can be filled with various types of concrete and strength, whilst the columns can be erected with various shapes of hollow steel sections. The most common types of composite columns are shown in Figure 1.1; namely steel-encased concrete column, concrete-filled circular hollow section (CHS), concrete-filled square (SHS), or rectangular hollow section (RHS). The steel-encased column comprises I or H steel cross-section placed within a traditional reinforced concrete or plain concrete. This structure is the earliest type of composite cross-section. A CFT column, on the other hand, is simply constructed by filling concrete into the hollow section, which is used as a casting mould to the concrete.



(a)



(b)



(c)



(d)

Figure 1.1: Typical cross-section of composite columns

The orientation of the steel and concrete member in the CFT column cross-section has a significant role in terms of enhancing the strength and stiffness of the structure. The steel section is located at the outer perimeter, where it performs most effectively in tension and bending moment. Furthermore, the stiffness of the CFT column is enhanced as the steel section has a greater modulus of elasticity compared with concrete members and a greater moment of inertia owing to the fact that the steel section is situated farthest from the centroid of the cross-section (Gourley et al., 2001). The concrete core, which acts as the inner structure (EFNARC, 2002), is considered to be ideal in terms of withstanding the compression loading, and is often found to prevent or delay the occurrence of local buckling in the steel section, particularly in rectangular CFTs (Gourley et al., 2001). The concrete core also prevents inward local buckling; thus, the steel tube can only buckle outwards, which therefore leads to an increase in ultimate strength and local buckling strength of the composite column (Liang et al., 2006). The CFT column is also popular as a structural member, as it has a number of significant advantages, such as higher strength and improved ductility (Ellobody et al., 2006, Ellobody and Young, 2006). Notably, saving construction time and labour costs is another keen advantage associated with the use of CFT column, as the steel column has the ability to eliminate the need of formwork since the steel section can also act as permanent formwork. Notably, longitudinal reinforcement and finished structure, including surface treatment, can be effectively achieved at the same time.

Recently, elliptical hollow sections (EHS) were introduced, drawing the attention from engineers and architects due to its aesthetic appearance and structural efficiency, predominantly owing to its major and minor axis. The

elliptical hollow sections also have greater bending capacity compared to circular hollow sections of the same area and weight, owing to its strong and weak axis directions (Packer, 2008). As a mark of acceptance, EHS have been employed in a number of applications, such as Terminal 5 Heathrow Airport in the UK, and the Legend Centre in Canada.

1.2.2 Composite Column Materials

The typical forming of hot-rolled hollow steel tubes is commonly utilised in the case of CFT columns. However, the cold-formed steel tube manufacturing and build-up steel section can also be found in the market. The build-up steel tube is formed by the welding of plates or channel sections. Moreover, the concrete member of the composite columns can be either normal strength concrete or high strength concrete. Notably, they should be designed and produced in accordance with relevant norms with at least 25 N/mm^2 cube strength and 2400 kg/m^3 concrete density. According to BS EN 1994-1-1:2004 the clause to design composite compression members only applies for normal weight concrete of cube strength classes C25 to C60. The typical density for the normal concrete is 2400 kg/m^3 .

Importantly, the development and application of high-performance materials have greatly increased all over the world. The materials have several advantages over ordinary strength materials. For example, the use of high-strength concrete (HSC) and high-strength steel (HSS) are proven to enhance the load-carrying capacity of structures and also significantly benefit in terms of saving material costs.

In the case of traditional reinforce high concrete strength columns, stirrup spacing is often reduced to prevent the brittle failure associated with the

characteristic of the high strength concrete and to obtain a higher ductility. However, the stirrups may create a form of natural plane separation between the confined concrete core and the unconfined concrete cover, and increases the risk of a premature spalling of the concrete cover (Johansson and Gylltoft, 2002). Nevertheless, this problem can be overcome with the use of composite columns consisting of concrete-filled steel tubes, CFT.

1.3 Research Significance

There has been a notable increase in the use of composite columns in engineering structures, especially in seismic zones. The presence of elliptical sections adds more choice for engineers and architects when employing such sections in numerous structures for aesthetic purposes. However, as with the newest section shape, there are many issues which are not well understood owing to a lack of knowledge in relation to its behaviour.

At this moment, there is limited understanding of structural performance on the section. The results on elliptical hollow sections are currently insufficient, and very limited experimental information can be found concerning elliptical CFT columns. Most of the researches on elliptical CFT columns focused on short columns such as work done by Dai and Lam (2010). The confinement effect is an issue which needs to be addressed, particularly in consideration of how it affects to the steel section. The interaction between local and global buckling also needs to be investigated, especially for long, slender columns. The works presented in this thesis highlight the study of mechanical behaviour in elliptical CFT columns. In order to comprehend the behaviour of elliptical CFT columns, it is first necessary to understand the

response of elliptical tubes in the composite structure and the interactions between individual materials in structure. Furthermore, the potential and advantages associated with the use of HSC in the composite column have been established. Thus, the knowledge gained from the experiments and FE analysis and the failure process in the columns are vital in order to add information which fundamentally benefits both the researcher and engineers.

1.4 Thesis Aims and Objectives

The study is mainly divided into experimental studies and Finite Element (FE) Modelling. The work emphasise on the investigation of behaviour and performance of concrete filled elliptical steel tube. Experiments were performed on both short and long columns tests and the results were used to verify the FE models. In this thesis, a long column is defined as a member whose length is considerably larger than any of its cross-sectional dimensions.

The principle aim of this research project is to gain an understanding into the behaviour of this form of constitution. Since the shape is relatively new and also as the data for this type of column is currently insufficient with very limited understanding, it therefore deserves further investigation. The objective of this project is mainly concerned with investigating the 2, capacity and failure patterns both up to and beyond the ultimate load of this cross-sectional shape of composite column. This is owing to the fact that the behaviour associated with such a shape is relatively unknown, especially in the case of long columns. The other objectives are to investigate the effects of the use of normal concrete strength and high concrete strength, the influence of slenderness on column strength, and the confinement provided

by the shape of steel tube, all of which are addressed in order to investigate the effects on CFT columns.

The main objectives of this study are outlined as follows:

1. To conduct an experimental investigation of elliptical CFT columns under axial load;
2. To investigate the influence of parameters such as column slenderness and concrete strength on load-bearing capacity;
3. To give an experimental base of information for the design of elliptical columns consisting of concrete filled hollow steel sections
4. To develop a numerical model in order to simulate the behaviour of the elliptical CFT columns under axial loading
5. To propose new equations for this form of structural sections.

1.5 Research Scope

In this study, tests concerning elliptical CFT columns were conducted on twenty-seven specimens, including two hollow stub columns, for the purpose of comparison. Parameters considered in this study include column slenderness (L/D), width-to-thickness ratio (D/t) and concrete strength. Reviews from previous studies have further highlighted that such parameters affect the behaviour and strengths of CFT columns. Moreover, experiments were carried out and studied in order to determine their influences on the ultimate strength of elliptical concrete-filled steel tube column. The results of the axial compression test on the specimens reflect the influences of such

parameters on the strength and behaviour of elliptical CFT columns. The experiments only considered concrete-filled elliptical hollow steel sections without the use of any mechanical connectors or reinforcement.

The experiments involved short and long elliptical columns. The stub columns tests were performed in order to establish the squash load of the structure. Meanwhile, in the case of long columns, the tests were carried out on various lengths for the purpose of studying the behaviour and influences of global buckling on the structure's capacity. It is noteworthy to state that there is limited research work available in the literature concerning long concrete-filled steel columns and none involved elliptical sections. Thus, the experiment was performed over a range of length where local buckling and overall flexural buckling were involved. Moreover, long columns tests were carried out on three different lengths in a range of 1500 mm to 2500 mm in order to study the reduction in strength and behaviour with increasing slenderness. Different typical concrete cube strength 30 N/mm^2 , 60 N/mm^2 and 100 N/mm^2 are used in this study and in the form of self-compacting concrete (SCC). Self-compacting concrete is facilitating the highly efficient filling of composite columns by offering reliable and segregation-free techniques for filling up to significant heights without additional compaction. The use of high-strength concrete is included in this study as it benefits the structures in terms of both strength and stiffness (O'Shea and Bridge, 2000).

Numerical modelling was carried out in parallel with the experimental programme. This analysis provides better behavioural understanding of the structural. In the numerical study, models were developed in order to predict the response of elliptical CFT column subjected to axial compression load.

Initial geometric imperfections were considered in the three-dimensional non-linear finite element models of long columns.

1.6 Dissertation Structure

This thesis presents the study of elliptical concrete-filled tube columns which involves reviews from related literatures, procedure of non-linear finite element models, the design of self-compacting concrete, and subsequent analysis from both experimental and FE results. The work developed in this thesis has been organised into eight chapters. The first chapter is the introduction of the research background. Research aims and the principles of CFT columns have been highlighted in this chapter.

Chapter 2 presents a review of the existing research work related to the area of interest covered in the thesis. This section discusses on the related findings in relation to investigations conducted on hollow and composite CFT columns.

Chapter 3 describes about the self-compacting concrete that has been chosen as concrete infill. This chapter covers the design and concreting procedure of the particular types of concrete.

Chapter 4 outlines the methodology used for the purpose of conducting the experimental work. This section explained in detail the procedure of specimen's preparation, the rig-frame setting-up and the tests involved in this study.

Chapter 5 encompassed the results of current study. Observation made from the experimental of elliptical columns under axial loading was highlighted in this chapter.

Chapter 6 discusses the numerical method performed in ABAQUS. It covers the procedure of modelling and verification of the results obtained throughout the FE analysis phase. A series of parametric study was also conducted.

Chapter 7 covers the analysis from the experimental results and numerical analysis. The influences of parameters involved in this study were discussed. The indicators such as strength enhancement index, SI and ductility index, DI were used to assess the compressive capacity and the ability of non-linear deformation respectively. Comparison of the results from both methods with current design codes are also highlighted in this chapter.

Chapter 8 is the final chapter that encompasses the conclusion drawn from the project analysis and its corresponding results. Significant findings were highlighted and recommendations for further research have been made.

Chapter 2

Literature Review

2.1 Introduction

This chapter is aimed towards providing an overview of the background literature. Key research findings relating to the experimental works, numerical modelling and design guide of the concrete infill columns structures are also covered.

Originally, the composite column started with a steel-encased concrete column type; however, the main disadvantage of this type of composite columns was that the structure required complete formwork and a reinforcement cage, which was needed in order to prevent the concrete core from spalling. On the other hand, the CFT column had the advantage of preventing such problems owing to the configuration of the structure.

As mentioned in the previous chapter, the combination of concrete and steel in the column structure was initially aimed towards achieving fire resistance. The composite action which occurred owing to the bonding between these materials was later found to have an effect on the structure's strength. As a result, an extensive study concerning the assessment of the composite action in the columns was conducted.

Studies on CFT columns have been on-going for many decades (Giakoumelis and Lam, 2004, Zeghiche and Chaoui, 2005). The use of CFT columns was first recorded and published by Sewell in 1901 (Johansson, 2002), and the earliest complete test on CFT columns was conducted in 1957 by Kloppel and Goder (Han, 2002). The aim of the concrete infill in the Sewell study was to protect the internal hollow tube from rusting. The enhancement of the structure stiffness was noticeable after some of the columns were accidentally overloaded. The development in studying the axial strength of the CFT columns continued since the columns first tested by Kloppel and Goder were various cross-sections structures, such as circular, square, and rectangular (Han, 2002).

Recently, the elliptical tube section was introduced in the hollow tube family. Since it is the newest steel section, only a handful of investigations on the application of this column structure shape had been undertaken. However, most of the researchers conducted so far have involved elliptical hollow sections and stub elliptical composite columns. Therefore, it is considered that further investigations and experimental data are needed in order to develop a better understanding of the elliptical CFT columns particularly on slender columns behaviour.

2.2 Behaviour of CFT Column

A column is a structural element which primarily loads in compression along its length. It can be either subjected to compression forces or combined with eccentric load or bending moment. The failure of short compression columns is the result of compression axial force, whereas in the case of longer

columns, compression members are affected by the strength and stiffness of the material, as well as the geometry of the members.

The steel hollow section is known to be a very efficient structure in terms of resisting compression loads, and has been widely used in the case of framed structures in industrial buildings. However, it is nevertheless recognised that the material is vulnerable to heat, and the potential of exposed steel section to be used in design might therefore be compromised. In spite of this, as the development in the steel industry has moved forward, there have been many approaches to fire protection offered for exposed steel columns. Furthermore, as the construction technology advances, concrete infill in the hollow section are not only expected to increase the capacity of the structure, but also to increase its overall fire resistance.

There are several factors which may have a considerable effect on the ultimate strength of CFT columns, such as slenderness ratio, thickness, cross-section shape, and the mechanical properties of steel and concrete (Shakir-Khalid and Zeghiche, 1989, Romero et al., 2005). Generally, the compression axially loaded CFT members can fail in two principal ways: in terms of slenderness and material properties. In the case of short columns, mechanical properties play an important role in their behaviour. The failure state is attained when the steel tube reaches the limit state of yielding and concrete crushing, which is known as a strength criterion. On the other hand, stability will essentially govern the ultimate load capacity of slender CFT columns, where the members are more likely to fail as a result of buckling and second-order effects becoming more critical (Gourley et al., 2001, Sakino, 2006); therefore, the critical buckling load, P_{ct} , which represents the

load at which slender column buckles is more crucial for the column. It can be seen that the stiffness fundamentally influences the column's strength more in slender columns, but that this is not the case for short columns where the strength is mainly depends on the material strength and cross-sectional area.

The shape of the column has also contributed to the strength and behaviour of CFT column. Comparing the open section and the hollow tube, the latter is considered to be the most efficient shape for the compression member owing to its material distribution, which is further away from the centre of the cross-section. However, the disadvantage remains that the structure member is difficult in terms of connection.

Nowadays, there are many types of hollow tubes available in the market. Amongst them, the circular hollow section is evidently the most efficient for compression members, as it has an equal second-moment of area and stiffness in all directions. The effect of the cross-section shape and thickness on the ultimate axial strength of CFT columns has been acknowledged from research carried out by Schneider (1998), Shams and Saadeghvaziri (1997), Huang et al., (2002). From the study, it was concluded that the short axially loaded circular CFT columns have an elastic-perfectly plastic behaviour, and also offer more post-yield axial ductility when compared with the square or rectangular CFT column. This was further exhibited by the significant strain-hardening behaviour of the circular column, whilst various post-yield behaviour—depending on the tube wall thickness of the tube column, were exhibited in the case of square and rectangular tubes.

2.2.1 Confinement

Confinement has a significant relation to the ductility of CFT columns besides providing a significant advantage in term of the column's ultimate strength. In the columns, compressive confining stress on the concrete core is induced via a passive confinement provided by the hollow steel tube (Johansson and Akesson, 2002). The confining effect, however, basically depends on a variety of factors, such as the dimension of the steel tube, concrete strength, tube thickness, the yield stress of the steel tube and the overall shape of the column cross-section (Ellobody and Young, 2006, Ellobody et al., 2006). The development of confinement at the steel-concrete interface is initiated partly from the difference in Poisson's ratios between materials in the structure. Concrete has a smaller Poisson's ratio, ν_{conc} (0.15-0.25) than steel, (0.3) during the elastic stage, which therefore leads to lateral separation of the steel tube and concrete core. Notably, however, ν_{conc} becomes higher than steel, particularly when the concrete core begins to crack or crush; thus, lateral deformation of the concrete reinitiates interactive contact with the steel tube (Gourley et al., 2001). Further loading results in the development of radial pressure and setting up a hoop tension in the tube. During this stage, the steel shell provides confining pressure to the concrete expansion of the concrete core, which subsequently puts the concrete under tri-axial stress and the steel in biaxial. Accordingly, it is expected that the steel tube in the CFT enhances the concrete core in axial compressive strength by its lateral confinement. The tri-axial compression concrete in the columns can withstand higher strains and stress (Grauers, 1993).

The section's shape effect on confinement was investigated by Nardin and El Debs (2007) and Fujimoto et al. (2004). As has been ascertained from the study, the confinement is found to be superior in circular and octagonal CFT columns, but not in CFT columns with a square steel section. This is owing to the uniformed lateral pressure in the circular tube which confines the concrete core; in the case of the square section, however, higher confining pressure only occurs at the centre and corner of the section compared to the other side. Further investigation also demonstrates that the thickness of the tube influences the ductility behaviour of the square section.

The investigation carried out by Shanmugam and Lakshmi (2001) on rectangular tubes, shows that the tension hoop developed along the side of the tube was not constant, and therefore seems to be the reason as to why a confinement effect was not present except in the corner of the steel tube. The same conclusion was drawn from the non-linear analysis conducted by (Hu et al., 2003). The nonlinear finite element program, *ABAQUS* in their study had been performed on circular section, square section, and square section stiffened by reinforcing ties. Thus, it is suggested that confinement is considered to be more significant in the case of circular CFT columns rather than square CFT columns, where the column only shows a small increment in axial strength (Fujimoto et al., 2004). As can be determined from the study of Nardin and Debs (2007), the confinement in the square section was found to be more effective than the rectangular section, which was represented by greater ductility in the post-peak behaviour. Notably, the circular section was still established as being more ductile compared with other shapes in their studies. CFT columns with circular sections provide a good confining effect; however, when the width-to-thickness ratio is small ($D/t < 40$), it was

established that the square section did not provide a large confining effect especially when the width-to-thickness ratio was large ($B/t > 30$). The effects of concrete confinement for columns with large plate slenderness ratios were also found to be less pronounced, as local buckling may occur (Uy, 1998).

The confining effect was noted to have enhanced considerably the strength of a short column; however, the effect was found to be insignificant in the case of slender columns (Oehlers and Bradford, 1995). This is primarily due to the fact that the column with large L/D ratios was generally found to fail owing to columns buckling before it reached the strain necessary to cause an increase in concrete volume (Han, 2002). From a numerical investigation carried out by Neogi *et al.* (1969), it was established that there was a gain in strength owing to a triaxial effect for columns with L/D ratios less than 15. In their study, complete interaction between steel and concrete was assumed; thus, triaxial and biaxial effects were not considered. The columns were subsequently analysed by tangent-modulus approach and compared with experimental results.

2.2.2 Axial Buckling

Buckling is one of the structural behaviour and an instability form which should be considered primarily for compression members, such as columns. Its presence obviously reduces the capacity of the structure. Eurocode 4 (EC4), for instance, has imposed some restrictions on the allowable diameter-to-thickness ratio, D/t in order to prevent local buckling from influencing structure capability as indicated in Table 6.3 in BS EN 1994-1-1:2004.

2.2.2.1 Local Buckling

There are two types of buckling: local buckling and overall buckling. Local buckling occurs when the thin steel elements are compressed in their planes (Oehlers and Bradford, 1995). With this in mind, and in order to fully utilise the steel strength, the failure mode should be prevented before the steel reaches its yield stress. In the case of thin walled steel tubes, the influence of local buckling is significant to its strength. This type of failure is indicated by the growth of bulges, waves or ripples. In the case of CFT columns, the presence of concrete infill has an effect in prolonging the local buckling of the tube wall (Baig et al., 2006, Schneider, 1998). Furthermore, the resistance in a local buckling of steel owing to the presence of concrete was first identified by Matsui (Uy, 1998). Other than delaying the presence of local buckling, the concrete core in CFT columns has also been established to significantly increase the structure's ductility. It also adds stiffness to the steel tube by preventing inward buckling, as the concrete core only forces the buckling modes outward, consequently increasing the stability and strength of the structure (Hu et al., 2003, Nardin and El Debs, 2007, Hu et al., 2005). As a result of the prevention of inward buckling by concrete core, it was found that the increment of buckling capacity was approximately 50% more when compared with the hollow steel column, as highlighted in (Shanmugam and Lakshmi, 2001). The contribution of concrete core in delaying the occurrence of inward local buckling could ensure that the steel would reach its longitudinal yield strength before buckling took place (Zeghiche and Chaoui, 2005). The other advantage of having only outward mode failure mechanism is the prevention of significant decreases in the section modulus. This is owing to the fact that the distance between the top

and bottom flanges of the steel increases rather than decreases (as without) the concrete core when local buckling occurred. The presence of local buckling is also known to affect the confinement in concrete-filled columns when failure occurs prior to concrete crushing where the effect of confinement is limited as the tube sections were prevented from providing a continuous restraint on the concrete for confinement. However, if the local buckling is inelastic, then the confinement of concrete can nevertheless develop (Uy, 1998).

The experiment conducted by Schneider (1998) proved that very similar local buckling behaviour was established in rectangular and square section results. The square tube has buckling effects occurring equally on each face, whereas the rectangular CFT has extensive local buckling owing to the fact that it has a wider face. In circular CFT, the wall buckling was found to be owing to a radial expansion of the tube. Generally, a tube with larger D/t ratios has more local buckling capability with higher apparent distortion compared to the sections with small D/t ratios.

2.2.2.2 Overall Buckling

Overall buckling generally occurred in the case of long or slender columns. The failure is illustrated by sideways bending where, for the particularly columns, the global stability is more vulnerable, as the columns tend to fail owing to flexural buckling (Oehlers and Bradford, 1995). This failure occurs when the condition of a stable equilibrium between the internal and external forces in the structure is no longer possible (Shanmugam and Lakshmi, 2001). The behaviour of these columns is influenced by the slenderness ratio, with the slenderness also contributing to the so-called second order effects.

2.2.3 Modes of Failure

A short or stocky columns failure mechanism is characterised by the yielding of steel and crushing of concrete, whilst the medium length CFT columns behave inelasticity and therefore fail owing to the partial yielding of steel, the crushing of concrete in compression, and the cracking of concrete in tension (Shanmugam and Lakshmi, 2001). Finally, slender columns are bound by the elastic limit. As the capacities of short columns are dominated by the strength limit of the material thus, the structures are known as material-dependent.

The type of buckling mode of stub CFT columns is also significantly influenced by the method of loading conditions. Study by Johansson and Gyltoft (2002) on the columns subjected to axial loading include various different loading conditions, namely loading on the steel tube, loading on the concrete core, and simultaneous loading of the steel and concrete. From the study, for those columns with the load applied to the entire section and those columns with the load applied to the concrete core, the combination of local buckling and crushing was found to affect the stability of the columns. From the experiment, bond strength was found to have no effect on the behaviour of the columns when simultaneous loading was applied; however, in the case when the load was applied only on the concrete core, the bond strength was found to significantly affect the confinement effects; this condition also greatly influenced the overall strength and behaviour of the columns.

Axially-loaded long CFT columns with an L/D ratio of between 12.5 and 25.0, and lengths from 2-4 m were tested by Zeghiche and Chaoui (2005). The results showed that the columns failed after they reached the steel yield

strain with small-lateral mid-length deflections. Furthermore, there was no sign of local buckling, and the overall instability fundamentally dominated the column's failure mode. The removal of the steel envelope for some specimens revealed no sign of concrete-crushing at the mid-length of the sections. This study also highlighted that the enhancement owing to concrete strength is essentially more significant for short columns.

2.2.4 Creep and Shrinkage

Both creep and shrinkage in terms of concrete structure is categorised as time-dependent deformation. The concrete creep can be defined as the deformation which commonly occurring in the direction, in which the force is being applied—of the structure under a sustained load which can generally change the shape of the concrete structure.

The concrete shrinkage is the volumetric change of concrete structures owing to the evaporation of water from the hardened concrete. Tensile stresses will be generated, with the presence of cracks. There are three shrinkage categories: plastic shrinkage, chemical shrinkage, and drying shrinkage. The effect of plastic shrinkage occurs in the case of wet concrete, and may result in significant cracking throughout the setting process. Cracking occurs owing to capillary tension in the pore water. Since the bond between the plastic concrete and the steel tube in CFT columns has not yet developed, the steel section is ineffective in controlling such cracks. Moreover, drying shrinkage is the reduction in volume caused principally by the loss of water during the drying process, whilst chemical (or endogenous) shrinkage results from various chemical reactions within the cement paste and includes hydration shrinkage, which is related to the degree of hydration of the binder in a sealed specimen. The high-strength concrete of SCC is

ultimately more prone to plastic shrinkage and chemical shrinkage due to its low water content and silica fume. On the other hand, the drying shrinkage for the high-performance concrete is smaller than in normal-strength concrete due to the lower quantities of free water following hydration. However, the effects of shrinkage in CFT columns have been found to be smaller compared with plain concrete (Uy, 2001). Furthermore, the shrinking effect hardly has any effect on the load resistance of CFT columns (Shams and Saadeghvaziri, 1997). As the concrete core in CFT columns is confined in the steel tube and isolated from the environment, the tube can act as a barrier for a better curing system which prevents the loss of moisture, which subsequently minimises the presence of shrinkage.

2.3 Composite Column Materials and Structure

Strength and stiffness are the most important properties in a material. The strength of the material dominates the determination of the collapse load of a structure, whilst its stiffness ensures that the structure does not deflect significantly under the load (Seward, 1998).

2.3.1 Concrete Infill

The strength for the concrete infill can be in the form of normal concrete with a compressive strength of less than 60 MPa, or high strength concrete with a compressive strength of more than 60 MPa. Notably, concrete core with lower concrete strength may experience failure through concrete splitting, whilst in the case of higher concrete strength, concrete sliding may cause failure. A comparison between a low concrete strength and a higher concrete strength in terms of stress-strain curves indicates that the concrete which possesses a higher strength has large elastic rigidity as the initial

elastic modulus of concrete increases parallel with the increase in the concrete strength.

The use of high-strength concrete (HSC) offers several advantages over normal-strength concrete due to its greater stiffness. Increasing the concrete strength also results in a greater strength capacity and the reduction of the external dimension of the composite columns (Nardin and El Debs, 2007). Nevertheless, the majority of research conducted on CFT columns has focused on circular and square sections with lower concrete strength (Lue, 2007); thus, for this research, the high-strength concrete is included in order to experimentally investigate the elliptical CFT column behaviour which is subjected to axial loading. The major concern regarding the use of HSC is brittleness, which is associated with ductility. Accordingly, the use of the HSC column is limited in high seismic zones. However, the ductility of HSC in columns can be significantly improved by encasing the concrete core in a steel shell, which can provide shear resistance as well as improvements in overall ductility, as described by Aboutaha and Machado (1998). The study highlights various weaknesses concerning the use of CFT columns; however, such considerations will not be discussed here.

The use of HSC as concrete infill in CFT columns has been considered in a study by Giakoumelis and Lam (2004). The study involved various concrete strengths, i.e. 30, 60 and 100 N/mm², with the overall aim of examining the bond strength and confinement effect. However, from the load-strain graph of the normal concrete and the high concrete strengths, it has been concluded that, for high-strength CFT columns, peak load was achieved for small shortening, whereas for normal concrete, the ultimate load was gained

with corresponding large displacement. This clearly illustrates that the use of HSC possibly made the structure stiffer. In the study, the confinement effect was further examined by performing non-greased and greased specimens; from the results, it was concluded that the effect of the bond between the concrete and the steel was more critical for high-strength concrete in terms of enhancing axial capacity.

In order to achieve the adequate strength and durability of the concrete material, compaction is needed. The purpose of compaction is to eliminate the air voids which are trapped in loose concrete, as the air voids can fundamentally reduce the concrete strength and thereby increase its permeability, which subsequently reduces durability. A study conducted by Han and Yao (2004) on the influence of the compaction technique on CFT columns shows that better compaction could enhance the overall strength of CFT members. The tests further exhibited the importance of compaction for concrete core in CFT columns; thus, it is considered crucial for any fresh concrete to fulfil the good concrete properties, such as maintaining its homogeneity. In this study, self-compacting concrete was used as concrete infill. Further explanations for this concrete type are described in Chapter 3.

2.3.2 Steel

As concrete infill, steel can also be categorised into two groups: normal strength tubes with yield strength of less than 400 MPa, and high-strength tubes with yield strength of above 400 MPa (Zhang and Shahrooz, 1999). The properties of the materials are assessed from the stress-strain curves of coupon tests in tension. In this study, mild steel strength was considered.

2.4 Finite Element Model

In order to further study the behaviour of the composite CFT columns structures, finite element analysis (FEA) was performed parallel to the experimental study using a commercial finite element package, ABAQUS. The use of numerical simulations is commonly accepted as a replacement owing to expensive experimental programmes. Many researchers have adopted the finite element analysis programme to model the CFT columns in order to predict the structural response and simulations with ABAQUS software package, as it was found to be the most preferred programme to model the structural.

2.4.1 Element Types

The correct choice of element type and mesh is significant when seeking to gather accurate results. Most of the researchers select different types of element when modelling the concrete infill and steel tube, whilst few select the use of only one type of element to model both concrete and steel tube. Non-linear analysis numerical models performed by Ellobody and Young (2006) on SHS and RHS columns were carried out by selecting element types of 4-noded doubly shell elements with reduced integration, S4R to model the steel tube, and C3D8 solid element in order to model the concrete infill. However, another study carried out by Ellobody *et al.* (2006) witnessed a solid element type of C3D8 selected to represent both the steel tube and the concrete. According to this study, the element type was found to be more efficient in the analysis of the axially loaded circular CFT columns. Notably, this was decided after several different types of elements had been tried to simulate the circular CFT columns' behaviour. By implementing the same

approach, a three-dimensional FE model based on a solid element type was established in studies by Hu *et al.* (2003) and Johansson and Gylltoft (2002).

2.4.2 Materials modelling

Material models play a key role in the realistic prediction of the performance of a structure. The main obstacle to finite element analysis is the difficulty in characterising the material properties. Notably, concrete can be regarded as a homogenous isotropic material, and its mechanical properties are related to hydrostatic pressure. Thus, the application of Drucker-Prager plasticity is applicable when seeking to represent the concrete material, and can be adopted to express the constitutive relationship.

The unconfined uni-axial stress-strain curve material property of the concrete core was adopted in a numerical study by Schneider (1998), as shown in Figure 2.1. The unconfined material characteristic was according to the experimental results by the author, which suggested that little confinement occurred for the concrete core prior to yield. In terms of the steel section, inelastic material and geometric non-linear behaviour were considered. Von Mises yield criterion to define the yield surface and the Prandtl-Reuss flow rule were used to determine inelastic deformations of the element. No strain hardening was taken into account in the study.

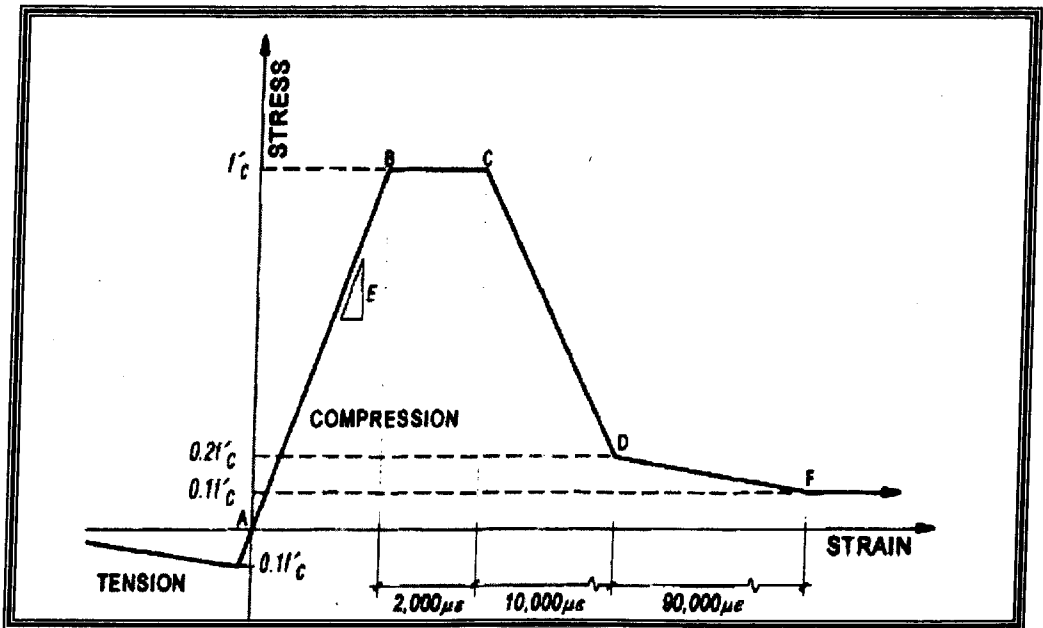


Figure 2.1: Concrete material model used by Schneider (1998)

A confined concrete material property was considered by many researchers. A study based on Hu *et al.* (2003), the circular CFT columns with D/t less than 40 was found to provide large confining effects to the concrete core. This ratio indicates that local buckling is unlikely to occur. To consider the confined concrete material property, an equivalent uni-axial stress-strain curve for confined concrete had to be obtained. Notably, the early development of confined concrete properties show the strength and corresponding longitudinal strain at the strength of concrete confined by an active hydrostatic fluid pressure by the following relationship;

$$f'_{cc} = f'_{co} + k_1 f_1 \quad (2.1)$$

$$\varepsilon_{cc} = \varepsilon_{co} \left(1 + k_2 \frac{f_1}{f_{co}} \right) \quad (2.2)$$

where f'_{cc} and ε_{cc} are the maximum concrete stress and the corresponding strain respectively, under the lateral fluid pressure, f_1 ; f'_{co} and ε_{co} are the

confined concrete strength and the corresponding strain respectively, whilst k_1 and k_2 are the coefficient that are functions of the concrete mix and the lateral pressure. The strength of concrete with active confinement from fluid pressure was approximately the same as the concrete with passive confinement pressure from closely spaced circular steel spirals which causing equivalent lateral pressure (Mander et al., 1988).

Confined concrete material properties was also considered by Ellobody and Young (2006) owing to the assumption that, in their case, the concrete strength was considerably improved, thus the concrete properties can be assumed as confined concrete model. Furthermore, the SHS and RHS steel tube considered in the study have small D/t ratio, and are acknowledged as providing remarkable confinement in the structure. The stress-strain curve of the confined concrete is shown in Figure 2.2. Three parts of the equivalent confined concrete curve have to be determined: elastic range, non-linear portion, and descending part. This proposed method has been considered in this study.

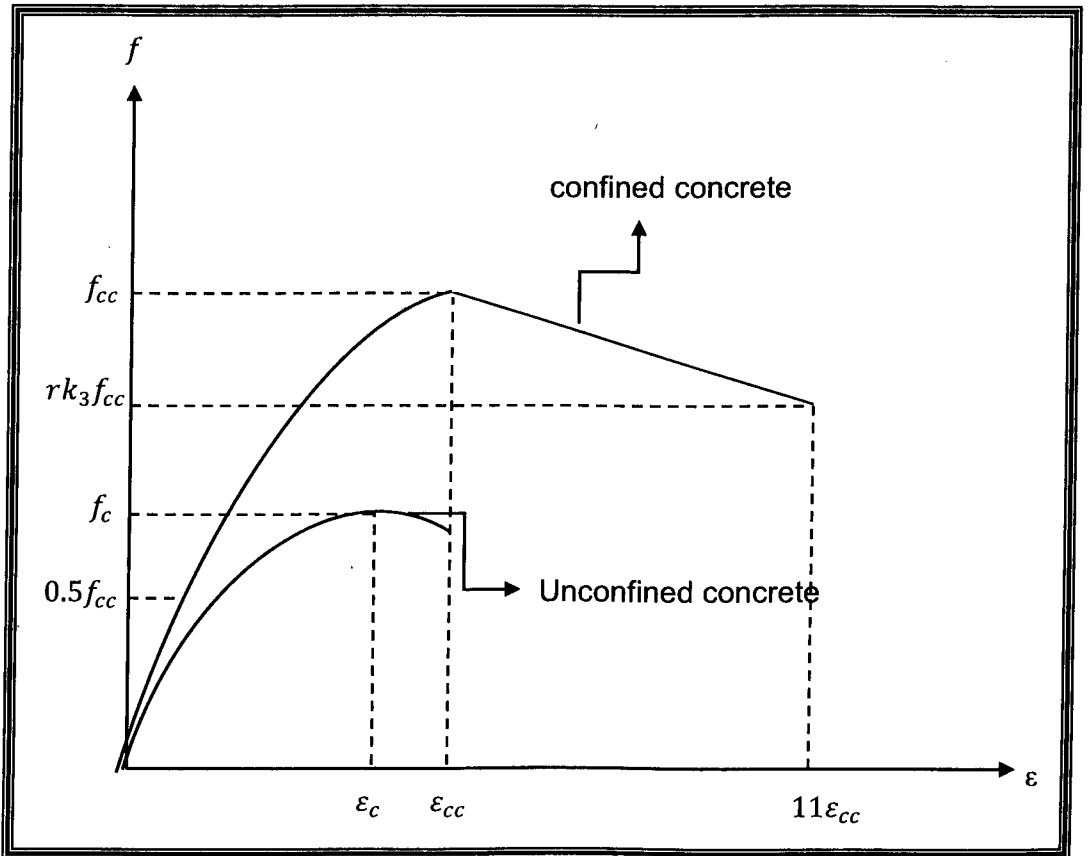


Figure 2.2: Equivalent stress-strain curves by Ellobody and Young (2006)

Notably, quadratic solid element and isoparametric shell element types were used to represent a concrete core and steel tube respectively in order to investigate the response of CFT columns by Sham and Saadegraziri (2000). The von Mises elasto-plastic material model with kinematics-hardening was used for the steel tube, whilst for the concrete core; Pramano-William's concrete material model was coded in FORTRAN and implemented in the ABAQUS using user the UMAT sub-routine in their study. Importantly, the FE model in the study was verified using a number of experimental works performed by other researchers, and it was found that the FEA and experimental data are in agreement.

Smearred crack plastic model was adopted for concrete properties in numerical model by Johansson and Gylltoft (2002). In this approach, the localised deformation of each crack is smeared out over a characteristic length, with the response in tension described as a continuum in terms of stress-strain relations. However, when the principal stress components are predominantly compressive, the response of the concrete is subsequently modelled by elastic-plastic theory where elastic stress state is limited by a Drucker-Prager yield surface. The uni-axial stress-strain relation in compression was used in the analysis; however, the relation registered only up to the maximum stress. The remaining part was subsequently determined by the researcher according to other sources; however, it was found that the material model was still not sufficient to describe a tri-axial stress state. Accordingly, in order to capture the increase in ductility owing to confinement, they assumed a straight line for a descending branch with only a small inclination. In the case of a steel tube, an elastic-plastic model with von-Mises yield criterion, associated flow rule and isotropic strain hardening was considered to describe the behaviour of steel material. The stress-strain relation taken from uni-axial tension tests was used with Poisson's ratio equal to 0.3.

As the confinement effects depend on the section shape, Dai and Lam (2010) propose a new stress-strain model for confined concrete for elliptical hollow stub CFT columns. It has been established that a circular tube provides effective confinement compared to square section. With this in mind, in their study, the confinement force in elliptical steel tube was found smaller than the circular tube and higher than the square tube. Various modifications on stress-strain model proposed by Ellobody and Young

(2006) were made, and a 'quick softening' section was included to consider the elliptical geometry effect. The first and second parts of the elliptical confined concrete properties were determined according to Mander, Hu and Saenz. The section starts at the maximum confined concrete core, f_{cc} and terminates at f_e as in equation 2.3 and the corresponding strain, $\varepsilon_e = 10\varepsilon_{ck}$.

$$f_e = v_a(f_{cc} + f_u) + f_u \quad (2.3)$$

with parameter v_a , dependant on the geometry of the tube. For $15r \frac{(a+b)}{t} \leq 30$ and $\frac{a}{b} = 2$; $v_a = 0.3$. The forth part continues from f_e and ends when $f_u = v_4 f_{cc}$ with the corresponding strain equal to $\varepsilon_u = 30\varepsilon_{ck}$. The parameter v_4 depends on the strength of concrete core where $v_4 = 0.7$ for concrete grade C30 and $v_4 = 0.3$ for C100. Linear interpolation can be used to determine the parameter with concrete grade between C30 and C100 with the condition the concrete strength not less than 30 MPa.

The investigation of the confinement concrete properties was carried out by analysing the contact forces of idealised circular and elliptical tube columns, each of which comprise the same areas of concrete and steel tube as shown in Figure 2.3. However, it is noteworthy to state that the contact stress distribution in stub elliptical concrete-filled columns is complicated and is affected by various different factors, such as column length, major-to-minor diameter ratio, and wall thickness, etc. However, in their study, the major-to-minor diameter ratio of the elliptical section was limited to 2:1.

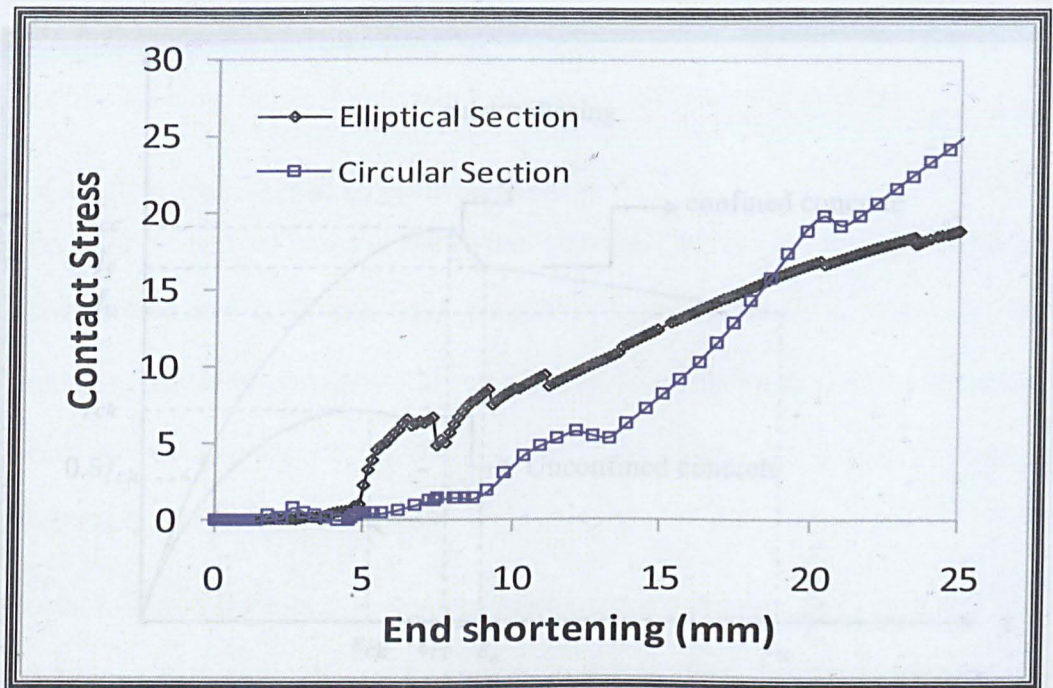


Figure 2.3: Comparison of average contact stresses in columns with EHS and CHS

Figure 2.4 shows the proposed stress-strain material properties in elliptical columns, including the quick softening section for the purpose of considering the effect of elliptical section. The accuracy of this newly proposed stress-strain model was verified by the experimental results, and it was further established that the maximum difference of axial compressive loads between experimental and numerical results was only 5%.

Another finite element model was carried out by the author (Jamaluddin et al., 2009). The method concerned with defining the equivalence of confined concrete properties, as suggested by Ellobody and Young (2006), was adopted in the study. Through the results analysis, the use of the stress-strain model was only deemed appropriate for specimens with low-strength concrete.

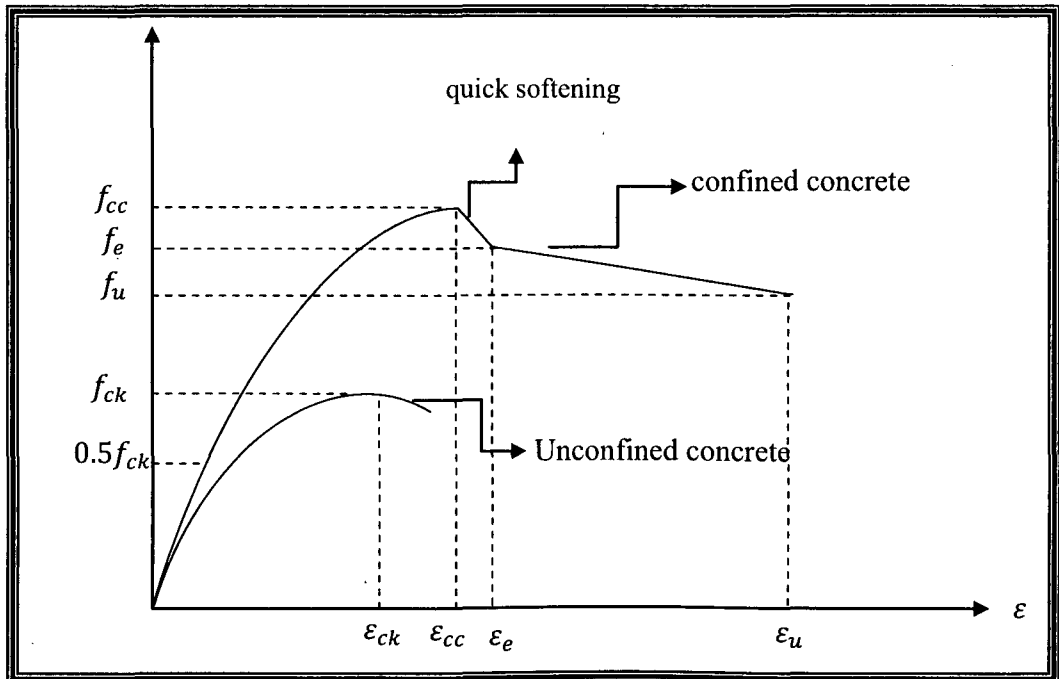


Figure 2.4: Stress- strain curves concrete properties of elliptical CFT stub columns proposed by Dai and Lam

2.4.3 Geometrical Imperfection

In practice, it is impossible to achieve a perfect condition of columns. Initial imperfections concerning the steel tube are owing to the manufacturing process, fabrication and also handling—all of which highly influence buckling behaviour (Bisagni, 2000). Typically, imperfection causes the column to move sideways or to otherwise buckle. Thus, a certain amount of scatter is to be expected throughout the analysis of the results. Accordingly, in order to obtain the ultimate loads of buckling analysis, initial geometric imperfections must be included in order to trigger the deformation (Yang and Hancock, 2004). The usual approach in performing this analysis involves two methods of analysis, which are run using the same model definition. Notably, an eigenvalue buckling analysis uses 'perfect' structure, whereas an imperfection in the geometry is introduced by adding the buckling modes to

the 'perfect' geometry. The most important characteristic in these analyses is to get a load multiplier. Normally, the lowest values are of interest.

2.4.4 Concrete-steel tube interface

The interaction and integral behaviour between the steel tube and concrete core makes the CFT columns an efficient structural. In a finite element analysis, contacts conditions are a special class of discontinuous constrain which allow forces to be transmitted from one part of the model to another (ABAQUS User's Manual, 2008).

Surface-based contact and contact elements are provided by ABAQUS with the objective to simulate contact between two bodies. The interface element in the commercial finite element software ABAQUS is often used by researchers, such as Ellobody and Young (2006) for the purpose of modelling the contact between the concrete and steel tube. The interface elements consist of two matching contact faces of steel tube and concrete elements. It allows the surfaces to separate under the influence of tensile force, but not for both contact elements to penetrate each other. The friction between the two faces is maintained as long as the surfaces remained in contact. In their study, the coefficient of friction between the two faces is taken as 0.25.

On the other hand, Hu *et al.* (2003) performed an interaction between the concrete and the steel tube by modelling a special nine-node interface element. The nodes of concrete and steel tube are connected by using the interface elements which require matching meshes on the two bodies. The elements can model infinitesimal sliding and friction between the concrete

and the steel tube. The friction coefficient used in all the analyses was taken as 0.25.

2.5 Elliptical steel section

Elliptical hot-finished structural sections are now available with outer dimension ranging from 150 x 75 mm to 500 x 250 mm and thicknesses in a range between 4 mm to 16 mm with aspect ratio of two for all sections.

As the profile is the newest steel section, only a handful of investigations on the application of this column structure shape had been undertaken. However, most of the researches conducted thus far have involved elliptical tubes, hollow column structure and stub elliptical composite column. Therefore, it is considered that further investigations and experimental data are needed in order to develop a better understanding of the elliptical CFT columns—particularly for slender columns, lead to the design recommendation.

2.5.1 Experimental works on elliptical tube

The lack of fundamental test data regarding elliptical tube shape as a column structure has attracted the attention of architects and engineers. A recent project carried out at Coach Station at Heathrow Terminal 5 in London has employed the use of oval section columns where a pragmatic and conservative approach was taken by the structural engineers in mind of the column design (Gardner and Ministro, 2005). Their aesthetic appeal with differing major and minor axis properties enabled the members to be orientated so as to most effectively resist the applied loading, which consequently made the section more popular.

Despite the fact that only a few researches have been carried out in the area of an oval section as a building column structure, an analytical examination on the shape was first carried out by the aeronautical industry on the elastic critical buckling and post-buckling behaviour in the 1950s and 1960s. From these initial studies, formulae concerned with predicting the elastic critical buckling and post-buckling response of oval hollow sections under axial load were proposed (Garner and Ministro, 2004), as in Equation 2.4.

$$\sigma_{cr} = \frac{Et}{\left[\frac{A^2}{B}\right]\sqrt{3(1-\nu^2)}} \quad (2.4)$$

The investigation on elliptical section classification was carried out by Gardner and Chan (2007). From their study, Class 3 slenderness limit from EN 1993-1-1 for CHS can be safely adopted for compression members. The study also proposed a system for cross-section classification limits for elliptical hollow sections in bending, and a combination of compression and bending. For a general slenderness parameters in major axis bending based on elastic stress the proposed formulation as below:

$$\frac{D_e}{t\varepsilon^2} = 1.3 \frac{(a^2/b)}{t\varepsilon^2} \quad \text{for } \frac{a}{b} > 1.155 \quad (2.5)$$

$$\frac{D_e}{t\varepsilon^2} = \frac{2a}{t\varepsilon^2} \quad \text{for } \frac{a}{b} < 1.155 \quad (2.6)$$

An experimental study on stub elliptical hollow column was carried by Gardner and Ministro (2004). The results show that the stub hollow columns exhibited a similar failure mode that buckled locally at wider faces. The specimens also experienced a single half-wave across the width which indicated that the characteristic was closer to plate behaviour rather than shell. Other experimental works on the elliptical hollow section structure have also been highlighted in recent works carried out by Chan and Gardner

(2008a, 2008b). In the study, the compression resistance and bending strength of the structure were investigated.

Previous researches have focused on structural behaviour and the design of elliptical hollow stub columns (Garner and Ministro, 2004, Chan and Gardner, 2008b). The study was conducted on one typical size of elliptical steel section with three nominal wall thicknesses. Varying concrete strengths of normal- and high-strength concrete were considered in the study. Three loading cases—loading through the whole section, loading through concrete alone, and loading through steel alone—were performed. From the results, it was seen that the increase in the concrete strength was found to have a significant effect on the increase of axial loading. Notably, however, the ductility of column was reduced. The study also indicates that the effect of the thickness of the steel tube is much more critical for lower-strength concrete, thereby suggesting that, for lower concrete strength, the concrete core begins to crack and expand earlier; thus, the majority of the columns' strength will fundamentally depend on the confinement that the steel tube offers to concrete core. As the concrete strength increases, the influence of thickness is less significant as the concrete core is able to sustain the load and not rely on the steel tube to provide better confinement. Further investigation by Testo (2007) was carried out in order to compare elliptical CFT behaviour with circular and square CFT from studies by Giakoumelis and Lam (2004) and Lam and Williams (2004). As shown in Table 2.1, comparisons of the ultimate strength between elliptical CFT columns and circular CFT columns were conducted. From the table, it may be seen that circular specimens achieved higher axial loads compared with elliptical columns. This suggests that circular tubes provide better confinement effects

on the CFT column structure. On the other hand, elliptical tubes do not provide as much confinement to the concrete core, as its longer sides are weaker and less able to provide a perpendicular pressure to restrain the concrete core. However, it is nevertheless noteworthy to recognise that higher axial loads were achieved by elliptical CFT columns compared with the square CFT columns. It is assumed that the curved shape in elliptical tube provides more circumferential tension, which thereby leads to the pressure to restrain the concrete core.

Table 2.1: Shape effect on ultimate strength CFT columns (Testo, 2007)

Concrete strength	Circular CFT	Elliptical CFT	Square CFT
30 MPa	1090	1000	780
60 MPa	1400	1100	1000
100 MPa	1790	1300	900

Works carried out by Testo (2007) were further investigated by Yang *et al.* (2008). From the investigation, it was found that there are various differences in column response for different tube thicknesses. The concrete infill in the thinner tube experienced inclined shear failure, which is believed to be due to the tube offering less confinement compared with thicker tubes. The relationship between the cylinder strength and concrete contribution ratio (CCR) shows thicker tubes have a greater capacity as the strength of concrete increases. The ductility of elliptical stub CFT columns was further assessed by the ductility index, DI. From the parameter, it was witnessed that thicker tube exhibit a greater ductility, as it is known to offer more confinement. However, it is believed that this depends on the concrete

strength as it has been found that higher concrete strength may increase the compression resistance, which results in detrimental ductility.

Another experiment on stub elliptical CFT columns was carried out by Zhao and Packer (2007, 2009). Both normal and SCC were considered as concrete infill in the study and, similar to that of Testo (2007), three loading conditions were adopted. By implementing a simple superposition approach, the prediction of the elliptical CFT columns' capacity was good. The authors also established the design rules of EC4 and CSA procedures were applicable in predicting the ultimate capacity by treating an EHS as an equivalent RHS.

2.5.2 Numerical works on elliptical steel sections

Numerical modelling on elliptical hollow section (EHS) has been reported in several researchers' works, such as Garner and Ministro (2004), Chan and Gardner (2008b) and Zhu and Wilkinson (2007). For instance, Gardner and Ministro (2004) carried out a finite element analysis parallel to the experimental study on stub oval hollow section. In the study, numerical models were performed by including various features, such as curved geometry, non-linear material properties, and initial geometric imperfections. Several amplitudes of initial geometric imperfections were considered; however, only column deformation was found to be sensitive to the level of imperfection, although the ultimate load was closely predicted and relatively insensitive to the imperfection amplitude.

Parametric studies on the compressive response of elliptical hollow sections with different aspect ratios and varying slenderness were reported in a study by Chan and Gardner (2008b). This study follows the satisfactory agreement

achieved between the experiment on compression resistance of EHS and numerical results. From the results, the authors have established a relationship between cross-section slenderness and cross-section compressive resistance. The results further demonstrate that the Class-3 for circular in Eurocode 3 was safely adopted for elliptical tube. Moreover, preliminary effective area formulation for slender EHS was also proposed in the studies.

The investigation on the local buckling behaviour of the elliptical hollow section (EHS) structure in compression was performed by Zhu and Wilkinson (2007). The 'equivalent CHS' was used to model the local buckling of EHS by replacing the diameter term, D in theoretical elastic buckling load of a circular hollow to D_1/D_2 , which represents the major and minor diameters of the ellipse. It was found that the use of an equivalent CHS was a reasonably good predictor of the capacity of slender sections and the deformation capacity of compact sections.

Three main components in CFT column have to be modelled properly in order to achieve an accurate simulation of the actual behaviour. They are hollow steel tube, concrete core and interface between these materials. It was found that most of the previous studies considered confined concrete in the analysis, as much evidence highlights the presence of the effect of concrete confinement on the overall strength and capacity—particularly for circular CFT. Numerical models on elliptical CFT columns have been carried out by the author (Jamaluddin et al., 2009) and Dai and Lam (2010). The initial FEA carried out by the authors (Jamaluddin et al., 2009) considered confined concrete properties method, as proposed by Ellobody and Young

(2006). In the study, the use of confined concrete properties was found to be appropriate for elliptical CFT columns with lower concrete core strength. As for columns with HSC, the confined concrete properties were considered to be less significant owing to the increment of compression strength and stiffness of the concrete core, which thereby resulted in less confinement at failure as the steel sections might have already yielded.

Moreover, further FEA on elliptical CFT columns was carried out by Dai and Lam (2010). Based on the parametric study, the equivalence of confined concrete properties in elliptical tube was proposed to be as detailed in 2.4.4. The new formulae have successfully predicted the axial compressive behaviour of short elliptical CFT columns.

Chapter 3

Self-Compacting Concrete

3.1 Introduction

Concrete is widely used as a construction material. Its popularity in engineering construction stems from its availability and also because it is economical. The material is generally a mixture of cement, water and aggregates and is easily moulded into virtually any required shape.

In 1986, a new method of concrete design was proposed to achieve durable concrete without the need for compaction, known as self-compacting concrete. The prototype of self-compacting concrete, or SCC, was first completed in 1988 (Okamura and Ouchi, 2003). This concept was first initiated in Japan in the mid-1980s, and the development began with the aim to achieve durable concrete structures by improving quality in construction process. The development was also a response to the decreasing number of skilled workers in the Japanese construction industry which was known to be affecting the quality of construction work (Gaimster and Dixon, 2003, Ahmadi et al., 2007, Goodier, 2003). This technology reached Europe in the 1990s, with Sweden being the first country in Europe to begin the development of SCC. It is noteworthy to state that this is not a new material but rather a

further extension of existing concrete technology but with improvements in various aspects of construction.

3.2 SCC Characteristics

Self-compacting concrete (SCC) is a special kind of concrete characterised by its high workability. A good SCC mixture should have the capability to flow through dense reinforcement under its own weight and adequately fill all voids without segregation or excessive bleeding. Without the need for vibration or other mechanical consolidation, this type of concrete is able to maintain its stability and homogeneity and still achieve the same out-comes of good compaction. Therefore, it has been successfully used in numerous applications where normal concrete is difficult to place as or in places with limited accessibility as the result of reinforcement congestion.

This method was first developed using an existing technology with a certain requirement of fresh concrete properties which have to be fulfilled without the need of additional compaction. These properties include good segregation resistance and high flowability. This further extension of an existing method is found to offer additional benefits and the potential for improvements in various aspects of construction over the conventional concrete, such as improving productivity due to the speed of construction and reduced labour costs. Although SCC does not require additional energy for compaction during the placing process, it can nevertheless still obtain good compaction owing to its rheological properties (Yu et al., 2007). Nonetheless, there is no difference between SCC and conventional vibrate concrete in terms of structural and durability requirements; therefore, an

existing design codes and standard for conventional concrete can also be adopted for SCC (VicRoads and GeoPave, 2006).

The advantages of not using a vibrator include that 'white finger syndrome' and high levels of noise can be eliminated, thereby improving the working environment and general health and safety. The elimination also offers a rapid rate of concrete placement and reduction in labour, energy and cost of equipment.

3.3 Self Compatibility Mechanism

SCC is made from the same basic constituent materials for conventional concrete but with the addition of various admixtures or fine materials with the objective to increase the cohesiveness and required rheological properties for SCC. Ground granulated blast furnace slag (GGBS), limestone powder and pulverised fuel ash (PFA) are common powders used in SCC. However, without the presence of additional fine materials, SCC may still be produced (Goodier, 2003). The mixed proportions are based on creating a high degree of flowability whilst simultaneously maintaining a low water/cementation ratio. The main difference between the conventional concrete and SCC is the actual materials proportion in view of the fact that it is the major element influencing the properties of SCC. Generally, SCC contains lower coarse aggregate, higher amounts of sand or fine aggregates, higher amounts of cementations content, including Portland cement, lower water/cementations material ratio, higher superplasticiser doses, and sometimes viscosity modifying admixtures (VicRoads and GeoPave, 2006).

Up until now, there has been no standardised method for designing the SCC mixture. The design based on a standard design for conventional vibrated

concrete was adopted in this study but with various adjustments to satisfy the performance requirements of fresh SCC properties. The general requirement that needed for the fresh concrete such as:

- filling ability: SCC must flow into forms and around obstacles, such as congested reinforcement under the force of gravity;
- passing ability: SCC should comprise this ability when passing through various obstacles, such as restricted spaces between reinforces bars without blocking and segregation; and
- segregation resistance: SCC has to have the ability to retain the component of mixes or homogeneity during mixing, transportation, placing and curing.

Trial mixing should be conducted in order to establish suitable proportions and to highlight the necessary adjustments—particularly when dealing with estimating the superplasticiser and viscosity-modifying admixture content. Superplasticiser produces a highly fluid concrete mix, and it is an essential component in SCC when seeking to provide the necessary workability. A large quantity of powder materials or viscosity-modifying admixture is often used in order to maintain the stability by providing sufficient viscosity for the mix; consequently, it also reduces bleeding and the segregation of materials (Zhu and Bartos, 2003).

In order to achieve the required properties of SCC, the design mix should consider the requirements for lower coarse aggregate content, higher amounts of sand and cementations materials, etc. The lower coarse aggregate can lead to the reduction of frictions, and therefore enhance the overall concrete fluidity. Increasing the amount of paste content by adding

more sand, cementations material and admixture will ultimately further increase fluidity, and cohesiveness and resistance to segregation (VicRoads and GeoPave, 2006). Notably, various general parameters are needed in order to produce the quality mixes of SCC, such as:

1. Coarse aggregates content: the content is much lower in SCC in order to reduce the risk of blocking by congested reinforcement and narrow openings in formwork. The maximum size for coarse aggregate is limited to 20 mm; however, the choice of larger sizes is possible but is only justified with low reinforcement content.
2. Lower water/cementations ratio was needed to achieve high deformability. The ratio also leads to higher viscosity of the SCC paste since higher viscosity is able to suspend aggregate particles. This characteristic is crucial and effective in preventing segregation.
3. Fine aggregates: fine aggregate content in SCC is higher than in conventional concrete at approximately 48-55% of the total aggregate weight, with 50% being the typical amount. The influence of fine aggregate is more significant than coarse aggregate in SCC.
4. Superplasticiser: the chemical was added to achieve the required rheological characteristics. The addition of superplasticiser at a later stage of mixing is carried out in order to obtain fluidity, which subsequently leads to improved workability.

3.4 SCC Constituent Materials

As has been mentioned, the constituent materials for SCC are the same as those used for vibrated concrete. However, to achieve the fresh property

required by the type of concrete, additional materials are commonly used to improve the characteristics of concrete materials.

3.4.1 Additions

Additions such as fly ash, silica fume and ground blast furnace slag (GGBS) are commonly used to improve and maintain cohesions and segregation resistance due to the requirements of fresh concrete properties in SCC. The additions can be categorised according to their reactive capacity with water. Fly ash and silica fume are pozzolanic additions whereas GGBS is a hydraulic addition. In this study, fly ash and silica fume were considered in SCC design. Fly ash is effective in increasing cohesion and reducing the sensitivity of changes in water content while silica fume improved segregation resistance (SCCEPG, 2005).

3.4.2 Admixture

High range water reducing admixtures or well known as superplasticisers are an essential component in producing a SCC. The admixtures can reduce water required in concrete mixture and producing a highly fluid concrete mix. Viscosity modifying admixtures (VMA) is another type of admixtures that may be used to improve segregation resistance and the sensitivity of the mix due to variations in other constituents. It can minimise the effect of variations in moisture content, fines in the sands and its grains size distribution. This admixture modifies the cohesion of the concrete without significantly altering its fluidity (SCCEPG, 2005). Other admixtures including air entraining, accelerating and retarding also may be used in the material composition.

3.5 Test Methods

There are several test methods which have been developed in order to examine the performance of SCC; however, none of these methods has, as yet, become standardised. Visual inspection is also carried out during the testing in order to substantiate the performance of fresh SCC. The following are the tests which are commonly carried out for SCC.

- Slump Flow Test: Other than visual inspection, the slump-flow test can also be conducted in order to measure the filling ability and flowability; this may evaluate the indication of segregation. In the case of severe segregation, most coarse aggregate will remain at the centre of the pool of concrete, and the mortar and cement paste at the concrete periphery (EFNARC, 2002).



Figure 3.1: Slump Flow Test (Ambedkar, 2008)

- Flow time test, T500: This is another approach concerned with assessing the viscosity of SCC. This is carried out concurrently with a slump-flow test. It measures the time required by SCC to flow and

reach at 500 mm diameter. The increasing flow time shows that SCC is more likely to improve segregation resistance (EFNARC, 2002) where as the spread of concrete is considered as an indication of the ability of SCC to freely flow under its self-weight.

- L-Box test: A test carried out with the objective to assess the passing ability of SCC through tight openings, including spaces, between reinforcing bars without segregation and blocking.

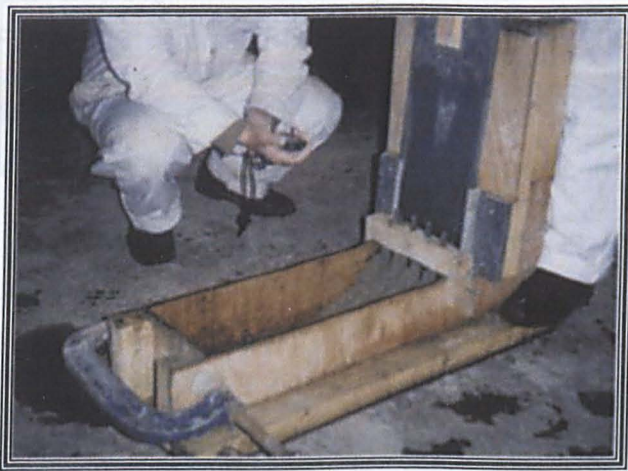


Figure 3.2: Typical L-Box test (Ambedkar, 2008)

- J-Ring: This is another passing ability test through an obstacle, in which a ring containing the reinforced bars of different diameters spaced at different intervals surrounding the slump cone. This test method is not carried out in this study, as CFT columns do not have any reinforcement.



Figure 3.3: Typical J-Ring test (Ambedkar, 2008)

- GMT: Segregation is a more important characteristic in this study owing to the fact that the concrete needs to be filled in long hollow tube columns. This test will be used in order to measure the segregation resistance. To carry out the test, some of the SCC samples are allowed to stand for a period of time so as to enable any internal segregation to occur. Subsequently, half of it is then poured into a 5 mm sieve. The mortar which passes through the sieve is then weighed. The percentage of the sample passing the sieve is calculated as follows, the weight of the material which had passed through the sieve, M_b , divided by the actual mass of the sample, M_c with some indications for corresponding percentage from the test listed in Table 3.1.

$$r = \frac{M_b}{M_c} \times 100 \quad (3.1)$$



(a) Samples poured into a sieve



(b) Laitance is collected

Figure 3.4: Typical sieve segregation resistance test (SCCEPG, 2005)

Table 3.1: GMT test results indication

$0\% \leq r\% \leq 5\%$	Excessive segregation resistance <ul style="list-style-type: none"> • Significant risk of blow holes on the hardened concrete surface.
$5\% \leq r\% \leq 15\%$	Satisfactory segregation resistance.
$15\% \leq r\% \leq 30\%$	Marginal segregation resistance <ul style="list-style-type: none"> • Risk of segregation
$r\% > 30\%$	Very bad segregation resistance <ul style="list-style-type: none"> • Systematic instability-unusable concrete

Precautions should be taken into account when dealing with SCC. For instance, it tends to dry very fast compared with traditional concrete owing to its high fines content and viscosity. This situation leads to potential plastic shrinkage cracking. The pouring process should be in a continuous motion to avoid this possibility from occurring.

3.6 SCC Mix Design Approach

Different typical concrete strengths, including both normal-strength and high-strength of 30, 60 and 100 N/mm² concrete strengths were design for concrete infill. The concrete mixes were designed for compressive cube strength, f_{cu} at 28 days, and actual concrete strength was measured on the testing day. The concrete was poured inside the hollow tube without any additional reinforcement provided inside the tube.

In this study the SCC was produced based upon the existing standard concrete design. Modifications to the mix design method were performed as the mineral admixtures; pulverified fuel ash (PFA) and silica fume were used and considered in the mix design. The admixtures were added in the concrete mixture to improve the properties of fresh concrete. Silica fume was considered only for the concrete strength of 100 MPa. It is a very fine powder with the particles size approximately 1/100 the diameter of portland cement grains which is great in reducing porosity. It is normally used to produce high-performance concrete and was added to produce C100 concrete grade in this study.

The mixture proportions were based on creating a high degree of flowability with a low water/cementitious materials ratio. The coarse and fine aggregates content were fixed and the compactibility of the concrete mixture was achieved by adjusting the water ratio and superplasticizer dosage. A trial mix was carried out prior to the concrete casting, as it is considered to be very important since there is no standard design for SCC; thus, the mix has to be designed and tested, with its fresh properties considered vital to being determined first.

A Portland cement class 42.5 and 20 mm maximum coarse aggregate was used in all concrete mixes. Superplasticizer by SIKA was mixed in SCC with the aim to achieving a required slump flow of 660 mm-750 mm, which was suitable for column application. Superplasticizer was used at a dosage rate of 1% to 3% by weight of cement and 30% proportion of PFA was specified in mix design, whilst the ratio of fine aggregate was 50% of the total aggregate weight. The mix composition was carefully designed in order to satisfy all the performance criteria for the concrete in both fresh and hardened states. Initial concrete mixes trials were performed prior to the actual mix being cast so as to ensure the design mix would fulfil the requirements of SCC.

Three methods of fresh concrete tests were adopted as they were considered to be more significant to the condition of the specified columns in the study. As there was no steel reinforcement used, there was therefore no need to specify the passing ability requirement of the fresh concrete. The tests performed on fresh concrete were, slump flow test, flow time and stability sieving test. These tests were conducted as a quality control with the aim of establishing that the mixtures were considered acceptable. Table 3.2 provides a summary of fresh concrete requirement as in (SCCEPG, 2005) and Table 3.3 shows the mix proportion for each typical concrete strength. The mixing time for SCC is longer than traditional vibrate concrete. This is viewed as being reasonable as SCC has more cementations and fine aggregate, thus a longer period should be provided in order to produce sufficient blending of these materials.

Table 3.2: Fresh concrete tests requirements

Tests	Requirement
Slump Flow	SF2 class: 660-750mm
T500	VS2' class: with 3.5-6.0 sec
Sieve segregation test	5% ≤ r ≤ 15% Satisfactory segregation resistance

Table 3.3: Mix design proportion of SCC

	C30	C60	C100
Cement	210 kg/m ³	390 kg/m ³	596 kg/m ³
Sand	902 kg/m ³	785 kg/m ³	724 kg/m ³
10 mm gravel	300 kg/m ³	268 kg/m ³	241 kg/m ³
20 mm gravel	602 kg/m ³	537 kg/m ³	483 kg/m ³
water	195 kg/m ³	190 kg/m ³	170 kg/m ³
PFA	90 kg/m ³	130 kg/m ³	-
Silica fume	-	-	107
Super-plasticiser	0.8 %	0.9 %	2.8 %

3.7 Mixing Procedure

All concrete mixes were prepared in a laboratory concrete mixer. The procedure of mixing process of SCC mix is described as follows;

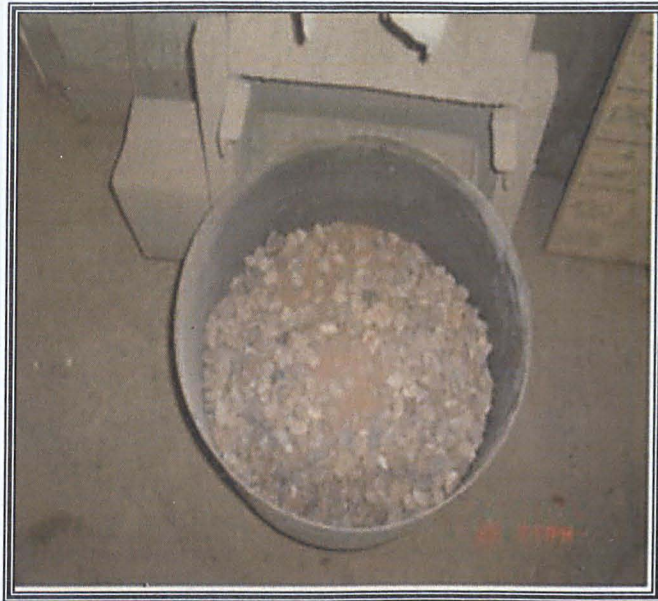


Figure 3.5: Sand and coarse aggregate are mixed first

- d. Cement and PFA are added and mixed for another minute. For high-strength concrete of 100MPa, only silica fume used as an additive.
- a. The sand and coarse aggregates are mixed together for 30 seconds.
- b. Superplasticizer is introduced and the concrete is mixed for a further 3 minutes. This admixture cannot be added directly to the concrete but should be dispersed together with mixing water. The
- c. The mixer is left for 5 minutes to allow the dry aggregate to absorb the water. Plastic is used to cover the mixer in order to minimise evaporation.



Figure 3.6: The mixer is covered with plastic

- d. Cement and PFA are added and mixed for another minute. For high-strength concrete of 100MPa, only silica fume used as an additive.
- e. Superplasticizer is introduced and the concrete is mixed for a further 3 minutes. This admixture cannot be added directly to the concrete but should be dispersed together with mixing water. The introduction of superplasticizer at a later stage of mixing processes leads to improved flowability.

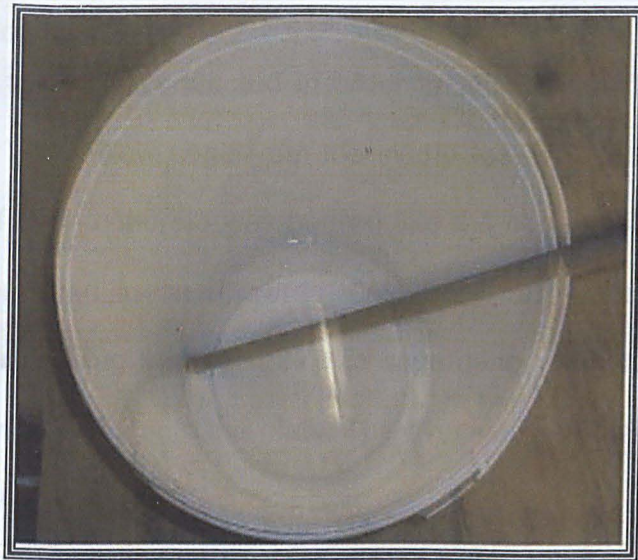


Figure 3.7: Superplasticizer is mixed with water

- f. Fresh concrete tests are performed immediately following the completion of mixing.

3.8 Concrete Tests

3.8.1 Fresh Concrete Tests

The major concern when dealing with SCC for long CFT columns is segregation. Poor segregation resistance can consequently cause poor deformability, high drying shrinkage, and non-uniform compressive strength; thus, evaluations on fresh concrete tests were carried out with the objective to examine the properties of fresh concrete.

As highlighted previously, only three fresh concrete tests were considered in this study as they were found to be more practical and suitable for the composite columns structural with plain concrete in-filled. These tests have to be performed prior to pouring the concrete into the hollow tube so as to ensure the mixtures can be accepted and also as a quality control measure.

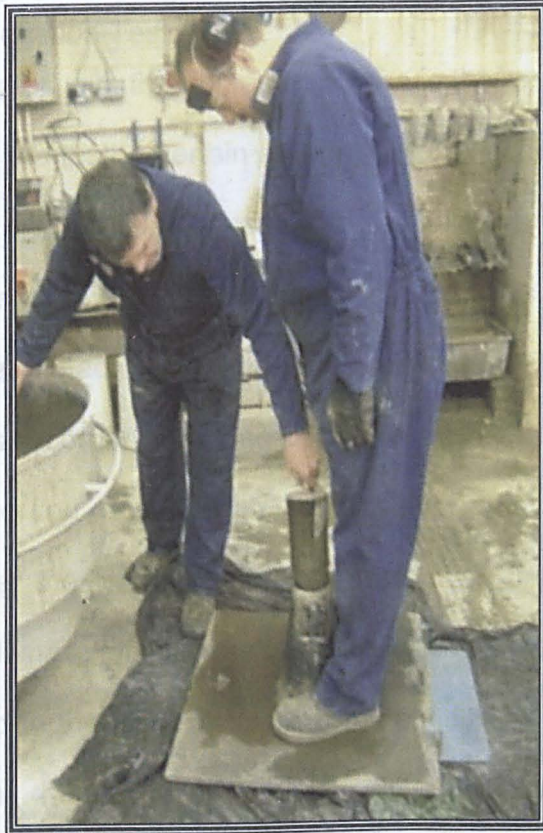
(a) Slump Flow Test

A slump flow test was conducted in order to assess the flowability of the concrete mix. The hollow cone from the slump test was placed on a plate. The sample of fresh concrete was poured into the cone until it was full. The cone was then lifted in an upwards movement, and visual inspection in conjunction of assessing the resistance to segregation was carried out when the concrete was flowing into the plate. The average diameter of final spread concrete was then recorded.

Visual inspection was also made during the testing. The distributions of aggregates particles in the concrete were observed to be relatively equivalent at all location indicated a good segregation was achieved.

(b) Flow Time Test, T500

This test represents another possible way of assessing the viscosity of a SCC, which is measured during the slump flow test. The marked 500 mm diameter was placed first on the plate surface, with the time recorded from the commencement of the upward movement of the cone to when the concrete spread had reached the 500 mm diameter. The VS2 class with 3.5-6.0 seconds was found to be more appropriate for this research as it shows segregation resistance improvement (SCCEPG, 2005). Figure 3.8 shows both tests that had been carried out.



(a)



(b)

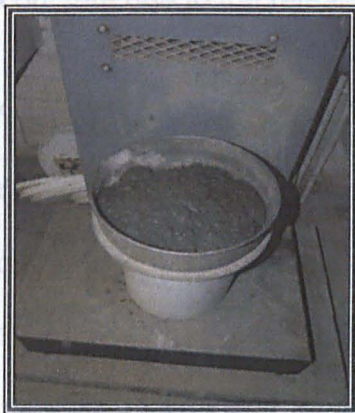
Figure 3.8: Slump flow test and T500

Figure 3.9: Sieve Separation Test

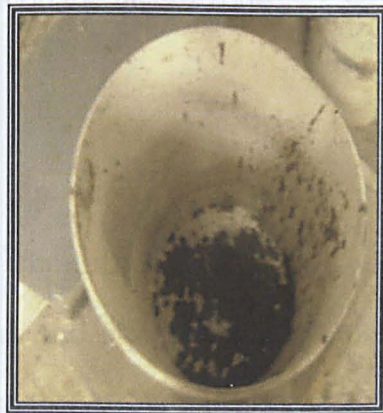
(c) Sieve Segregation Test

This test was adopted with the objective to assess the resistance of the SCC to segregation. In the test, a certain amount of fresh concrete was placed in a container with a fitted lid. The sample was allowed to stand on a flat surface without disturbance for approximately 15 minutes. Any separation for water bleeding was noted. The weight of the sieve (5 mm square apertures) receiver (W_p) was recorded and placed on the receiver, and the mass was subsequently recorded again. With the receiver and sieve still on the weighing machine, the top part of the sample was then poured into the sieve. The actual mass of the sample (W_c) was recorded. Concrete was permitted to stand in the sieve for approximately 120 seconds, upon which time the sieve was then removed vertically without agitation. The weight of the material which had passed through the sieve, including the receiver (W_{ps}), was measured. The segregation ratio was then calculated using equation 3.2;

$$r = \frac{(M_{ps} - M_p)}{M_c} = \frac{M_b}{M_c} \times 100\% \quad (3.2)$$



(a)



(b)

Figure 3.9: Sieve Segregation Test

3.8.2 Hardened Concrete Properties

As the basic ingredients used in the SCC mixes are practically the same as those used in the conventional vibrated concrete, thus the tests for hardened properties were carried out using the same method as conventional concrete. The hardened properties of the SCC are also expected to be similar to those obtained with the conventional concrete. Cubes and cylinders concrete were prepared and cast at the time of concrete placement in the elliptical tubes.

The hardened tests were conducted on 7, 14, 28 and on the day of the corresponding columns testing. For each batch, concrete cubes of 100 mm and standard 150 mm x 300 mm cylinders were cast and cured under the same conditions as the elliptical CFTs columns, and subsequently tested in compression in order to achieve an accurate representation of its strength. The concrete cylinder test results were assumed as accurately representing the concrete core of the in-filled columns. This assumption was made owing to the fact that there had been no witnessed failure dominated at the top and bottom of the cylinders, which would affect the true stress-strain relationship of the concrete due to the release of strain on the failure zone.

3.9 Trial concrete mixing

The SCC was designed for compression strength of 30 N/mm². The mixing time for SCC is longer than traditional vibrate concrete. It is reasonable because of SCC has more cementations and fine aggregate thus longer period should be provided in order to produce sufficient blending of these materials.

3.9.1 Fresh concrete tests results

The average diameter of spread concrete obtained from this trial for slump flow test was within the range needed for class SF2. The diameter of concrete spread of 700 mm was obtained from the mixture and it is found to fit the requirement for suitable application for column structure. Through observation there was no tendency for segregation occurred as there is no concrete remained at the centre of the pool of concrete.

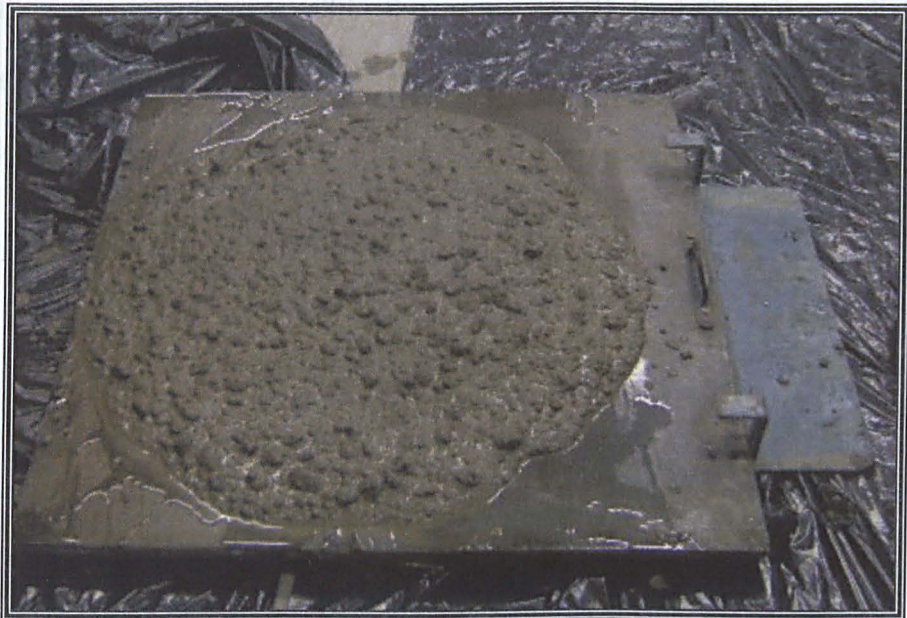


Figure 3.10: Spread of SCC fresh concrete for trial mixing

From T500 test the viscosity of the mixture was estimated and the recorded time for concrete to reach 500 mm was 5 seconds. As suggested in Brite Eurem Report (2000) the measurement indicates that the concrete was satisfied for criteria in civil engineering concrete application as shown in Table 3.4.

Table 3.4: Proposed criteria for used test methods by Brite EuRam (2000)

Application	Slump flow [cm]	T50 [s]
Civil Engineering	> 60	3-7
Housing	> 60	2-5

As for segregation evaluation, the mixture falls into the category which is indicated that the SCC design mix has no risk of segregation. Based on the equation, the result was within the range of 5% to 15% which satisfy the segregation resistance which is needed and significant for column application.

$$r = \frac{M_b}{M_c} \times 100$$

$$r = \frac{0.84}{7.67} \times 100$$

$$r = 13.6\%$$

From the fresh concrete tests results, it was found that the design mix meets the entire requirement for SCC. The fresh concrete tests which were conducted to assess the performance of fresh mixture are presented in Table 3.5. It is clearly shown that the mixture fit to exhibit self-compacting characteristics.

Table 3.5: Fresh concrete tests results for trial mix

Tests	Requirement	Achieve
Slump Flow	SF2 class: 660-750mm	700 mm
T500	VS2 class: with 3.5-6.0 sec	5 s
Sieve segregation test	$5\% \leq r \leq 15\%$ Satisfactory segregation resistance	$r = 13.6\%$

3.9.2 Hardened concrete testing

Hardened concrete tests of SCC are the same as normal concrete tests. Concrete cubes with dimension of 150 mm are conforming to BS EN 12390-1-2000 and BS 1881-108:1983. The compaction and steel rod was prevented during the placement of fresh concrete into the cubes and cylinder moulds after it discharges from skip. Grease was applied to concrete mould in order to allow easy release of cube and cylinder concrete.

Immediately after the making, the specimens in their moulds were transferred to a moist curing environment for at least 16 hours before demoulding as stated in BS EN 12390-2-2000. The next day after concrete casting, the cubes and cylinders were de-moulded. Figure 3.11 shows cubes and cylinder concrete from the same batch after they were de-moulded. The surface of some concrete cubes shows the present of air void. Fortunately only 3 of the concrete cubes shown some concentration of voids as shown in Figure 3.12.



Figure 3.11: Cubes and cylinder concrete



Figure 3.12: Present of some air voids in the concrete cubes

These specimens then were covered with Hessian and plastic cover for curing and were left until testing as shown in Figure 3.13. These specimens were not left in curing room or submerge into the water as it will not represent the actual condition for composite CFT column. More over the steel tube tends to get rust in humid condition.

Figure 3.14: Concrete cube after failure



Figure 3.13: Curing of concrete cubes and cylinder

The cubes for this trial mix were tested at 7, 21 and 28 days after casting with 3 cubes were used for testing at each specified age. The testing procedure was according to BS EN 12390-3:2002 with the cubes still in wet condition. Figure 3.14 and Figure 3.15 shows the concrete cubes after the tests were complete and the development of compression test results respectively.



Figure 3.14: Concrete cube after failure

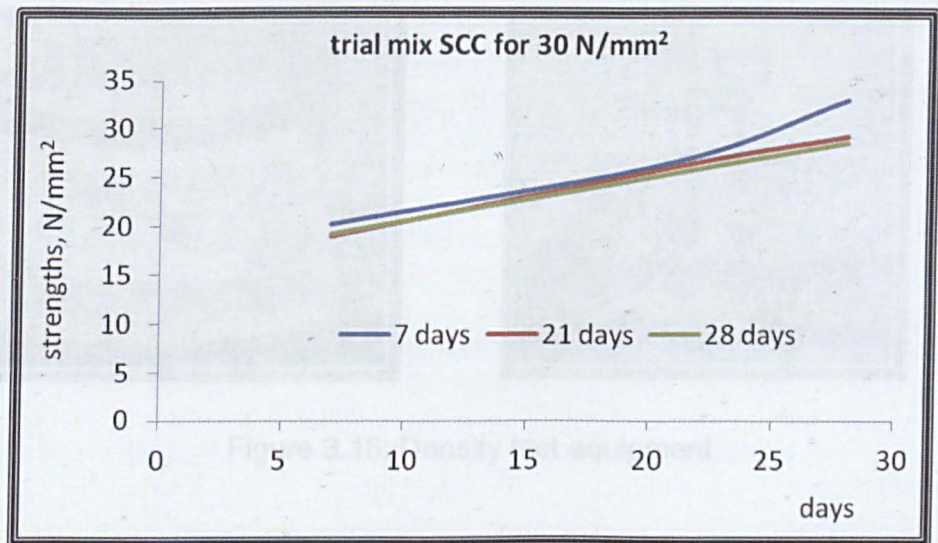


Figure 3.15: Concrete strength development for $f_{cu} = 30 \text{ N/mm}^2$

Density tests for hardened cube were also conducted. This test is very important as it shows the quality of freshly mixed concrete. Figure 3.16 shows the apparatus used for this test with the balance is equipped with a stirrup for weighed the cube. The concrete cube was weighted on the balance (Figure 3.17) and then the cube was put on the stirrup which it will be fully submerged (Figure 3.18) in the water tank at a constant depth. Specific gravity was calculated and the result is shown in Table 3.6. The results show that the densities of concrete cubes were in the typical range of normal weight concrete density thus indicate that any present of small voids is not significant.

Figure 3.18: Concrete cube has to be fully submerged

Table 3.6: Density of cubes concrete

S.G1 = 2346 g/mm³ S.G2 = 2339 g/mm³ S.G3 = 2341 g/mm³

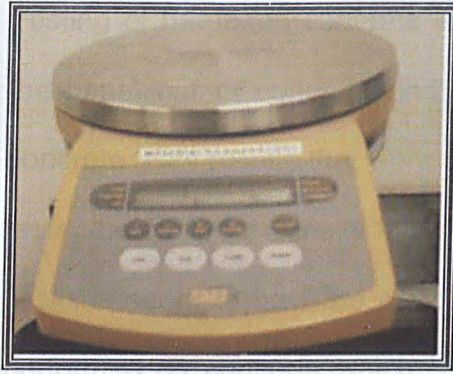


Figure 3.16: Density test equipment

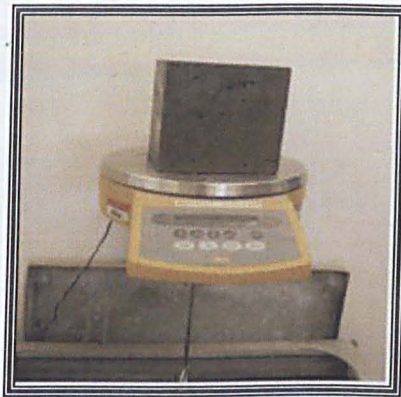


Figure 3.17: Concrete cube was weighted

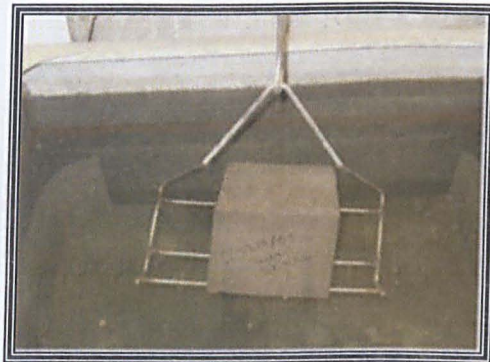


Figure 3.18: Concrete cube has to be fully submerged

Table 3.6: Density of cubes concrete

S.G1 = 2346 g/mm ³	S.G2 = 2338 g/mm ³	S.G1 = 2341 g/mm ³
-------------------------------	-------------------------------	-------------------------------

Testing of hardened concrete is important as it can be used to investigate the behaviour of concrete and the strength characteristics. The hardened concrete tests results that were conducted are satisfactory. From the density tests, the concrete density fall within normal concrete range and the present of voids seem to have no effects on the concrete. The most common test performed on concrete which is compressive test was conducted on both cubes and cylinders concrete and the results are acceptable.

Chapter 4

Experimental Studies

4.1 General

This chapter describes an experimental work which has been carried out. Details of the experimental investigation, including the description of the specimen's preparation, are presented.

In this study, a series of compression tests have been carried out on elliptical composite columns, with both short and long columns tested for failure under axial concentric loading. The experimental investigation was performed on hot-finished elliptical sections produced by Corus Tubes. The main purposes of such tests were to understand and establish the elliptical CFT columns' behaviour and the load-carrying capacity of the structure. Notably, the information obtained would serve as an aid to formulate the design criteria.

An elliptical hollow stub column for each selected column size was included in the study for comparison purposes. The identified parameters considered in this study are intended to examine their influences on the strength and behaviour of elliptical CFT columns. An experimental programme was conducted not only to determine the maximum load capacity of the elliptical CFT columns, but also to investigate the failure pattern up to and beyond the

ultimate load. The experiments were also designated so as to provide information regarding the stress-strain characteristics, failure modes, including the effects of geometric dimension, concrete strength and column length. Following the experimental investigation, a numerical analysis adopting a finite element programme was performed. Numerical models—which have been developed both with and without the confinement effect taken into consideration—were verified with the experimental results and have been accordingly explained in Chapter 6.

4.2 Experimental Programme

4.2.1 Properties of Ellipse

EHS is defined by the length of two principal axes—major and minor, as outlined in Figure 4.1. The A-A' axis is the major axis with a length of $2a$, whilst the B-B' axis is the minor axis with a length of $2b$, with the area of ellipse given by the general formulation of πab . EHS are produced by Corus Tubes in the U.K and all the sections are produced, with major-to-minor axis dimensions of 2:1, as hot finished hollow structures.

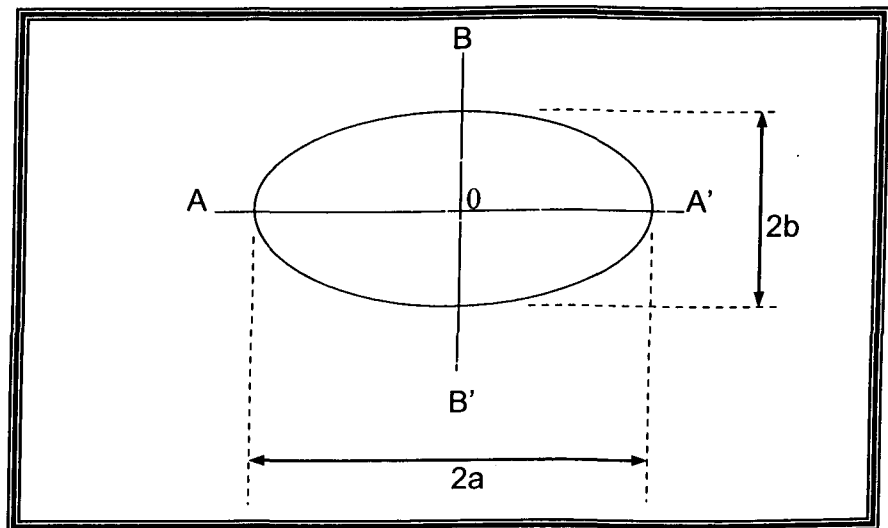
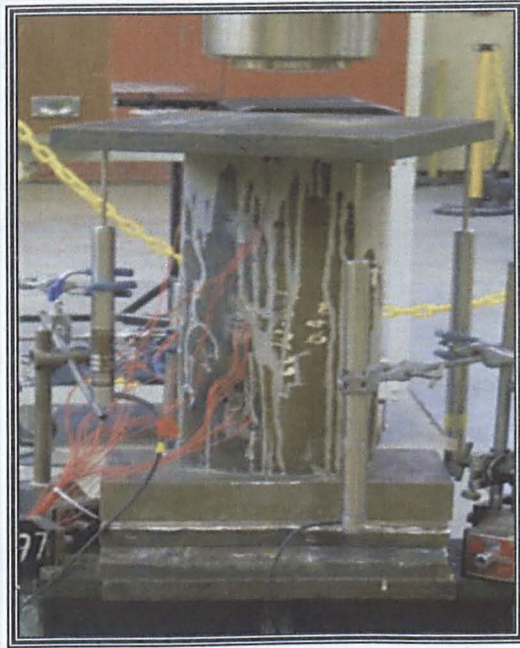


Figure 4.1: Definition of ellipse

4.2.2 Instrumentation

Various instruments, such as linear vertical displacement transducers (LVDTs) and strain gauges were used during the experimental. The LVDTs were used to measure the out-of-plane deflection and strain gauges, which located at the outer circumference of the steel tube, were able to ascertain the local effects on the cross-section.

The axial shortening was captured by LVDTs, which were positioned between the plates of the stub columns and the end plates of the testing machine for long columns (Figure 4.2). The lateral displacements of the long columns were mainly measured at the centre and quarter points of the columns as well as the strains (Figure 4.3 and Figure 4.4j). For all columns, six strain gauges were attached to each specimen. Vertical gauges were affixed at the top, middle and bottom of the major axis, whereas one horizontal gauge was affixed at the middle column of the major axis. On one side, only one vertical gauge was affixed at the middle. Similarly, one vertical gauge was affixed on the other side, at the middle (Figure 4.3). The load gauges, LVDTs and strain gauges were connected to a data logging system that was controlled by an automatic data acquisition system and operated by a personal computer.



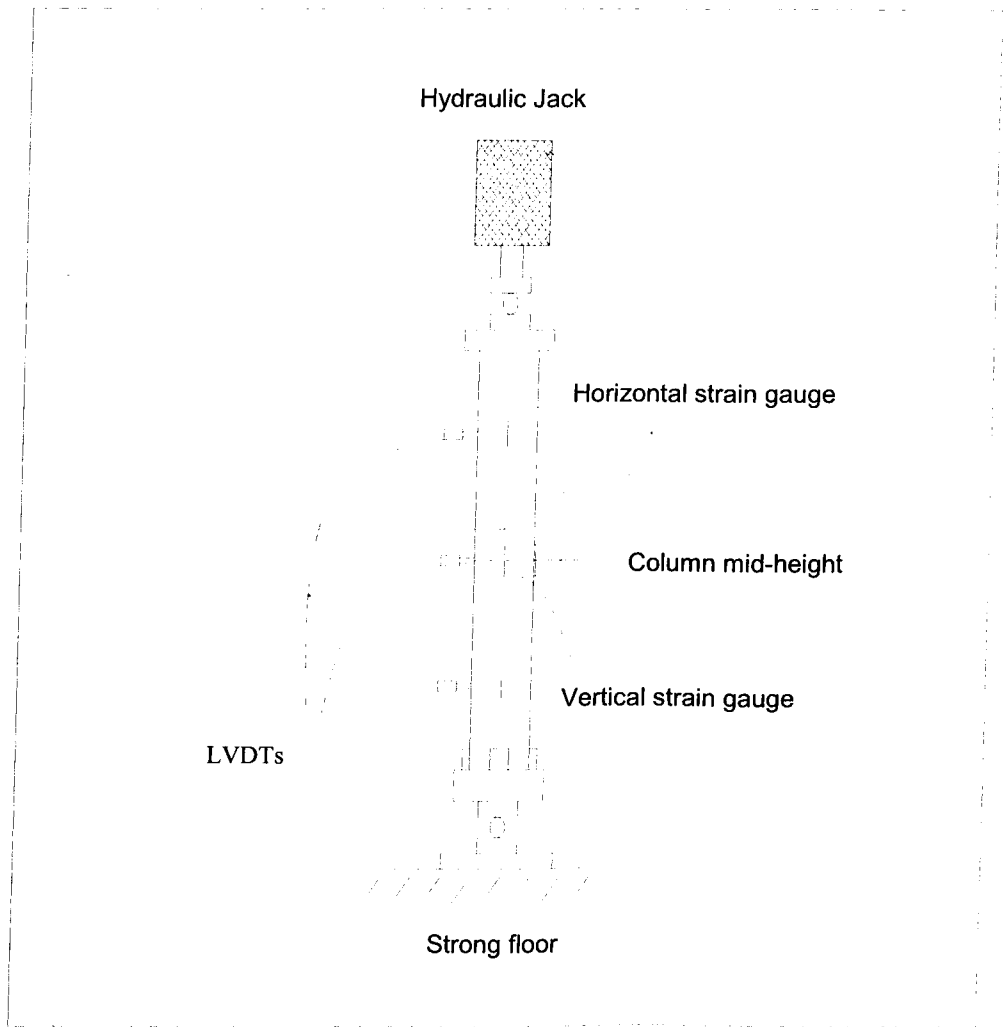
(a) Stub columns



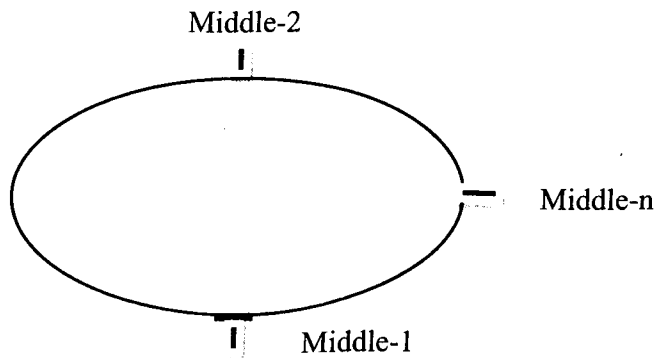
(b) Long columns

Figure 4.2: Location of LVDTs for axial shortening measurement

Figure 4.3: Instrumentation of columns



(a) Location of LVDTs and strain gauges for long column



(b) Location of strain gauges at mid column

Figure 4.3: Instrumentation of columns

4.2.3 Columns' Set-up and Test Procedure

A total of twenty-five CFT columns and two elliptical hollow columns were tested to failure. All columns were tested in a vertical position and subjected to a compressive axial loading. Tests were performed on pin-ended long columns and on fixed-ended stub columns. Prior to the test, a layer of plaster of Paris was added to flush the top concrete core in order to ensure the loading was evenly distributed across the cross section.

For stub columns, both its ends were capped by the steel plates so as to ensure full contact between specimens and end bearings (Figure 4.2a), whereas for long columns, only the bottom end was welded to a steel plate in order to facilitate the placing of concrete whilst the other end was secured by a slotted plate, as shown in Figure 4.4c. Notably, when each column was placed in the test rig, a small load was applied so as to hold the specimen upright.

The typical setting-up of long columns is shown in Figure 4.4. The column was rested on top of the bottom support plates where the bricks were used to stabilise the column's base. In order to ensure the stability of the column following the top support having been fixed, the column would then be loaded with a small load from the load cell. A laser, spirit level and plumb-bob were used to ensure the column was straight so as to avoid initial inclination and also to put to centre with the load cell. The specimens were centred in the testing machine to ensure that the compressive axial load was applied without any eccentricity. Moreover, to guarantee the loading was applied uniformly, a preload test was conducted. The top and bottom strain gauges were used to assess the uniformity of the load. Prior to performing the test, a small load of approximately 100 kN was applied to the specimens

and the values of strain gauges around the cross section were observed and clarified. The measurements of both strain gauges were considered by comparing the values to their average strain measurement. Adjustments of the column were made until the differences between the measured strain and their average value was less than 5% (Hanbin and Tsutomu, 1992).

Two test frames were used to perform experiments on all long columns. A four-legged test frame which height can be regulated enables experimentations on specimens from series I, II and III. A 3000 kN hydraulic jack is located at the top of the frame. Due to the restriction of column length available for the 4-legged test frame, specimens from series IV were tested at two-legged test rig with a 1000 kN hydraulic jack that was designed to be overloaded safely to at least 1500 kN while some stub hollow columns were tested in compression machine in which the concrete cubes and cylinders were tested. The hollow specimens were among the earlier tests conducted in this study before the new hydraulic jack arrived. Thus the tests were conducted slightly different in terms of the testing procedure, where only load controlled can be applied to the machine.

Precautions were taken prior to the testing. Wire mesh cage was used to avoid the steel ball from flying out and a string was used to tie the column to ensure the specimen is within the test rig during the testing. An extra precaution was taken for series IV tests where steel bars were fixed to the test rig as shown in Figure 4.4j.

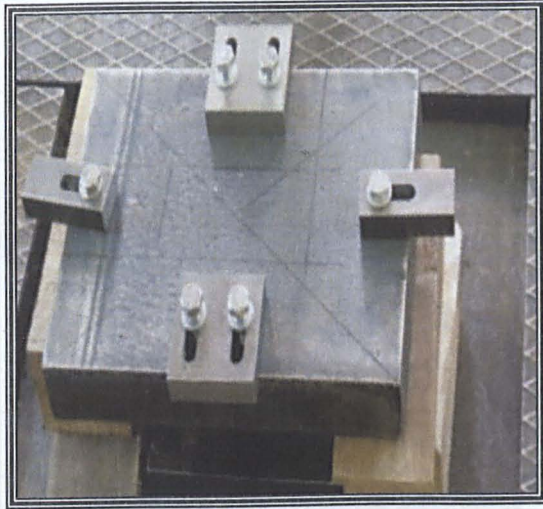


(a) Laser was used to ensure the column was in centre with the load cell



(b) Timber wedges are used to stabilise the ball support.

(c) The column is set up vertically on top of 2.5 m x 2.5 m plate



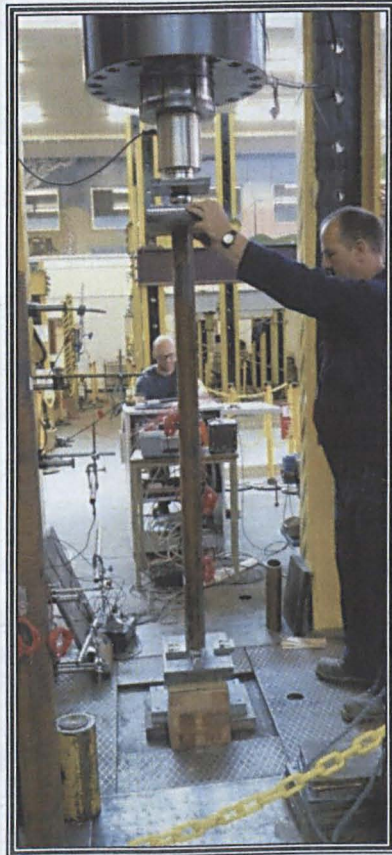
(c) Slotted plate is placed on top of the ball support and bricks are used to replace the timber wedges to stabilise the support system.



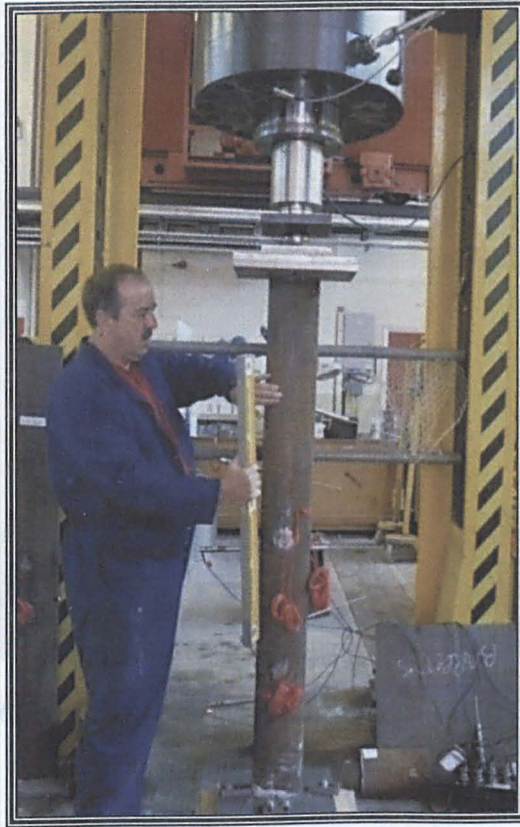
(d) The column is set up vertically on top of the slotted plate



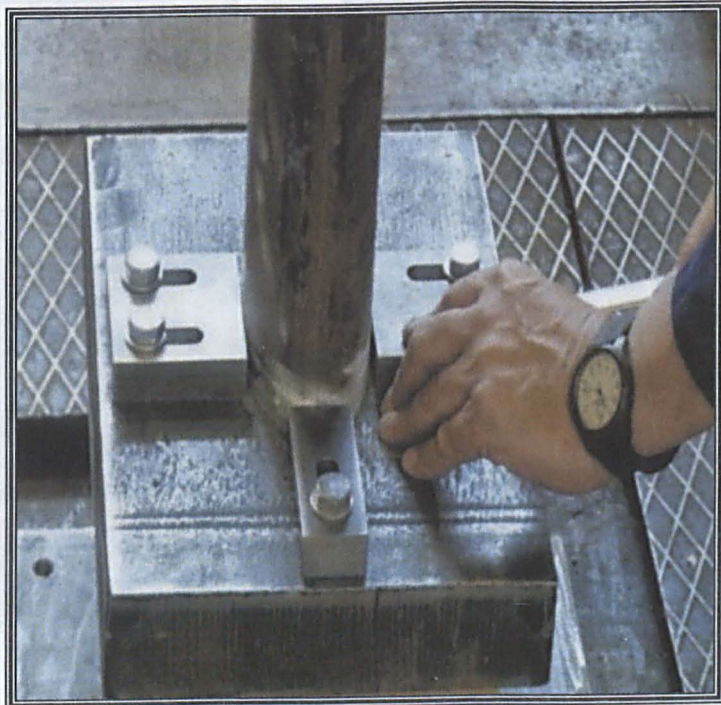
(e) Once the column is in position, the upper supporting plates are placed on top of the specimen.



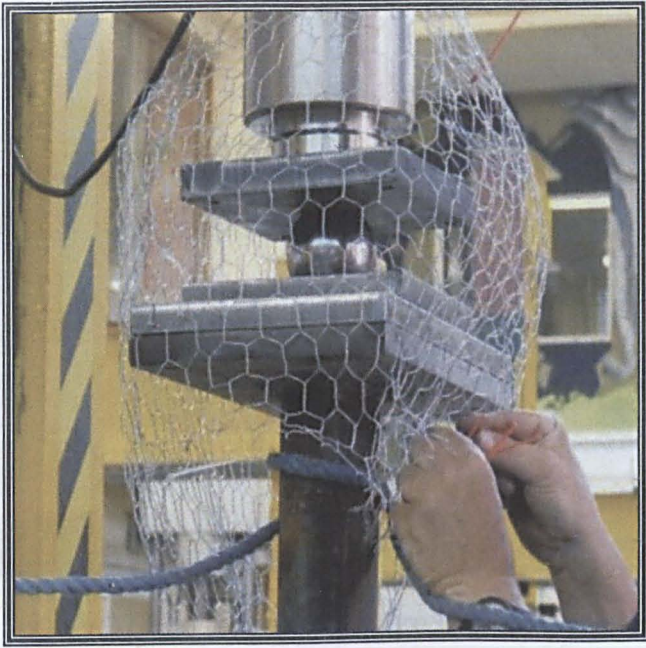
(f) To ensure the stability of the column after the top support has been fixed, the column is loaded with a small load from the load cell.



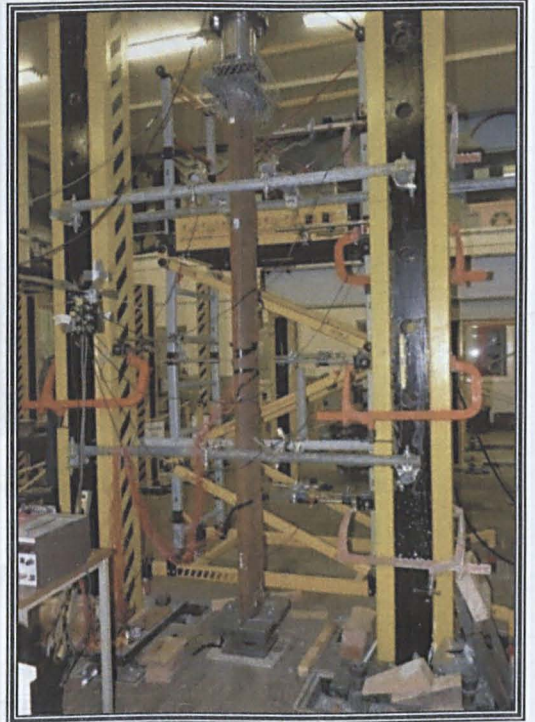
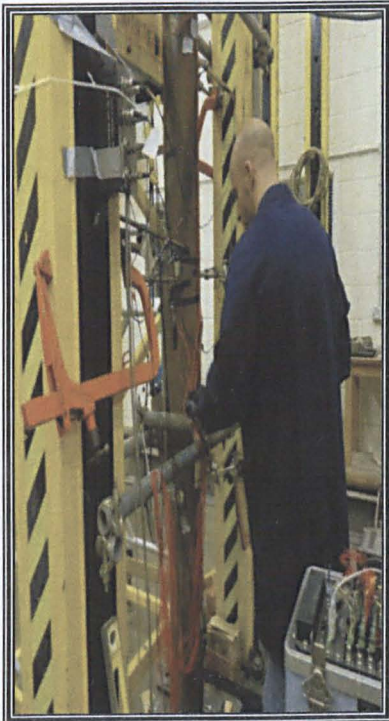
(g) The verticality of the column is checked using spirit level.



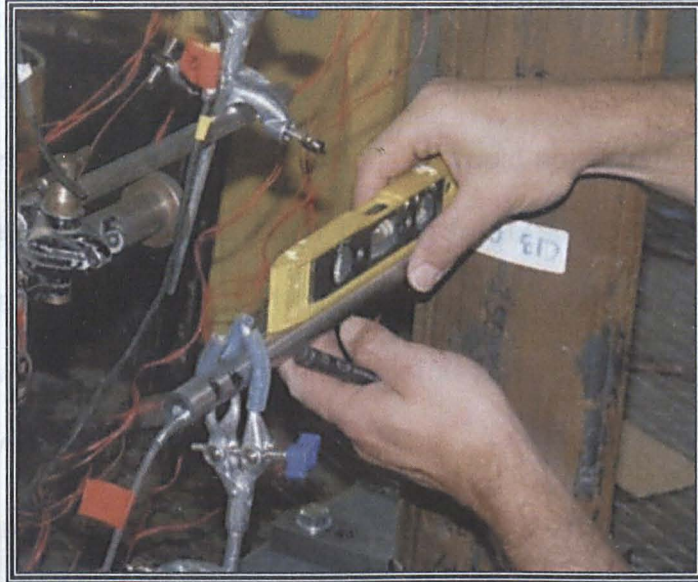
(h) The bottom specimen is secured by the slotted plate.



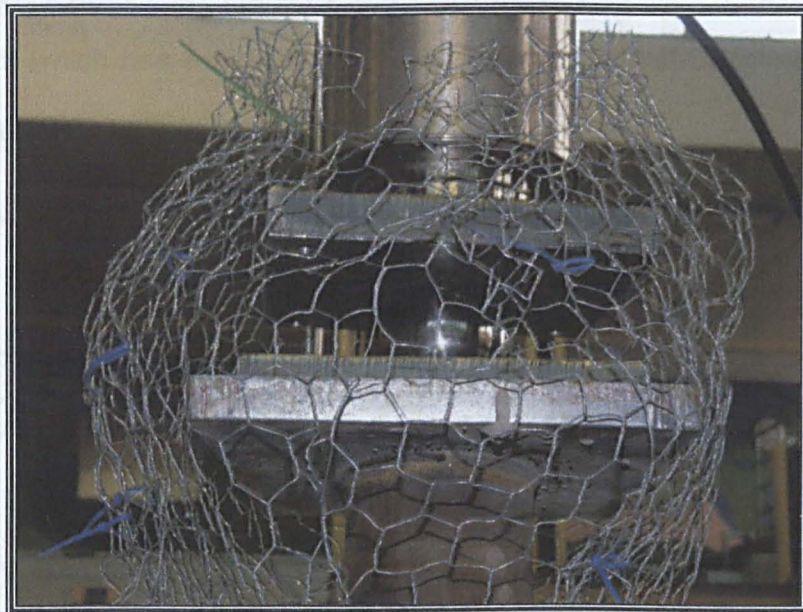
(i) Encased protection is placed around the test frame to prevent materials from flying out.



(j) Steel bars are fixed to the test rig



(k) LVDT is checked to ensure it in horizontal



(l) Wire mesh cage to avoid the steel ball from flying out

Figure 4.4: Long columns test setup.

4.2.4 Column Labelling and Dimension

All specimens were classified into four series depending on the height of columns, as summarised in Table 4.1. In Series I, columns with heights of 300 mm and 400 mm were considered as stub columns. For Series II, Series

III and Series IV, they represented long columns with tube heights of 1500, 1790 and 2500 mm respectively. Initially column length as high as 3000 mm has been prepared, however the dimension could not fit in the available test rig thus, the columns have been cut to the 1790 mm. In Series II the experiments for columns with typical concrete strength of C60 have been repeated two times. These columns, CII-150-C58, CII-150-C64 were tested in order to verify the results.

All specimens were labelled such that the length, size and nominal concrete strengths could be identified from the label. For instance, CIII-150-C65, the first letter and Roman number: therefore, CIII symbolises a column from Series III which has a typical length of 1790 mm, whilst C65 indicates the actual cube strength and 150 represents the tube size.

There were two nominal sizes of specimens chosen in this study; 150 x 75 x 4 mm and 200 x 100 x 5 mm. The tubes were supplied by a manufacturer in total length of either 12 m or 10 m each. The specimens were accordingly cut to the desired lengths, ranging from 300 mm to 2500 mm. In the case of the stub column, its length was decided based on the study by Gardner and Ministro (2004). In this study, the stub columns' lengths for elliptical concrete filled tube (CFT) were selected to be two times the larger diameter, so that the length was sufficiently short and would not fail by overall buckling, and would be long enough to have a representative residual stress pattern. According to Gardner and Ministro (2005), an elliptical stub column which has a length of three times the larger dimension displays evidence of an overall buckling effect. Therefore, for this study, the length of the stub columns was taken as two times the larger cross-sectional

dimension of the tube. This was also applied so as to ensure that the specimens would be stub columns with a minimum effect from slenderness, as the tests were intended to demonstrate the overall column performance at a very low slenderness ratio. On the other hand, the elliptical long columns were tested on three different lengths in order to examine the influence of slenderness on column strength.

To summarize, the experiments were conducted on columns with steel tubes of typical diameter-to-thickness ratio (D/t) of 37.5 and 40, and yield stress of f_y in the range of 348-431 MPa, and were accordingly filled with normal and high-strength self-compacting concrete. The value of D is taken as a broad face dimension. Meanwhile, the columns' slenderness ratio, L/B ratios range from 16 to 143. The column length referred in this study is the length of the composite column itself excluding arrangements for loading application and support bearing whereas the buckling length is the length between the hinges as shown in Figure 4.5.

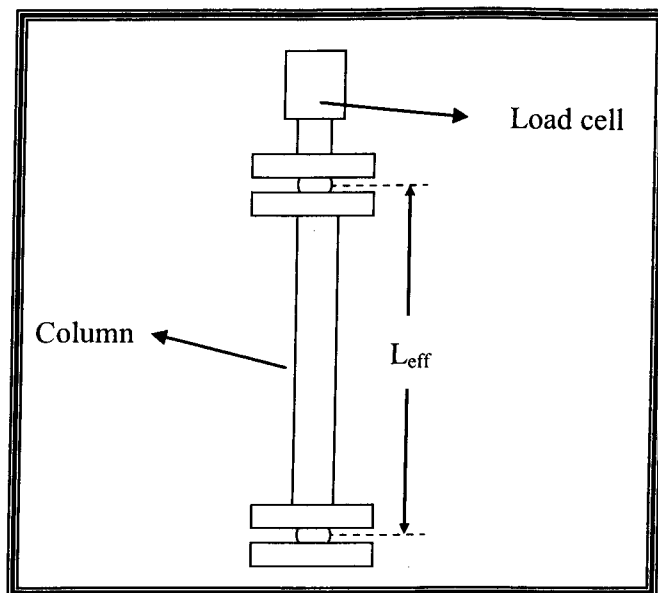


Figure 4.5: Buckling length of long column

Table 4.1: Summary of dimension and columns' properties

	Label	2a mm	2b mm	L mm	t mm	D/t	L/D
Series I	CI-150h	150.3	75.2	299.5	4.2	35.8	2
	CI-150-C47	150.1	75	300	4.1	36.6	2
	CI-150-C62	150.2	75.1	301	4	37.6	2
	CI-150-C106	150.1	75.2	299	4.2	35.7	2
	CI-200h	197.8	100.1	400	5.2	38.0	2
	CI-200-C34	197.8	100.1	398	5.1	38.8	2
	CI-200-C67	197.5	100.2	398	5.1	38.7	2
	CI-200-C116	197.4	100.1	398	5.1	38.7	2
Series II	CII-150-C26	150.9	75.4	1497	4	37.7	9.9
	CII-150-C58	150.2	75.2	1499	4.2	35.8	10
	CII-150-C64	150.4	75.2	1498	4.1	36.7	10
	CII-150-C91	150.3	75.2	1496	4.1	36.7	10
	CII-200-C29	197.5	100.2	1499	5.2	38.0	7.6
	CII-200-C55	197.4	100.1	1498	5.1	38.7	7.6
	CII-200-C93	197.7	100.1	1498	5.1	38.8	7.6
Series III	CIII-150C20	150.5	75.4	1785	4.1	36.7	11.9
	CIII-150C65	150.7	75.2	1785	4.2	35.9	11.8
	CIII-150C100	150.7	75.4	1786	4.1	36.8	11.9
	CIII-200-C42	197.6	100.2	1785	5.1	38.7	9
	CIII-200-C63	197.7	100.1	1786	5.1	38.8	9
	CIII-200-C98	197.3	100	1786	5.2	37.9	9.1
Series IV	CIV-150-C23	150	75.1	2500	4.2	35.7	16.7
	CIV-150-C63	150.2	75	2502	4	37.6	16.7
	CIV-150-C100	150.1	75	2501	4.1	36.6	16.7
	CIV-200-C29	197.5	100.3	2498	5.2	38.0	12.6
	CIV-200-C59	197.8	100.1	2499	5.1	38.8	12.6
	CIV-200-C101	197.7	100.1	2498	5.1	38.8	12.6

4.2.5 Column Supports

Tests were performed on pin-ended long columns and fixed-ended stub columns. Pin supports were constructed from groove plates and a steel ball in order to ensure rotations in every direction. So as to simulate this simply supported end condition, plates with spherical grooves at their centres (Figure 4.6) were used to accommodate the steel ball and were then fixed at both ends of the long columns.

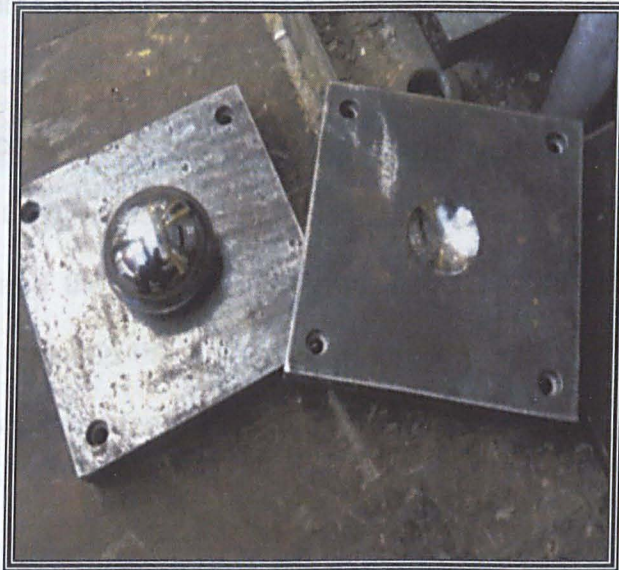
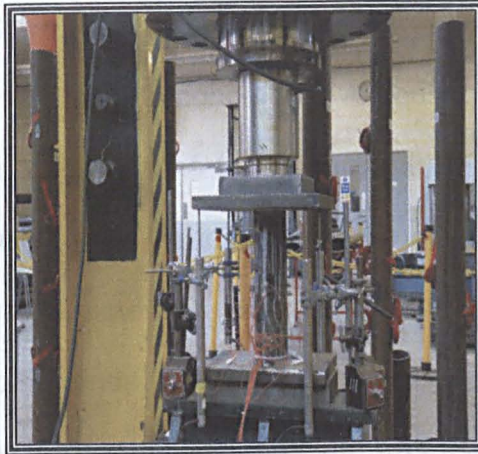


Figure 4.6: Groove plate and steel ball

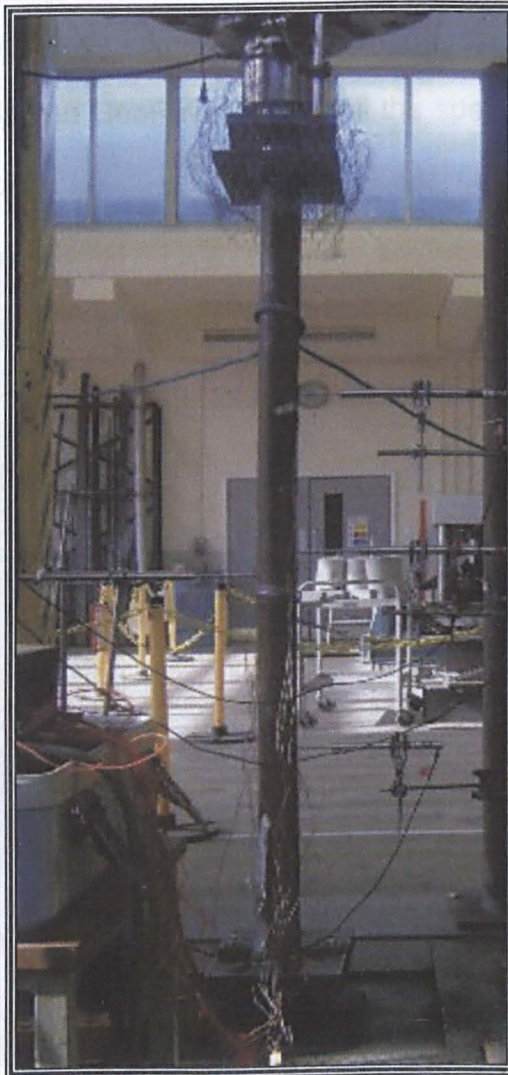
For stub columns test, both ends were capped with steel plates so as to ensure full contact between the specimen and end bearings. This was to guarantee the load was distributed evenly across the cross section. On the other hand, for long columns, only the bottom ends were welded to a steel plate whilst at the other end, a slotted plate was fixed and secured. The slotted plate arrangement was adopted for the purpose of accommodating a range of different section sizes, whereas the welded end plate was to facilitate the casting process.

4.2.6 Testing Procedure

Figure 4.7 shows the typical test arrangements for both stub and long columns. The compression load was applied monotonically increasing, and load, strain and displacement data were recorded during the testing process until the load was observed to be dismissing. The tests results concerning failure mode, circumferential strain distribution, load-deformation behaviour, buckling, and evaluation of the strength of the columns were documented during the course of the testing. The specimens were loaded at a very slow stroke control at a rate of 0.2 mm/min, such that the local buckling behaviour of the CFT could be carefully observed. Each testing normally lasted between 45 – 60 minutes. Prior to testing, the top surfaces of all specimens were levered and the ground smoothened so as to remove imperfections and to further maintain the uniformity of loading on the surface. A layer of plaster of Paris was added to flush the top of the concrete core.



(a) Stub column



(b) Long column

Figure 4.7: Test arrangement for elliptical composite columns

4.3 Casting of Composite Column

All CFT columns were filled with concrete in vertical position where the SCC was poured into the tube from the top (Figure 4.8). For short columns, the end plate was tack-welded so as to facilitate the concrete pouring from the other end. Moreover, the plate was removed before tested was initiated. For long columns, one of its ends was welded to a steel plate for this purpose. On each long column a 20 mm thick end plate was used. The concrete was poured into the columns in a continuous manner to avoid the concrete from being left for a long period of time which, in turn, had the potential to create a cold joint (VicRoads and GeoPave, 2006). All the specimens were then air-cured at room temperature.



(a) End-plate is welded to the tube



(b) Tube is secured with strings and a cone is used for concrete filling

Figure 4.8: Preparation of long tube for concrete casting

4.4 Material Properties Tests

In order to establish the material properties of steel and concrete elements, several tests were performed. In the case of the concrete infill, it is considered very important that the characteristics of fresh concrete material be defined for quality control owing to the fact that SCC mixture is more susceptible to quantity and material fluctuations. Only fresh concrete with the necessary characteristics should be used, whereas for steel material, its response under tensile load was obtained and the results were subsequently utilised in the analysis of the column test results and in the development of numerical models.

4.4.1 Steel

The steel tubes used were hot-rolled EHS with steel grade of S355. These tubes were cut into several pieces for the preparation of tensile coupon specimens. The material properties of the steel element were accordingly determined from mechanical testing on steel coupons with an approved shape. The coupons were subsequently prepared and tested according to the guidelines as outlined in the EN 10002-1:1990.

The basic material stress-strain response of the steel element was obtained by means of tensile tests on the coupon. The yield stress, f_y determined from the tensile strength is generally accepted as being the same for compression. As the columns under axial compression, the stress-strain characteristics of the steel section are roughly the same as those in tension up to the plastic range. The test pieces were accordingly machined from a batch of material specimens with two longitudinal coupons, which were cut from the flat surface of each elliptical tube. Linear strain gauges were affixed

at the midpoint of each side of the coupons. The behaviour of steel is described through the stress-strain relationship from the test. The curves were plotted and the ultimate stress, yield stress and Young's Modulus, E were obtained. Coupon specimens and a typical load-deformation curve for these coupons are shown in Figure 4.9.

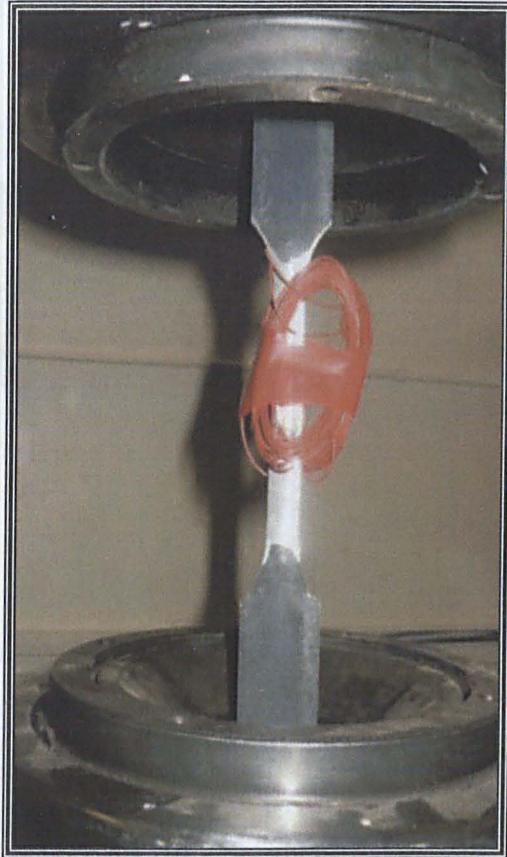
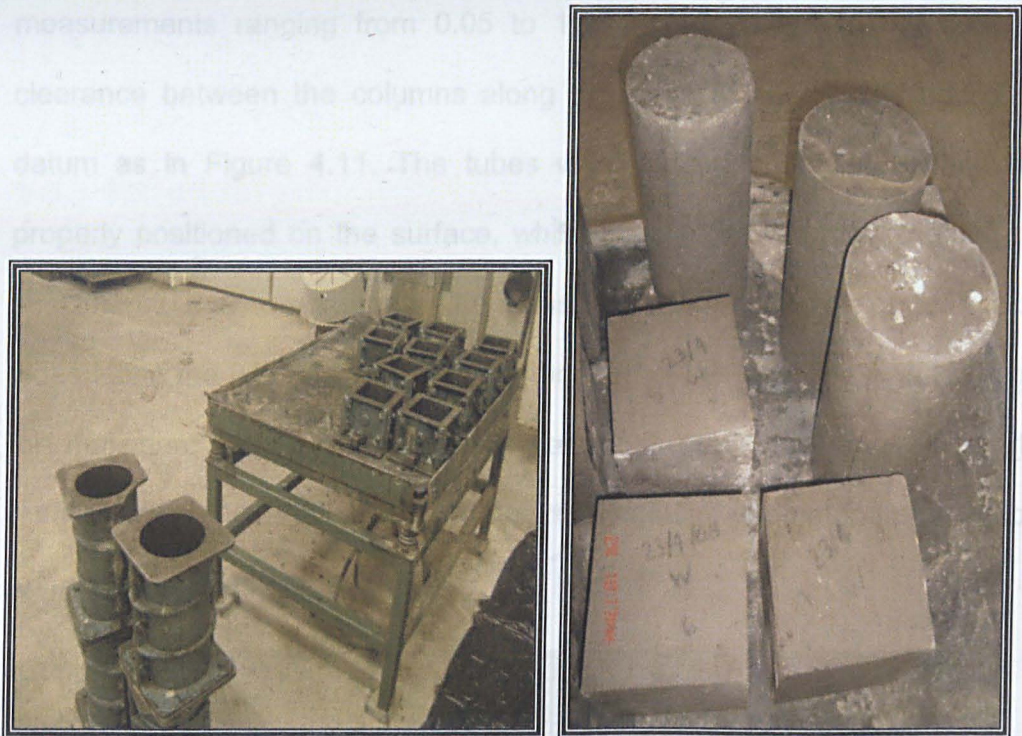


Figure 4.9: Coupon tests

4.4.2 Concrete infill

For each batch, concrete cubes of 100 mm and standard 150 x 300 mm cylinders were cast and cured under the same conditions as those of the elliptical CFT columns. The cubes and cylinders were tested in compression in order to achieve an accurate representation of their strengths. The concrete cubes were tested on days 7, 14 and 28, and also on the same

days the CFT column was tested to gather the actual cubic compressive strength, f_{cu} whereas—the cylinders were tested on 28 days and on the day the specimens were tested in order to obtain the mean compressive strength of the cylinders, f_c .



(a)

(b)

Figure 4.10: Preparation for specimens of hardened concrete properties tests

4.5 Initial out-of-straightness

The initial tube imperfection of long columns was measured prior to concrete casting taking place. The geometric imperfections were measured for all long column specimens, as for short columns, this parameter was considered not to play an important role. The measurement of the imperfection owing to the behaviour of columns was obviously influenced by initial imperfections, particularly for thin-walled steel sections (Zhang et al.,

2007) and long columns. Furthermore, the overall buckling and strength of the columns were also generally affected by the imperfection.

The reading of the imperfections was obtained using a feeler gauges from one end to another end of the steel tubes. A feeler gauge with measurements ranging from 0.05 to 1.3 mm was used to measure the clearance between the columns along the minor or weak axis and a flat datum as in Figure 4.11. The tubes were placed on a flat surface and properly positioned on the surface, whilst the gauge was moved along the specimen to measure the gap. The measurements were made on both wider sides along the tubes length. The primary aim of this exercise was to record the maximum amplitudes of imperfections inherent in the tubes. From the measurement it was found that the maximum initial geometric imperfection, ω_0 ranges from 0.03 to 1.2 mm.

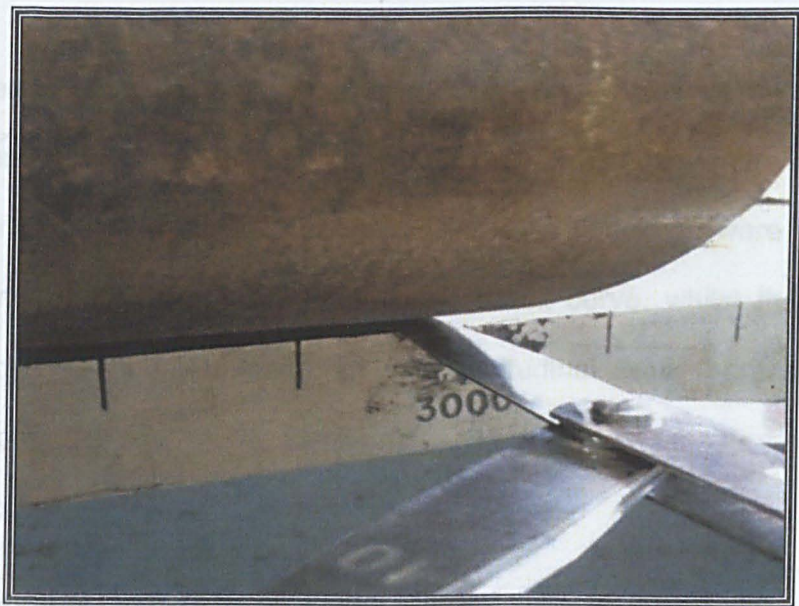


Figure 4.11: Imperfection measurement using feeler gauges

Chapter 5

Experimental Results

5.1 Introduction

A comprehensive testing programme on elliptical columns, manufactured by Corus, was conducted at Leeds University. A total of twenty-seven column specimens were prepared from two different tube sizes with the major-to-minor outer dimensions of 2:1, and were accordingly categorised into four series. Both short and long columns were considered and tested to failure with the aim of assessing their behaviour. In this study, a long column is defined as a member whose length is considerably larger than any of its cross-sectional dimensions. From each test, the behaviour of the axial load-displacement and axial load-strain were recorded. The maximum load, point of yielding and post-buckling behaviour for each specimen were measured and identified from the axial load-displacement curve, whilst the onset of local buckling was determined from load-longitudinal strain characteristics. In this chapter, the test results were analysed and typical structure responses are described.

5.2 Material Properties

5.2.1 Concrete Properties

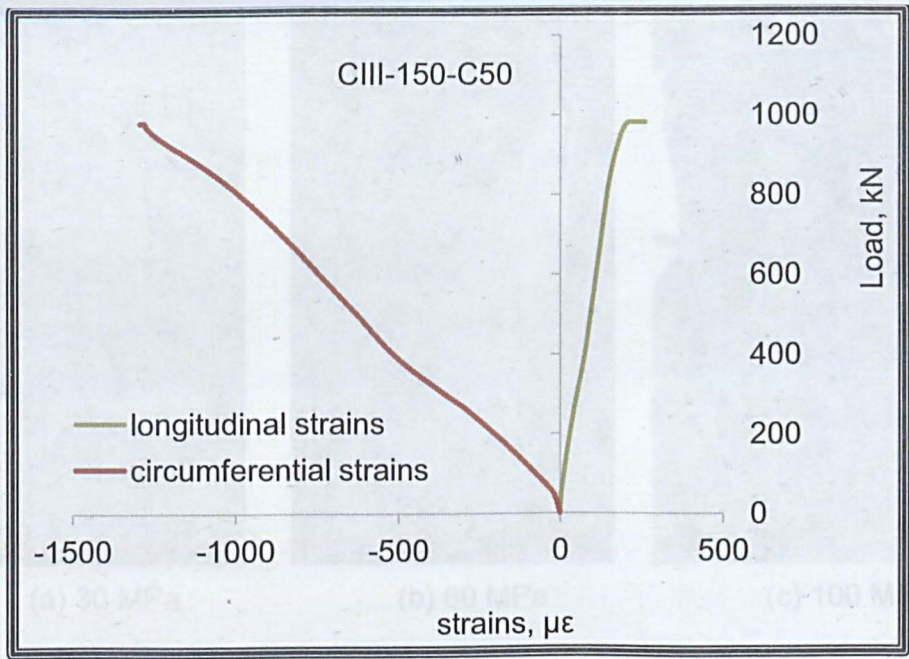
In addition to the overall column tests, a set of materials tests were conducted on the elements used to construct the column specimens. As explained in 3.8.2, the tests of the hardened properties of SCC were carried

out using the same method as normal concrete. The tests were conducted at various stages to ascertain the compressive strength of the concrete. The compressive cube strength, f_{cu} , compressive cylinder strength, f_{ck} and the modulus of elasticity, E_o are tabulated as shown in Table 5.1.

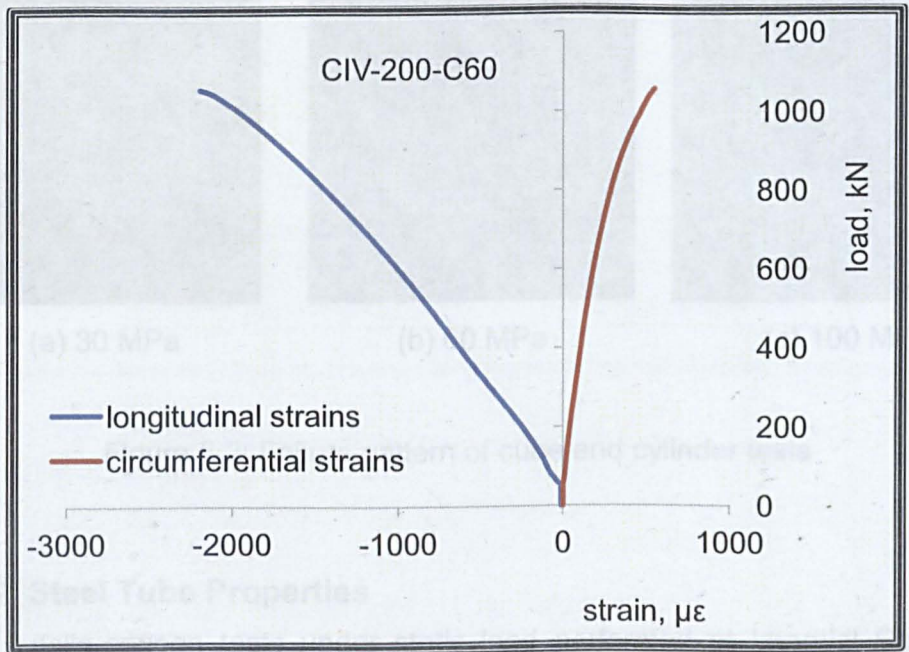
From the cylinder compression tests, the stress-strain curves of the concrete cylinders which represent the behaviour of plain concrete under uni-axial loading were plotted and the modulus of elasticity, E_o , and the strain at peak stress, ϵ_o were determined. From the tests, it was observed that the peak stress for all concrete cylinders vary from 1800 $\mu\epsilon$ -2500 $\mu\epsilon$ and higher modulus of elasticity was observed for HSC. Figure 5.1 shows typical load-strain relationship results of the compression tests. From the observation on compression results, there appeared to be differences in the crushing pattern between lower and higher concrete strengths. The nature of the failure of high strength concrete can be observed in the tests as illustrated in Figure 5.2, where mass crushing and spalling of the concrete occurred.

Table 5.1: Material properties

	Label	f_{cu} N/mm ²	f_{ck} N/mm ²	f_y N/mm ²	f_u MPa	ϵ_y $\mu\epsilon$	E_o N/mm ²	E_a N/mm ²
S-I	CI-150h	-	-				-	
	CI-150-C47	47.1	37.4				34552.9	
	CI-150-C62	62.1	45.2	424.35	517.2	2000	33084.4	201000
	CI-150-C106	105.9	90				41527.8	
S-II	CI-200h	-	-				-	
	CI-200-C34	34.2	23.2				31435.7	
	CI-200-C67	66.5	41.6	361.7	472.9	2000	33084.4	209000
	CI-200-C116	115.8	72.3				41527.8	
S-III	CII-150-C26	26	19.8				31649.4	
	CII-150-C58	58	43				34218.3	201000
	CII-150-C64	64.1	52.2	424.35	517.2	2000	35039.9	
	CII-150-C91	90.8	77.5				39889.3	
	CII-200-C29	29	23				31718.8	
	CII-200-C55	55	41.8	361.7	472.9	2000	34149.2	209000
S-III	CII-200-C93	92.9	71.1				38698.2	
	CIII-150-C20	20	15				32122.4	
	CIII-150-C65	64.5	50	424.35	517.2	2000	36249.8	201000
	CIII-150-C100	99.9	72.3				36390.0	
	CIII-200-C42	42	29.4				33688.5	
	CIII-200-C63	63	40.6	361.7	472.9	2000	37000.5	209000
S-IV	CIII-200-C98	97.7	76.4				43699.7	
	CIV-150-C23	23	18.4				25422.0	
	CIV -150-C63	62.9	53.5	424.35	517.2	2000	34480.2	201000
	CIV -150-C100	99.9	72.3				44026.7	
	CIV-200-C29	29	21.6				27018.3	
	CIV -200-C59	58.6	49.8	361.7	472.9	2000	35900.5	209000
	CIV -200-C101	101.1	73.8				45686.1	



(a)



(b)

Figure 5.1: Stress-strain relation of concrete cylinders

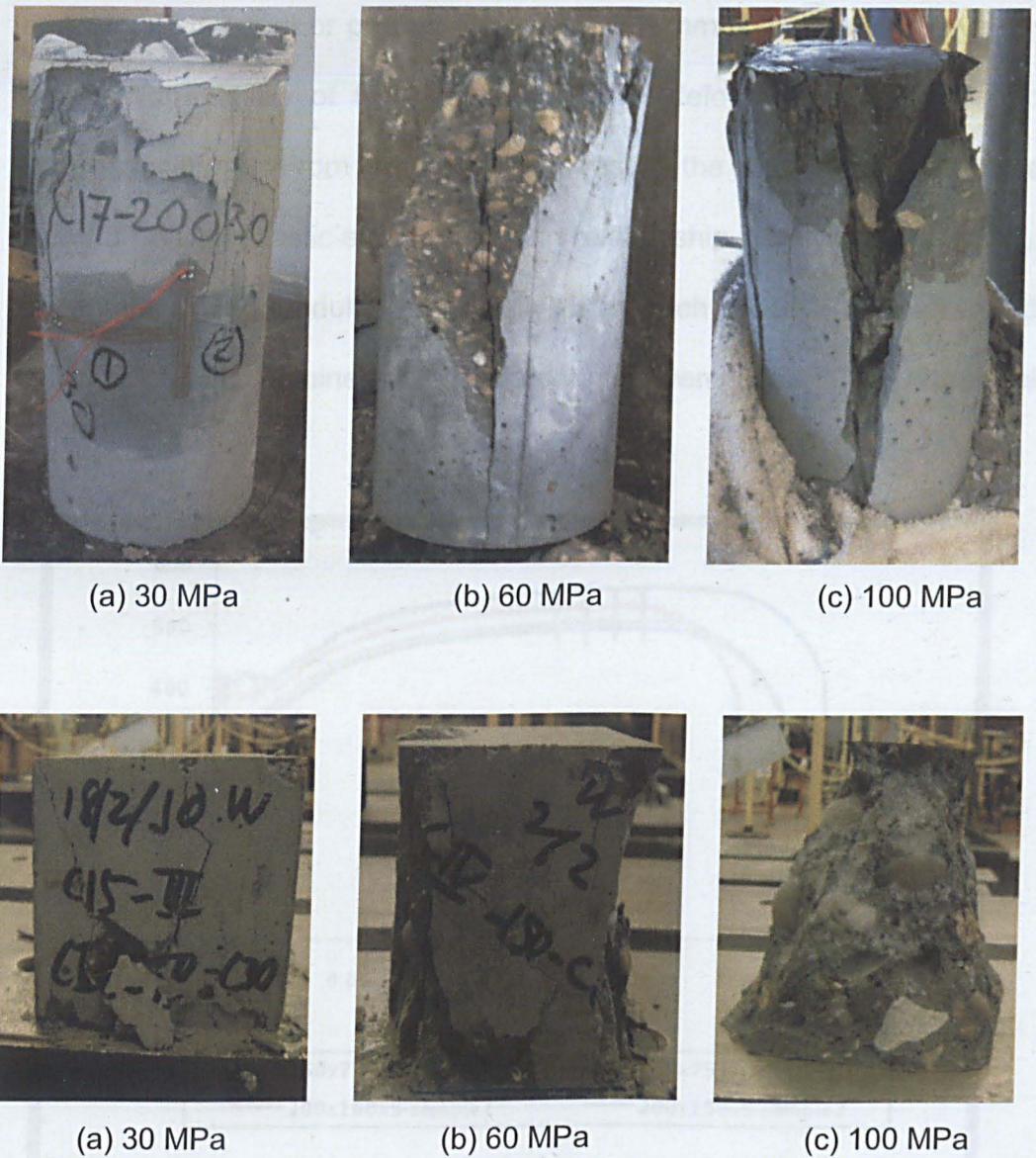


Figure 5.2: Failure pattern of cube and cylinder tests

5.2.2 Steel Tube Properties

The tensile-coupon tests under static load performed at Imperial College were conducted according to BS EN 10002-1:1990 with the aim of establishing the mechanical behaviour of the steel element. From the tensile tests, Young's modulus and yield strength were determined based on the engineering stress versus engineering strain curves. As depicted in Figure 5.3, there is a linear stress-strain relationship at the beginning with elastic

modulus, E_a is equal or greater than 201000 N/mm^2 . The measured values represent the ability of the material to resist deformation, which is also known as stiffness. From the tensile tests results the stress-strain steel tube shows an elastic-plastic-strain hardening relationship. The yield strength, f_y , yield strain, ϵ_y and modulus of elasticity, E for each specimen are tabulated in Table 5.1. The obtained material properties were used in the numerical simulations.

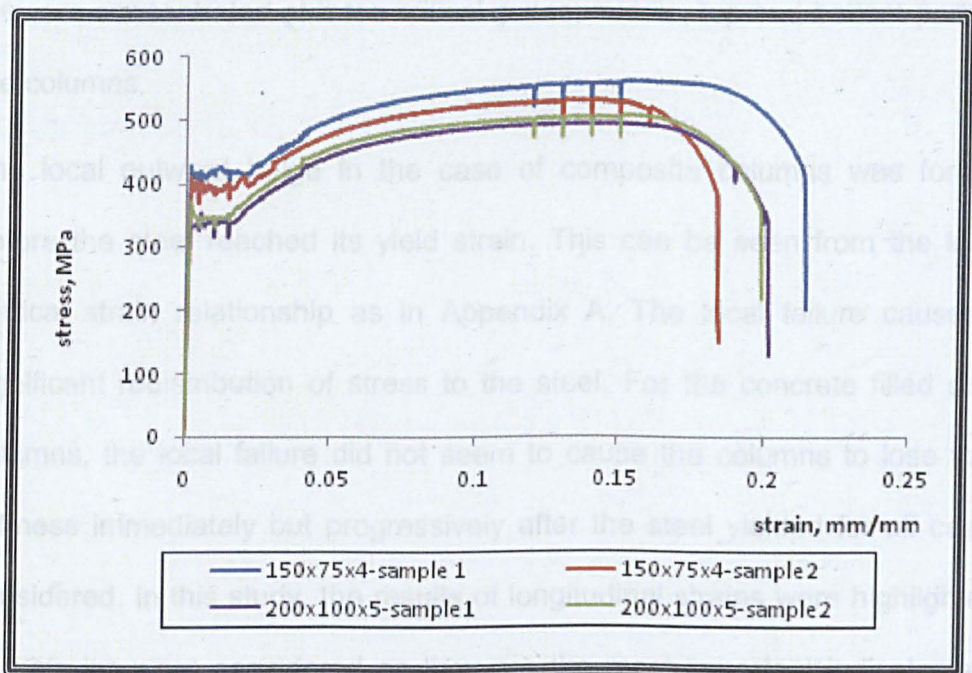


Figure 5.3: Coupon tests results

5.3 Experimental Results of Stub Tests

5.3.1 Observation on the Short Columns Tests

The ultimate strength of composite columns has been the subject of many investigations. Essentially, it can be defined as the highest load at which the column stiffness becomes zero. In this study, the ultimate load of the columns was taken as the maximum load achieved during the tests.

The maximum capacities of all composite short columns were observed to achieve after the local buckling and steel yielding occurred. For instance, steel tubes had yielded when the load reached 851 kN for specimen CI-150-C30 and 1132 kN for CI-200-C30 that have maximum capacity of 900 kN and 1232 kN respectively. This indicates that most of the columns are able to sustain further loading even after the steel has yielded as the result of strain hardening. The locations of the yielding vary among all columns and they are concentrated at three critical zones; middle, top and bottom parts of the columns.

The local outward bulge in the case of composite columns was formed before the steel reached its yield strain. This can be seen from the load-vertical strain relationship as in Appendix A. The local failure causes a significant redistribution of stress to the steel. For the concrete filled steel columns, the local failure did not seem to cause the columns to lose their stiffness immediately but progressively after the steel yielded for all cases considered. In this study, the results of longitudinal strains were highlighted. The strains were considered as they are the most important indicator and are critical for the specimens with axial compression loading. Observation from the experiment shows that the steel tube of all columns yielded first in the longitudinal or axial direction.

From the load versus vertical strain curves for specimen CI-150-C30, the occurrence of local buckling could not be observed due to the uneven distribution of the strains. Thus, no firm conclusion of the failure could be made as the strains results might not give accurate strain values. The occurrence of local buckling failure observed in all CFT columns was also

thought to be due to the force of the locally crushed concrete on the steel wall. The bulge started to grow with the load and resulted in the increase of the lateral movement because the steel tube was pushed out by the compressive concrete core. In the case of hollow columns, it was observed that the local failure occurred before the maximum load for both specimen of CI-150-h and CI-200-h. Table 5.3 summarises the experimental results for all columns. From the table, stub columns results show that the axial displacement getting lower as the concrete infill increases.

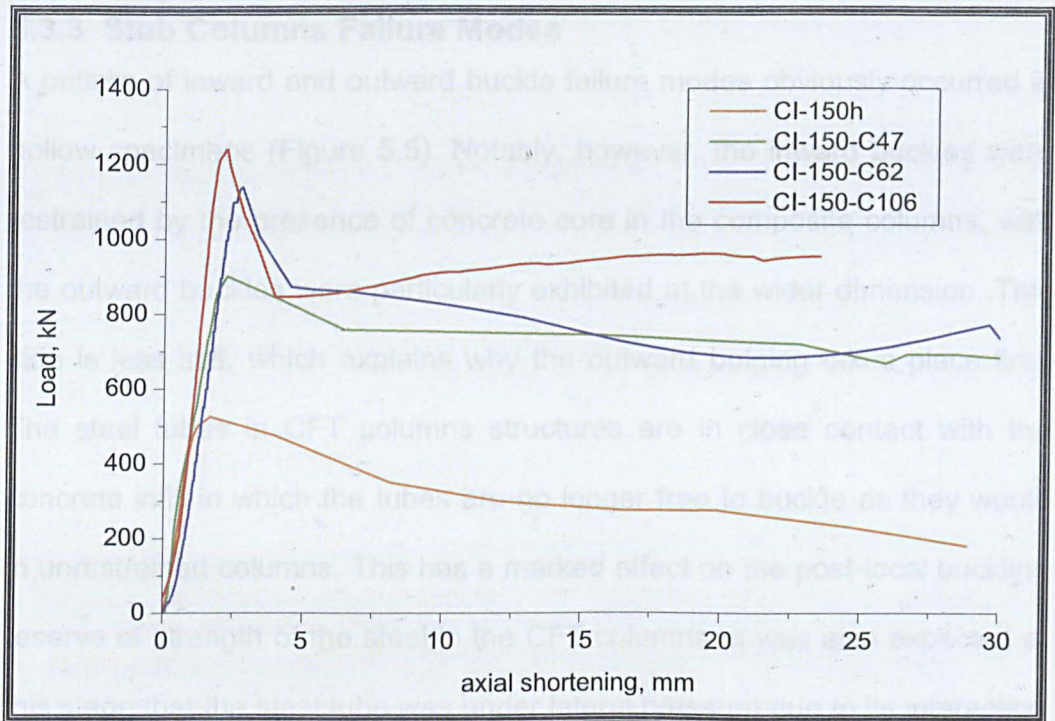
Table 5.2: Summary of experimental results of stub and long columns

	Label	P_u (kN)	Lateral displacement δ_u (mm)	Axial displacement Δ_u (mm)
Series I	CI-150h	525	-	4.2
	CI-150-C47	900	-	2.2
	CI-150-C62	1139	-	2.8
	CI-150-C106	1239	-	2.2
	CI-200h	810.7	-	4.7
	CI-200-C34	1232	-	3.02
	CI-200-C67	1737	-	2.55
	CI-200-C116	2116	-	1.80
Series II	CII-150-C26	520.6	10.0	7.2
	CII-150-C58	742.8	6.8	8.8
	CII-150-C64	828.8	8.0	7.7
	CII-150-C91	923.2	6.66	8.67
	CII-200-C29	938.4	4.12	8.8
	CII-200-C55	1064	6.9	9.85
	CII-200-C93	1480	6.3	11.47
Series III	CIII-150C20	483.8	4.07	6.44
	CIII-150C65	663.2	5.95	8.23
	CIII-150C100	871.2	3.11	8.45
	CIII-200-C42	967.5	3.36	11.53
	CIII-200-C63	1237	2.49	10.41
	CIII-200-C98	1411	6.45	13.77
Series IV	CIV-150-C23	326.6	20.4	8.1
	CIV-150-C63	427	16.4	7.7
	CIV-150-C100	547.4	10.7	10.1
	CIV-200-C29	839	12.32	7.97
	CIV-200-C59	947	13.41	15.75
	CIV-200-C101	1072	6.03	16.71

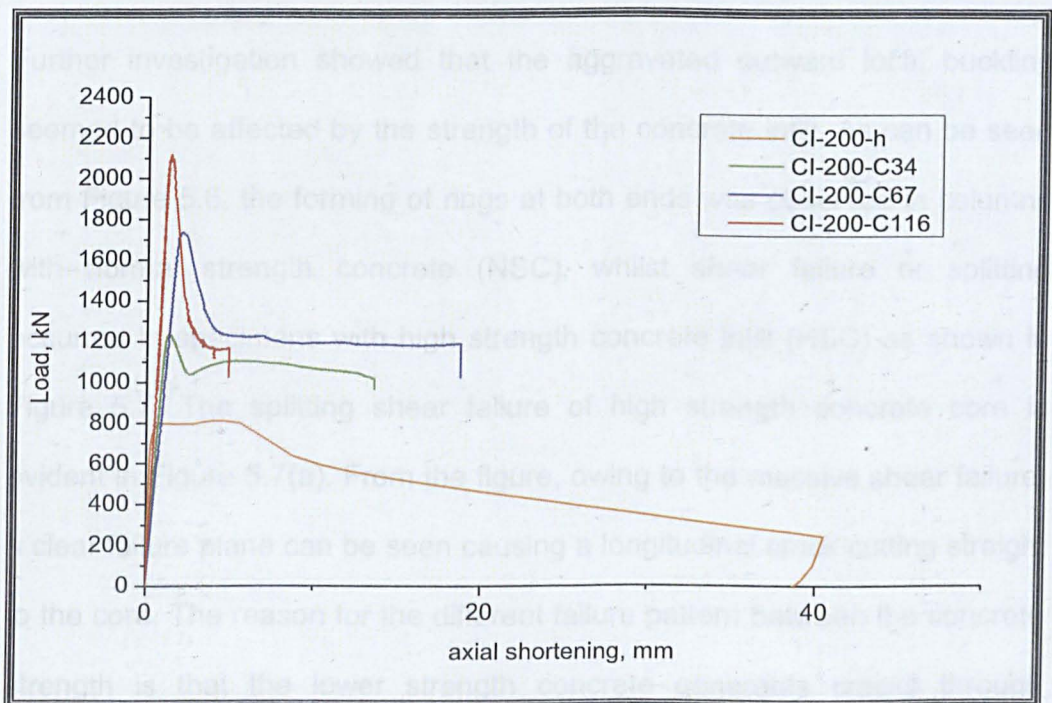
5.3.2 Axial Load-Shortening Relationship of Short Columns

In this series of experiments, four LVDTs were used to measure the shortening of the columns tested. The axial load-shortening diagrams provide useful information in identifying the point of yielding, the ultimate load and the post-peak behaviour of the columns.

The relationship of the load and vertical displacement of the 150 x 75 x 4 mm and 200 x 100 x 5 mm short columns are represented in Figures 5.4(a) and 5.4(b) with the vertical displacement taking an the average values measured from the LVDTs. As illustrated in the figures, the load-shortening relationships are seen to be fairly linear prior to reaching the peak load. These columns generally behave in a stiff manner when axial shortening is small at the beginning of the loading, and subsequently increases as the columns approaching the ultimate load. Generally the columns with concrete infill displayed a superior performance compared to hollow sections in sectional strength, however this does not happen in terms of initial stiffness as can be seen from Figure 5.4. By comparing the strength of the infill, the stiffness of the specimens with lower concrete strength decreases much more gradually than that of other columns. It also can be observed from the figures, that the stub CFT specimens show a drop in the curves after the maximum load was achieved. The slope of the curve drops slowly after the peak for columns with lower concrete infill strength. On the other hand the post-peak curves in specimens with HSC infill are steeper which suggest that the load drops suddenly as a result of the characteristics of the concrete infill. Nevertheless it can be seen that the gain in strength considerably more when using concrete of a higher compressive strength.



(a) 150 x 75 x 4 mm



(b) 200 x 100 x 5 mm

Figure 5.4: Load-axial shortening relationship of stub columns

5.3.3 Stub Columns Failure Modes

A pattern of inward and outward buckle failure modes obviously occurred in hollow specimens (Figure 5.5). Notably, however, the inward buckles were restrained by the presence of concrete core in the composite columns, with the outward buckles were particularly exhibited at the wider dimension. This side is less stiff, which explains why the outward bulging takes place first. The steel tubes in CFT columns structures are in close contact with the concrete infill in which the tubes are no longer free to buckle as they would in unrestrained columns. This has a marked effect on the post-local buckling reserve of strength of the steel in the CFT columns. It was also expected at this stage that the steel tube was under lateral pressure due to its interaction with axially loaded concrete core, which consequently lead to local buckling of the steel tube.

Further investigation showed that the aggravated outward local buckling seemed to be affected by the strength of the concrete infill. As can be seen from Figure 5.6, the forming of rings at both ends was observed in columns with normal strength concrete (NSC), whilst shear failure or splitting occurred in specimens with high strength concrete infill (HSC) as shown in Figure 5.7. The splitting shear failure of high strength concrete core is evident in Figure 5.7(a). From the figure, owing to the massive shear failure, a clear failure plane can be seen causing a longitudinal crack cutting straight to the core. The reason for the different failure pattern between the concrete strength is that the lower strength concrete generates cracks through splitting, while the higher strength concrete generates cracks by sliding. In the case of specimens with higher concrete infill strength, during the experiment these columns did not show obvious deformation even after the

loading had started to decrease. As indicated by the strain gauges results, these steel tubes experienced local failure just before they reached ultimate strength. However, the sign of local failure was only visible some time after the columns lost their capacity. This phenomenon may also resulted by the occurrence of splitting crack. Furthermore the characteristics of the SCC may influence the failure mode and further explanation will be made in Chapter 7.

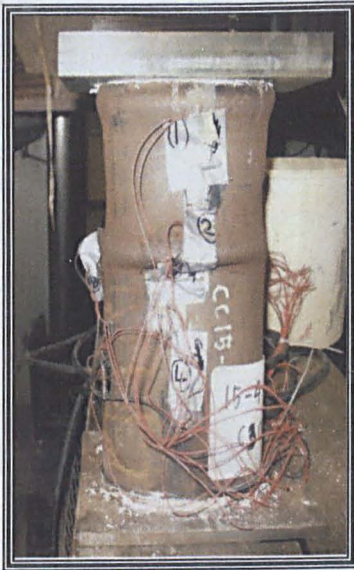


(a) C1-150h



(b) C1-200h

Figure 5.5: Typical failure modes of elliptical hollow column



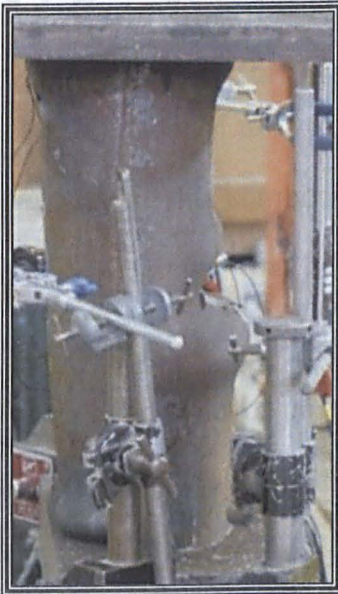
(a) CI-150-C30



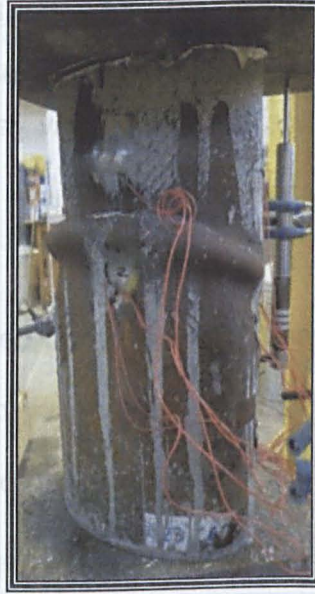
(b) CI-150-C60



(c) CI-150-C100



(d) CI-200-C30



(e) CI-200-C60



(c) CI-200-C100

Figure 5.6: Typical failure modes of elliptical stub composite columns

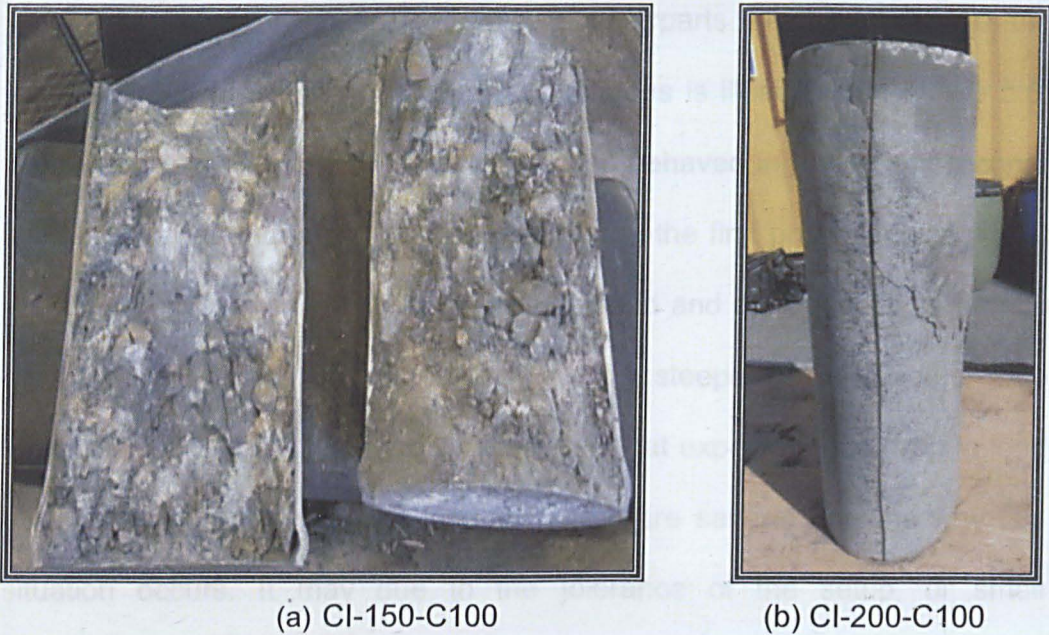


Figure 5.7: Concrete failure of C100 concrete strength in stub CFT columns

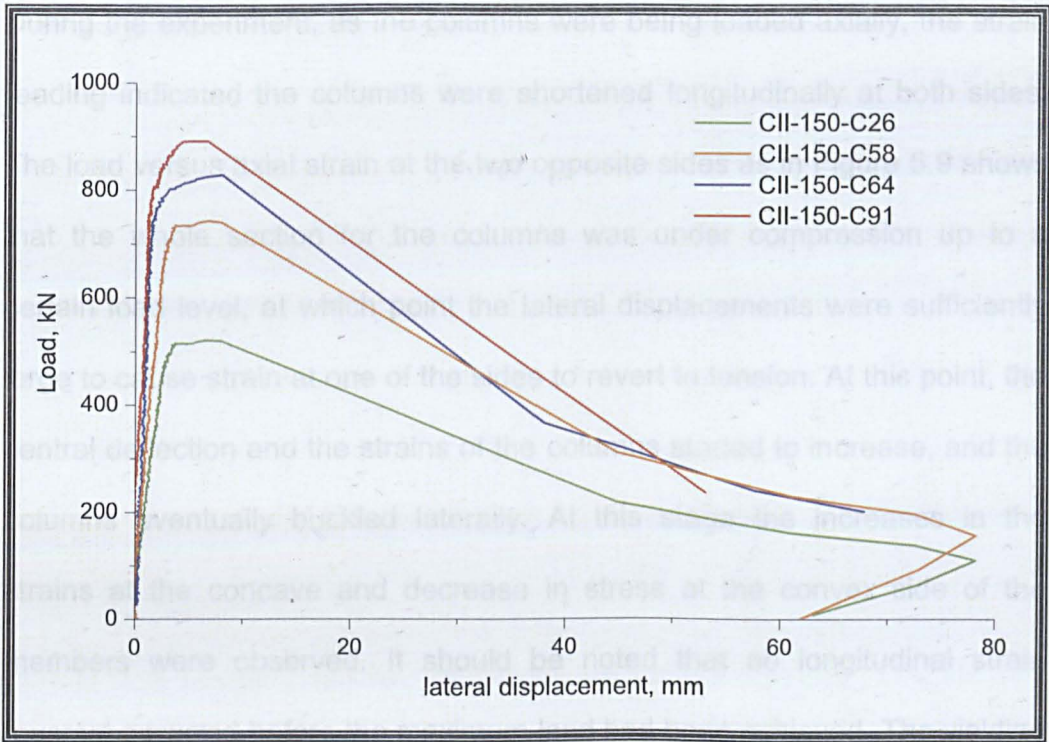
5.4 Experimental Results of Long Column Tests

5.4.1 Observation on Series II columns

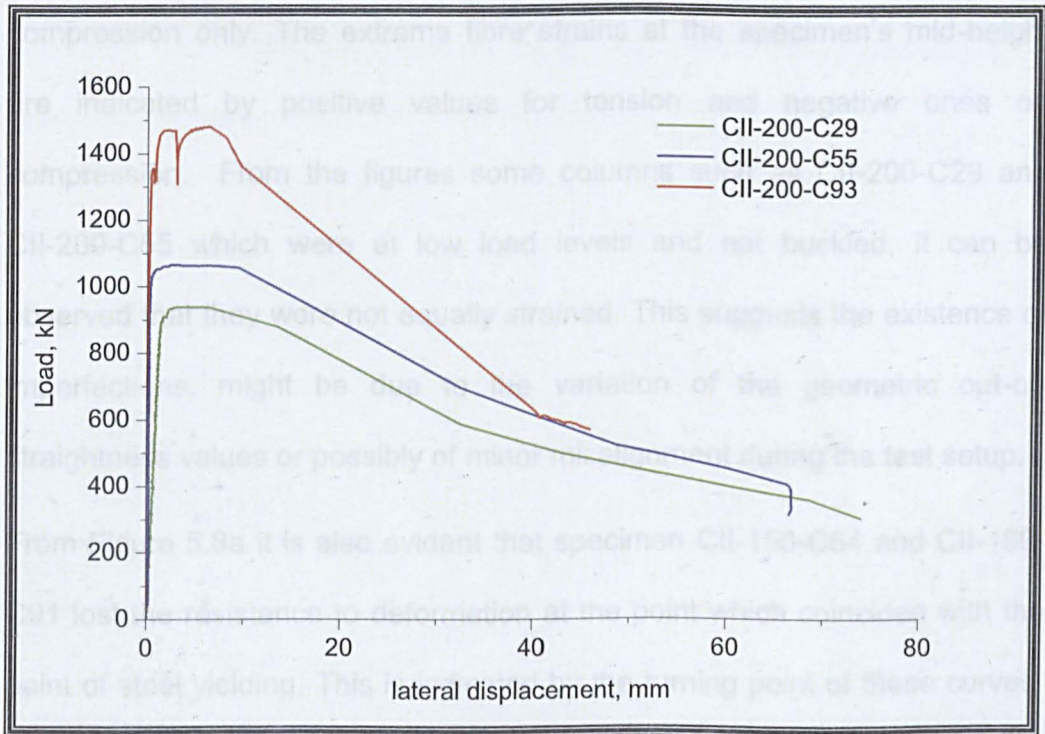
The definition of failure may vary, but in this study as far as the maximum capacity of the composite members were concerned, it was taken as the stage at which the load carrying capacity of the structures begins to decrease. As been observed from the experimental data, Series II columns failed by plastic column buckling. It was indicated by the occurrence of lateral deflection when the columns reached their ultimate strengths.

There was significant difference in bearing capacities from section dimensions point of view. The ultimate loads achieved by the columns with smaller tube size were in the range of 520.6 kN to 923.2 kN and the ultimate loads increased as the columns' size increased. In the case of columns with bigger tube size such as specimens CII-200-C29, CII-200-C55 and CII-200-C93, the columns were able to achieve higher loading at 938.4 kN, 1064 and

1480 kN respectively compared to their counterparts. The relationship of the load-lateral displacements for Series II columns is illustrated in Figure 5.8. Similar to stub columns, these columns also behaved in a very stiff manner with small axial and lateral deformation during the first phase of loading. At the maximum load, the displacement increased and the descending branch of the load-deformation curve was getting steeper. From Figure 5.8b specimen CII-200-C93 is the only specimen that experiences a drop in load bearing at the early stage of loading. There are several reasons why this situation occurs. It may be due to the tolerance of the setup, or small gap that exist between members or due to the local defect existed at the particular specimen.



(a)



(b)

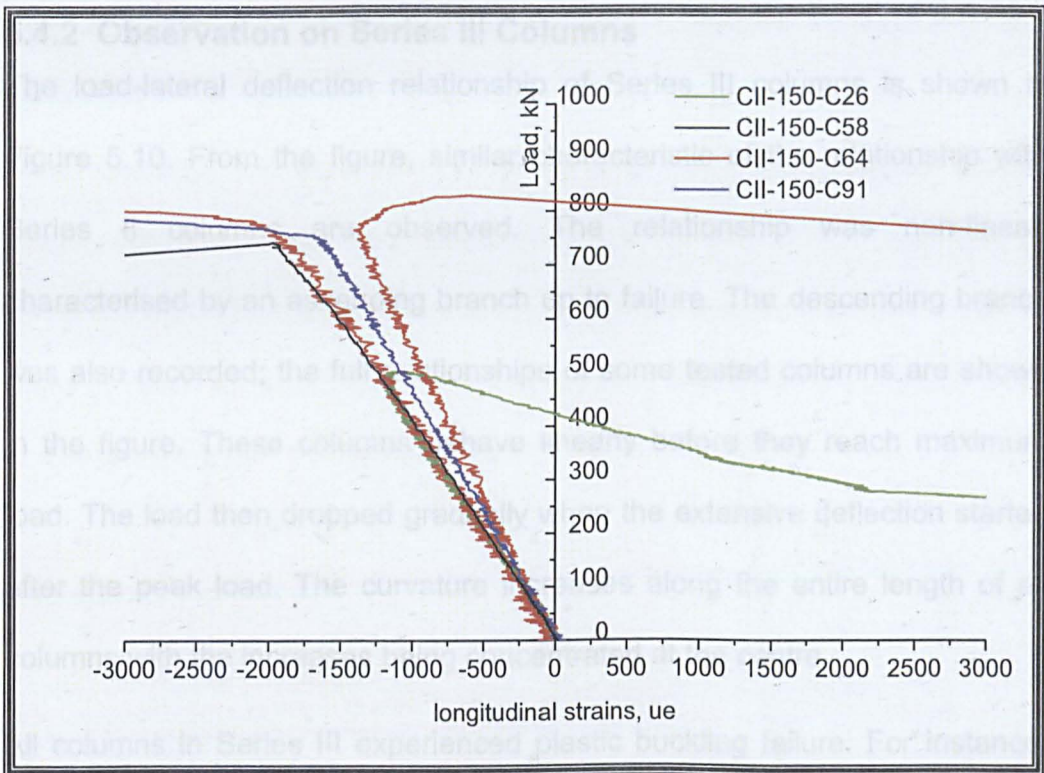
Figure 5.8: Load-lateral displacement series II

During the experiment, as the columns were being loaded axially, the strain reading indicated the columns were shortened longitudinally at both sides. The load versus axial strain at the two opposite sides as in Figure 5.9 shows that the whole section for the columns was under compression up to a certain load level, at which point the lateral displacements were sufficiently large to cause strain at one of the sides to revert to tension. At this point, the central deflection and the strains of the columns started to increase, and the columns eventually buckled laterally. At this stage the increases in the strains at the concave and decrease in stress at the convex side of the members were observed. It should be noted that no longitudinal strain reversal occurred before the maximum load had been achieved. The yielding also has been observed occurred at the central part of the members in compression only. The extreme fibre strains at the specimen's mid-height are indicated by positive values for tension and negative ones on compression. From the figures some columns such as CII-200-C29 and CII-200-C55 which were at low load levels and not buckled, it can be observed that they were not equally strained. This suggests the existence of imperfections, might be due to the variation of the geometric out-of-straightness values or possibly of minor misalignment during the test setup.

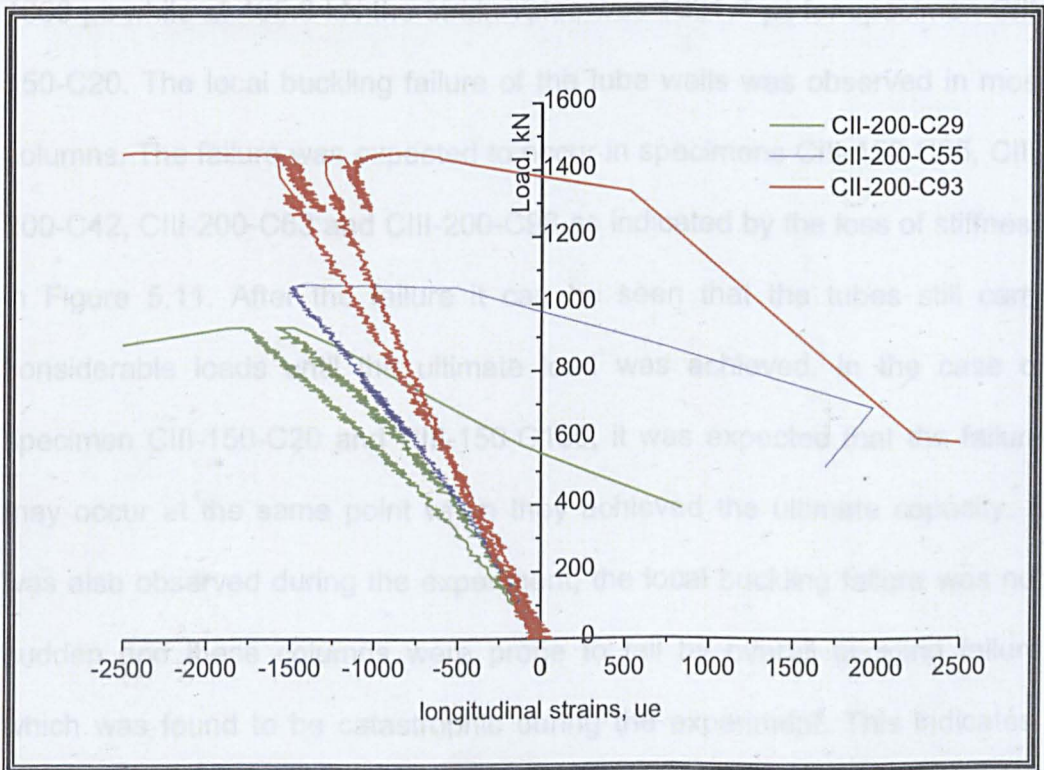
From Figure 5.8a it is also evident that specimen CII-150-C64 and CII-150-C91 lost the resistance to deformation at the point which coincided with the point of steel yielding. This is indicated by the turning point of these curves. From the figures, it is also clear that the steel yielded almost at the same point for both specimens. As the concrete strength infill for specimen SII-150-C91 was high thus, the column was able to achieved higher ultimate load.

In the case for columns with bigger tube size, these columns also achieved the maximum load at and after the steel had yielded with the local buckling expected to occur at the same point for specimens CII-200-C29 and CII-200-C93. However, it is quite difficult to observe from the Figure 5.9(b), at which point the maximum load actually achieved. From a careful observation on the strain data, the results demonstrate that for specimen CII-200-C29 the maximum load was achieved at $1803 \mu\epsilon$ whereas, specimen CII-200-C93 reached the load of 1478 kN at $2098.67 \mu\epsilon$ which was before it reached maximum load of 1480 kN.

The overall buckling failure dominated the columns failure. Despite this failure mode, the local buckling of the steel tube was observed in all specimens except for CII-200-C55 and occurred generally near the specimen mid-height. As mentioned the local failure was observed exist before the maximum load had been reached.



(a) 150 x 75 x 4mm



(b) 200 x 100 x 5mm

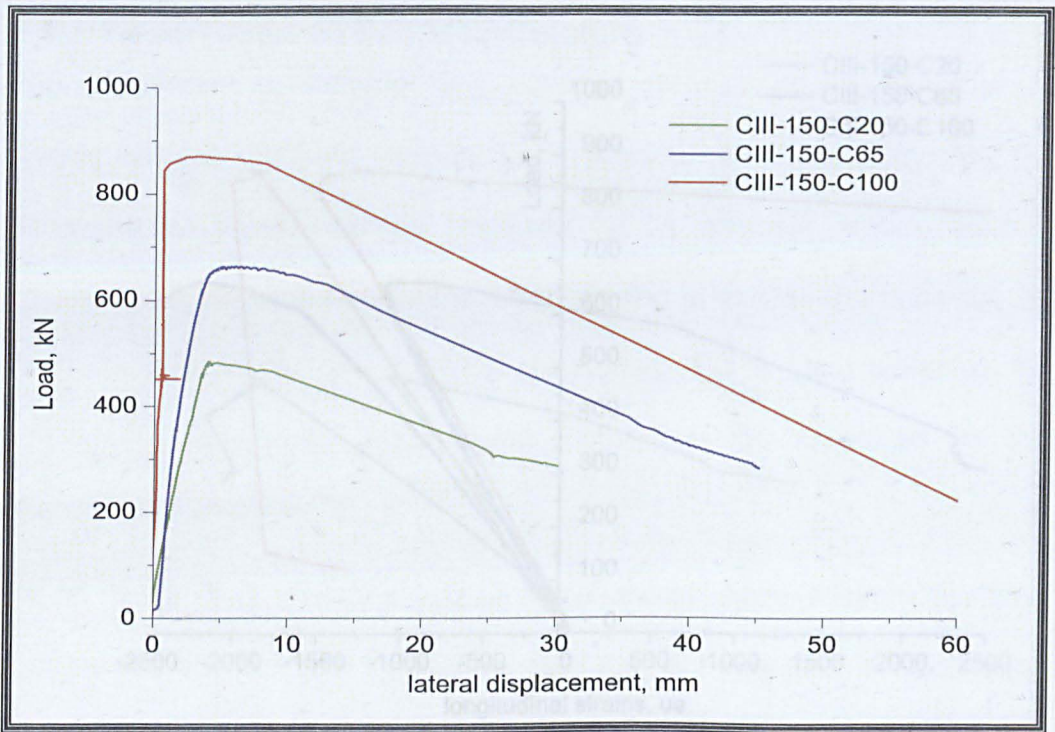
Figure 5.9: Load-mid-height vertical strain of series II

5.4.2 Observation on Series III Columns

The load-lateral deflection relationship of Series III columns is shown in Figure 5.10. From the figure, similar characteristic of the relationship with Series II columns are observed. The relationship was non-linear, characterised by an ascending branch up to failure. The descending branch was also recorded; the full relationships of some tested columns are shown in the figure. These columns behave linearly before they reach maximum load. The load then dropped gradually when the extensive deflection started after the peak load. The curvature increases along the entire length of all columns with the increases being concentrated at the centre.

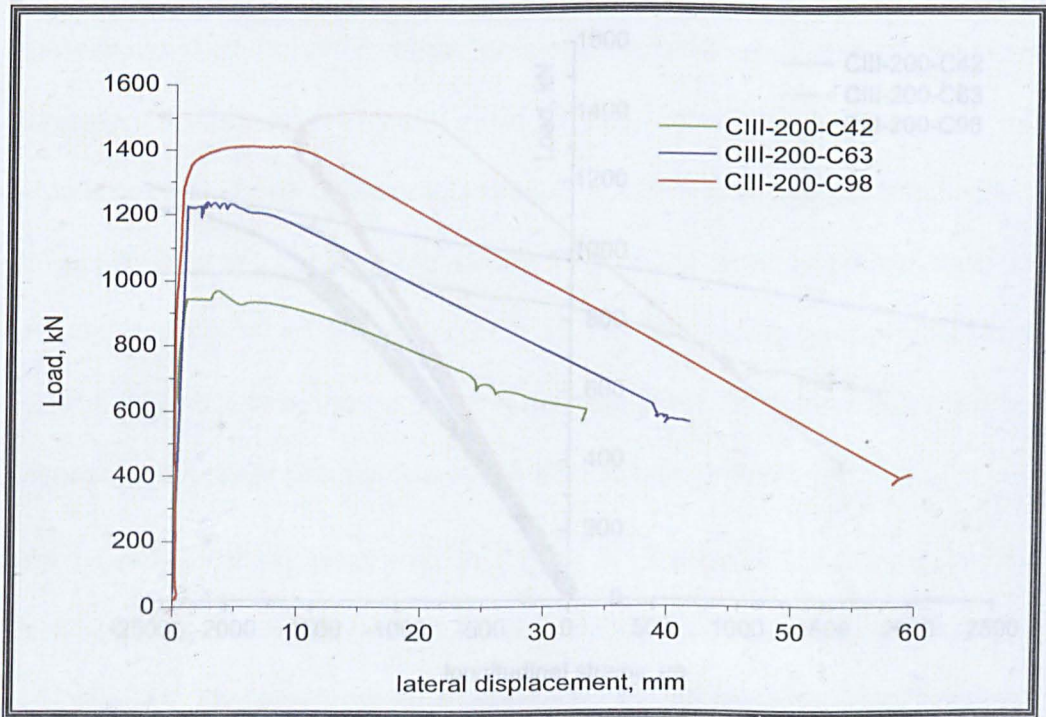
All columns in Series III experienced plastic buckling failure. For instance, specimen CIII-150-C100 reached a load of 840 kN when the strain was at $1800 \mu\epsilon$ while at 465.9 kN the strain value was $1801.7 \mu\epsilon$ for specimen CIII-150-C20. The local buckling failure of the tube walls was observed in most columns. The failure was expected to occur in specimens CIII-150-C65, CIII-200-C42, CIII-200-C63 and CIII-200-C98 as indicated by the loss of stiffness in Figure 5.11. After the failure it can be seen that the tubes still carry considerable loads until the ultimate load was achieved. In the case of specimen CIII-150-C20 and CIII-150-C100, it was expected that the failure may occur at the same point when they achieved the ultimate capacity. It was also observed during the experiment, the local buckling failure was not sudden and these columns were prone to fail by overall buckling failure which was found to be catastrophic during the experiment. This indicates, despite the observed local buckling, the failure of the columns is not due to the stresses in those locations, hence its influence is not critical.

The maximum axial displacement at failure increased considerably with increasing of the concrete infill strength, and consequently the columns were under bending. The deflections at failure of axially loaded columns at mid-length were very small and varied from 3.36 to 6.45 mm. It also can be observed that it had been difference between stiffnesses from both columns sizes in which lower influence in initial stiffness as indicated in Figure 5.10b is due to their larger size in diameter.



(a)

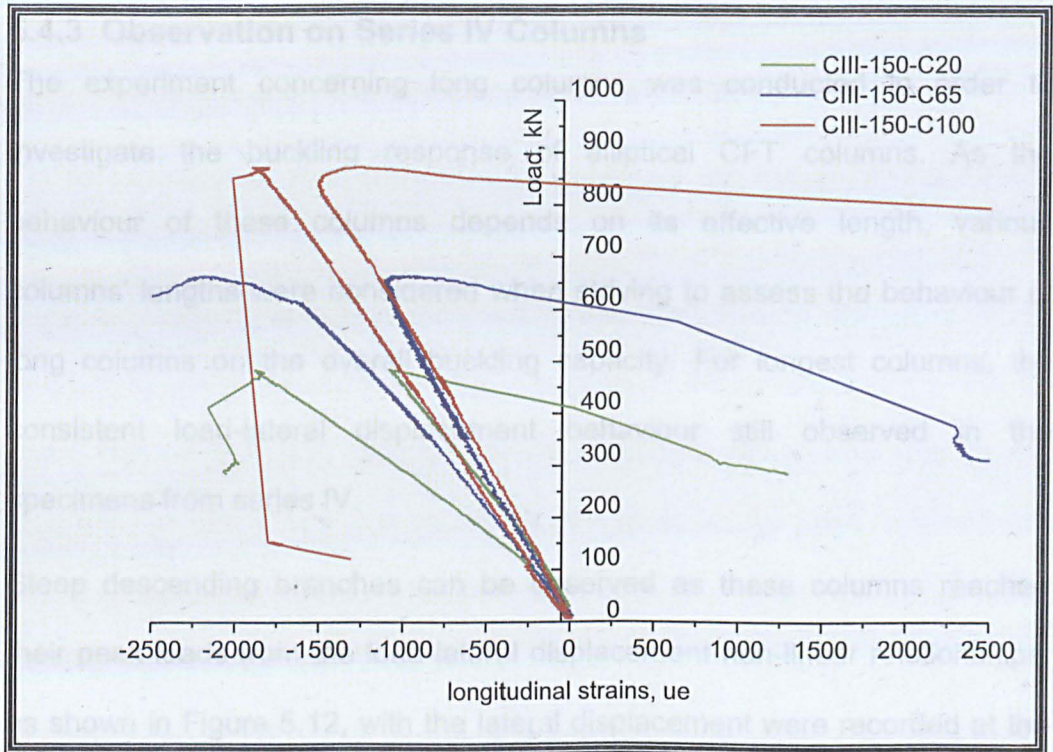
(a) 150 x 75 x 4mm



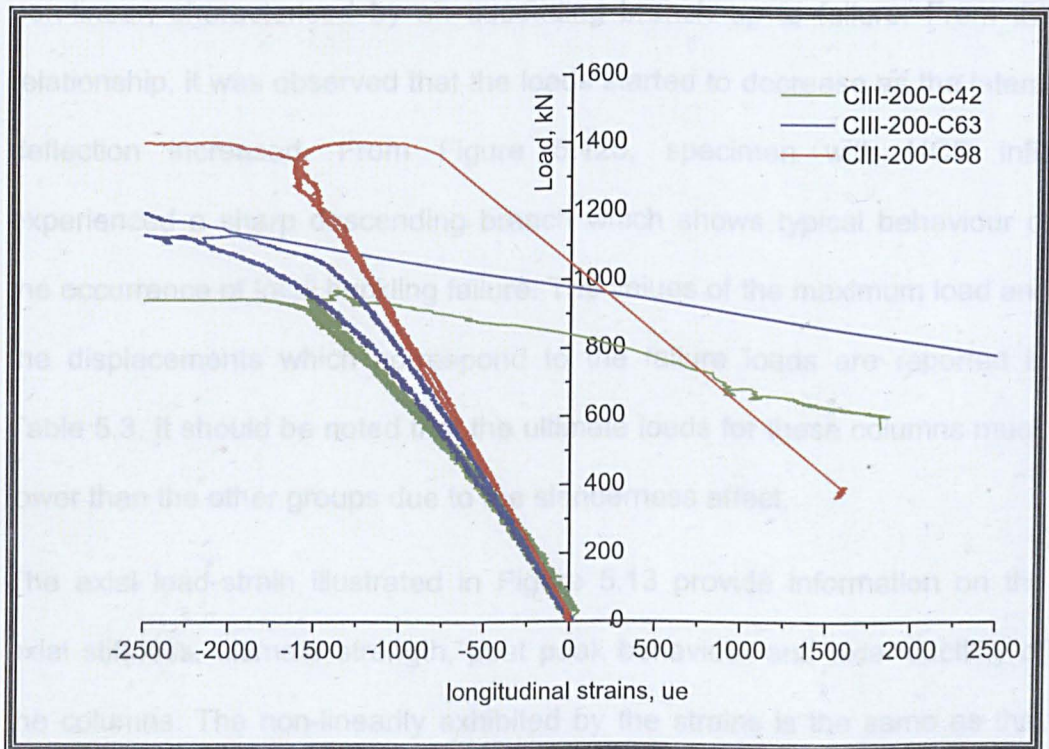
(b)

(b) 200 x 100 x 5mm

Figure 5.10: Load-horizonal displacement series III



(a) 150 x 75 x 4mm



(b) 200 x 100 x 5mm

Figure 5.11: Vertical strains characteristics at mid-height of series III

5.4.3 Observation on Series IV Columns

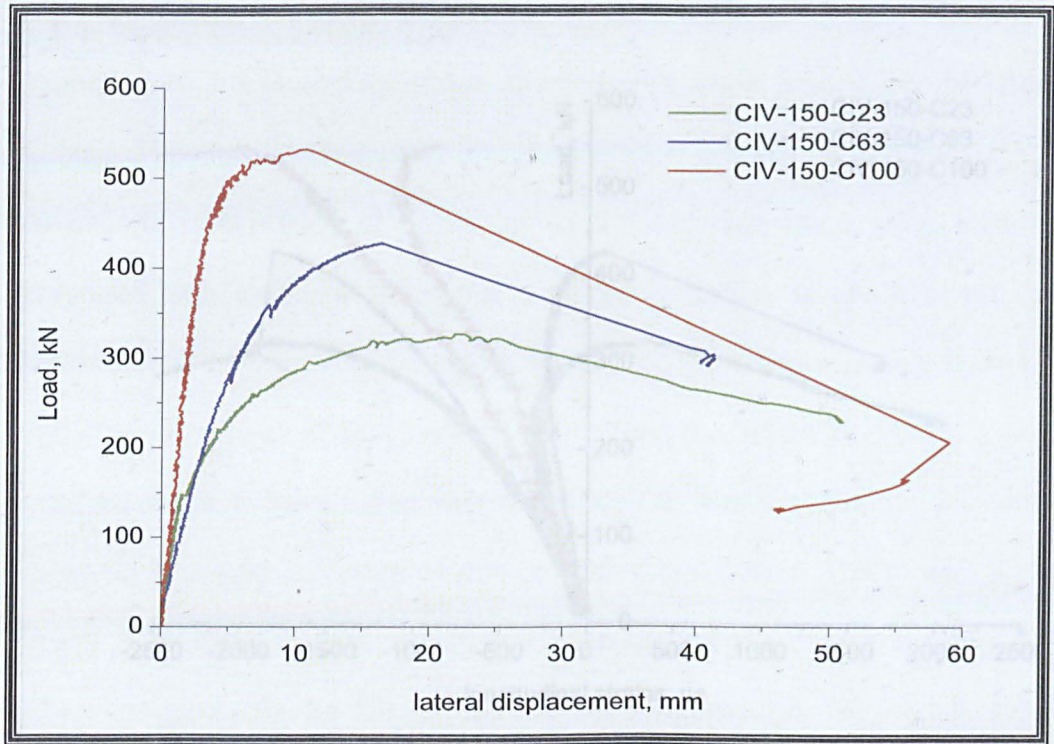
The experiment concerning long columns was conducted in order to investigate the buckling response of elliptical CFT columns. As the behaviour of these columns depends on its effective length, various columns' lengths were considered when striving to assess the behaviour of long columns on the overall buckling capacity. For longest columns, the consistent load-lateral displacement behaviour still observed in the specimens from series IV.

Steep descending branches can be observed as these columns reached their peak loads from the load-lateral displacement non-linear relationships, as shown in Figure 5.12, with the lateral displacement were recorded at the middle of the columns length. The relationship of load-lateral deflection was non-linear, characterised by an ascending branch up to failure. From the relationship, it was observed that the loads started to decrease as the lateral deflection increased. From Figure 5.12b, specimen with HCS infill experienced a sharp descending branch which shows typical behaviour of the occurrence of local buckling failure. The values of the maximum load and the displacements which correspond to the failure loads are reported in Table 5.3. It should be noted that the ultimate loads for these columns much lower than the other groups due to the slenderness effect.

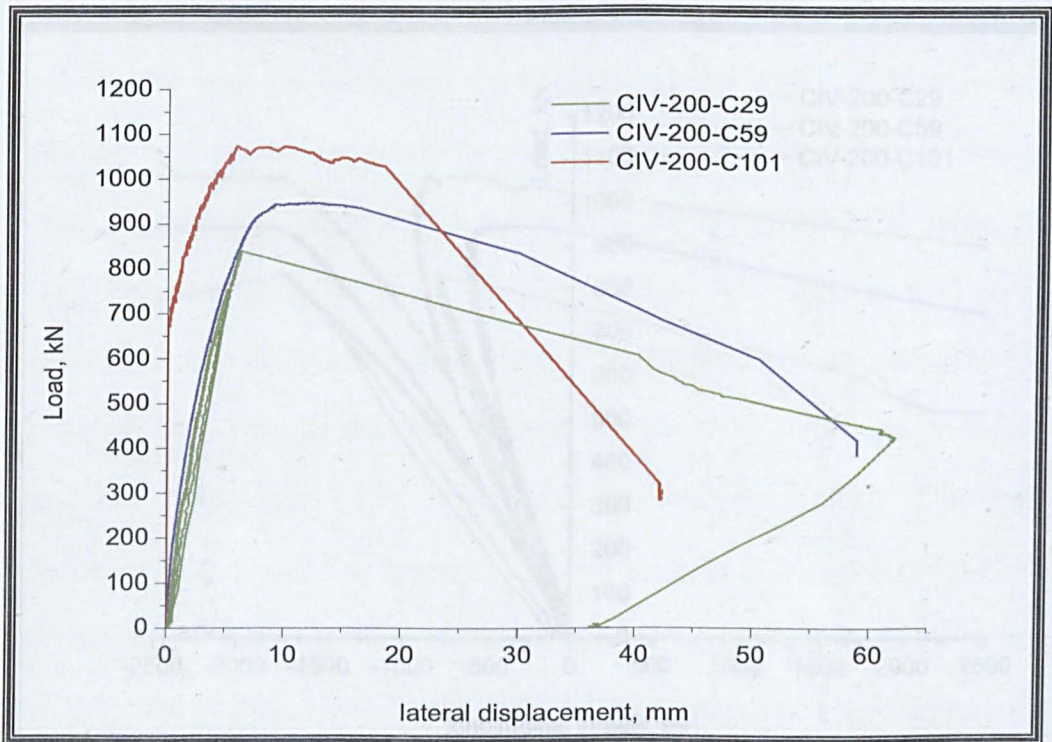
The axial load-strain illustrated in Figure 5.13 provide information on the axial stiffness, ultimate strength, post peak behaviour and axial ductility of the columns. The non-linearity exhibited by the strains is the same as that exhibited by other specimens from the other groups. All columns in this series failed by buckling at plastic stage with some of the columns are showing signs of local buckling. In all the column tests, and as can be seen

from the figure, the recorded strains in the steel section reached their yield strain values at loads which are close to the failure loads.

For instance specimens CIV-200-C101 reached the maximum capacity of 1072 kN after the steel tube yielded at around the load of 1062 kN. As expected, yielding was first recorded in the compression side at columns' mid-height where bending was most significant. From this figure it can be seen that all the long columns failed elastic-plastically and due to the slenderness effect with the values of plastic strain in these columns are small. These columns also failed in a rapid manner with an increasing rate of deflection. During the post-peak stage, the deflection curves were approximately in the shape of half-sine wave as illustrated in Appendix B.

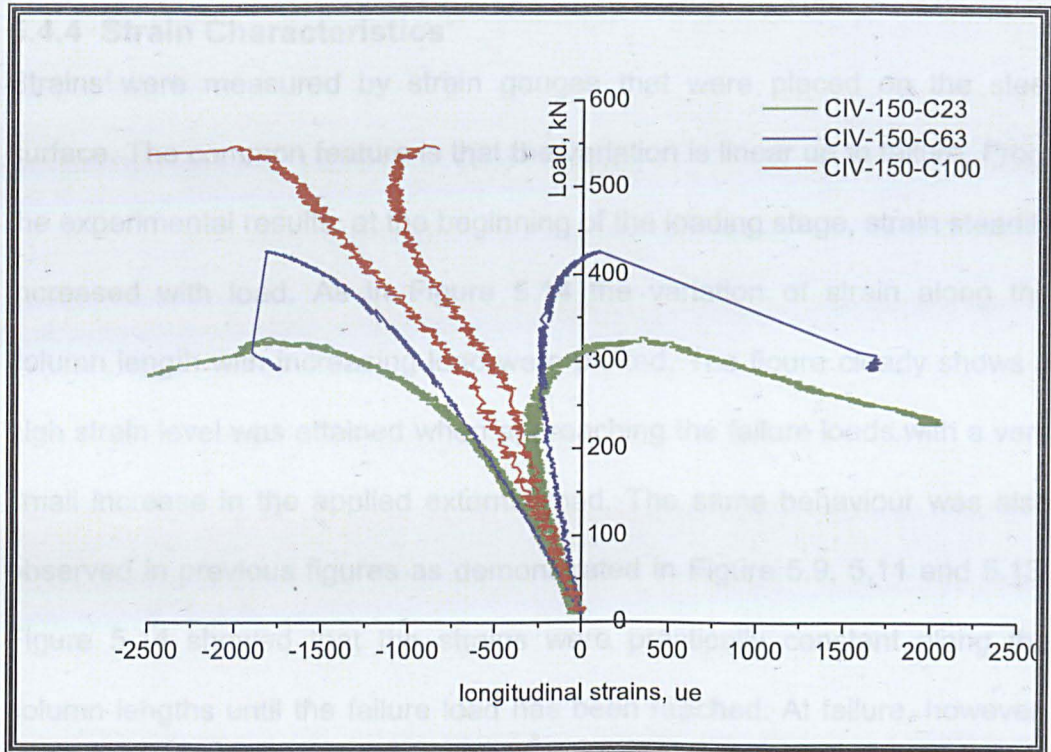


(a)

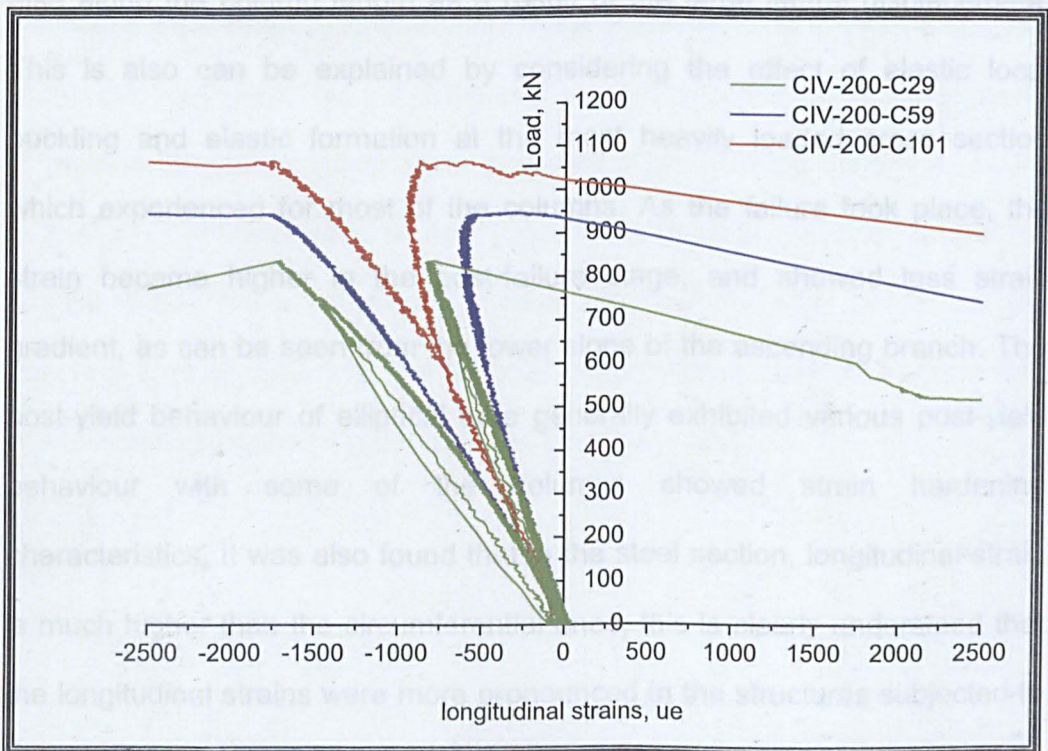


(b)

Figure 5.12: Load-horizontal displacement series IV



(a) 150 x 75 x 4mm



(b) 200 x 100 x 5mm

Figure 5.13: Mid-height vertical strain characteristics of series IV columns

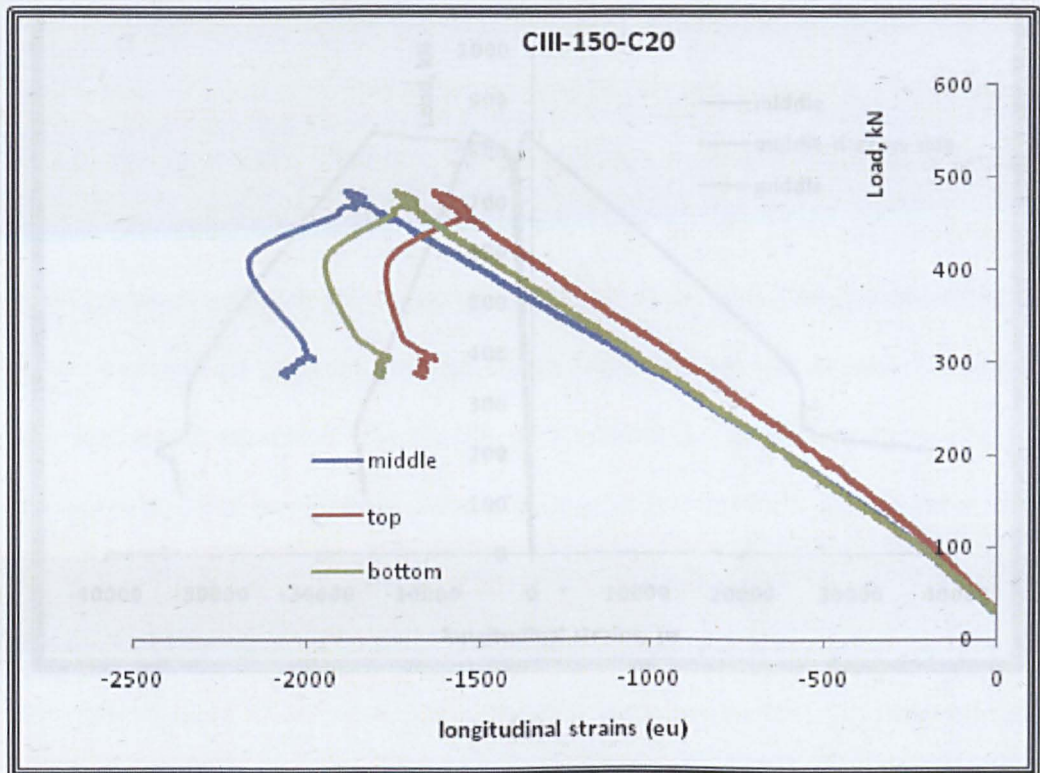
5.4.4 Strain Characteristics

Strains were measured by strain gauges that were placed on the steel surface. The common feature is that the variation is linear up to failure. From the experimental results, at the beginning of the loading stage, strain steadily increased with load. As in Figure 5.14 the variation of strain along the column length with increasing load were plotted. The figure clearly shows a high strain level was attained when approaching the failure loads with a very small increase in the applied external load. The same behaviour was also observed in previous figures as demonstrated in Figure 5.9, 5.11 and 5.13. Figure 5.14 showed that the strains were practically constant along the column lengths until the failure load has been reached. At failure, however, strains recorded at columns' mid-height were found larger than anywhere else along the column length as a result of the large lateral displacement. This is also can be explained by considering the effect of elastic local buckling and elastic formation at the most heavily loaded cross section which experienced for most of the columns. As the failure took place, the strain became higher in the post-failure stage, and showed less strain gradient, as can be seen from the lower slope of the ascending branch. The post-yield behaviour of elliptical tube generally exhibited various post-yield behaviour with some of the columns showed strain hardening characteristics. It was also found that in the steel section, longitudinal strain is much higher than the circumferential ones; this is clearly understood that the longitudinal strains were more pronounced in the structures subjected to axial load.

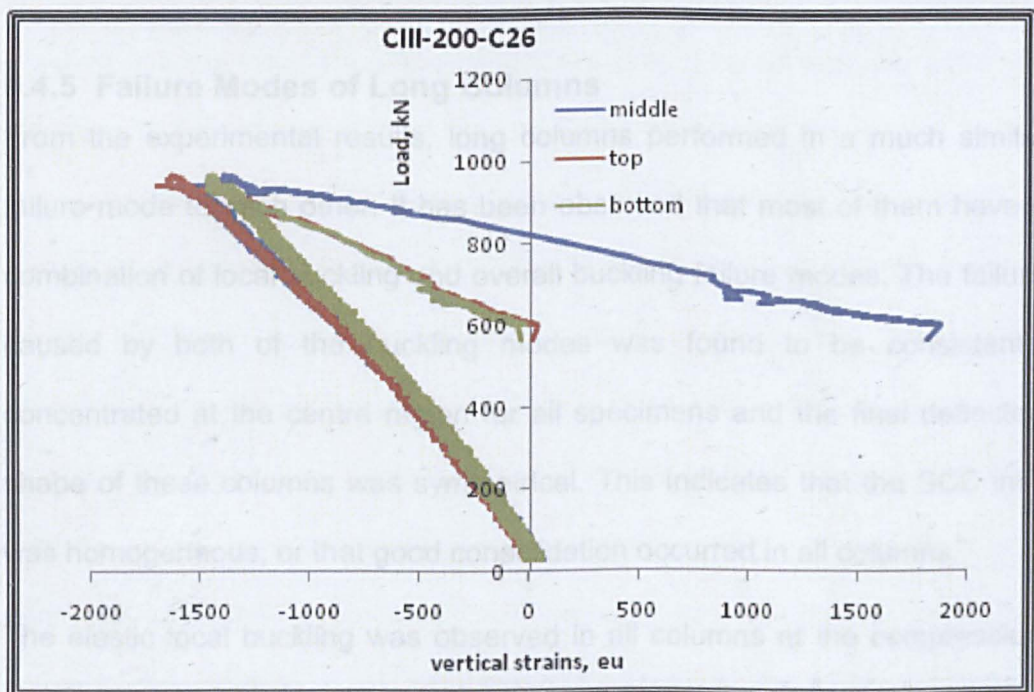
As observed in the experiment, the yield strain was reached first in the compressive zones. The strains reached just before (approximately at 90%

of failure load) or at failure and exceeded in the post failure stage. This shows that for that particular column, the load bearing capacity was always determined by the yielding at the compressive edge of the structures. However, this is only significant for columns with lower slenderness ratio. Inspection on the stress distribution at failure for higher slenderness columns showed that the maximum strength was achieved not long after the steel tubes reached their yield strength at failure which suggests that the global instability was significant in controlling the failure of those particular columns. It has been observed that columns in Series II-IV failed by inelastic buckling and these columns can be referred to as intermediate columns.

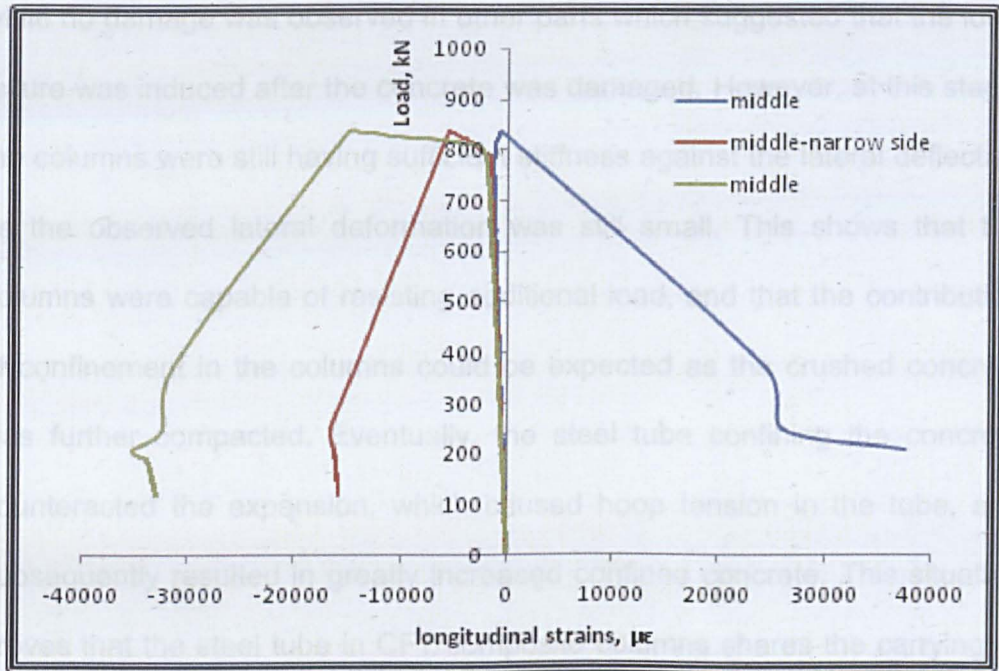
Strain variations across the elliptical cross section are shown in Figure 5.14. Non-uniformed strain distributions on the cross-section as demonstrated in the figure show that the longitudinal strains were higher at the flattest portion of the elliptical tube. This indicates that the portion of the tubes were unable to provide as much perpendicular pressure which indicate the limited ability to restrain the concrete core and susceptible to local buckling. Unlike the circular tube, these conditions caused the compressive stress on the concrete core to vary over the elliptical cross-section, and the confinement effect was consequently lower than the circular section.



(a) CIII-150-C20



(b) CIII-200-C26



(c)

Figure 5.14: Load versus axial strain at middle length of CFT column

5.4.5 Failure Modes of Long Columns

From the experimental results, long columns performed in a much similar failure mode to each other. It has been observed that most of them have a combination of local buckling and overall buckling failure modes. The failure caused by both of the buckling modes was found to be consistently concentrated at the centre region for all specimens and the final deflected shape of these columns was symmetrical. This indicates that the SCC infill was homogeneous, or that good consolidation occurred in all columns.

The elastic local buckling was observed in all columns at the compression edge. Again, this was expected due to the increased compression and the concrete crushing that pushed the steel tube outward. This phenomenon was further proven by the observation on the concrete after the steel enveloped was removed. The concrete within the middle area was crushed

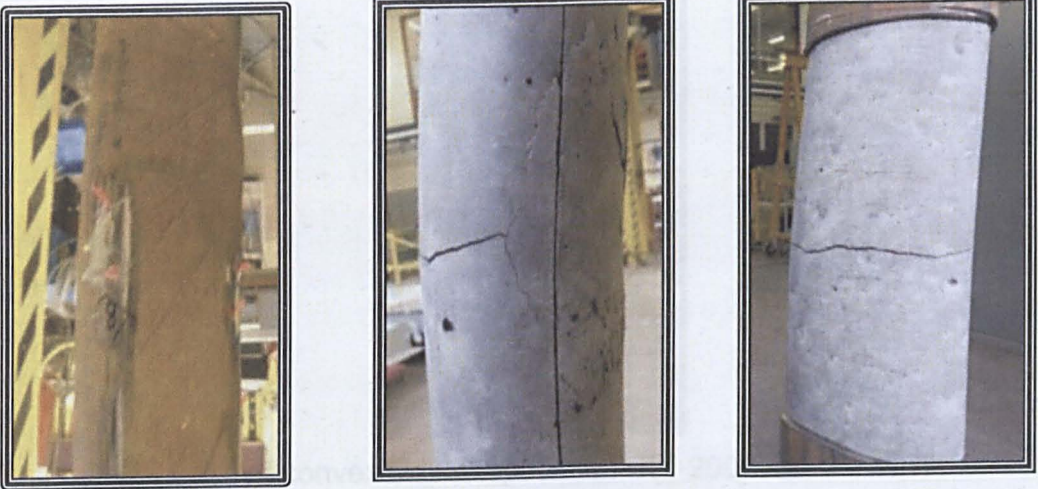
while no damage was observed in other parts which suggested that the local failure was induced after the concrete was damaged. However, at this stage, the columns were still having sufficient stiffness against the lateral deflection as the observed lateral deformation was still small. This shows that the columns were capable of resisting additional load, and that the contribution of confinement in the columns could be expected as the crushed concrete was further compacted. Eventually, the steel tube confining the concrete counteracted the expansion, which caused hoop tension in the tube, and subsequently resulted in greatly increased confined concrete. This situation proves that the steel tube in CFT composite columns shares the carrying of the compressive load with the concrete core, even though the primary purpose of the element is to carry the tensile stresses. The drastic changes in terms of the lateral displacement were only observed after the columns reached ultimate load. Thus, the capacity of long columns was characterised by the initiation of overall buckling, and was further proven as this failure causes higher stress concentration at the centre region of all columns as can be expected from buckling analysis. This is the kind of failure mode that the design engineer constantly vigilant against because the buckling is particularly dangerous which can cause a catastrophic failure. Further investigation of the load-vertical strain curve has observed that the ultimate load for some of the columns, it was expected that ultimate load was achieved after the steel tubes had yielded, which indicated that these columns were able to resist further load due to the reserved steel strength. However, for higher slenderness columns they could behave elastically.

In order to investigate the failure of the concrete core, some of the steel tube envelopes were removed. The concrete crush took the shape of the

deformed tube, as can be seen in Figure 5.15 (a) and (b). Although the compressive crack was developed, the concrete core seems to have remained intact and been well contained by the steel tube, which therefore suggests that a composite action occurred in the specimen. However, upon the removal of the steel envelope from various tested columns from Series IV, no sign of concrete crushing was seen to have occurred in the longer columns. Apart from the compression crack failure, the tension crack failure also occurred in long CFT columns, but it was only observed in columns with C100 grade concrete infill as illustrated in Figure 5.15(b). Notably, this phenomenon can be related to the characteristics of higher strength concrete of SCC. Due to having higher fine material as compared to other strength and less coarse aggregates, the friction in the mixture is minimised and affects the mechanical bond in the concrete filling.



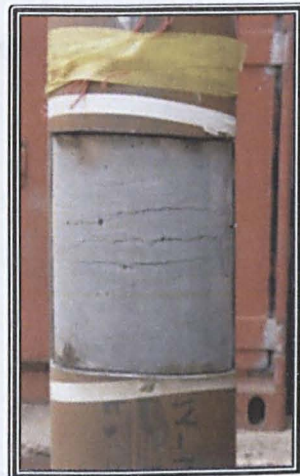
(a) Series II (CII-150-C60)



(b) Series II - CII-200-C100

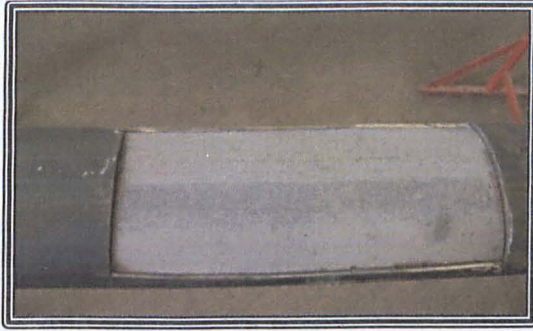


Compression failure of CIII-150-C100

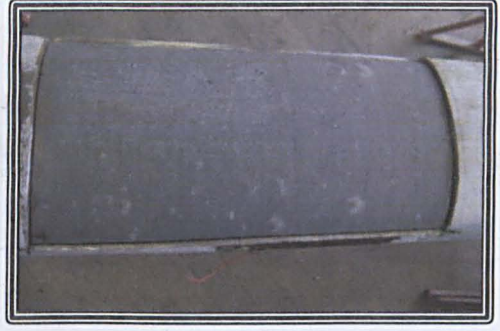


Tension failure of CIII-200-C100

(c) Series III



CIV-150-C63



CIV-150-C100



At convex side of specimen CIV-200-C30

(d) Series IV

Figure 5.15: The removal of steel enveloped

Chapter 6

Numerical Modelling

6.1 Introduction to the Finite Element model

This chapter outlines the development of the finite element (FE) models carried out in this study. The computational procedures were developed and performed in parallel with the testing programme. Physical testing has a significant role but it is very expensive, time-consuming and difficult to carry out extensively. Therefore, numerical FE analysis has been an alternative and broadly used to provide supplementary information and conduct parametric study.

In the research reported in this thesis, the general purpose nonlinear FE package programme, ABAQUS Version 6.8, was employed to perform numerical simulation of the elliptical CFT columns subjected to axial compressive forces. In order to study the behaviour of the elliptical CFT columns, reliable three-dimensional non-linear FE models subjected to axial load were modelled considering the nonlinear geometrical and material properties of the concrete core and steel tube.

6.2 Description of the Finite Element model

There are two main analysis solvers in ABAQUS, which are ABAQUS/Standard and ABAQUS/Explicit. The ABAQUS/Standard is used for general purpose analysis. It applies implicit equation at each user-defined increment to solve a wide range of linear and nonlinear problems involving the static, dynamic, thermal, and electrical responses of components. ABAQUS/Explicit is a special purpose analysis product that uses an explicit dynamic FE formulation. It is appropriate for modelling transient dynamic events, such as impact and blast problems. This analysis solver is efficient in solving highly nonlinear problems involving changing contact conditions, such as forming simulations. Choice between these two approaches of analysis depends on the nature of the problem.

In the studies of elliptical CFT columns, the three-dimensional FE models were developed by defining the steel tube, concrete core and plates as individual bodies. Elements considered in the simulations of the behaviour of concrete filled elliptical steel tube columns are shown in Figure 6.1 and Figure 6.2. The dimensions of these model sections are the same as the columns used in the experimental works.

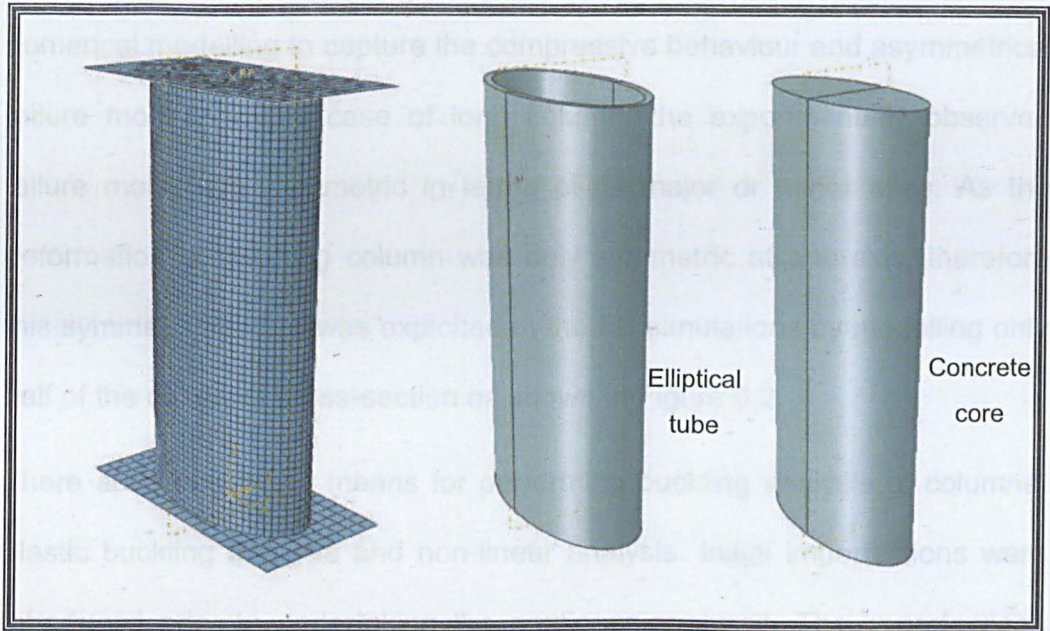


Figure 6.1: Typical FE model of stub columns

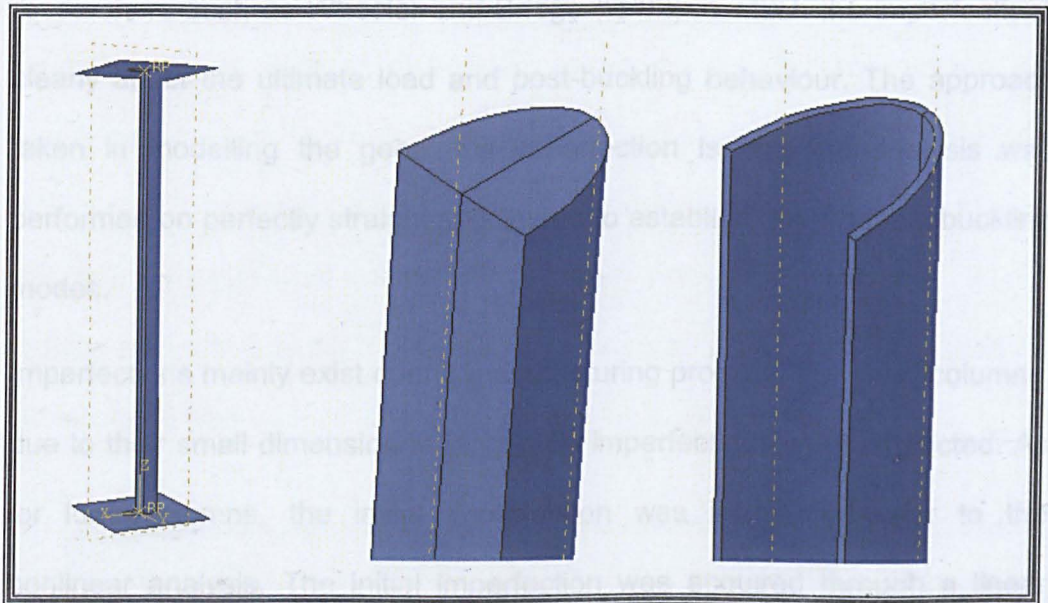


Figure 6.2: Typical FE model of long columns

As observed from experimental studies, the failure modes of short columns are the local buckling of steel section, concrete crushing and shearing. The deformations of these columns include symmetric and asymmetrical shapes. Therefore full short composite column as in Figure 6.1 was adopted in the

numerical modelling to capture the compressive behaviour and asymmetrical failure modes. In the case of long column, the experimentally observed failure mode was symmetric in terms of its major or minor axes. As the deformation of the long column was only symmetric at one axis, therefore this symmetric feature was exploited in the FE simulations by modelling only half of the columns' cross-section as shown in Figure 6.2.

There are two primary means for performing buckling analysis of columns; elastic buckling analysis and non-linear analysis. Initial imperfections were introduced prior to undertaking the nonlinear analyses. The imperfections were taken into consideration parallel with the findings by several researchers such as Wheeler and Bridge (2002) in which the imperfections clearly affect the ultimate load and post-buckling behaviour. The approach taken in modelling the geometric imperfection is that the analysis was performed on perfectly straight specimens to establish the probable buckling modes.

Imperfections mainly exist during manufacturing process. For short columns, due to their small dimension in length the imperfections were neglected. As for long columns, the initial imperfection was introduced prior to the nonlinear analysis. The initial imperfection was acquired through a linear perturbation analysis of the identical CFT column in which the eigen modes shape were extracted. The lowest mode shape combined with the maximum measured column out of straightness was employed as the total imperfection in the numerical modelling. The mode shape of the lowest eigen mode was considered sufficient to adequately characterise the most influential geometric imperfection.

Elastic buckling analysis is followed by the non-linear load-displacement analysis. This is a more accurate approach as this technique incorporates features such as initial imperfection geometry, plastic behaviour and large-deflection response. In this stage, the models were loaded to failure to predict the full response and ultimate loads of the columns. In this study, the Static, General method was used to carry out an incremental load in this analysis. The displacement control loading method was used in the analysis, in which identical to the loading method used in the tests.

6.2.1 Boundary conditions and load application

Following the testing procedures, fixed end boundary conditions were applied to the top and bottom of the short CFT columns. This was achieved by restraining all degrees of freedom except for the displacements at the loaded end to allow for vertical deformation during loading course. As shown in Figure 6.3, at the fixed end, degree of freedom of displacements in x,y,z direction (U_1, U_2, U_3) as well as their rotation were set to be zero. At the loading end; which is the movable end, the degree of freedom in longitudinal direction, U_3 was free.

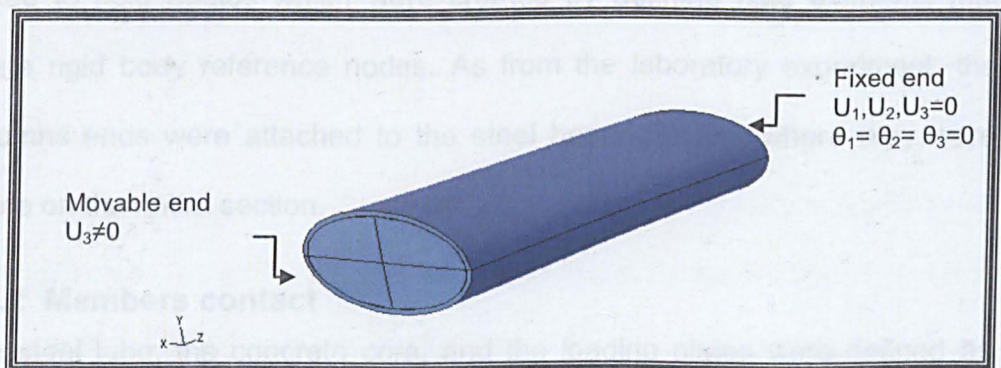


Figure 6.3: Boundary condition for stub columns

The boundary conditions applied to long columns were similar to the conditions used in the stub columns simulations. However, both ends of the long columns were free to rotate about the x and y-axis to allow for the pin-ended joints simulation as imposed during the laboratory experiments.

For simplification of the model and to prevent convergence problems, the rotation about the y-axis was then fixed. This was adapted considering that there were no buckling observed about the y-axis during the laboratory experiment. The effect of this approach was investigated and it was found that there was no significant difference in the columns capacities and behaviour if the rotation of the y-axis was fixed. Subsequently, only rotation about the x-axis was considered in the models.

The load was applied as an increased deformation on the columns. The nonlinear parameter (*NLGEOM) was included to deal with the large displacement analysis. An increment of deformations in z-direction was applied to the reference point at the centre node of the top rigid base plate of all specimens. Each columns ends were divided into an immovable end and a movable end, which was the loaded end. The top end of the columns was linked to rigid bodies which were created by defining rigid elements that share rigid body reference nodes. As from the laboratory experiment, the columns ends were attached to the steel bearing plates where they were borne on the entire section.

6.2.2 Members contact

The steel tube, the concrete core, and the loading plates were defined as individual bodies in the numerical modelling. Contact pairs option with small sliding parameter to model infinitesimal sliding between

these separated deformable bodies were introduced and used in the simulations. These elements will then interact with each other such as the load plate will transfer the axial load to the steel tube and concrete core and the concrete core will be confined by the steel tube. Instead of normal interaction between the interface of steel tube and concrete core during the loading course, this contact surface allows sliding of the elements when the columns experience larger deformation. To simulate these interactions, the contact function provided by ABAQUS software was adopted.

ABAQUS offers a variety of contact functions to simulate such interaction between the contact pair. The two most common used in ABAQUS/Standard solver is the surface or node based contact pair. The surface based contact pair function was used in the study to define the contact interaction between the contact pair; i.e. the inner surface of the steel tube, and the concrete core. A penalty function contact algorithm was used. To simulate the bond between the inner steel tube and the circumferential of concrete core, a contact pressure-over closure model in normal direction and a Coulomb friction model in the direction tangential to the surface were used by considering the definition of master and slave contacting surfaces (Brite-EuRam, 2000).

The inner surface of the steel tube is chosen as the master surface as this surface is considered the stiffer body. Different values of friction coefficients, μ ranging from 0.1 to 0.5 were investigated in the tangential direction. From the sensitivity study, no significant effect to the axial resistance of the composite column was found, but smaller coefficient is likely to cause convergent problem at large deformation. The coefficient of friction, μ

between the surface pair was taken as 0.3 and the friction was maintained as long as the surface pair remained in contact. The contact surface pair between the concrete and steel tube was allowed to separate and slide relative to each other, as well as transmit contact pressure and shear stresses but do not penetrate each other. In the basic form of the Coulomb friction model, the contacting surfaces can carry shear stresses across their interface up to a given magnitude before they start sliding relative to one another. The Coulomb friction model defined this critical shear stress, τ_{crit} , at where sliding between the surfaces starts. The critical shear stress defined as a fraction of the contact pressure, p between the surfaces. The contact pressure is given by the pressure-over closure relationship (Johansson and Gylltoft, 2002). The critical shear stress is defined in Equation 6.1 with the coefficient of friction, $\mu = 0.3$ for all models.

$$\tau_{crit} = \mu p \quad (6.1)$$

Contact pairs between end plates and the column ends are also simulated using the contact function provided in ABAQUS/Standard solver. 'Hard contact' was assumed for normal contact behaviour whereas 'rough' friction was used in the tangential direction between the contact pairs to restrain the slip.

6.2.3 Elements types and meshes density

Type of element and the size of mesh are important in the FE modelling as they affect the results accuracy and simulation speed. To select appropriate element type, the 4-noded doubly curved with reduced integration shell element, S4R and 8-node solid element, C3D8R were selected for analysis in a so-called sensibility study. The S4R element type was found to be

negligible as the simulated failure mode did not replicate the experimental results. Therefore, the C3D8R was selected in the simulation of the concrete core and the steel tube. This is similar to what was found by other researchers Ellobody and Young (2006), Ellobody et al. (2006), Dai and Lam (2010) that this type of element is more efficient. According to Dai and Lam (2010), although the shell element would reduce the total number of elements but the element could not follow the curved contact boundary well and finally lead to an impairment of the simulation accuracy of the concrete confinement and bond action of the members. Thus, C3D8R, reduced integration solid continuum element was selected to represent both the steel tube and concrete core. The advantage of the reduced integration element is that the strain and stresses calculated at the locations provide optimal accuracy.

Steel plates at the ends of the columns were defined as rigid elements body in the numerical model. The rigid plate was considered to eliminate the concern that the top and bottom edges are being damaged through the analysis and to apply axial compressive load uniformly to the column end. The rigid plates were meshed using four-node three dimensional bilinear rigid quadrilateral elements, R3D4 with element size of 10 mm. The surfaces of these elements are also defined to connect with the edge of the column. The load was applied as static uniform displacement through the top of the rigid plate's reference point.

A mesh size sensitivity study was conducted to determine the most suitable finite element mesh size. The mesh size should be fine enough to achieve accuracy. However, excessively fine mesh should be avoided as it requires

more processing time and disk usage. Element sizes ranging from 5 mm to 30 mm were considered in the study to obtain a suitable mesh size that would produce accurate results whilst remaining computationally efficiency.

The sensitivity study that compares the numerical prediction to the experiment results suggested that mesh size of 10 mm to 15 mm gives an acceptable degree of accuracy. A uniform mesh along the circumferential and longitudinal direction was employed in all models. An example is shown in Figure 6.4.

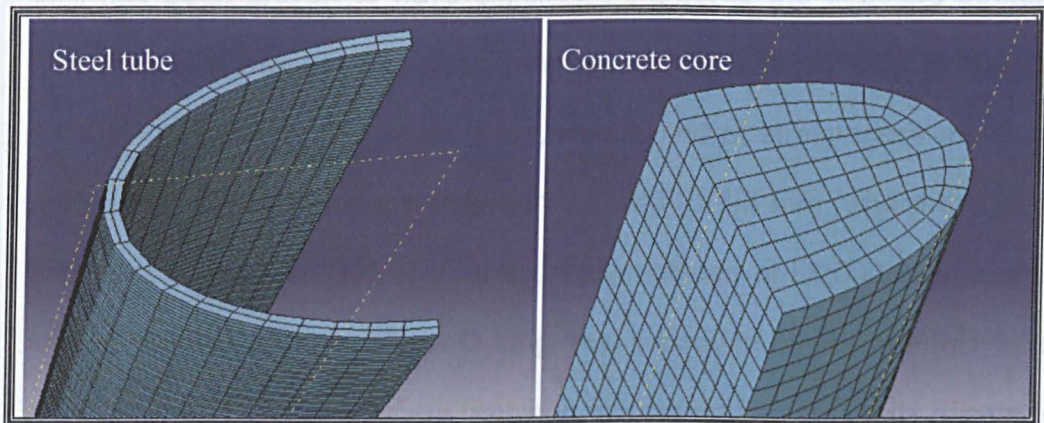


Figure 6.4: Three-dimensional finite element mesh for steel tube and concrete core

6.2.4 Imperfection and Residual Stress

Initial global geometric imperfections were incorporated in the numerical model. According to Chan and Gardner (2009), imperfection amplitude of $L/1000$ provides the best agreement between FE and test results of elliptical hollow columns. In present study a range several fixed fractions of the specimen length L , i.e. $L/250$, $L/500$, $L/1000$, $L/2000$ and $L/6400$ were studied. The anticipated sensitivity to imperfection has been reflected in the

numerical results which showed greatest variation in response. In the CIII-150-C20 model, the ultimate load reduces by approximately 22% with increment of imperfection amplitude from L/2000 to L/250. It should be noted that the amplitude of L/250 and L/500 reflected the current allowable out-of-straightness tolerance for elliptical section tube in Europe and the L/500 amplitude also is the tolerance limit in North America (ASTM) and Australia (Standards Australia 1991) for other tubular members (Chan and Gardner, 2009) whereas L/1000 has been found to satisfied for elliptical hollow columns. It is acceptable that for composite columns, the present concrete infill has been proven to have significant impact to the structure strength. Thus, smaller imperfection magnitude seems more reasonable to consider for this structure. In this study, the scope of out of straightness measured from all tested specimens is between 0.3 mm to 1.3 mm, where the global imperfect is about L/2000. Therefore, the amplitude of L/2000 was adopted for the numerical simulation. During the validation, this imperfect scale provided very good agreement between the experimental results except for specimen CII-150-C55 which is further explained in 6.4.2.

In this study, the residual stress which is normally induced during the manufacturing process of the steel hollow section is not considered. Gardner and Nethercot (2004) have shown that the residual stress is not significant in reducing the stiffness and it only has small influence on the ultimate capacity of the stub CFT column.

6.3 Material properties

6.3.1 Steel section

All models are assumed to have isotropic strain hardening material properties as justified by the stress-strain. The stress-strain relationship of the steel tube was adopted from the coupon test results of Figure 5.3. The ABAQUS software requires material properties for finite-strain calculation in terms of true stress and log plastic strain. The results from the coupon tests do not give a true representation of the deformation characteristics as it is based on the initial dimension of the specimen and the dimensions change continuously during the test. Equations 6.2 and 6.3 relate the true stress to the nominal stress, and the true strain to the nominal strain, respectively. The incremental plasticity model requires only a range of the true stress-strain curve from the point corresponding to the last value of the linear range of the static engineering stress-strain curve to the ultimate point of the true stress-strain curve (Yan and Young, 2004).

$$\sigma_{true} = \sigma_{nom}(1 + \epsilon_{nom}) \quad (6.2)$$

$$\epsilon_{ln_{pl}} = \ln(1 + \epsilon_{nom}) - \sigma_{true}/E \quad (6.3)$$

An elastic-plastic model with the Von-Mises yield criteria used to define the yield surface and the Poisson's ratio in the elastic part was set to 0.3.

6.3.2 Concrete material

Different approaches to determine the actual stress in the confined concrete have been developed as explained in the previous chapter. According to Shams and Saadeghvaziri (1997), the geometrical configuration of the columns and the material properties of the concrete have significant influences on the enhancement of the mechanical properties of the confined

concrete core in composite columns. To date however, there has been very limited research conducted on the stress-strain concrete core relationship and the mathematical expression developed for material properties of confined concrete in elliptical steel tubes. To the author's knowledge, the only study on confined concrete properties was reported by Dai and Lam (2010).

Numerical analysis is initially performed by considering both conditions of the confined and the unconfined uni-axial stress-strain curve of concrete. This was conducted with the aim of further assessing the influence of concrete confining pressure properties in the elliptical CFT columns. Although, it appears that the stub elliptical tubes provide significant confinement for the concrete during experiment, it is not certain whether the simplified FE models are able to capture the behaviour of the confined concrete. Thus, for the case of confined concrete properties, the equivalent stress-strain relationships for the confined concrete under monotonic loading as described by Hu et al.(2003), Ellobody and Young (2006), Dai and Lam (2010), and Han et al. (2007) were adopted for elliptical CFT column models. For long column FE models, both the confined and unconfined concrete properties are crucial for assessing the presence of the confinement effect in the columns, as has been found from the experiment.

The elastic-plastic confined concrete properties were considered in three regions. The uniaxial compressive strength, f'_{cc} and the corresponding strain, ϵ'_{cc} of concrete subjected to lateral confining pressure were much higher than those of unconfined concrete. Figure 6.5 shows the equivalent uniaxial stress-strain curve of concrete as presented in Hu et al.(2003).

Elastic portion for confined concrete is considered from origin up until proportional limit stress. Proportional limit stress is taken as the value of $0.5f_{cc}$ and its corresponding strain is equal to $0.5f_{cc}/E_{cc}$. Young's modulus for confined concrete is given by the empirical equation of equation 6.3 with the Poisson's ratio, ν_{cc} is taken as 0.2.

$$E_{cc} = 4700\sqrt{(f_{cc})} \text{ MPa} \quad (6.4)$$

The second part of the stress-strain properties specifies the nonlinear portion starting from proportional limit stress to the compressive confined concrete strength, f_{cc} and its corresponding strain, ε_{cc} which were determined from equations 6.5 and 6.6, respectively. Unconfined concrete cylinder compressive strength, f_c was obtained from the cylinders test results. The corresponding unconfined strain, ε_c was taken as 0.002, as found in the average SCC compression cylinders tests. The value of ε_c is usually in the range of 0.002 - 0.003, with $\varepsilon_c = 0.003$ adopted from Hu et al. (2003) and Ellobody and Young (2006), as suggested by ACI.

$$f_{cc} = f_c + k_1 f_1 \quad (6.5)$$

$$\varepsilon_{cc} = \varepsilon_c \left[1 + k_2 \frac{f_1}{f_2} \right] \quad (6.6)$$

where,

k_1 and k_2 = 4.1 and 20.5 respectively

f_1 = lateral confining pressure imposed by the steel tube.

Many studies on the CFT columns have found that the lateral confining pressure f_1 depends on the D/t ratio and the yield stress, f_y . Higher confining

effect is seen in lower D/t ratio due to restraining action. Conversely, the confining pressure, f_1 proposed by Dai and Lam (2010) suggests that the confining pressure increases with increasing D/t ratio. The formulation worked well in the FE simulations carried out for the elliptical stub CFT columns in their study. However, no experimental result is available to prove the situation. Although steel tube of various sizes were involved in this study, no firm conclusions regarding the effect of the D/t parameter on the columns' capacity can be made since there is difference in the length of the columns considered. It should be emphasised here that the proposed equations by Dai and Lam (2010) are based on a study that has similar aspect ratio of 2 as in this study but only considered one column size.

The curve for the second part analysis is plotted with the strain value between the proportional strain and the confined strain, ε_{cc} .

$$f = \frac{E_{cc}\varepsilon}{1+(R+R_E-2)\left(\frac{\varepsilon}{\varepsilon_{cc}}\right)-(2R-1)\left(\frac{\varepsilon}{\varepsilon_{cc}}\right)^2+R\left(\frac{\varepsilon}{\varepsilon_{cc}}\right)^3} \quad (6.7)$$

where,

$$R_E = \frac{E_{cc}\varepsilon}{f_{cc}} \quad (6.8)$$

$$R = \frac{R_E(R_\sigma-1)}{(R_\varepsilon-1)^2} - \frac{1}{R_\varepsilon} \quad (6.9)$$

and R_σ and R_ε are taken equal to 4.

In a similar approach to Ellobdy and Young (2006), this study treated the part after the proportional limit stress with the Drucker-Prager yield criterion model. The criterion includes two parameters: *Drucker-Prager and *Drucker-Prager hardening which were used to define the yield stage of confined concrete. The concrete core was found to be subjected to tri-axial

compressive stresses in CFT columns. The compressive failure surface dominated in the structure which increases the hydrostatic pressure. Therefore, an elastic-plastic model based on Drucker-Prager yield criterion was used to model the yield surface of the concrete. The material angle of friction, β and the ratio of flow stress in tri-axial tension to that in compression, K are taken as 20° and 0.8, respectively, as adopted by Hu et al. (2003) and Ellobody and Young (2006) however, these material parameters should be determined from the experimental data. The same method was applied for circular, rectangular and square CFT columns in the study by Ellobody et al. (2006).

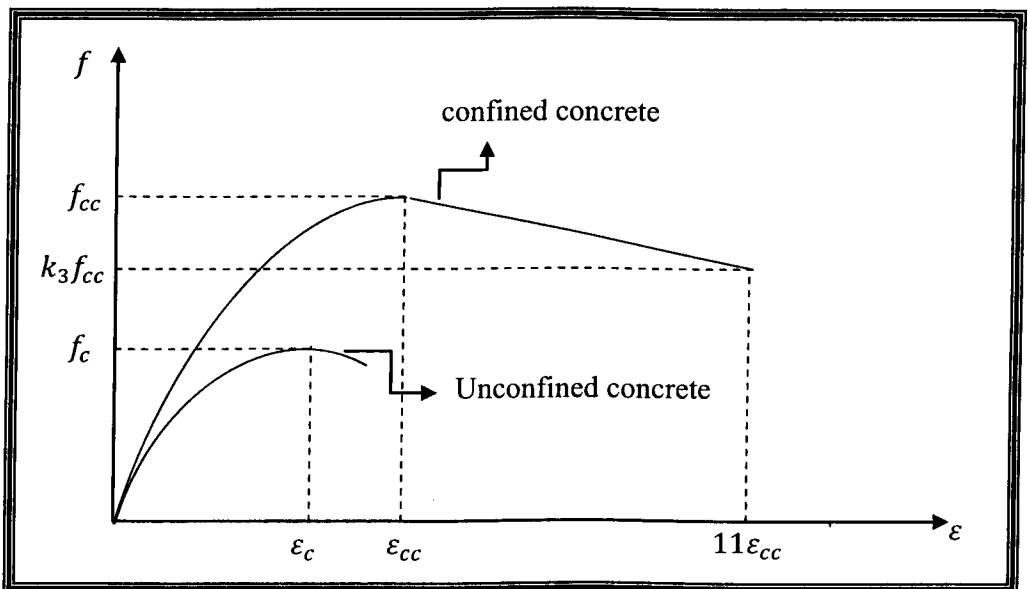


Figure 6.5: Equivalent stress-strain curve of concrete by Hu et al (2003)

In this study an approach proposed by Han et al. (2007) for simulating plastic behaviour of the confined concrete in circular CFT columns was

considered. In this approach the plastic behaviour depends on the confinement factor, ξ expressed as follows:

$$\xi = \frac{A_s f_y}{A_c f_{ck}} = \alpha \frac{f_y}{f_{ck}} \quad (6.10)$$

where $\alpha = A_s/A_c$ and the stress-strain relationship was calculated as the following;

$$y = \begin{cases} 2x^2 - x^2 & (x \leq 1) \\ \frac{x}{\beta_o(x-1)^\eta + x} & (x > 1) \end{cases} \quad (6.11)$$

where $x = \varepsilon/\varepsilon_o, = \sigma/\sigma_o$; $\sigma_o = f'_c$ (N/mm^2), $\varepsilon_o = \varepsilon_c + 1800\xi^{0.2} \times 10^{-6}$;
 $\varepsilon_c = (1300 + 12.5f'_c) \times 10^{-6}$;

$\eta = 2$ for circular and $1.6 + \frac{1.5}{x}$ for square section;

$$\beta_o = \begin{cases} (2.36 \times 10^{-5})^{[0.25+(\xi-0.5)^7]} (f'_c)^{0.5} \times 0.5 \geq 0.12 & \text{circular} \\ \frac{(f'_c)^{0.1}}{1.2\sqrt{1+\xi}} & \text{square} \end{cases} \quad (6.12)$$

In this study circular section approach was considered. The initial modulus of elasticity and Poisson's ratio are $E_c = 4730\sqrt{f'_c}$ and $\mu_c = 0.2$ respectively. Preliminary analysis was conducted to assess all the formulations adopted from other researchers. However, some of the proposed behaviour of confined concrete did not produce the volumetric strain behaviour accurately for elliptical CFT columns. Comparisons of results obtained from different approaches have found that the confined stress-strain relationships suggested by Han et al. (2007) is more reliable for elliptical long CFT columns and therefore adopted in this study. The numerical models have satisfactorily replicated the experimentally observed main structural

behaviour which is the initial stiffness, ultimate capacity and general load-deformation response and failure patterns. Both numerical and laboratory experiments found that flexural buckling dominates the failure modes. Thus, the effect of the tensile behaviour of a concrete core was considered and the plastic concrete properties were simulated based on the concrete damaged plasticity approach. The concrete damaged plasticity model is an isotropic plasticity model that resembles Drucker-Prager model in terms of the compressive behaviour of concrete. The uni-axial compressive stress-strain response of concrete is assumed to be linear up to 40% of its compressive strength. Beyond this point, it is in the plastic region and the plastic strain data are used to define the stress-strain relationship in the FE models.

The tensile strength of concrete is much lower than the compressive strength. The uni-axial tensile strength of concrete, f'_t is set at 10% of the compressive strength, $\sigma_{t0} = f'_c/10$ (Goto et al., 2010). In the damaged model, the stress strain response under uni-axial tension follows a linear elastic relationship until the maximum tensile strength is reached. The total strain at which the tensile stress is zero is normally taken as ten-fold of the strain at failure in the tension stiffening model for the case of heavily reinforced concrete slabs. It has been found that this value is not adequate in the case of concrete slabs in composite beams and a total strain of 0.1 is used for reinforced concrete slab in composite beams (Liang et al., 2004). This value is adopted in this study.

The Poisson's ratios for concrete under uniaxial compressive stress is in range of 0.15 to 0.22 (Hu et al., 2005) and the value of 0.2 is assumed for the concrete core in CFT columns. The other material constants necessary

to specify the concrete damaged plasticity models are parameters such as ψ , K_c , σ_{bo}/σ_{co} and eccentricity, e . For the in-filled concrete of the CFT columns specimens, there is no available data for these parameters and $K_c = 0.7$, $\sigma_{bo}/\sigma_{co} = 1.1$ and $e = 0.2$ were used as the standard values recommended by the ABAQUS. The dilation angle, ψ for concrete defines the plastic strain direction with respect to the deviatoric stress axis in the meridional plane. In this study, a value of 20° is used as the dilation angle of concrete.

In regards to the unconfined concrete properties, the stress-strain behaviour of plain concrete in uniaxial compression were calculated in accordance to BS EN 1992-1-1: 2004 (EC 2). The schematic diagram of the stress-strain relationship for nonlinear structural analysis based on the design code is shown in Figure 6.6 and the properties were calculated using Eq. 6.13 to Eq. 6.15.

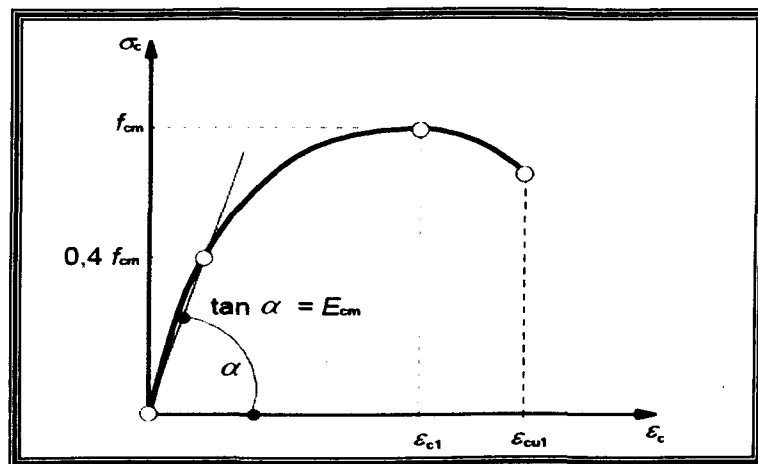


Figure 6.6: Schematic representation of the stress-strain relation
(BS EN 1992-1-1)

$$E_{cm} = 22 \left[\frac{f_m}{10} \right]^{0.3} \quad (6.13)$$

$$f_{cm} = f_{ck} + 8 \quad (6.14)$$

where,

f_{cm} = mean value of concrete cylinder compressive strength

f_{ck} = characteristic compressive cylinder strength of concrete at 28 days

The relationship between compressive stress, σ_c and shortening strain, for short term uniaxial loading calculated in Eq. 6.11 is;

$$\frac{\sigma_c}{f_{cm}} = \frac{k\eta - \eta^2}{1 + (k-2)\eta} \quad (6.15)$$

where,

σ_c = compressive stress in the concrete

$$\eta = \frac{\varepsilon_c}{\varepsilon_{c1}}$$

ε_c = compressive strain in concrete

From the numerical analysis, the nonlinear analyses were obviously sensitive to the assumptions in the stress-strain curves. Nevertheless, the proposed concrete material properties of Han et al. (2007) were able to predict more realistic responses.

6.4 FEM Verification

6.4.1 Introduction

The verification of the developed models is crucial in any numerical study. Accordingly, it was conducted in order to assess the accuracy and effectiveness of the numerical models in terms of simulating the response of elliptical CFT columns. Comparisons between the main results obtained

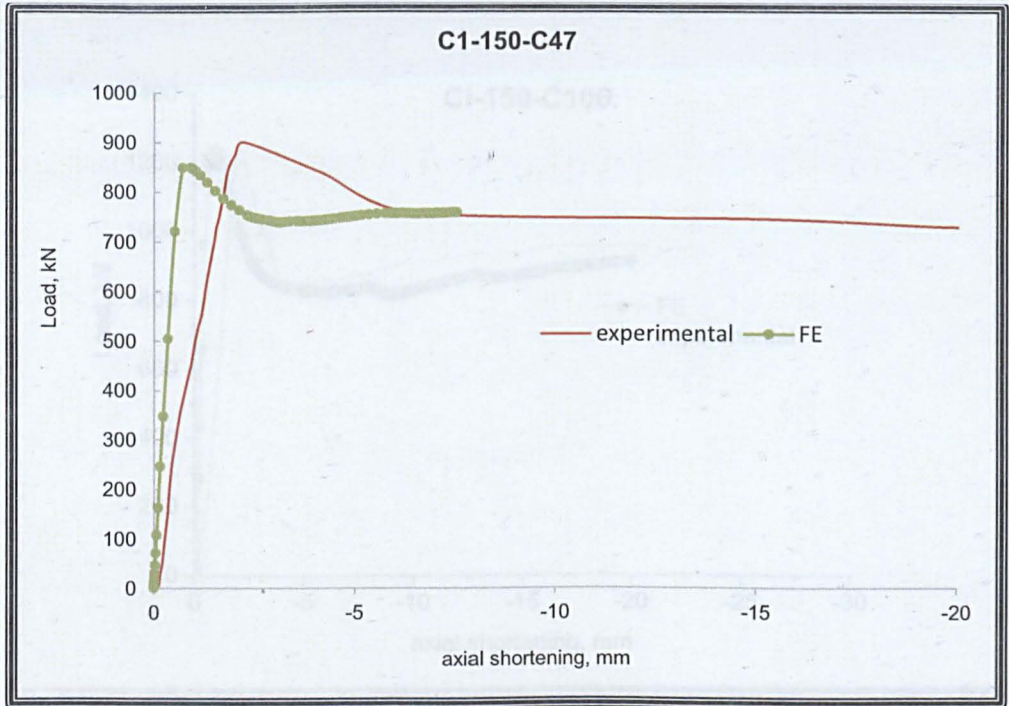
from the experimental and those generated by FE models were made. The main results are the column strengths, load-axial shortening curve, load-lateral displacement curve, and failure modes among others.

6.4.2 Validation of Stub Columns

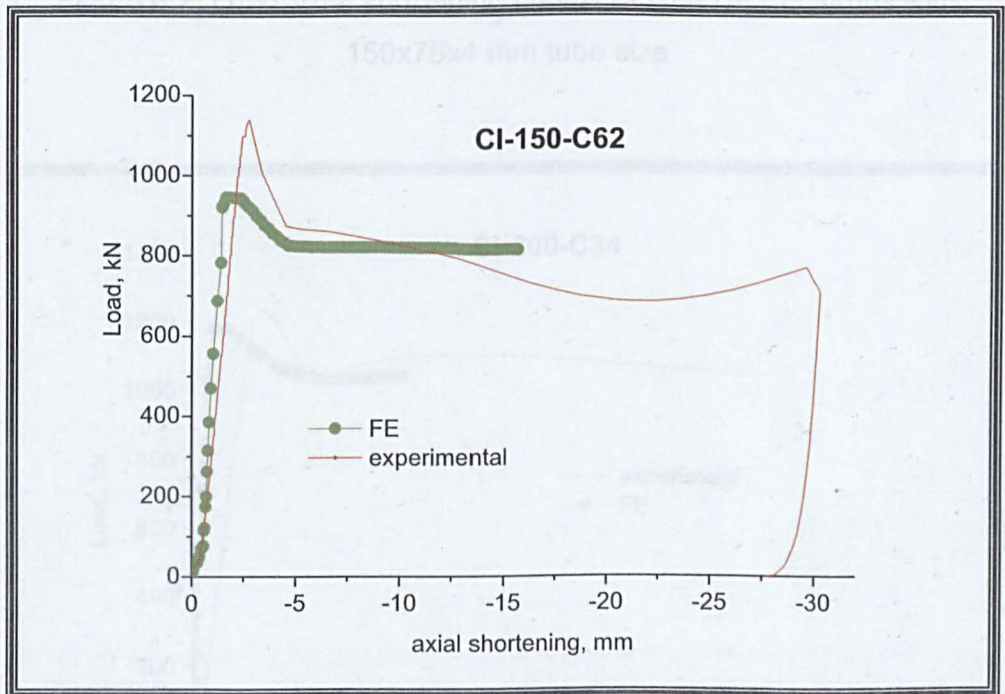
Figure 6.7 and Figure 6.8 show the comparisons of axial compressive load via end shortening curve obtained from the experiments with the numerical models. Both elastic and inelastic responses of the specimens predicted by numerical method were closely correlated with the experimental results. However, the FE results produced higher initial stiffness than observed in the experiment. This discrepancy might be primarily attributed to the difference of material properties between tested specimens and specified in the model. It was expected that this is due to the material concrete properties used in FE models might not represent the actual behaviour in CFT columns. Finite element analysis, as used in structural engineering, determines the overall behavior of a structure by dividing it into a number of simple elements, each of which has well-defined mechanical and physical properties. However the development of a model for the behaviour of concrete is a very challenging task. In addition concrete is a quasi brittle material and has different behaviour in compression and tension. Other factors that may cause the higher stiffness in the finite element modes include the micro cracks produced by drying shrinkage present in the concrete to some degree. These would reduce the stiffness of the actual structure, whereas in the finite element modes the presence of micro cracks were not considered. Perfect bond between the concrete and steel was assumed in the finite element analyses. This situation might not be true for the actual structures. As bond slip occurs, the composite action between the

concrete and steel is lost. Thus, the overall stiffness of the actual beams could be lower than predicted by the finite element models, due to factors that are not incorporated into the models. Stiffness which characterises the response to the applied load depends on several factors, such as the shape, material and support. It is defined as the slope of axial load-deflection curve and is equal to the sum of axial stiffness of the concrete core and steel tube.

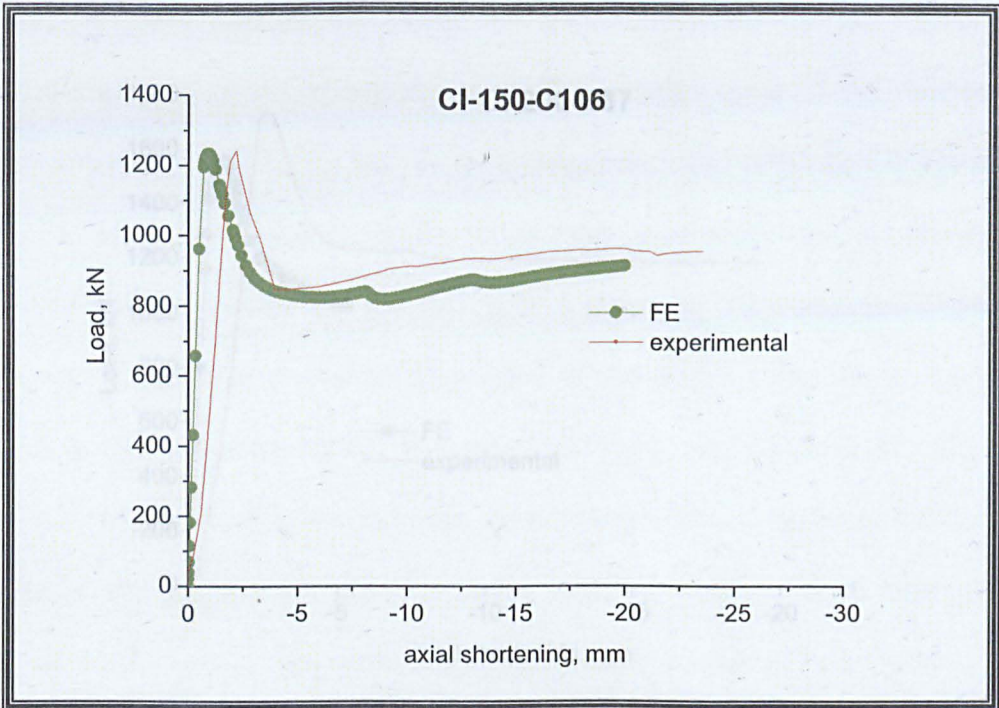
The initial set-up and tolerance may also cause lower initial stiffness. In addition, the axial shortening experimental data was obtained from the LVDTs, and the results were expected not to reflect the true deformation of the column. It is observed in the experiment that the displacements were influenced by early deformation due to the usage of Paris plaster at the capped ends. It is also suspected that the stiffer behaviour of the elliptical columns than the numerical models curve is due to the difference of the significant contribution of the confinement effect to the elliptical cross-sections specimens.



(a)

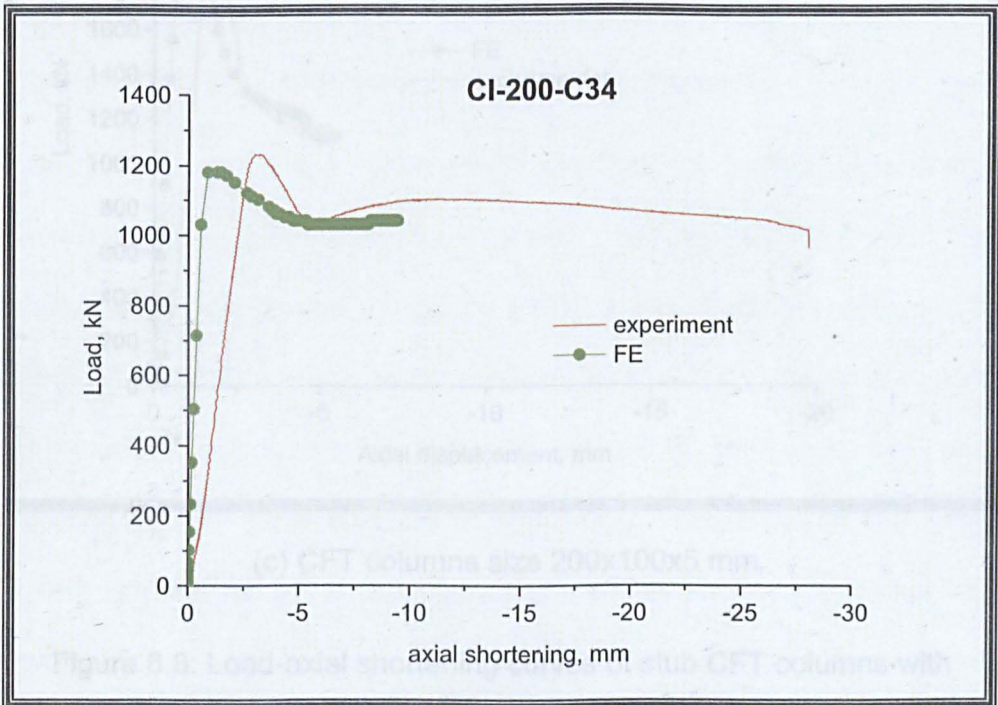


(b)

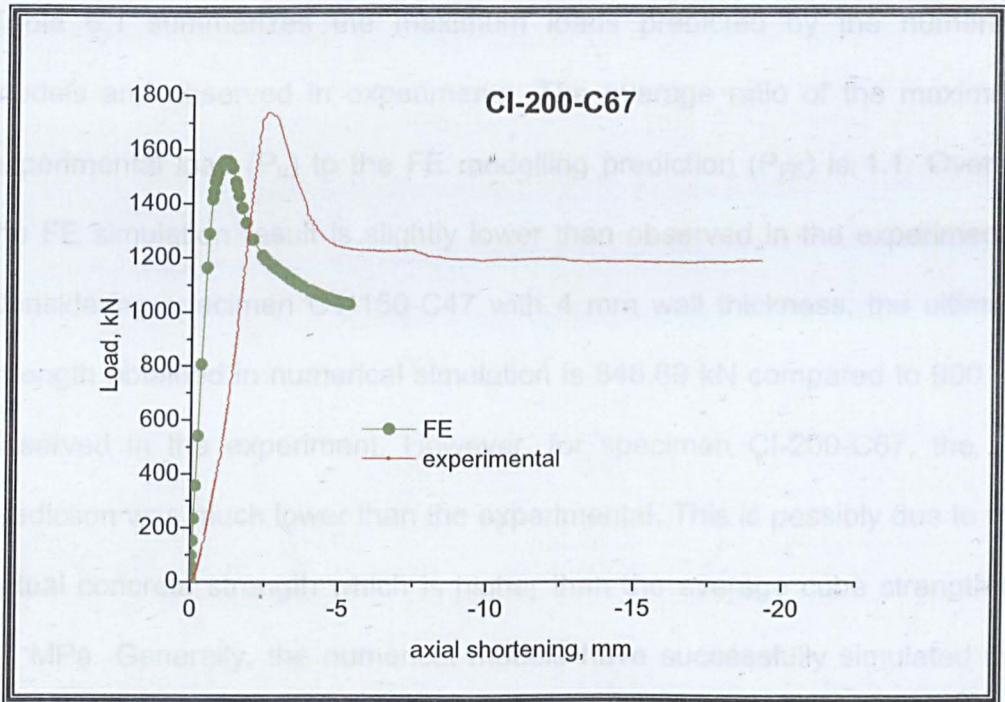


(c)

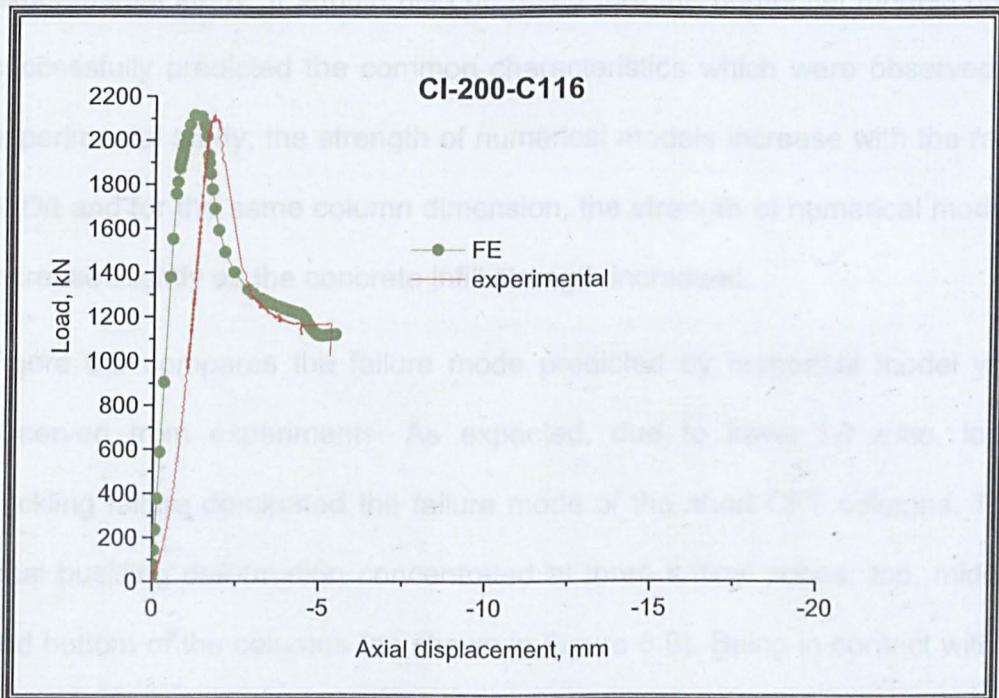
Figure 6.7: Load-axial shortening curves of stub CFT columns with 150x75x4 mm tube size



(a)



(b)



(c) CFT columns size 200x100x5 mm

Figure 6.8: Load-axial shortening curves of stub CFT columns with 200x100x5 mm tube size

Table 6.1 summarizes the maximum loads predicted by the numerical models and observed in experiments. The average ratio of the maximum experimental load (P_u) to the FE modelling prediction (P_{FE}) is 1.1. Overall, the FE simulation result is slightly lower than observed in the experiments. Considering specimen C1-150-C47 with 4 mm wall thickness, the ultimate strength obtained in numerical simulation is 848.69 kN compared to 900 kN observed in the experiment. However, for specimen CI-200-C67, the FE prediction was much lower than the experimental. This is possibly due to the actual concrete strength which is higher than the average cube strength of 67 MPa. Generally, the numerical models have successfully simulated the maximum load capacity of short CFT columns as have been observed in the experimental study. It should also be noted that the numerical models have successfully predicted the common characteristics which were observed in experimental study; the strength of numerical models increase with the ratio of D/t and for the same column dimension, the strength of numerical models increase slightly as the concrete infill strength increased.

Figure 6.9 compares the failure mode predicted by numerical model with observed from experiments. As expected, due to lower L/r ratio, local buckling failure dominated the failure mode of the short CFT columns. The local buckling deformation concentrated at three critical zones: top, middle and bottom of the columns (as shown in Figure 6.9). Being in contact with a rigid medium, the local buckling of steel tube takes place in the form of outward buckles, which is due to the restraining action of the steel tube. However, these models were not successful in simulating the shear failure of high strength concrete core. This is possibly due to the constitutive concrete

properties model adopted in the FE models which did not accurately reflect the behaviour of SCC in the elliptical hollow tube particularly for HSC.

Table 6.1: Comparison of maximum loads

	Label	Test failure load P_U (kN)	FE failure load P_{FE} (kN)	P_U/P_{FE}
Series I	CI-150-C47	900	848.69	1.06
	CI-150-C62	1139	945.13	1.21
	CI-150-C106	1239	1232.4	1.01
	CI-200-C34	1232	1183.87	1.04
	CI-200-C67	1737	1558.96	1.11
	CI-200-C116	2116	2111.69	1.00
				average
			Standard deviation	0.1

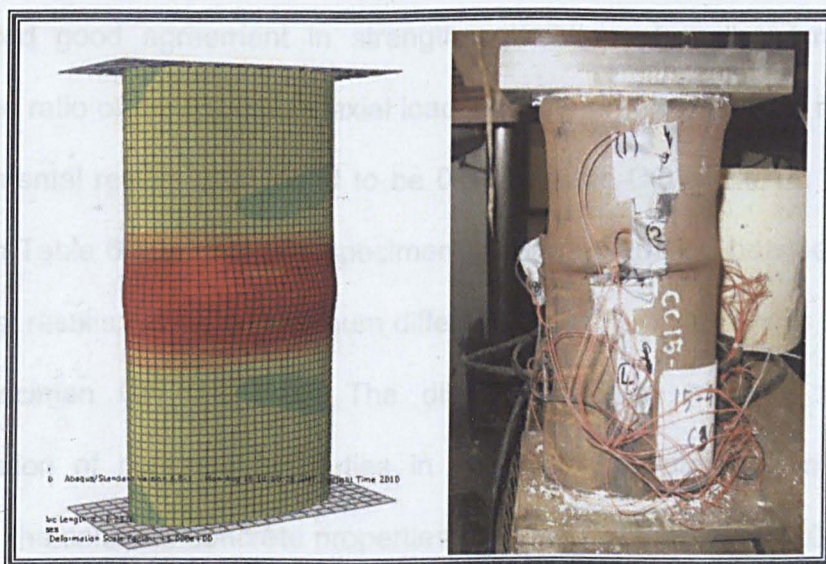


Figure 6.9: Comparison of failure mode observed in stub FE model

6.4.3 Validation of Long Columns

As described in earlier sections, geometric imperfection has significant effect to the structural behaviour of long CFT columns. With the measured out-of-straightness in the range of between 0.3 to 1.3 mm, the global imperfection amplitude of $L/2000$ was employed through-out the study except in the case of specimen CII-200-C55. The amplitude value of approximately $L/500$ is found to be suitable for this case than the smaller imperfection measured by $L/2000$. For this particular case, the difference between the numerical results with the test results is 8.6% which suggested that larger geometric imperfection may have actually existed for the specimen.

In order to verify the FE modelling method for long CFT columns, axial maximum loading capacity, compressive load versus mid-height lateral displacement curves, deformed shape obtained from experiments were compared with results from FE models. Table 6.2 summarizes the maximum axial compressive loads of all specimens measured in experiments and predicted by the FE models. Overall, the proposed numerical models produced good agreement in strength estimations for all columns. The average ratio of the maximum axial load capacity predicted by FE models to experimental results was found to be 0.98 with the COV of 0.14. It can be seen in Table 6 that only one specimen has large variation between the FE and test results; with the maximum difference of 31% higher—was observed for specimen CIV-150-C100. The discrepancy may attribute from the domination of concrete properties in this typical section. As mentioned before, the confined concrete properties proposed by Han et al. (2007) were considered in this study. It is noteworthy to state that there are many variables which are known to affect the confinement on CFT columns, such

as the concrete compressive strength, shape of the tube cross section, L/D ratio and D/t ratio. Moreover, there is currently no analytical model which is able to take into account of the entire variables. The compressive cylinder values which were used in the analysis may not represent the true values of the concrete columns due to the size and different curing environment. All these factors may cause the differences between the numerical results and experimental results. In addition, it is difficult to use FE modelling to analyse columns under large deformation owing to the cracking in the tensile zone of concrete, which has potential to affect the convergence.

Figure 6.10 shows typical buckling deformation of long columns under axial compressive load. Generally the deformation predicted by the FE study replicated the failure mode observed in the experimental work. From the figure, local buckling at compression region observed in some of the tested specimens was not captured by the numerical models. This possibly is due to the local imperfection which was not introduced in the numerical models. In this study global imperfection was taken into account in FE models as it was observed in the experiments that the predominant failure mode of the elliptical columns under axial compressive loads was the global buckling. However local imperfection could also be considered in the models. Nevertheless, higher stress concentration mainly attributable to the excessive overall buckling of the specimens was observed at the columns' mid-height in both experiments and numerical models.

Table 6.2: Comparison of ultimate strength obtained from experiments and predicted by FE models

	Column labels	Length (mm)	Test failure load P_U (kN)	FE failure Load P_{FE} (kN)	FE/Test
Series II	CII-150-C26	1.5m	520.6	613.1	1.18
	CII-150-C58		742.8	711.9	0.96
	CII-150-C91		923.2	800.9	0.87
	CII-200-C29		938.4	1052	1.12
	CII-200-C55		1064	1164	1.09
	CII-200-C93		1480	1568.6	1.06
Series III	CIII-150-C20	1.79m	483.8	508	1.05
	CIII-150-C65		663.2	574.7	0.87
	CIII-150-C100		871.2	699.1	0.80
	CIII-200-C42		967.5	1014	1.05
	CIII-200-C63		1237	1256	1.02
	CIII-200-C98		1411	1473.5	1.04
Series IV	CIV-150-C23	2.5m	326.6	300.5	0.92
	CIV-150-C63		427	341	0.80
	CIV-150-C100		547.4	375.1	0.69
	CIV-200-C29		839	813.6	0.97
	CIV-200-C59		947	941.6	0.99
	CIV-200-C101		1072	1082.6	1.01
				average	0.98
				COV	0.14

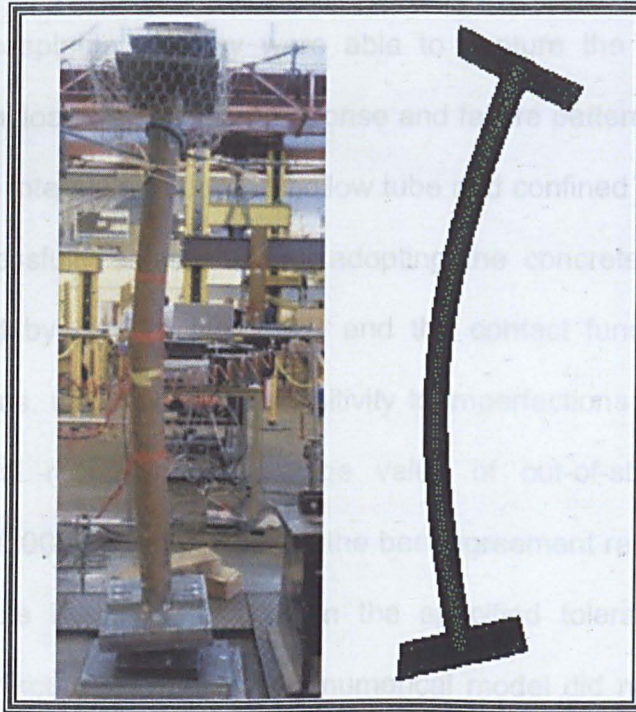
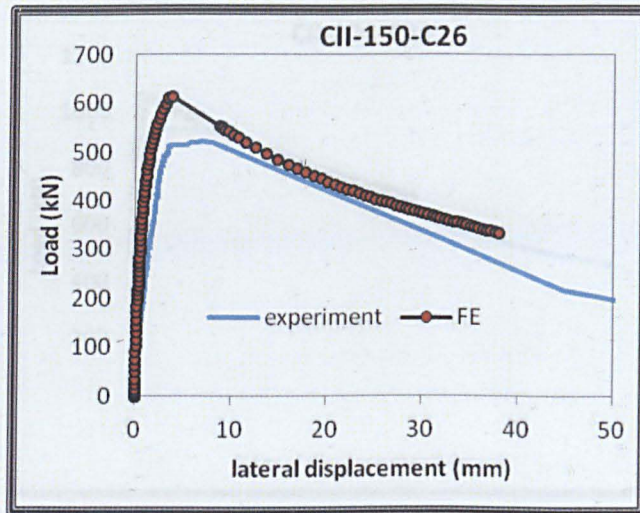


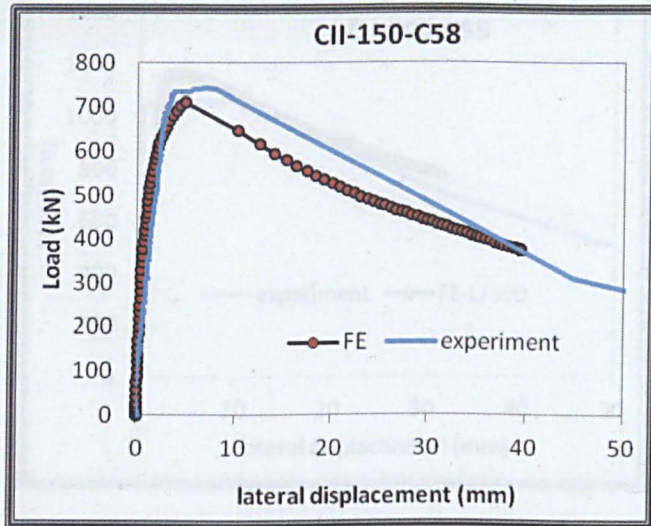
Figure 6.10: Typical deformation of long column FE model

The computed axial compressive load mid-height lateral deflection responses as compared with their experimental counterparts are depicted in Figures 6.11, 6.12 and 6.13. Overall, satisfactory agreement is achieved between the test results and those obtained from the numerical models, with the numerical models being able to predict accurately the initial stiffness, ultimate capacity, general load-lateral deformation response and failure mode observed in the experimental. From these figures, it is also evident that the increases in infill concrete strength increase the capacity of the columns. On the other hand, as the columns' slenderness increases, the load-carrying capacity drops significantly. It is also clear that most of the FE models were able to show the overall response of steeper decline in column strength once the ultimate loads were reached. Based on the comparisons

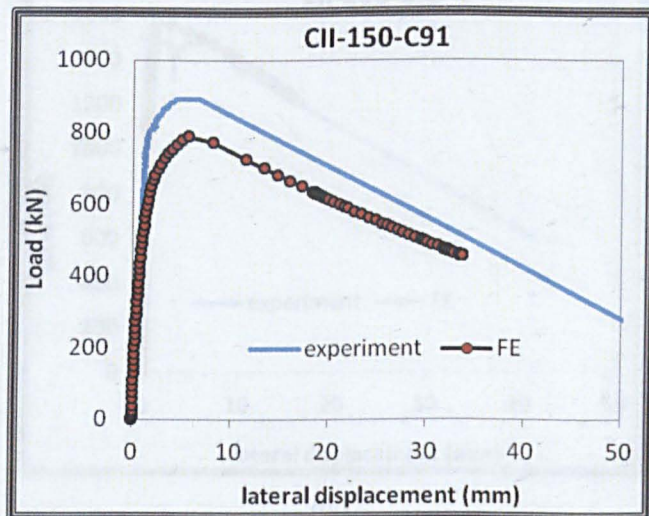
between numerical simulations and experimental results, the FE models was found to be acceptable as they were able to capture the ultimate load capacity, general load-deformation response and failure pattern as observed in the tests. The interaction between hollow tube and confined concrete core has been successfully established by adopting the concrete stress-strain model proposed by Han et al. (2007) and the contact function. For the particular columns, the anticipated sensitivity to imperfections was reflected in the numerical results. The average value of out-of-straightness of approximately $L/2000$ not only provides the best agreement results between the FE and tests but it is also within the specified tolerance with the measured imperfection. However, one numerical model did not predict the ultimate load very well. The accuracy of the material properties adopted during the modelling may have accounted for such discrepancy. It could also been seen from the trend pattern of the numerical models that the discrepancy may be dominated by the concrete properties for typical long column of size 150x75x4 mm. On the other hand steel properties dominated on the column of size 200 x100 x 5 mm. Nevertheless, the simplification considered in the FE model and the confined concrete constitutive model is sufficient in the prediction of the axial compressive response of the elliptical CFT columns.



(i)



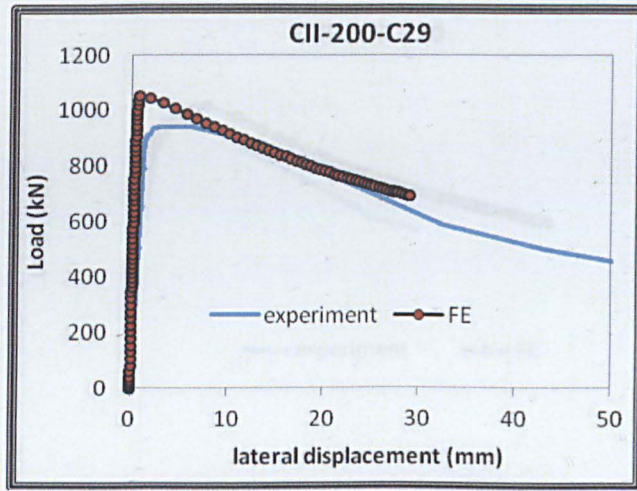
(ii)



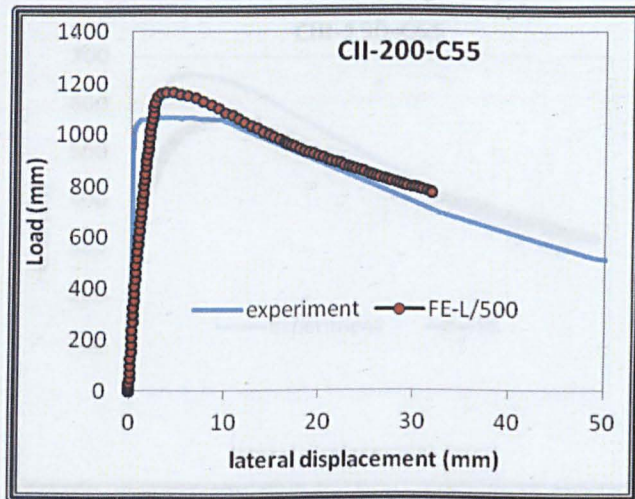
(iii)

(a) 150x75x4 mm tube size

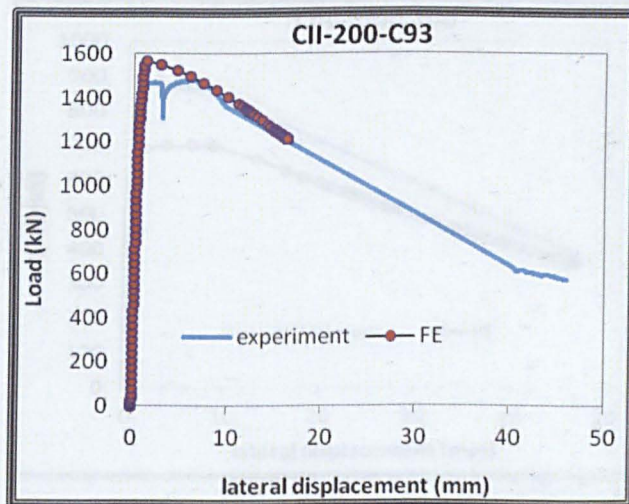
Figure 5.11: Comparison of experimental and FE results for Series II columns



(i)



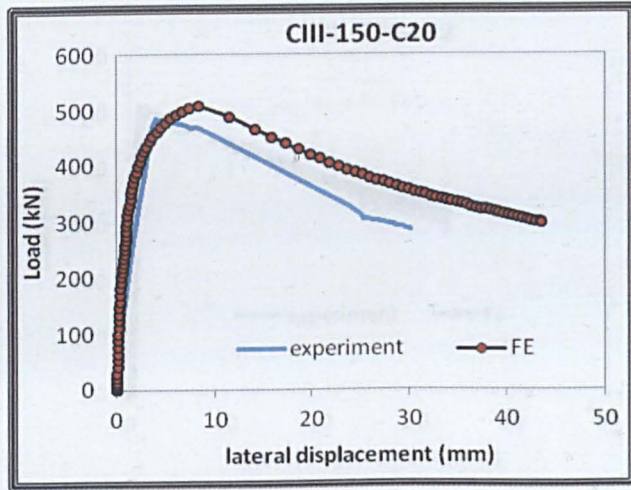
(ii)



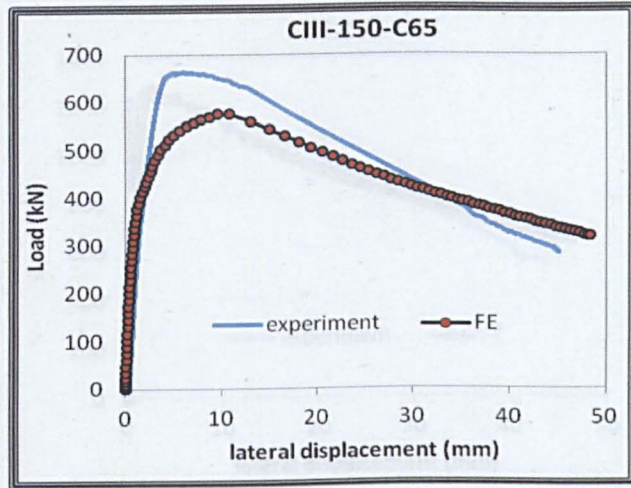
(iii)

(b) 200x100x5 mm tube size

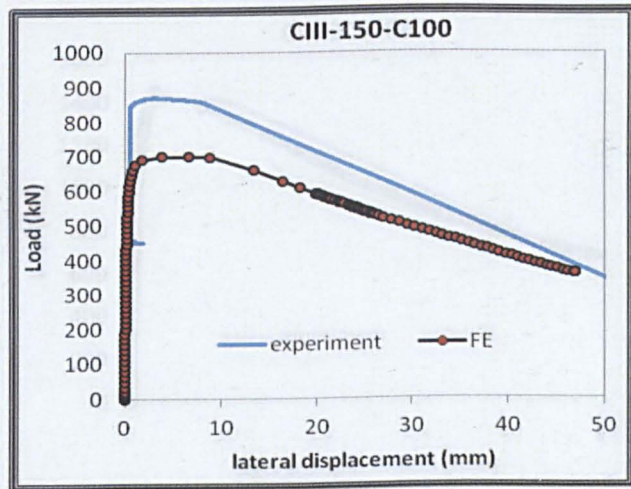
Figure 6.11: Comparison between test and FE models of Series II columns



(i)



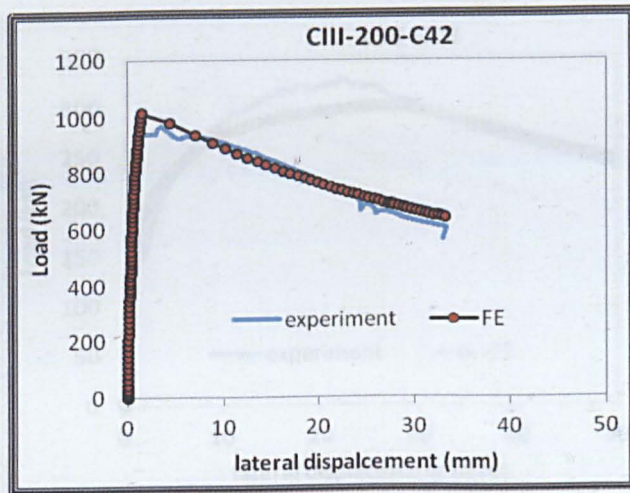
(ii)



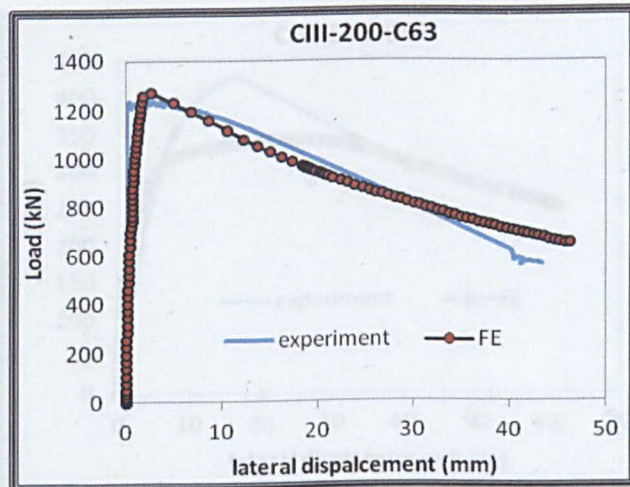
(iii)

(a) 50x75x4 mm tube size

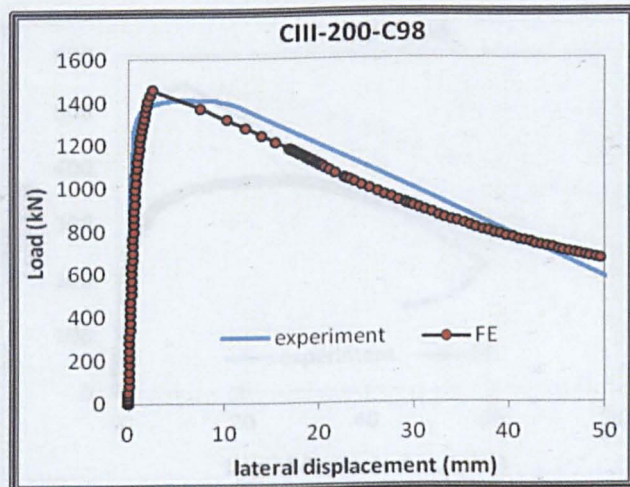
Figure 6.12 Comparison between test and FE models of weak III columns



(i)



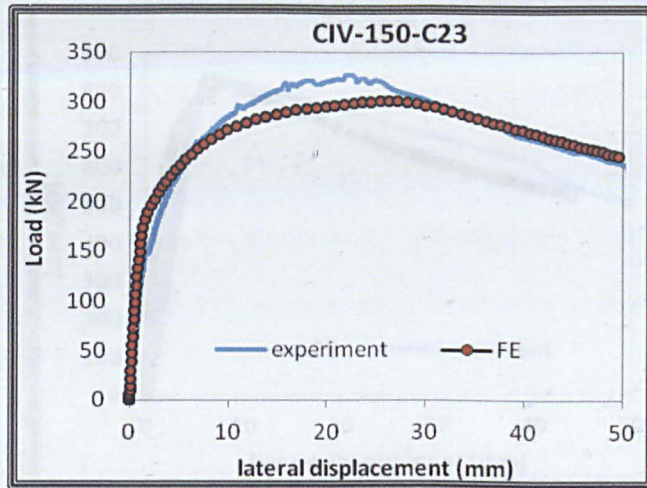
(ii)



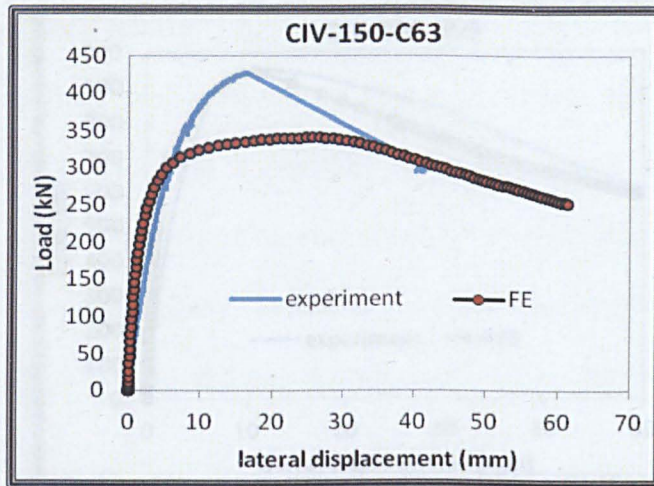
(iii)

(b) 200x100x5 mm tube size

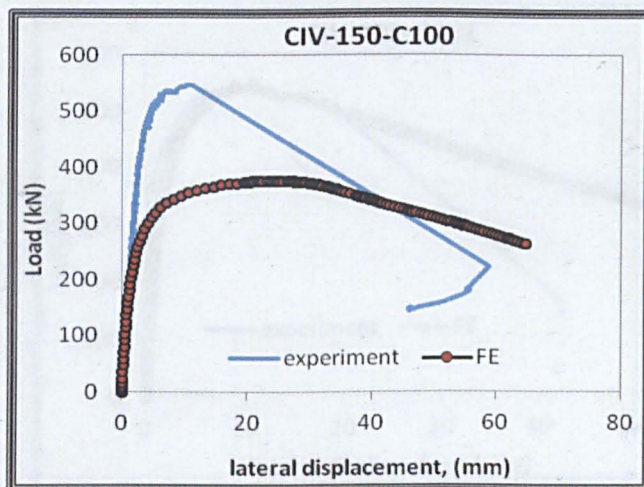
Figure 6.12: Comparison between test and FE models of Series III columns



(i)



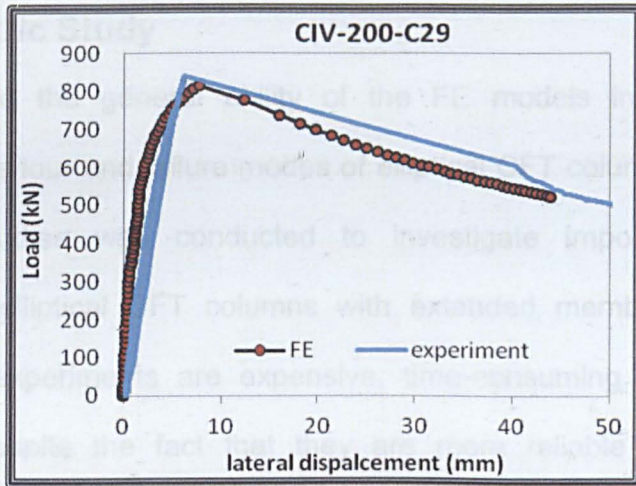
(ii)



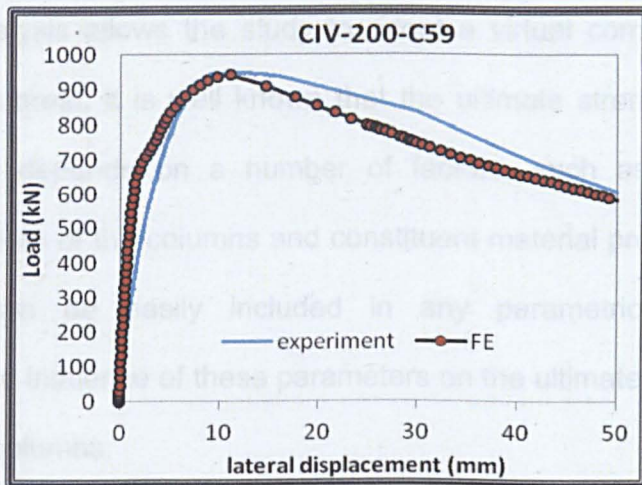
(iii)

(a) 150x75x4 mm tube size

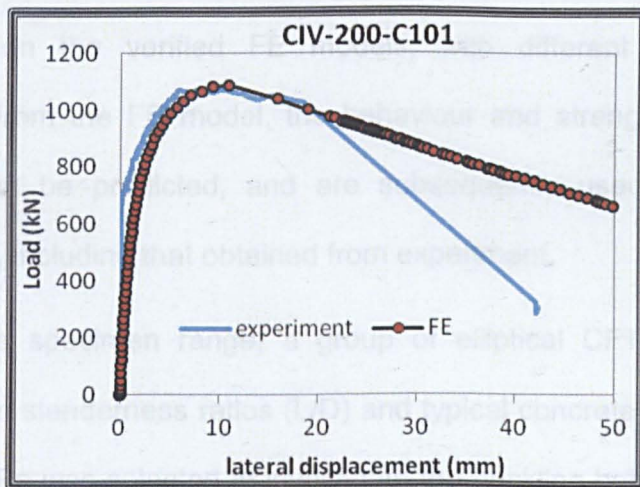
Figure 9.13 Comparison between test and FE results for CIV-150-C23, CIV-150-C63 and CIV-150-C100



(i)



(ii)



(iii)

(b) 200x100x5 mm tube size

Figure 6.13: Comparison between test and FE models of Series IV columns

6.5 Parametric Study

Having verified the general ability of the FE models in capturing the structural behaviour and failure modes of elliptical CFT columns, a series of parametric studies was conducted to investigate important structural behaviour of elliptical CFT columns with extended member geometrical features. As experiments are expensive, time-consuming and practically impossible, despite the fact that they are more reliable and played a significant role in research, the finite element model is more affordable. Numerical analysis allows the study to adopt a virtual combination of the parameters' interest. It is well known that the ultimate strength of elliptical CFT columns depends on a number of factors, such as cross-section dimension, length of the columns and constituent material properties. These parameters can be easily included in any parametric study which investigates the influence of these parameters on the ultimate strength of the elliptical CFT columns.

The parametric study is generally conducted by executing one application many times on the verified FE models, with different sets of input parameters. From the FE model, the behaviour and strength of the 'new' specimens can be predicted, and are subsequently used to add more available data, including that obtained from experiment.

To extend the specimen range, a group of elliptical CFT columns with various column slenderness ratios (L/D) and typical concrete strength of 30, 60 and 100 MPa was selected to investigate the buckling behaviour. A total of 21 column specimens were analyzed in the parametric study. The studies covered three tube size sections and various column lengths up to 4.5 m. A

global imperfection of $L/2000$ was assumed for all columns due to their greater slenderness. The FE modelling method was similar to the approach adopted for the previous numerical study.

Table 6.3 lists the selected specimen dimensions and maximum load capacity obtained from numerical modelling. As expected, the load capacity of CFT columns was influenced by column slenderness and the concrete infill strengths. Figure 6.14 shows the relationship of the column strengths and concrete cube strength obtained from the parametric study. From the table and figure, it can be seen that the column strengths increase linearly with the concrete cube strength. The parametric results are used to evaluate the reduction factor and the non-dimensional slenderness relationship as further described in Section 7.4.4.

Table 6.3: Parametric studies for flexural buckling

Group	Specimen	Dimensions (mm)	Cube concrete grade	Length (mm)	P_{FEM} (kN)
C1	S1	150x75x4	C30	3000	242.6
	S2		C60		275.7
	S3		C100		300.5
C2	S4	150x75x4	C30	3500	179.7
	S5		C60		205.1
	S6		C100		220.3
C3	S7	200x100x5	C30	3000	696.2
	S8		C60		801.8
	S9		C100		906.7
C4	S10	200x100x5	C30	3500	534.3
	S11		C60		620.0
	S12		C100		688.2
C5	S13	300x150x8	C30	1500	2584
	S14		C60		3304
	S15		C100		3997
C6	S16	300x150x8	C30	2500	2470.8
	S17		C60		3090.6
	S18		C100		3605.2
C7	S19	300x150x8	C30	3500	2200
	S20		C60		2608.6
	S21		C100		2988.9
C8	S22	300x150x8	C30	4500	1625
	S23		C60		1851.5
	S24		C100		2078.1

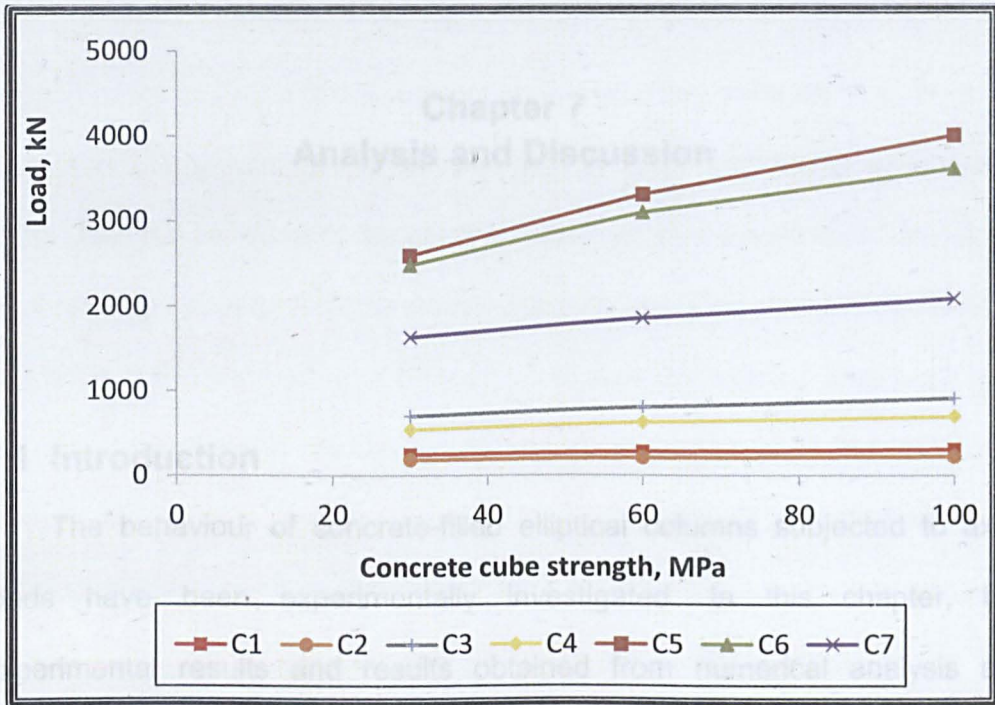


Figure 6.14: Column strength and concrete cube strength relationships obtained from parametric study.

7.2. Stub Columns

A review of available experimental studies shows that there are several parameters affecting the behaviour and strength of concrete-filled columns. These include geometrical parameters, such as the slenderness, the D/t ratio as well as the mechanical parameters, such as the strength of the steel and concrete, the loading and boundary conditions and the degree of concrete confinement. In the stub columns series, the test parameters were column slenderness, concrete test strengths and column dimensions. The test results demonstrate the influence of these parameters on the strength and behaviour of concrete-filled steel tubular columns.

Chapter 7

Analysis and Discussion

7.1 Introduction

The behaviour of concrete-filled elliptical columns subjected to axial loads have been experimentally investigated. In this chapter, the experimental results and results obtained from numerical analysis are discussed. Indicators such as Strength Enhancement Index, SI and Ductility index, DI were introduced to quantify section ductility and to assess the contribution of composite action and strain hardening in the structures respectively.

7.2 Stub Columns

A review of available experimental studies shows that there are several parameters affecting the behaviour and strength of concrete-filled columns. These include geometrical parameters, such as the slenderness, the D/t ratio as well as the mechanical parameters, such as the strength of the steel and concrete, the loading and boundary conditions and the degree of concrete confinement. In the stub columns series, the test parameters were column slenderness, concrete infill strengths and columns' dimensions. The test results demonstrate the influence of these parameters on the strength and behaviour of concrete-filled steel tubular columns.

One of the main benefits of the concrete filling is that it is substantial in load bearing capacity of the composite columns. Referring to Figure 5.4, the load-axial shortening relationship of stub hollow and concrete filled sections shows that the increase of the concrete strength has a positive effect on the load carrying capacity of concrete-filled steel tubes. One should note that the presence of the concrete infill not only increases the ultimate load but it also increases the flexural rigidity as evidenced by the slope of the curves. In comparison to the hollow columns, the strength of the composite is approximately more than 50% higher as a result of the presence of concrete core.

The laterally restrained concrete has also been recognised to withstand more loads compared to similar unrestrained concrete. This fact has been exploited in CFT columns in which the concrete core is subjected to lateral pressure due to confining stress. From the experimental investigation, it becomes apparent that the ultimate load, P_u for short CFT columns is considerably higher than the nominal strength, which is probably due to the occurrence of confinement effect in the structures. From Figure 5.4 it can be seen that a horizontal plateau softening branch was obtained after the peak load was achieved. This phenomenon shows that the stub CFT columns are able to achieve stability following the ultimate load before its failure, which is due to the concrete confinement as expected. It is well known that the beneficial effect of the confinement which exists in advanced stages of loading is due to the difference of poisson ratio, μ in steel and concrete. Notably, the effects could be predicted since the crushed concrete was compacted as the deformed concrete core was further loaded. Since the stub columns were able to carry further loading after the ultimate load was

achieved as compared to the steep drop of load in the long columns, this clearly suggests that the concrete confinement was more pronounced in the case of the short columns. Observations on the experimental results also highlighted the fact that the columns' capacity increases as the concrete core strength increases as tabulated in Table 7.1. The increase in strength of a steel tube due to concrete filling is given by the ratio P_{CFT}/P_h . For the columns tested, the value of this ratio ranges from 1.71 to 2.61. The values show a clear pattern of increase in the ratios which indicated that the strengths of CFT columns were dominated by the concrete strength.

Table 7.1: Analysis of experimental results of stub columns

	Label	P_u (kN)	P_{CFT}/P_h	DI	SI
Series I	CI-150h	525			
	CI-150-C47	900	1.71	2.78	0.96
	CI-150-C62	1139	2.17	1.41	1.14
	CI-150-C106	1239	2.36	1.36	0.87
	CI-200h	810.7			
	CI-200-C34	1232	1.52	1.74	1.01
	CI-200-C67	1737	2.14	1.39	1.15
	CI-200-C116	2116	2.61	1.23	1.07

Progress in concrete technology has utilised the high strength concrete in CFT columns. When the high strength concrete and the hollow steel tubes were used together, thus the more brittle nature of the concrete strength was partially mitigated by the confinement from the steel tube. This can be seen as the increments in capacity which was found to be insignificant for

columns with HSC since the columns exhibited smaller confinement effects due to low dilatation of concrete which prevented any confinement effect. Confinement is known as providing an advantage in the ultimate strength of CFT column. It is achieved when the micro cracking of the concrete core increases so as to enable the concrete infill to expand and exert the lateral compressive stress on the steel tube. However, as the compressive strength increases, the stiffness of the concrete also increases. Therefore it will result in less lateral expansion of concrete core which requires mobilising the restraint offered by the steel tube, which is reflected in less confinement. Greater confinement normally occurs in NSC owing to the nature of the concrete characteristic that contains a greater volume percentage of coarse aggregate. The micro cracking in NSC also starts earlier than the HSC. It has been reported in Grauers (1993), that the compression micro cracking starts at about 30% of the ultimate stress. However, a very little micro cracking below 65% of the maximum stress has been observed in HCS; thus, the confinement effect was not effective in the respective columns. As the lower strength concrete infill began to crack and expand earlier, it can therefore be predicted that the majority of the columns' strength will depend on the confinement which the steel tube offers to the concrete core. In comparison with traditional concrete, the micro cracking in SCC was expected to take place earlier on, as the composition required lesser coarse aggregates and higher cementation ratio. Further support for this hypothesis comes from the experiment on cylinder concrete tests. From the tests, it had been shown that the corresponding longitudinal strains at the maximum load were in between 0.002-0.0025 $\mu\epsilon$. It had been expected that this is the strain at which the concrete core commenced to increase in volume. From Figure

5.4, for the case of specimens with high strength concrete infill columns, a very high inclination was observed compared to the other concrete strength infill which was also expected due to the brittleness of the concrete infill.

In order to facilitate higher efficient filling, good flowability should be achieved; thus, in SCC, there is higher fine material and less coarse material should be used in order to minimise friction in the mixture. However, this is thought to affect the contribution of aggregate interlocking or mechanical bonding in the concrete filling, and thereby results in having lower shear strength due to reduced shear friction. It should be noted that the local buckling occurred before the steel tubes reached the yielding stress. This indicates that it might be due to the failure of the concrete infill making the load carrying capacity of the stub column specimens with HSC of C100 being affected more significantly. This is because the concrete infill is more brittle than normal strength concrete which resulted in the failure of the specimen to resist further loading. Due to this reason the increment in load carrying capacity was not really significant compared to other concrete infill strengths.

7.2.1 Strength Enhancement Index, SI

The strength enhancement index, SI is introduced to assess the axial compressive capacity of CFT columns. This parameter is defined as the ratio of the maximum load capacity to the sum of nominal strengths or theoretical plastic capacity of the individual components in the composite columns; $N_{nom} = A_s f_y + A_c f_{ck}$. The ratio of this parameter is described as in Equation 7.1 whereas the results were tabulated in Table 7.1 and illustrated in Figure 7.1.

$$SI = \frac{P_u}{A_s f_y + A_c f_{ck}} \quad (7.1)$$

From this parameter, the contribution of composite action and strain hardening in the composite columns was reflected for the SI values higher than 1.0. This suggested the positive interaction between the components in the columns and confinement effect can be expected in such columns. In general the strength index, SI increases with the increase in the sectional dimension and decreases as the slenderness ratio increase. From Figure 7.1, this condition is further proven. The figure illustrates the ultimate load from the experiment and FE results have been normalised by the nominal strength. Like most of the values for the ratio greater than unity, this indicates that the cross-sections are capable of reaching the yield load—as observed from the results of the experiment. This is also due to the effect of confinement. Thus, the improvement in load carrying capacity for stub columns is believed to result from the strain hardening of steel tube which is expected from the stiffer region of the elliptical section that have low radius of curvature. From the figure, it can also be seen that the scale effect of concrete and steel from D/t ratio between these specimens is not significant to the strength of the columns.

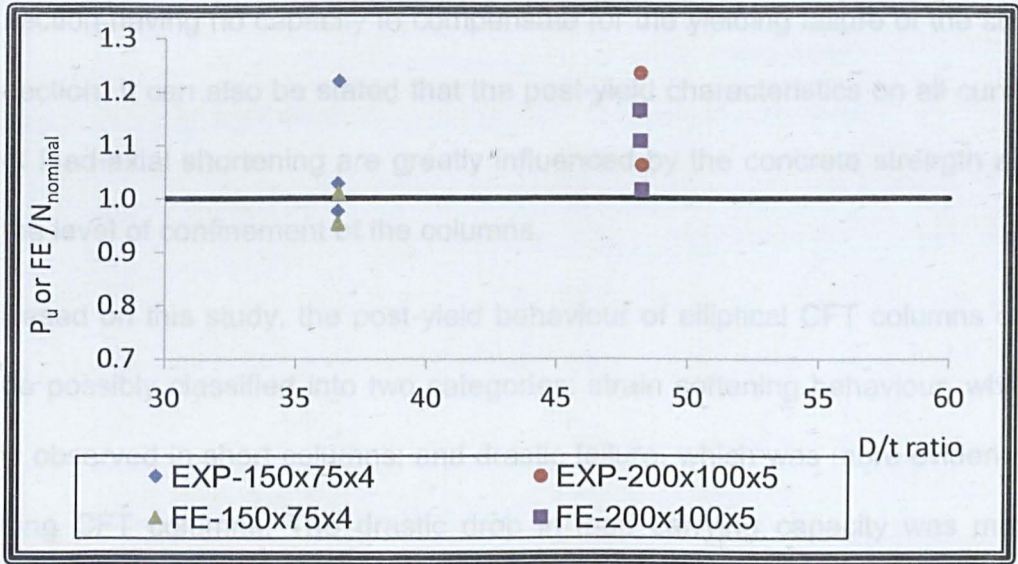


Figure 7.1: Strength and nominal ratio versus D/t ratio of stub columns

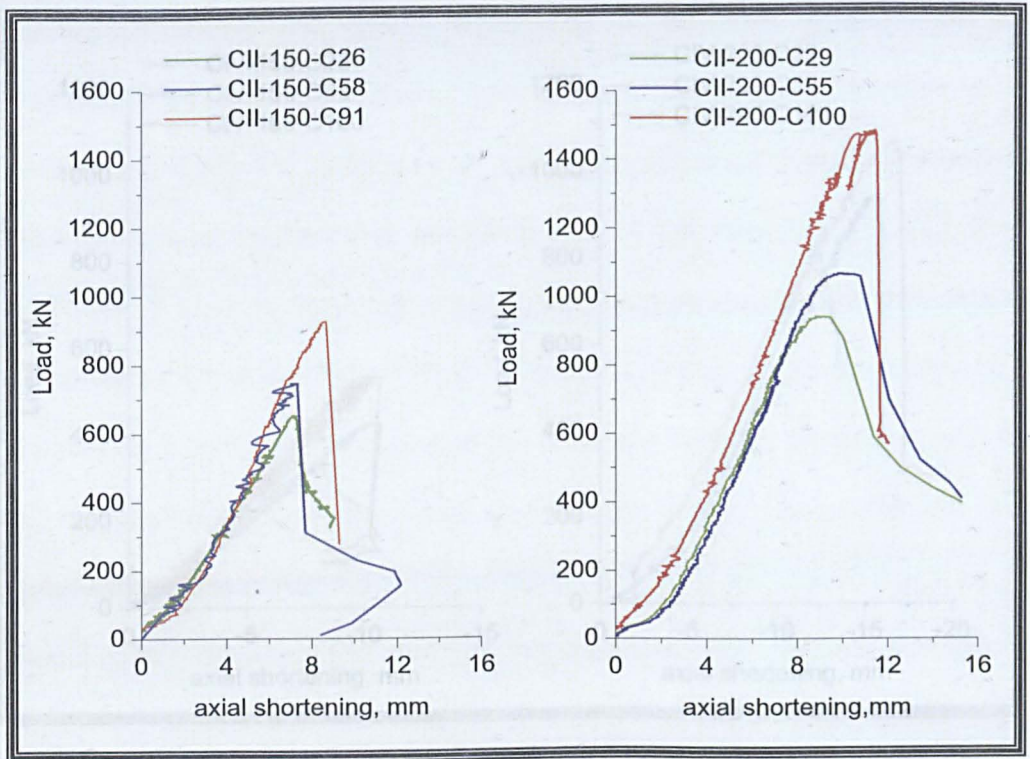
7.3 Long Columns

From the investigation, the increases in carrying capacity of the columns, is the result of being filled with concrete material. Apart from that it also depends on the characteristics of the materials used, the size of steel section, and columns lengths.

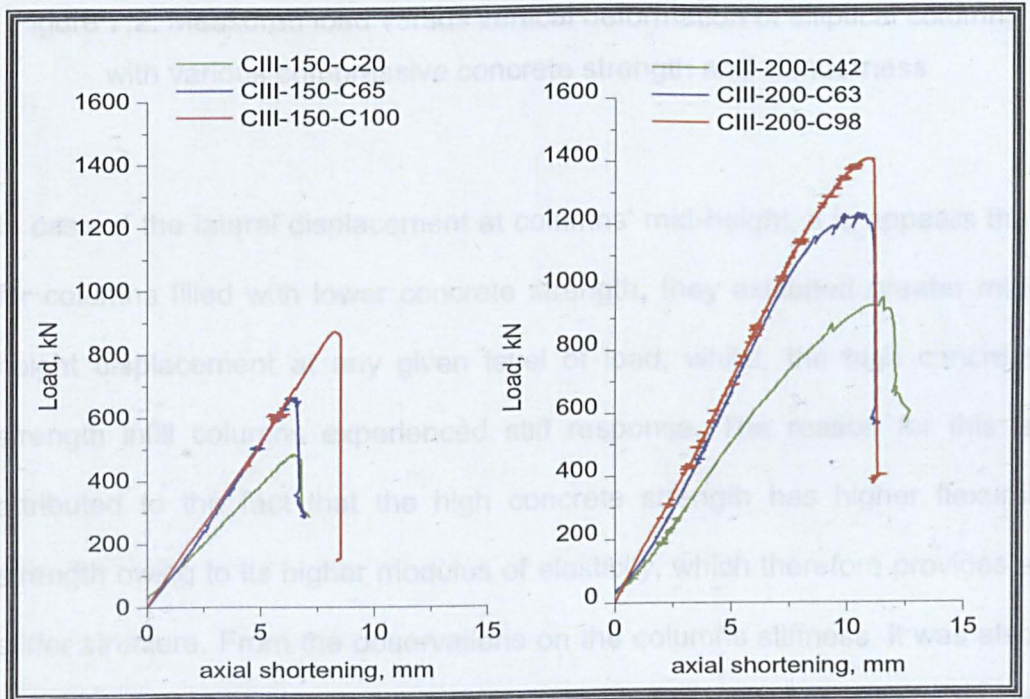
The load-axial displacement characteristic plotted in Figure 7.2 presents the responses of all long columns according to their lengths and sizes. From these curves, the information on the columns' carrying capacities and ductility were obtained. As illustrated, rapid deterioration in the axial capacities following after peak load in long columns was more obvious as the concrete strength increased. The effect resulted in a steeper descending branch, which indicates that the post-buckling strength of the columns is relatively low. A reason for this may be that the columns' vertical maximum strains were higher than the concrete core's compressive strains at its maximum compressive capacity, which therefore resulted in the concrete

section having no capacity to compensate for the yielding failure of the steel section. It can also be stated that the post-yield characteristics on all curves of load-axial shortening are greatly influenced by the concrete strength and the level of confinement of the columns.

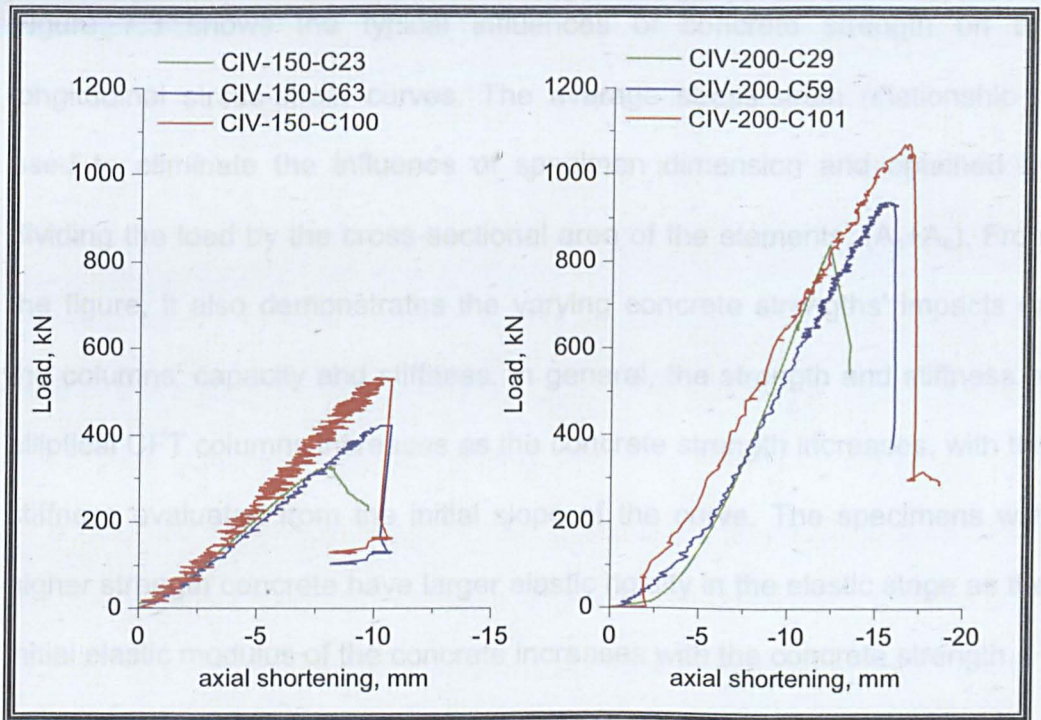
Based on this study, the post-yield behaviour of elliptical CFT columns can be possibly classified into two categories: strain softening behaviour, which is observed in short columns: and drastic failure, which was more evident in long CFT columns. The drastic drop in load carrying capacity was more pronounced in columns with higher concrete strength infill columns, as the columns were also observed to have flexural cracks at the tension side (Figure 5.9d), which is expected to cause the columns' flexural stiffness to decrease more quickly than in the case of the other concrete strength infill. Notably, this phenomenon can be related to the characteristics of higher strength concrete of SCC: the higher concrete strength of SCC was achieved by having highly fine material as compared to other strength and less coarse aggregates; this minimises friction in the mixture, which affects the mechanical bond in the concrete filling.



(a) Series II (Tubes' Length = 1.5m)



(b) Series III (Tubes' Length = 1.79m)



(c) Series IV (Length = 2.5m)

Figure 7.2: Measured load versus vertical deformation of elliptical columns with various compressive concrete strength and slenderness

In case of the lateral displacement at columns' mid-height, it appears that for columns filled with lower concrete strength, they exhibited greater mid-height displacement at any given level of load, whilst, the high concrete strength infill columns experienced stiff response. The reason for this is attributed to the fact that the high concrete strength has higher flexural strength owing to its higher modulus of elasticity, which therefore provides a stiffer structure. From the observations on the columns stiffness, it was also found that all long columns reached lateral deflections of more than 7 mm at maximum load.

Figure 7.3 shows the typical influences of concrete strength on the longitudinal stress-strain curves. The average stress-strain relationship is used to eliminate the influence of specimen dimension and obtained by dividing the load by the cross-sectional area of the elements, $(A_s + A_c)$. From the figure, it also demonstrates the varying concrete strengths' impacts on the columns' capacity and stiffness. In general, the strength and stiffness of elliptical CFT columns increases as the concrete strength increases, with the stiffness evaluated from the initial slope of the curve. The specimens with higher strength concrete have larger elastic rigidity in the elastic stage as the initial elastic modulus of the concrete increases with the concrete strength.

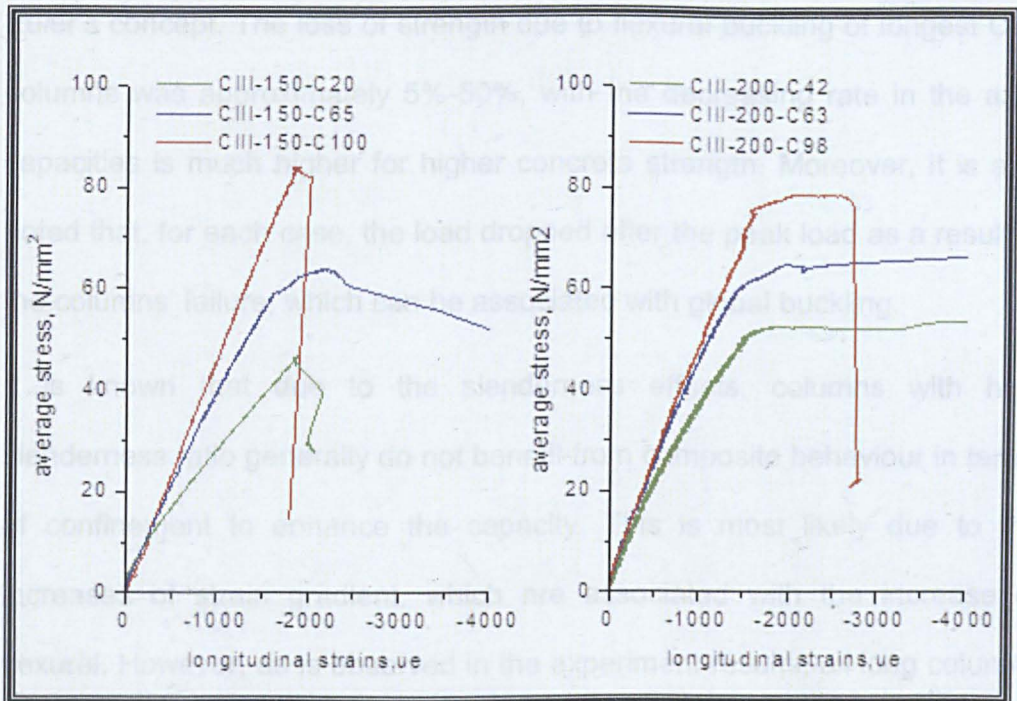


Figure 7.3: Stress-strain relationship curves of long columns

7.3.1 Slenderness

The effects of slenderness ratio, λ is important to consider as, in practise, the slenderness ratio varies in multi-storey building. The slenderness ratio, λ

is defined as the ratio of effective length of a column to the radius of gyration of its cross section, L/r . To study the effects of slenderness on the behaviour of elliptical composite columns, slenderness ratios varying from 16 to 143 were considered.

The increments in axial strength varied substantially, with the slenderness ratio of the columns being seen from Figure 7.4 and Table 7.2. The effects then were examined by comparing specimens of the close concrete strength. The experimental failure load is seen to be adversely affected when the height of the columns increases. The trend of a detrimental effect upon the column capacity as the slenderness ratio increases agrees with the Euler's concept. The loss of strength due to flexural buckling of longest CFT columns was approximately 5%-50%, with the decreasing rate in the axial capacities is much higher for higher concrete strength. Moreover, it is also noted that, for each case, the load dropped after the peak load as a result of the columns' failure, which can be associated with global buckling.

It is known that due to the slenderness effects, columns with high slenderness ratio generally do not benefit from composite behaviour in terms of confinement to enhance the capacity. This is most likely due to the increases of strain gradient, which are associated with the increase of flexural. However, as is observed in the experiment results, all long columns failed by inelastic buckling which can be categorised as intermediate columns. The intermediate columns will undergo some steel yielding and/or concrete crushing before buckling occurs whereas the failure mode of slender columns is characterised by overall elastic buckling. This type of columns has a sufficiently large l/d ratio to cause buckling before any

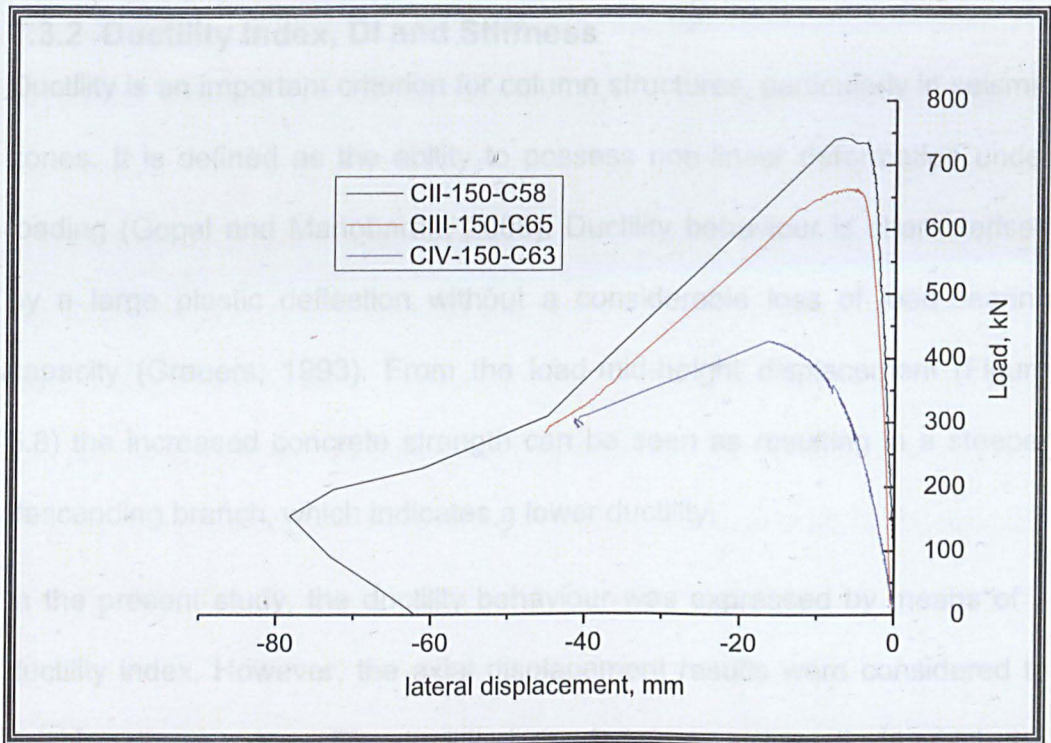
significant yielding occurs in the columns. However, from the observation, all long columns in the current study experienced steel yield before the buckling occurred and no concrete crushing was observed for higher slenderness columns.

Table 7.2: Analysis of long columns results

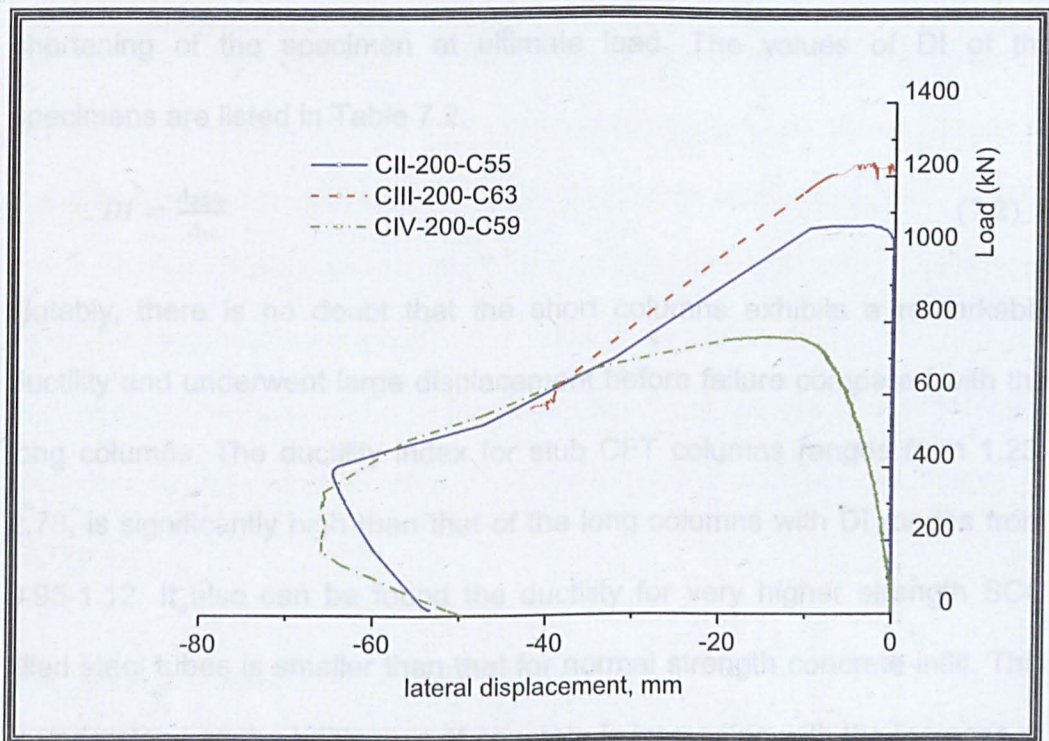
	Label	Pu (kN)	DI	λ
Series II	CII-150-C26	650.8	1.04	61.65
	CII-150-C58	742.8	0.97	61.73
	CII-150-C64	836	1.02	61.69
	CII-150-C91	923.2	1.01	61.62
	CII-200-C29	938.4	1.12	46.13
	CII-200-C55	1064	1.10	46.10
	CII-200-C93	1480	1.00	46.10
Series III	CIII-150C20	483.8	1.06	72.24
	CIII-150C65	663.2	1.01	72.24
	CIII-150C100	871.2	1.02	72.28
	CIII-200-C42	967.5	1.04	53.98
	CIII-200-C63	1237	1.06	54.01
	CIII-200-C98	1411.2	1.01	54.01
Series IV	CIV-150-C23	326.6	1.08	98.53
	CIV-150-C63	427	1.01	98.60
	CIV-150-C100	547.4	0.95	98.57
	CIV-200-C29	839	1.10	73.57
	CIV-200-C59	947	1.00	73.60
	CIV-200-C101	1072.3	1.01	73.57

The highest slenderness columns have greater flexibility which resulted in having greater mid-height displacement at any given load and lower stiffness compared to other tube lengths due to the instability phenomena. These phenomena were proven from the experimental results and as illustrated in Figure 7.4. Notably, as can be seen from the figures, the columns with higher slenderness (buckling length of 2680mm) have a lower maximum load than lower slenderness columns (buckling length of 1680mm) and they shed load much more quickly once the ultimate load is reached, therefore these columns are more ductile. From the curves, it is also evident that the elastic stage decreases and becomes shorter as the slenderness increases. This shows that the second-order effects are more evident with an increase of the slenderness ratio (Zhang and Guo, 2007).

The experimental results also indicate that all long column specimens failed at column's mid-height with buckling occurring at the major axis: such findings run parallel with the findings of the hoop strains at major vertices, where the strains were almost constantly larger than those at minor vertices which led to the failure at major vertices. The comparison between strains at different locations along the columns found the strain concentrating was recorded at the columns' mid-height. This is due to the global buckling mode of failure in these columns, which caused a higher stress concentrate at the region. It was also observed that all columns failed in a flexural mode with large lateral deflection as shown in Appendix B. Despite this failure mode, the local buckling of the steel tube was also observed in most of the columns and occurred generally near the specimen's mid-height.



(a) 150 x 75 x 4mm



(b) 200 x 100 x 5 mm

Figure 7.4: Load-mid height lateral displacement relationship with various columns' slenderness

7.3.2 Ductility Index, DI and Stiffness

Ductility is an important criterion for column structures, particularly in seismic zones. It is defined as the ability to possess non-linear deformation under loading (Gopal and Manoharan, 2006). Ductility behaviour is characterised by a large plastic deflection without a considerable loss of load-bearing capacity (Grauers, 1993). From the load-mid-height displacement (Figure 5.8) the increased concrete strength can be seen as resulting in a steeper descending branch, which indicates a lower ductility.

In the present study, the ductility behaviour was expressed by means of a ductility index. However, the axial displacement results were considered to calculate these values. The ductility index is taken as the ratio at which the strength of the specimen dropped to 85% of the ultimate load to the end shortening of the specimen at ultimate load. The values of DI of the specimens are listed in Table 7.2.

$$DI = \frac{\Delta_{85\%}}{\Delta_u} \quad (7.2)$$

Notably, there is no doubt that the short columns exhibits a remarkable ductility and underwent large displacement before failure compared with the long columns. The ductility index for stub CFT columns ranges from 1.23-2.78, is significantly high than that of the long columns with DI ranges from 0.95-1.12. It also can be found the ductility for very higher strength SCC filled steel tubes is smaller than that for normal strength concrete infill. This is understood as the brittleness of concrete is increasing with the increase of its strength.

In the case of long columns, from the values in Table 7.2, one can observe that the ductility decreases when the slenderness ratio increases. It is also

found that the ductility index decreases as the concrete strength increases, which is in-line with normal concrete behaviour. This can be expected due to the smaller confining effects arising in the columns compared with the columns with lower-strength concrete. The higher compressive strength concrete has less micro-cracking resulting in less lateral expansion, which accordingly leads to less restraint offered by the steel tube. Consequently, the concrete experiences less confining pressure and affects the columns' ductility and resistance. Furthermore, the load on columns with HSC tends to drop quickly after the peak load had been achieved; therefore, there is no obvious ductility improvement on the columns.

Stiffness in the present context is defined as the ability to resist lateral deformation. The stiffness of the CFTs columns is complicating due to the concrete core and interaction between the different materials (4). From the experimental results, load-axial shortening represents the axial stiffness of the member studied. It was found that the columns filled with NSC exhibit lower flexibility compared to HSC due to the fact that HSC has higher flexural strength as mentioned in 7.2. This is also likely to be influenced by the values of elastic modulus of the concrete infill whilst, columns with higher slenderness ratio were observed as having lower stiffness as shown in Figure 7.4.

7.4 Design Codes

Load carrying capacity of the structure is the most important aspect to consider in design. However, there is currently no capacity prediction in the case of elliptical composite column covered in any current design codes. Nevertheless, in this study the test results obtained from the experiment with

the design strengths as predicted by the Eurocode 4 (EC4) and American Specifications (AISC). The squash load of stub columns was regarded as an upper limit for the ultimate capacity of the corresponding long columns.

7.4.1 Eurocode 4 (BS EN 1994-1-1:2004)

Eurocode 4 (EC4) covers the design rules for encased, partially encased and concrete-infill columns both with and without reinforcements. The code applies to the column with steel grades S235 to S460 and with the normal weight concrete of strength classes C20/25 to C50/60. The design procedure for composite columns in this code was treated by a combination of both steel and concrete design approaches; however, the steel contribution ratio has to be checked in order to ensure the design method applicability for composite columns.

The simplified design method was adopted in this study. The method presented for the composite columns is of doubly symmetrical and uniform cross-section over the column height. For the long columns design, European buckling curves BS EN 1993-1-1 for steel columns were considered. The application of this method should fulfil its limit of applicability listed in the codes, otherwise the general method should be considered.

The resistance of the cross-section is calculated by assuming a fully plastic cross-section, the load of which must be distributed between the steel and the concrete. The resistance of stub CFT columns subject to compression was calculated as in equation 7.3 and equation 7.4. Equation 7.3 can be applied to composite CFT columns for CHS, RHS and SHS with the confinement effect neglected. The coefficient of 0.85 in the expression is replaced by 1.0 in the case of concrete filled section. It is notable that

equation 7.3 is similar to the sum of the general nominal strength of steel and concrete materials.

The nominal capacity of the cross-section is calculated under the assumption that the compressive capacity of the concrete and the yield capacity of the steel can be added. The compressive resistance, $N_{pl,RK(2)}$ of the CFT columns, as in Equation 7.4 is provided for CHS with consideration of the contribution of confinement provided by the tube.

$$N_{pl,RK(1)} = A_s f_y + 0.85 A_c f_c \quad (7.3)$$

$$N_{pl,RK(2)} = \eta_s A_s f_y + \left[1 + \eta_c \left(\frac{t}{D} \right) \left(\frac{f_y}{f_{ck}} \right) \right] A_c f_c \quad (7.4)$$

where η_s is a factor to reduce the tube strength to account for hoop stress whilst η_c is the increased strength of concrete core due to the confinement effect, both of which are determined to consider the interaction between the steel tube and concrete elements, and to account for the changes in the strength due to concrete confinement. The diameter, D of the CHS steel tube defined in the code was taken as an equivalent diameter, $D_o = \frac{2a^2}{b}$ and was considered. It is important to recognise that the columns exhibit enhanced resistance due to the tri-axial containment effects. However, according to the code, if $\bar{\lambda} > 0.5$ (as in equation 7.11), this effect should not be considered.

In this study, A_s and A_c were calculated as in Equation 7.5-7.7. The area of elliptical hollow cross-sectional of steel, A_s , was based on the study by Chan and Gardner (2008).

$$A_c = \pi ab \quad (7.5)$$

$$A_s = P_m \times t \quad (7.6)$$

$$P_m = \pi(a_m + b_m)(1 + 0.25h_m) \quad (7.7)$$

where P_m is the mean perimeter and t is the thickness of the elliptical section whilst $a_m = \frac{2a-t}{2}$ and $b_m = \frac{2b-t}{2}$ and $h_m = \frac{(a_m-b_m)^2}{(a_m+b_m)^2}$. The values of $2a$ and $2b$ are taken as the larger and smaller outer dimensions of the elliptical section.

Two methods of design which are general method and simplified method are available to design concrete-infill columns. In the former method, the second-order effects including residual stress, creep, and shrinkage of concrete are taken into consideration for the composite columns design. In the case of the simplified method, columns curves are used in order to determine the strength of long composite columns, which are restricted to doubly symmetrical and uniformed cross-section over the columns' length. Further assessment on the capacities of long CFT columns using the simplified method were based on the buckling curves. The squash load of the corresponding long columns was reduced by the reduction factor, χ which takes into consideration the influence of buckling in terms of the relative slenderness ratio and relevant buckling curve. A composite column with sufficient axial is given when:

$$N_{sd} \leq \chi \cdot N_{pl,Rk} \quad (7.8)$$

The reduction factor, χ for the relevant buckling mode, which is a function of modified slenderness, $\bar{\lambda}$ is determined from:

$$\chi = \frac{1}{\varphi + [\varphi^2 - \bar{\lambda}^2]^{\frac{1}{2}}} \leq 1 \quad (7.9)$$

where:

$$\varphi = 0.5[1 + \alpha(\bar{\lambda} - 0.2) + \bar{\lambda}^2] \quad (7.10)$$

The imperfection factor, α correspond to the relevant buckling curve.

The relative slenderness λ for the plane of bending being considered is given by;

$$\bar{\lambda} = \sqrt{\frac{N_{pl,Rk}}{N_{cr}}} \quad (7.11)$$

where, $N_{pl,Rk}$ is the resistance of the cross section to compression force and N_{cr} is the elastic critical normal force. For the determination of the relative slenderness $\bar{\lambda}$ and the elastic critical force N_{cr} , the characteristic value of the effective flexural stiffness $(EI)_{eff}$ of a cross section of a composite column should be calculated from;

$$EI = E_a I_a + 0.6 E_{cm} I_c + E_s I_s \quad (7.12)$$

where E_{cm} is the modulus of elasticity of concrete, I_a , I_c , and I_s are the second moments of area of the structural steel section, the un-cracked concrete section and the reinforcement for the bending plane being considered.

7.4.2 AISC 360-05

This code addresses the design of rolled and built-up composite columns. Two methods can be used in order to determine the nominal strength of composite sections: plastic stress distribution method and the strain-compatibility method, the former of which is used for the comparison of experimental results. Some limitations were imposed to the code: the concrete compressive strength shall be in a range of 21MPa to 70MPa and steel minimum yield stress shall not exceed 525 MPa.

The axial member strength, $\phi_c P_n$ and allowable compressive strength, $\frac{P_n}{\Omega_c}$ for axially loaded filled composite columns were determined for limiting the state of flexural buckling with the following:

Compressive strength design,

$$\phi_c P_n \quad (7.13)$$

Allowable compressive strength,

$$\frac{P_n}{\Omega_c} \quad (7.14)$$

With $\phi_c = 0.75$ (LRFD) and $\Omega_c = 2.00$. However, in all design calculation, these factors were set to unity. The value of P_n depending on $\frac{P_o}{P_e}$ relation;

$$P_o = A_s F_y + A_{sr} F_{yr} + C_2 A_c f'_c \quad (7.15)$$

$C_2 = 0.85$ for rectangular

$C_2 = 0.95$ for circular sections

$$P_e = \frac{\pi^2 E I_{eff}}{(KL)^2} \quad (7.16)$$

$$E I_{eff} = E_s I_s + E_s I_{sr} + C_3 E_c I_c \quad (7.17)$$

$$C_3 = 0.6 + 2 \left(\frac{A_s}{A_c + A_s} \right) \leq 0.9 \quad (7.18)$$

where KL is the effective length of the column.

For $P_e \geq 0.44 P_o$

$$P_{AISC} = P_o \left[0.658 \left(\frac{P_o}{P_e} \right) \right] \quad (7.19)$$

For $P_e < 0.44 P_o$

$$P_{AISC} = 0.877 P_e \quad (7.20)$$

7.4.3 Design Capacities

To evaluate the feasibility of available design codes in predicting the capacity of elliptical composite columns, the calculated ultimate loads predicted from the codes are compared with the column test results and numerical model. The main goal of this is to gauge the success of these two methods for computing the capacity of CFTs and, if necessary, to propose adjustments. To gauge the success of available design procedures in EC4 and AISC, the capacity of the aforementioned specimens was computed and compared against experimental results and numerical results. The reported study revolves around experimental data which was tested by the writer and it is associated to the FE results available from current study. The results are presented and discussed separately for short and slender columns.

7.4.3.1 Member strength of short columns

The column strengths, P_u obtained from the experimental works are compared with the un-factored design column strengths calculated using the EC 4 and the AISC. The P_u -to-design column strength ratios, P_u/P_{EC4} and P_u/P_{AISC} are summarized in Table 7.3. The column strengths predicted by AISC standard codes were conservative. The average ratio between the loads measured and computed strength, was, however, small for EC4. For the circular CFT columns, the AISC only allows for an increase of the usable concrete stress to account for the beneficial effects of the restraining hoop action arising from transverse confinement by increasing the multiplier of 0.85 to 0.95 (Lu and Zhao, 2010) and only EC4 presents a detailed formulation to estimate this contribution. From the results, it seems that the confinement corresponds to the higher differences of ultimate load between these codes. Therefore the confinement effect can be expected to occur in

the columns section which is attributed to from the composite action between the constituent elements. Consequently, it leads to the increment of the short elliptical columns' strength.'

For each column, the ratio of P_u/P_{EC4} is normally somewhat greater than unity as shown in Table 7.3. The results also indicate that the Eurocode 4 predicts a lower value than the test and thus 'safe' results were obtained. The average failure load ratio, P_u/P_{EC4} of 1.2 with coefficient of variation, COV of 0.1 was determined between the comparison of the experimental and the code prediction.

The equivalent diameter, D_e has been proposed by Chan and Gardner (2008) based upon the point along the circumference of an ellipse at which local buckling initiates. From this study, the considerations of equivalent diameter of $2a^2/b$ for elliptical CFT columns reasonably estimate the elliptical CFT columns capacities. Thus, there is no doubt that the EC4 method is generally comparable to those from experimental and numerical. The influences of concrete enhancement, steel reduction due to biaxial effects and column slenderness were all incorporated in the design rules of circular concrete-filled tubes is reliable to be considered for elliptical CFT columns.

Table 7.3: Calculated strength comparison for stub CFT columns

Label	P_u	P_{EC4}	P_{AISC}	P_{FE}	P_u/P_{EC4}	P_u/P_{AISC}	P_u/P_{FE}
CI-150-C47	900	909.6	677.4	848.69	1.0	1.3	1.06
CI-150-C62	1139	968.2	725.7	945.13	1.2	1.6	1.21
CI-150-C106	1290	1299.3	1002.5	1232.4	1.0	1.3	1.01
CI-200-C34	1232	1050	808.5	1183.87	1.2	1.5	1.04
CI-200-C67	1737	1298.2	1128.3	1558.96	1.3	1.5	1.11
CI-200-C116	2116	1710.8	1616.4	2111.69	1.2	1.3	1.00
Average					1.1	1.4	1.1
COV					0.1	0.1	0.1

7.4.3.2 Member strength of long columns

Research on CFT columns has often been restricted to short specimens. Based on the evaluation made for stub columns, the best estimation of strength was obtained from EC4 due to the inclusion of concrete enhancement from confinement. In the case of long columns, there is little evidence of an increase in concrete strength due to the confinement. As in EC4 method, this effect was assumed insignificant for the columns when the non-dimensional slenderness of $\bar{\lambda} > 0.5$. In this case, the non-dimensional slenderness for all columns exceeds the value 0.5 and according to this code, the factors of η_s and η_c should be taken as 1 and 0 respectively. In this method, the uses of column design curves are all incorporated in the design rules.

The ratio between measured strength, P_u to the calculated strength, P_{EC4} and P_{AISC} is summarised in Table 7.4 and Table 7.5. The computed capacities from AISC tend to overestimate the reported values particularly for columns with higher slenderness; on the other hand, the capacities from

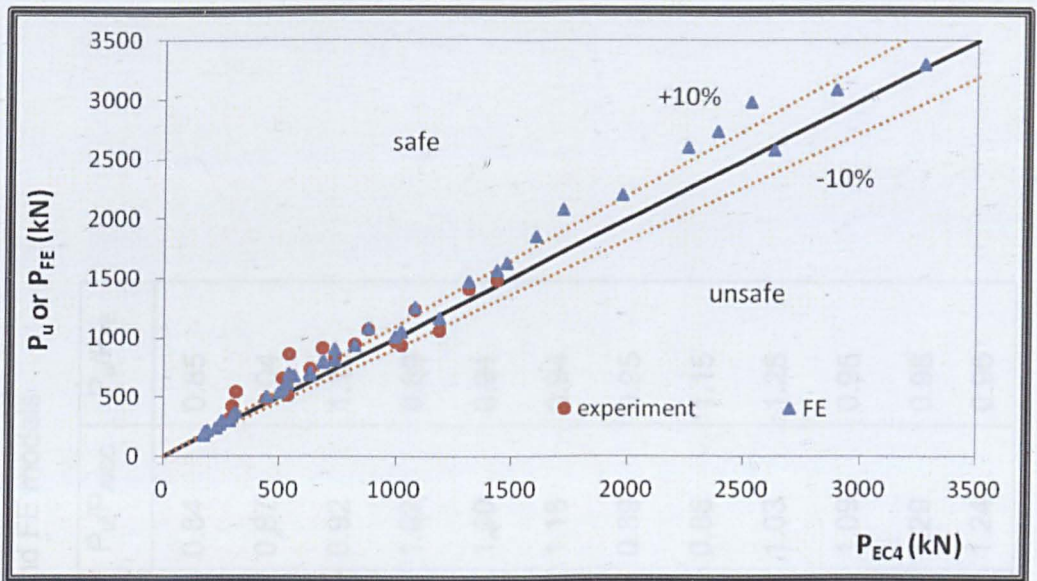
EC4 are smaller than measured values. On the average, the ratio of the measured capacity from experimental to calculated capacity is 1.19 with a COV of 0.19 (Table 7.4). As can be noticed, the values recommended by the EC4 showed good agreement with the experimental results. The highest difference was found for specimen CII-200-C55, where the experimental was 10% lower than EC4 values. In general, despite ignoring strain hardening in the steel material properties, the computed results by the EC4 procedure are fairly close to those measured from experimental.

Great differences between the axial capacities obtained from the experiment to the prediction of EC4 were also observed for HSC infill, but on the safe side. It should be noted that the standard code do not give any recommendations when high strength concrete is used in CFT columns. Nevertheless, with the developments in technology, the use of HSC member has proved to be most promising in terms of strength and stiffness as observed in current studies. However, it becomes brittle as the strength increases. The lack of ductility also may result in sudden failure. The strength and ductility may be improved by the use of spiral confinement, rectangular and circular ties in concrete members. As in CFT columns, the steel tube itself able to provide continued binding with the concrete member which may contribute to the higher columns' resistance.

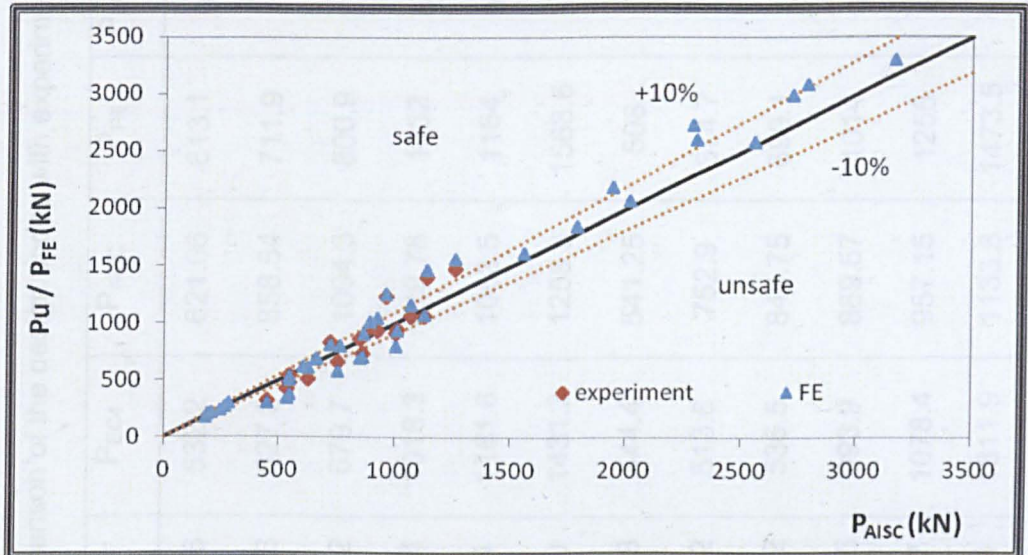
The ratio between the maximum experimental load and the design codes are also presented in Figure 7.5. Most of the tests and numerical prediction fall on the safe side within 10% of the difference predicted by EC4 code. However, for some results the ratio increases as the experiment load getting higher. In view of the aforementioned results which restricted within the limits

of the investigations reported above, it appears that the EC4 technique can reasonably provide a simple and reliable estimate column of both stub columns and long columns of elliptical concrete-filled tubes.

In the design of axial loaded CFT columns, either the strength of the cross-section or the stability of the member will govern the load carrying capacity is depending on the length of the columns. In the case of long columns, the increment in strength from confinement effect also could be expected in such columns as it was found the steel material has reached its yield strength and inspection on the concrete infill has found that most of the concrete, visually crushing. The situation may specify that these materials have reached their ultimate strength in the long columns however; due to the slenderness this effect was not fully developed. These show that the L/D ratio affects the confinement degree as well as load capacity. Lateral instability with low deformation and before the mobilization of the confinement is more prominent for higher L/D ratio columns. Thus, the approach from EC4 is the best estimation due to the exclusion of the concrete enhancement from confinement and the use of the column curve for column slenderness.



(a) Comparison to EC4



(b) Comparison to AISC

Figure 7.5: Ratio between experimental ultimate load, numerical results and codes provision

Table 7.4: Comparison of the design codes with experimental and FE models

Label	P_u	P_{EC4}	P_{AISC}	P_{FE}	P_u/P_{EC4}	P_u/P_{AISC}	P_u/P_{FE}
CII-150-C26	520.6	532.2	621.06	613.1	0.98	0.84	0.85
CII-150-C64	742.8	627.8	858.54	711.9	1.18	0.87	1.04
CII-150-C91	923.2	679.7	1004.3	800.9	1.36	0.92	1.15
CII-200-C29	938.4	1018.3	919.78	1052	0.92	1.02	0.89
CII-200-C55	1064	1181.6	1063.5	1164	0.90	1.00	0.91
CII-200-C93	1480	1431.3	1258.8	1568.6	1.03	1.18	0.94
CIII-150-C20	483.8	444.4	541.25	508	1.09	0.89	0.95
CIII-150-C65	663.2	513.6	752.9	574.7	1.29	0.88	1.15
CIII-150-C100	871.2	536.5	846.75	699.1	1.62	1.03	1.25
CIII-200-C42	967.5	993.9	889.57	1014	0.97	1.09	0.95
CIII-200-C63	1237	1078.4	957.15	1256	1.15	1.29	0.98
CIII-200-C98	1411	1311.9	1133.8	1473.5	1.08	1.24	0.96

Label	P_u	P_{EC4}	P_{AISC}	P_{FE}	P_u/P_{EC4}	P_u/P_{AISC}	P_u/P_{FE}
CIV-150-C23	326.6	284.9	448.77	300.5	1.15	0.73	1.09
CIV-150-C63	427	297.8	530.86	341	1.43	0.80	1.25
CIV-150-C100	547.4	311.1	542.01	375.1	1.76	1.01	1.46
CIV-200-C29	839	733.4	720.5	813.6	1.14	1.16	1.03
CIV-200-C59	947	818.5	1008.1	941.6	1.16	0.94	1.01
CIV-200-C101	1072	875.0	1122.8	1082.6	1.23	0.95	0.99
Average					1.19	0.99	1.05
COV					0.19	0.16	0.15

Table 7. 5: Comparison of the design codes with parametric study

Label	Length, L	P_{FE}	P_{EC4}	P_{AISC}	P_{FE}/P_{EC4}	P_{FE}/P_{AISC}
P 150x75x4	3000	242.6	229.3	244	1.06	0.99
		275.7	240.8	264	1.14	1.04
		300.5	251.9	284	1.19	1.06
	3500	179.7	173.2	179	1.04	1.00
		205.1	181.1	194	1.13	1.06
		220.3	188.7	209	1.17	1.05
P 200x100x5	3000	696.2	628.5	662.2	1.11	1.05
		801.8	684.8	763.5	1.17	1.05
		906.7	735.5	864.6	1.23	1.05
	3500	534.3	496.5	541.7	1.08	0.99
		620.0	530.8	603.9	1.17	1.03
		688.2	562.3	654.4	1.22	1.05

Label	P_{FE}	P_{FE}	P_{EC4}	P_{AISC}	P_{FE}/P_{EC4}	P_{FE}/P_{AISC}
P 300x150x8	1500	2584	2622.6	2551.4	0.99	1.01
		3304	3267.8	3161.2	1.01	1.05
		3997	4105.4	3955.9	0.97	1.01
	2500	2740.8	2379.8	2286.0	1.15	1.20
		3090.6	2888.1	2783.5	1.07	1.11
		3605.2	3485.7	3404.1	1.03	1.06
P 300x150x8	3500	2200	1972.4	1938.8	1.12	1.13
		2608.6	2252.5	2299.9	1.16	1.13
		2988.9	2520.1	2717.3	1.19	1.10
	4500	1625	1476.1	1556.4	1.10	1.04
		1851.5	1601.8	1783.1	1.16	1.04
		2078.1	1715.9	2012.1	1.21	1.03
Average					1.12	1.06
COV					0.07	0.05

7.4.4 Summary of Evaluation on Design Codes

The increase in the column slenderness decreases the load carrying capacity of composite columns. The obvious explanation for this condition is that for the short columns the steel section was expected to exert a lateral pressure on the concrete core and resulted in increases the capacity. The use of high concrete strength enhanced the load carrying capacity of the tested columns, but with a load–slenderness relationship decreasing at a higher rate compared to that for columns using normal strength concrete.

Figure 7.6 shows the ratio of the measured strength and predicted strength by the codes against slenderness ratio, L/r . Based on the limitations of the experimental results and on the basis of the comparisons, it appears that EC4 and AISC methods have satisfactorily predict the capacity of most of the columns. However, as can be observed in the figure, it clearly shows that the specimens demonstrate that the AISC method overestimates the capacities for columns in series IV. This is indicated by the unconservative results of P_u/P_{AISC} as the columns become slender. However, the EC4 predictions for axially loaded elliptical CFT columns were on the safe side. Nevertheless, an alteration needs to be considered for AISC design code, such as the use of higher slenderness reduction factor for the longest columns. In this study, the use of the actual yield stress and the concrete strength were considered in the calculation. It should be noted that, it is desirable for the material and load factor to be included to compensate any uncertainty such as the event of buckling due to accidental eccentricity.

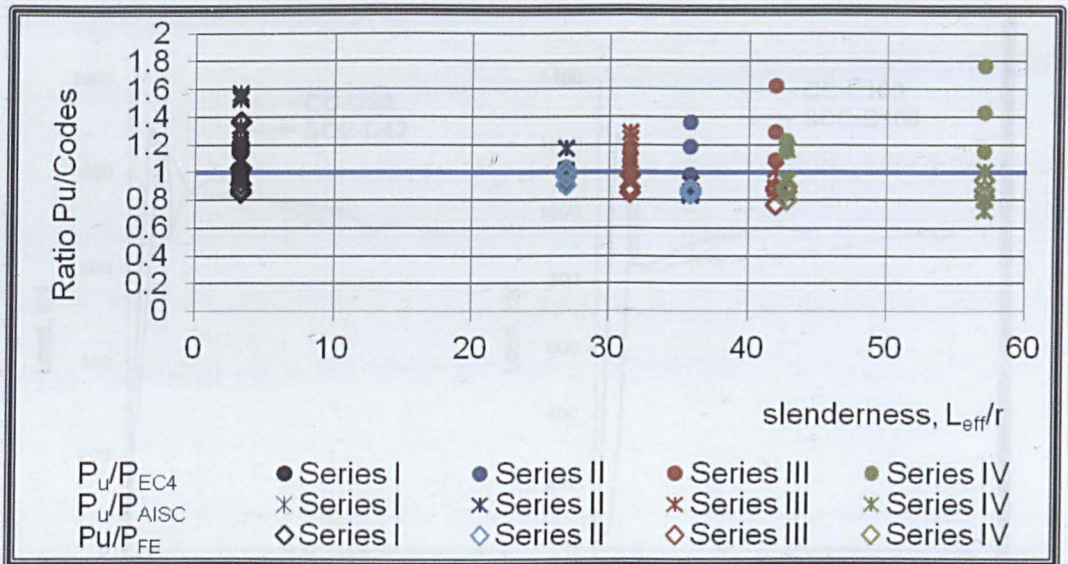


Figure 7.6: Ratio of measured strength and predicted strength from codes against slenderness

As far as the infill concrete is concerned, the used of SCC was found to be similar to those of the CFT columns with traditional concrete in terms of the strength. Shown in Figure, the results of stub columns were compared with the results of elliptical CFT columns with normal concrete which were carried out by Testo (2007). Overall, the experimental results show that the strength of SCC columns is less than the strength of conventional concrete, CC (Figure 7.7). This could be argued from the different mixture design of the SCC in which the fraction of fine particles is high and produces a preliminary micro cracking at low load. However, the comparisons also indicate that the strength prediction using the existing design codes developed for normal concrete-filled seems valid for SCC filled.

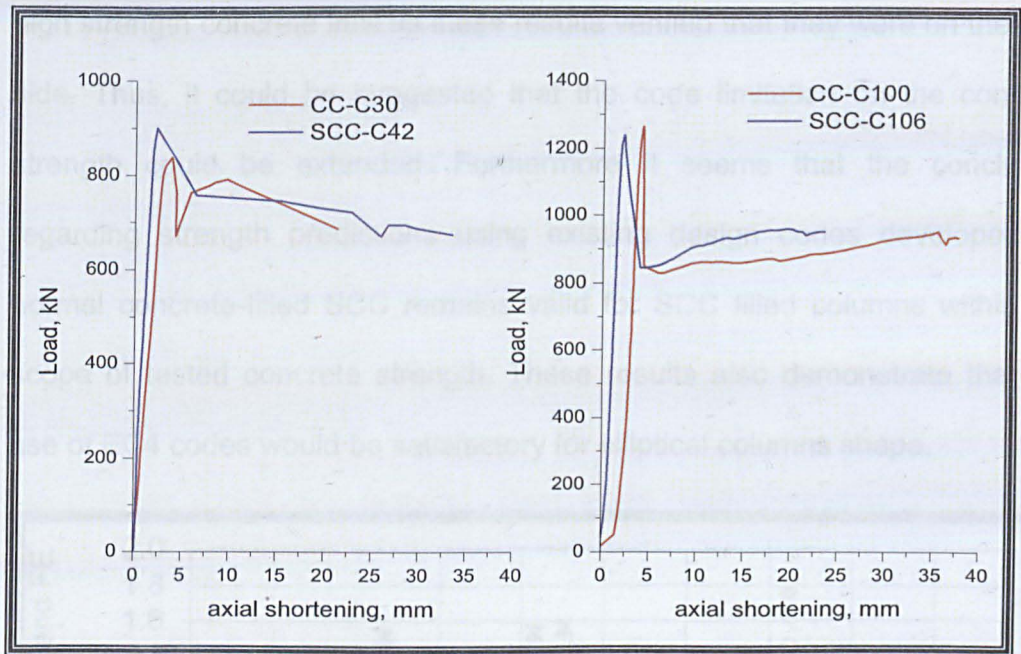


Figure 7.7: SCC infill versus conventional concrete infill

It should be noted that the design of elliptical CFT columns in the analysis was applied for a concrete grade of up to C100. The EC4 codes only restricted to concrete of strength classes C20/25 to C50/60 as specify in the design rules whereas concrete strength in range of 21MPa to 70MPa according to AISC codes. Some of the specimens' concrete cylinder strength did not satisfy the Eurocode 4 criteria. Further observation could be made from Figure 7.8, where the ratio of measured capacity and predicted capacity from both codes were plotted against the cylinder strength. As can be seen, points for columns with concrete infill less than 25 MPa are below the lines in which they overestimate the tests results, however this does not indicate that more 'safe' results could be obtained when the concrete strength was within the permitted range. There were no decreases in the ratio as the high strength concrete was used for other specimens. In addition it is clearly shows that both methods are suitable in predicting the resistance of elliptical CFT columns with normal and

high strength concrete infill as these results verified that they were on the safe side. Thus, it could be suggested that the code limitation on the concrete strength could be extended. Furthermore it seems that the conclusion regarding strength predictions using existing design codes developed for normal concrete-filled SCC remains valid for SCC filled columns within the scope of tested concrete strength. These results also demonstrate that the use of EC4 codes would be satisfactory for elliptical columns shape.

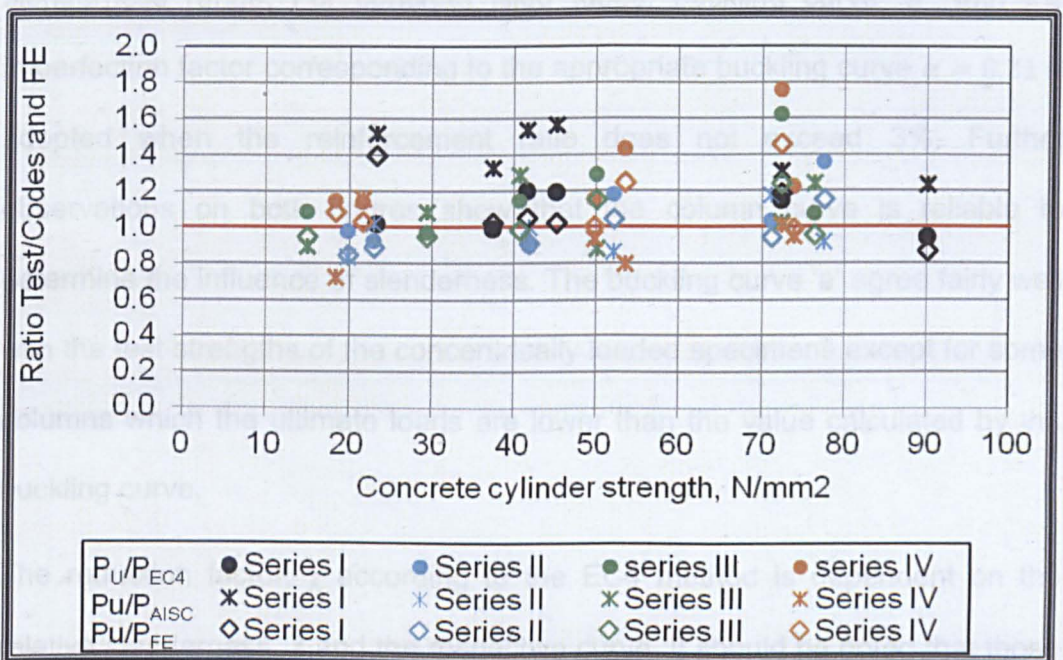


Figure 7.8: Ratio of measured strength and predicted strength from codes against concrete cylinder strength

The European buckling curves for steel columns were adopted as the basis of CFT column design. As illustrated in Figure 7.9 and Figure 7.10, the maximum compression strength obtained experimentally (P_u) and FE results (P_{FE}), is normalised with the nominal compression strength and plotted against the slenderness as specified in EC4. The buckling curves in accordance to the Eurocode 3 (EC3) are also plotted in the same figure. The calculation was

made using simplified method according to the code. The reduction buckling factor, χ depends on the relative slenderness, $\bar{\lambda}$ given in the form of $\sqrt{\frac{N_{pLRk}}{N_{cr}}}$.

The EC3 buckling curve generally provides a lower bound to the elliptical CFT columns test data and to the numerical results. As almost of tests and FE points lay above the buckling curve, therefore this indicated that the buckling curves are deemed safe for elliptical CFT columns, particularly in higher slenderness range. For concrete filled tubes, buckling curve "a" with the imperfection factor corresponding to the appropriate buckling curve $\alpha = 0.21$ is adopted when the reinforcement ratio does not exceed 3%. Further observations on both figures show that the column curve is reliable to determine the influence of slenderness. The buckling curve 'a' agree fairly well with the test strengths of the concentrically loaded specimens except for some columns which the ultimate loads are lower than the value calculated by the buckling curve.

The reduction factor, χ according to the EC4 method is dependent on the relative slenderness, $\bar{\lambda}$ and the respective curve. It should be noted that those five curves reflect the differences in imperfections including geometric imperfection; lack of verticality, straightness, flatness and accidental eccentricity of loading. Therefore the failure loads for the under-predicted of the specimens can be seen to depend not only on its slenderness ratio but also their mechanical properties of material. However, as most of the tests results lie above the buckling curve, hence the use of current design column curve, in general, a lower bound to the structural performance data and it is therefore recommended that it can be safely used for the design of elliptical concrete-filled columns.

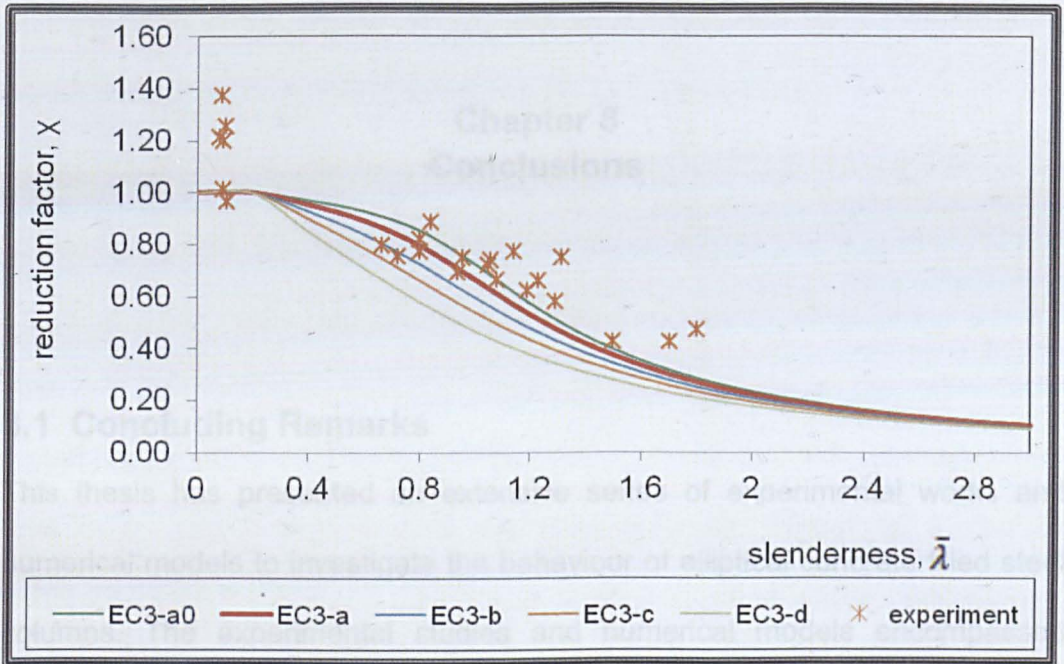


Figure 7.9: Normalised experimental results and buckling curves

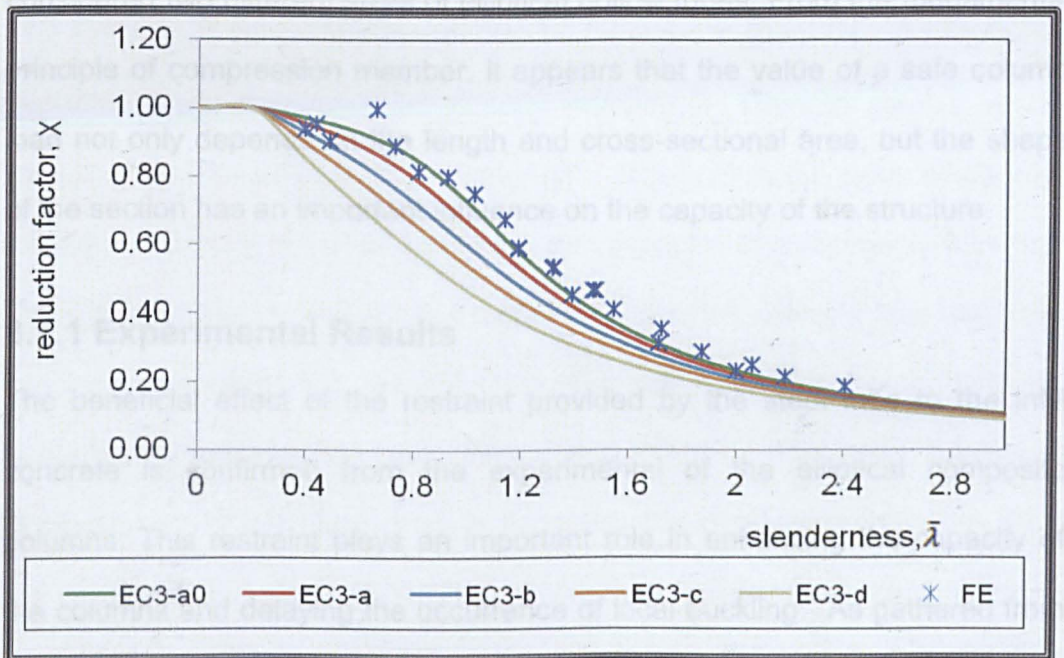


Figure 7.10: Normalised FE results and buckling curves

Chapter 8 Conclusions

8.1 Concluding Remarks

This thesis has presented an extensive series of experimental works and numerical models to investigate the behaviour of elliptical concrete filled steel columns. The experimental studies and numerical models encompassed different strengths of concrete infill and different columns lengths. These columns were tested under axial loading and the experiments have considered two different sizes of elliptical hollow tubes. From the fundamental principle of compression member, it appears that the value of a safe column load not only depends on the length and cross-sectional area, but the shape of the section has an important influence on the capacity of the structure.

8.1.1 Experimental Results

The beneficial effect of the restraint provided by the steel tube to the infill concrete is confirmed from the experimental of the elliptical composite columns. This restraint plays an important role in enhancing the capacity of the columns and delaying the occurrence of local buckling. As gathered from the experimental studies, two buckling failure modes were encountered in the tests. The combination of local buckling and overall flexural buckling were found in most of the long columns tests. Local buckling is a major

consideration in the design of thin wall steel tubes subject to compression, which was to the dominating failure modes in the stub column tests.

In comparison to the column capacity, in general, the ultimate strength (P_u) of the columns with concrete infill was found to be greater than that of the hollow columns. The comparison of the stub hollow and stub CFT columns showed that the concrete delayed the onset of the buckling of the steel tube. Consequently, the maximum strength was achieved by CFT columns, which was much larger than that of the steel columns. Therefore, it can be concluded that the elliptical CFT columns show good structure performance. However, the compressive response and ductility for CFT columns were found to be sensitive to steel tube dimension, concrete strength and the slenderness ratio. Generally, the ductility decreased as the concrete strength increased. The increase in concrete strength also had a positive effect on the specimens' capacity. From the investigation, the increase in strength gained by the presence of concrete core and the gain is significantly more when high strength concrete is used. However, the capacity of specimens with high strength concrete decreased at a higher rate after the ultimate load had been reached compared with the columns filled with normal strength concrete. Notably, it is believed that the sudden drop might be due to the brittleness characteristic in the high strength concrete; the over strength in the short column can be explained by the confinement of concrete core which is exhibited in the columns.

It is also interesting to see to what extent the capacity of the columns could reach by varying the concrete infill strength. From the results, it can be noted that there is a positive impact on the use of high concrete strength on the

composite columns. There were enhancements in load carrying capacity, where increases in lateral stiffness were noted. Another finding gathered as a result of increasing concrete core strength was a reduction in vertical strain, which is expected due to the concrete core providing more stability, thereby preventing or limiting the amount of local buckling from accruing.

There is a significant contraction in the NSC column leading to a gradual ductile failure; on the other hand, the contraction of the HSC column is much lower, which may be attributed to the fact that HSC is brittle and the tensile fracture failure was found at tensile zone for the concrete strength. The steel yielding process has also been observed to first start in the compressive zones, with tensile strain being found as not reaching the yield strain of steel.

In comparison to elliptical stub CFT columns with conventional concrete as conducted by Testo (2007) has found that the strength of elliptical stub columns with SCC infill was much lower. This situation can be related to the characteristic of the SCC infill. It is expected that the steel tube has begun to exert a lateral pressure due to the confinement at an earlier stage of loading.

Instability of the structures occurred before the composite cross-section reaches squash load in the case of long columns. Based on the limited range of slenderness account in this study, it was found that all specimens failed by overall flexural buckling, most of which occurred after the steel yielding, with the columns continued to resist further loading even after the local buckling.

Several methods to predict the ultimate strength of slender CFT columns are available in most common codes. However, their applications for HSC and SCC have yet not been investigated. From the comparison between the ultimate strength of elliptical concrete-filled tube columns (CFT) to the

prediction of the AISC LRFD, it has been determined that the current design provisions were inadequate. The application of EC4 method however, displays more reliable results compared to other code when the confinement effect was considered. This study also examined the applicability of design standards of EC4 and AISC for the design of elliptical CFT with high strength concrete infill. The principle limitation as far as EC4 code is concerned is that the normal weight of concrete strength classes is C20/C25 to C50/C60. Nevertheless, it was found that the utilisation of HSC could also be safely extended to predict the capacity of elliptical columns.

The simplified method which has been adopted in the analysis of EC4 procedure provides a simple yet reliable method for short and long columns. From the comparison and discussion it can also be reaffirmed that the EC4 standard procedure can reliably be used for computing the capacity of elliptical CFT columns. However, AISC method does not accurately estimate the capacity of the columns with higher slenderness. Nevertheless, from the comparison with the design codes considered in this study shows that EC4 can be used with confidence and generally give good agreement with test results. The average of P_u/P_{EC4} and P_u/P_{AISC} ratio for long columns tests for instance being 1.2 and 1.0 (for long columns) respectively with all safety factors were taken as unity.

A numerical model was developed for elliptical CFT columns under axial loading which the influence of the concrete confining properties on the behaviour of the uni-axial behaviour of CFT the columns was crucial to consider during the analysis. A constitutive model of the mechanical behaviour of the confined concrete under load was considered based on

currently available stress-strain relationships suggested by Dai and Lam (2010), Hu et al. (2003), Ellobody and Young (2006), Han et al. (2007). The column strengths, load–lateral displacement curves and deformed shapes of the columns have been predicted to be using the finite element model and compared well with the experimental results. The comparison between the finite element results and the experimental results for the columns with different concrete strengths and different geometric dimensions showed good agreement in predicting the capacities of the columns by using concrete material properties suggested by Han et.al (2007). However, it is expected that the use of SCC may influence the FE results, as there is no study regarding the behaviour of the concrete type. Based on the study conducted by Lin *et al.* (2008), it can be stated that the SCC properties, such as stiffness and ductility, were lower than in the case of traditional normal concrete. This is due to the SCC material composition, which influences the bond between the particles in concrete. From the cylinder SCC tests, it can be observed that the corresponding strains are much lower than a representative value, suggested by ACI Committee 318, which was considered in the analysis by Han et al. (2007). Thus, it is expected that this could potentially affect the concrete model properties, which may not be able to represent the failure process in SCC in a realistic way and which therefore resulted in the numerical results not capturing the plateau before or after the ultimate load which was observed in the experimental results. It should be stressed here that the merit of the proposed simplified models is not intended to claim to be a simple model for design purposes, but rather that the models could be used to estimate the ultimate strength of the newest elliptical tube section. The simplified models have also been found to satisfy the most critical attributes. In general the

results produced by the model show that the response of the columns before and after the peak are in good agreement with the experimental results. The proposed FE models were also shown to be a promising method to obtain data for the development of design aid.

8.2 Suggestion for Future Research

Overall, within the limits of the investigation reported, it may be concluded that the objective of this research have been achieved. The results obtained from the study are useful to be employed for the design of elliptical concrete-filled columns. The simplified numerical modelling also reasonably estimates the failure load and has provided safe predictions for the axially loaded column. However, there are nevertheless various recommended for future research, which are outlined as follows:

1. There is a need to develop a good understanding of the fundamental behaviour associated with SCC as concrete infill in tubular steel section. The SCC concrete core in CFT columns has a very complex material behaviour; thus, in-depth studies are necessary on the mechanical properties of SCC as the constitutive model for SCC core in CFT columns should represent major load-deformation mechanisms, such as the brittle fracture of high-strength concrete. Furthermore, owing to the SCC characteristics, it is expected that the structure will fracture at an early stage of deformation. Therefore, the concrete structure damage can be assumed as quantified by the volumetric expansion, which is caused by the propagation of micro cracks which built up progressively as it approached failure.

2. Owing to the limited research works carried out concerning the slender CFT columns, extensive data experiments should be conducted. The experiment concerning on the effect of local buckling behaviour and the effects of the width-to-thickness ratio on the confinement behaviour should also be carried out. More experimental data are needed for concrete-filled tubular columns with height equal to 3–4.0 m, which represent a typical storey height in multi-storey buildings; using different sizes of the cross section are needed.
3. An analytical study and analytical approaches to simulate the behaviour of elliptical confined concrete with reasonable accuracy are needed. The analytical work will extend the investigation in order to study the mechanics of the behaviour of the CFTs in more detail. The author hesitated in recommending a more complicated FE model approach using a variation method—particularly in representing the concrete properties to obtain more accurate numerical results. As there is still uncertainty surrounding the behaviour of confinement in elliptical sections, such models could be used to investigate the stress transfers which are not able to be otherwise obtained from experiments, and which are so far not well understood.
4. As the findings are in general accordance with the limited compressive data available on the elliptical section, therefore it is important to carry out a study on the volume strain behaviour under axial load in interpreting its confined response. Analytical analysis could be conducted in order to investigate the effective confinement pressures that are able to take the shape effect into account. It may also be

suggested that for SCC the initiation and propagation of cracks may be dominant mechanisms of the material response. However, it is worth mentioning that the concrete in the CFT columns has a very complex material behaviour: the material is not plastic but brittle, and the brittleness is more for SCC; thus, it is expected that the post-peak strain softening characteristic is important in the material properties. This owes to the progressive development of the damage in the form of micro-cracks and localisation of the failure, may which influence the behaviour of the entire structure when the concrete infill under compression and tension as observed in higher slenderness columns with HSC infill.

References

- ABAQUS User's Manual, Hibbitt, Karlsson and Sorensen, Inc. Version 6.8 (2008), USA.
- Aboutaha, R.S., and Machado, R. (1998) Seismic Resistance of Steel Confined Reinforced Concrete (SCRC) Columns. *The Structural Design of Tall Building*, 7(3), p.251-260.
- Ahmadi, M.A., Alidoust, O., Sadrinejad, I. and Nayeri, M. (2007) Development of Mechanical Properties of Self Compacting Concrete Contain Rice Husk Ash. *International Journal of Computer, Information and Systems Science, and Engineering*, 1(4), pp.258-261.
- Ambedkar, P.P. self compacting concrete - Its properties and test. [online] Available at: <http://www.scribd.com/doc/6120276/Self-Compacting-Concrete>. [Accessed 9 February 2012]
- Baig, M.N., Jiansheng, F. and Jianguo, N. (2006) Strength of Concrete Filled Steel Tubular Columns. *Tsinghua Science and Technology*, 11(6), pp.657-666.
- Bisagni, C. (2000) Numerical analysis and experimental correlation of composite shell buckling and post-buckling. *Composites, Part B*, 31(8), pp.655-667.
- Brite-EuRam (2000). *Gudelines; Task 9-End Product*. [online] Available at: http://www.cege.ucl.ac.uk/data/assets/pdf_file/0016/3607/task9.pdf. [Accessed 10 February 2012].
- Chan, T. M. and Gardner, L. (2008a) Bending strength of hot-rolled elliptical hollow sections. *Journal of Constructional Steel Research*, 64(9), pp.971-986.
- Chan, T. M. and Gardner, L. (2008b) Compressive resistance of hot-rolled elliptical hollow sections. *Engineering Structures*, 30(2), pp.522-532.

Chan, T. M. and Gardner, L. (2009) Flexural Buckling of Elliptical Hollow Section Columns. *Journal of Structural Engineering*, 135(5), pp.546-557.

Dai, X. and Lam, D. (2010) Numerical modelling of axial compressive behaviour of short concrete-filled elliptical steel columns. *Journal of Constructional Steel Research*, 66(7), pp.931-942.

EFNARC (2002) Specification and Guidelines for Self-Compacting Concrete. Association House, Surrey, UK

Ellobody, E. and Young, B. (2006) Nonlinear analysis of concrete-filled steel SHS and RHS columns. *Thin-Walled Structures*, 44(8), pp.919-930.

Ellobody, E., Young, B and Lam, D. (2006) Behaviour of normal and high strength concrete-filled compact steel tube circular stub columns. *Journal of Constructional Steel Research*, 62(7), pp.706-715.

Fujimoto, T., Mukkai, A., Nishiyama, I. and Sakino, K. (2004) Behavior of eccentrically loaded concrete-filled steel tubular columns. *Journal of Structural Engineering*, 130(2), pp.203-212.

Gaimster, R. and Dixon, N. (2003) Self-compacting Concrete. In: J. Newman and B.S. Choo, *Advance Concrete Technology, Processes*. Oxford: Butterworth Heinemann.

Gardner, L. and Chan, T. M. (2007) Cross-section classification of elliptical hollow sections. *Journal of Steel and Composite Structures*, 7(3), pp.185-200.

Gardner, L. and Ministro, A. (2005) Structural steel oval hollow section. *The Structural Engineer*, 83, pp.32-36.

Gardner, L. and Nethercot, D. A. (2004) Experiments on stainless steel hollow sections - Part 2: Member behaviour of columns and beams. *Journal of Constructional Steel Research* 60(9), pp.1319-1332.

Gardner, L. and Ministro, A. (2004) Testing and numerical modelling of structural steel oval hollow sections. *Research Report No.04-002-ST*. Imperial College, London, U.K.

- Giakoumelis, G. and Lam, D. (2004) Axial capacity of circular concrete-filled tube columns. *Journal of Constructional Steel Research*, 60(7), pp.1049-1068.
- Goodier, C. I. (2003) Development of self-compacting concrete. *Proceeding of the Institution of Civil Engineers, Structures and Building*, 156(4), pp.405-414.
- Gourley, B. C., Tort, C., Hajjar, J. F., and Schiller, P. H. (2001) A Synopsis of studies of the monotonic and cyclic behavior of concrete-filled steel tube beam-columns. *Structural Engineering Report No. ST-01-4*, Institute of Technology, University of Minnesota.
- Jamaluddin, N., Lam, D. and Ye, J. (2009) Finite Element Analysis of Elliptical Stub CFT columns. In: Lam, D, *Proceedings of the 9th International Conference on Steel Concrete Composite and Hybrid Structures (ASCCS 2009)*, Leeds, UK, 8-10 July 2009, Singapore: Research Publishing.
- Gopal, S. R. and Manoharan, P. D. (2006) Experimental behaviour of eccentrically loaded slender circular hollow steel columns in-filled with fibre reinforced concrete. *Journal of Constructional Steel Research*, 62(5), pp.513-520.
- Gota, Y., Kumar, G. P. and Kawwanishi, N. (2010) Nonlinear Finite Element Analysis for Hysteretic Behaviour of Thin-Walled Circular Steel Columns with In-Filled Concrete. *Journal of Structural Engineering*, 136(11), pp.1413-1422.
- Gourley, B. C., Tort, C., Hajjar, J. F. and Schiller, P. H. (2001) A Synopsis of studies of the monotonic and cyclic behaviour of concrete-filled steel tube beam-columns. *Structural Engineering Report No. ST-01-4*, Institute of Technology, University of Minnesota.
- Grauers, M. (1993) Composite Columns of Hollow Steel Sections Filled With High Strength Concrete. PhD, Thesis, Division of Concrete Structures, *Chalmers University of Technology*, Sweden.
- Han, L.H. (2002) Tests on stub columns of concrete-filled RHS sections. *Journal of Constructional Steel Research*, 58(3), pp.353-372.

Han, L.H., Yao, G.H. and Tao, Z. (2007) Performance of concrete-filled walled steel tubes under pure torsion. *Thin-Walled Structures*, 45(1), pp.24-36.

Han, L. H. and Yao, G. H. (2004) Experimental behaviour of thin-walled hollow structural steel (HSS) columns filled with self-consolidating concrete (SCC). *Thin-Walled Structures*, 42(9), pp.1357-1377.

Hanbin, G. and Tsutomo, U. (1992) Strength of Concrete-filled thin-walled Steel Box Columns: Experiment. *Journal of Structural Engineering*, 118(11), pp.3036-3054.

Hu, H.T., Huang, C.S. and Chen, Z.L. (2005) Finite element analysis of CFT columns subjected to an axial compressive force and bending moment in combination. *Journal of Constructional Steel Research*, 61(12), pp.1692-1712.

Hu, H.T., Huang, C.S., Wu, M.H. and Wu, Y.M. (2003) Nonlinear analysis of axially loaded concrete-filled tube columns with confinement effect. *Journal of Structural Engineering*, 129(10), pp.1322-1329.

Huang, C. S., Yeh, Y. K., Liu, G. Y., Hu, H. T., Tsai, K. C., Weng, Y. T., Wang, S. H. and Wu, M. H. (2002) Axial load behaviour of stiffened concrete-filled steel columns. *Journal of Structural Engineering*, 128(9), pp.1222-1230.

Jamaluddin, N., Lam, D. and Ye, J. (2009) Finite Element Analysis of Elliptical Stub CFT columns. In: Lam, D, *Proceedings of the 9th International Conference on Steel Concrete Composite and Hybrid Structures (ASCCS 2009)*, Leeds, UK, 8-10 July 2009, Singapore: Research Publishing.

Johansson, M. (2002) Composite action and confinement effects in tubular steel-concrete columns. PhD, Thesis, Department of Structural Engineering, *Chalmers University of Technology*, Sweden.

Johansson, M. and Akesson, M. (2002) Finite element study on concrete-filled steel tubes using a new confinement sensitive concrete compression model. *Nordic Construction Research*, 27, 43-62.

- Johansson, M. and Gylltoft, K. (2002) Mechanical behaviour of circular steel-concrete composite stub columns. *Journal of Structural Engineering*, 128(8), pp.1073-1081.
- Lam, D. and Williams, C. A. (2004) Experimental study on concrete filled square hollow sections. *Steel and Composite Structures*, 4(2), pp.95-112.
- Liang, Q. Q., Uy, B., Bradford, M. A. and Ronagh, H. R. (2004) Ultimate strength of continuous composite beams in combined bending and shear. *Journal of Constructional Steel Research*, 60(8), pp.1109-1128.
- Liang, Q. Q., Uy, B. and Liew, J. Y. R. (2006) Nonlinear analysis of concrete-filled thin-walled steel box columns with local buckling effects. *Journal of Constructional Steel Research*, 62(2), pp.581-591.
- Lin, C.H., Hwang, C.L., Lin, S.P. and Liu, C.H. (2008) Self-consolidating concrete columns under concentric compression. *ACI Structural Journal*, 105(4), pp.425-432.
- Lu, Z.H. and Zhao, Y.G. (2010) Suggested empirical models for the axial capacity of circular CFT stub columns. *Journal of Constructional Steel Research*, 66(6), pp.850-862.
- Lue, D. M., Liu J.L., and Yen, T. (2007) Experimental study on rectangular CFT columns with high-strength concrete. *Journal of Constructional Steel Research*, 63(1), pp.37-44.
- Mander, J. B., Priestley, M. J. N. and Park, R. (1988) Theoretical stress-strain model for confined concrete. *Journal of Structural Engineering*, 114(8), pp.1804-1826.
- Nardin, S. D. and EL Debs, A. L. H. C. (2007) Axial load behaviour of concrete-filled steel tubular columns. *Proceeding of the Institution of Civil Engineers, Structures and Building*, 160, pp.13-22.
- Neogi, P. K., Sen, H.K, and Chapman, J.C (1969) Concrete-filled tubular steel columns under eccentric loading. *The Structural Engineer*, 47(5), pp.187-195.

- Nethercot, D. A. (2004) Fundamentals, In: D.A. Nethercot, ed. 2004. *Composite Construction*. London: Taylor and Francis, pp.1-22.
- O'Shea, M. D. and Bridge, R. Q. (2000) Design of circular thin-walled concrete filled steel tubes. *Journal of Structural Engineering*, 126(11), pp.1295-1303.
- Oehlers, D. J. and Bradford, M. A. (1995) Composite steel and concrete structural members: *Fundamental behaviour*. Pergamon.
- Okamura, H. and OUCHI, M. (2003) Self-Compacting Concrete. *Journal of Advance Concrete Technology*, 1(1), pp.5-15.
- Packer, A. J. (2008) Going Elliptical. *Modern Steel Construction*, American Institute of Steel Construction. March Issue, pp. 65-67.
- Romero, M. L., Bonet, J. L. and Ivorra, S. (2005) A Review of Nonlinear Analysis Models for Concrete Filled Tubular Columns. In: B.H.V. Topping, eds. 2005. *Innovation in Civil and Structural Engineering Computing*. Stirling, UK: Saxe-Coburg Publications. pp.119-142.
- Sakino, K. (2006) Confined concrete in concrete-filled steel tubular columns. *American Concrete Institute, ACI*, 238 (Special Publication), pp.267-287.
- SCCEPG (2005) *The European Guidelines for Self-compacting Concrete - Specification, Production and Use*. [online] Available at: <http://www.efnarc.org/pdf/SCCGuidelinesMay2005.pdf>. [Accessed 10 February 2012].
- Schneider, S. (1998) Axially loaded concrete-filled steel tubes. *Journal of Structural Engineering*, 124(10), pp.1125-1138.
- Seward, D. (1998) Understanding structures: *Analysis, materials, design*, Basingstoke: Macmillan.
- Shakir-Khalid, H. and Zeghiche, J. (1989) Experimental behaviour of concrete-filled rolled rectangular hollow-section columns. *The Structural Engineer*, 67(19), pp.346-353.

Shams, M. and Saadeghvaziri, M. A. (1997) State of the art of concrete-filled steel tubular columns. *ACI Structural Journal*, 94(5), pp.558-571.

Shams, M. and Saadeghvaziri, M. A. (2000) Non-Linear behaviour of concrete-filled steel tubular columns under axial and lateral loadings. Composite and Hybrid Structures. In: Y. Xiao and S.A. Mahin (eds). *Proceeding of the Sixth ASCCS International Conference on Steel-Concrete Composite Structures*. University of Southern California, 22-24 March 2000, California, U.S: Univ. of Southern California.

Shanmugam, N. E. and Lakshmi, B. (2001) State of the art report on steel-concrete composite columns. *Journal of Constructional Steel Research*, 57(10), pp.1041-1080.

Testo, N. (2007) Axial capacity of elliptical concrete-filled steel tube columns. *Research Report of School of Civil Engineering*, University of Leeds.

Uy, B. (1998) Concrete-filled fabricated steel box columns for multi-storey buildings: behaviour and design. *Progress in Structural Engineering and Materials*, 1(2), pp.150-158.

Uy, B. (2001) Static long-term effects in short concrete-filled steel box columns under sustained loading. *ACI Structural Journal*, 98(1), pp.96-104.

Vicroads (2006) *Self-compacting concrete*. [online] Available at: <http://www.bookshop.vicroads.vic.gov.au/redirectpdf/pdfs/tn073.pdf>.

[Accessed 9 February 2012]

Vrcelj, Z. and Uy, B. (2002) Strength of slender concrete-filled steel box columns incorporating local buckling. *Journal of Constructional Steel Research*, 58(2), pp.275-300.

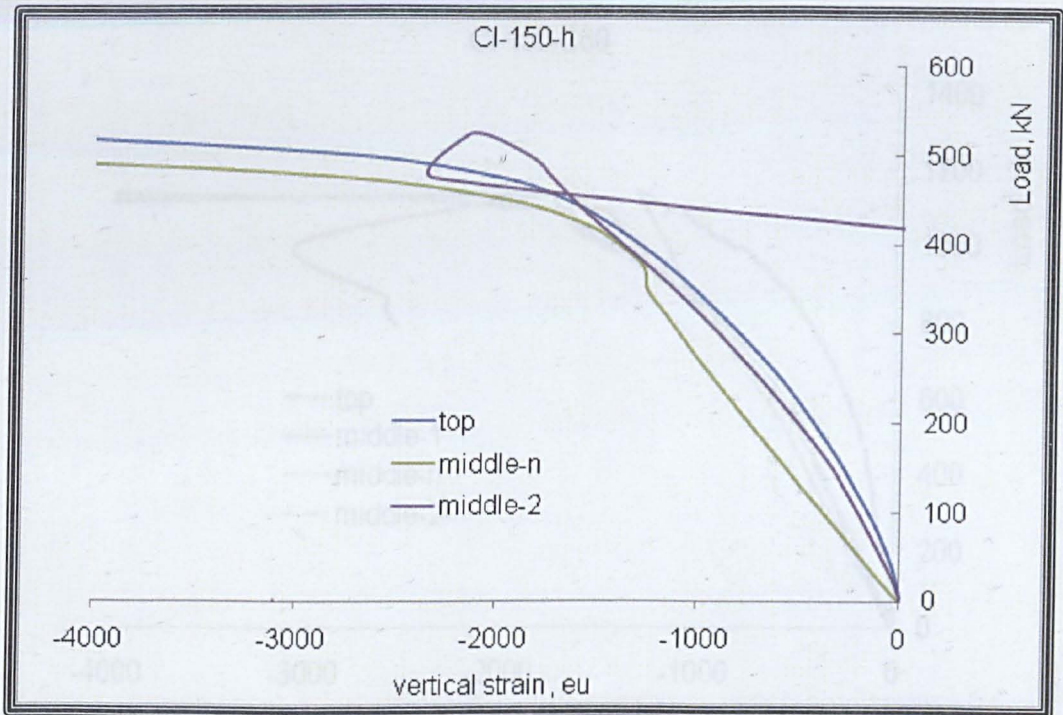
Wheeler, A. T. and Bridge, R. Q. (2000) Thin-walled steel tubes filled with high strength concrete in bending. In: ASCE Conf. Proc. *Composite Construction in Steel and Concrete IV Proceedings of the Fourth International Conference on Composite Construction in Steel and Concrete*. Alberta, Canada, May 28–June 2, 2000. ASCE

- Yan, J. and Young, B. (2004) Numerical investigation of channel columns with complex stiffeners—Part I: Test verification. *Thin-Walled Structures*, 42(6), pp.883-893.
- Yang, D. and Hancock, G. J. (2004) Numerical simulations of high strength steel lipped-channel columns. Research Report No R843, *Centre of Advance Structural Engineering*, Department of Civil Engineering, Australia.
- Yang, D., Lam, D. and Gardner, L. (2008) Testing and analysis of concrete-filled elliptical hollow sections. *Engineering Structures*, 30(12), pp.3771-3781.
- Yu, Z.-W., Ding, F.-X. and CAI, C. S. (2007) Experimental behaviour of circular-filled steel tube stub columns. *Journal of Constructional Steel Research*, 63(2), pp.165-174.
- Zeghiche, J. and Chaoui, K. (2005) An experimental behaviour of concrete-filled steel tubular columns. *Journal of Constructional Steel Research*, 61(1), pp.53-66.
- Zhang, S. and Guo, L. (2007) Behaviour of High Strength Concrete-Filled Slender RHS Steel Tubes. *Advances in Structural Engineering*, 10(4), pp.337-351.
- Zhang, W. and Shahrooz, B. M. (1999) Comparison between ACI and AISC for concrete-filled Tubular Columns. *Journal of Structural Engineering*, 125 (11), pp.1213-1223.
- Zhang, Y., Wang, C. and Zhang, Z. (2007) Tests and finite element analysis of pin-ended channel columns with inclined simple edge stiffeners. *Journal of Constructional Steel Research*, 63(3), pp.383-395.
- Zhao, X. L., Lu, H. and S, G. (2007) Tests of elliptical sections filled with SCC (self-compacting concrete). *Proceeding of the 5th International Conference on Advances in Steel Structures*, Singapore, pp.950-955.
- Zhao, X. L. and Packer, J. A. (2009) Tests and design of concrete-filled elliptical hollow section stub columns. *Thin-Walled Structures*, 47 (6-7), pp.617-628.

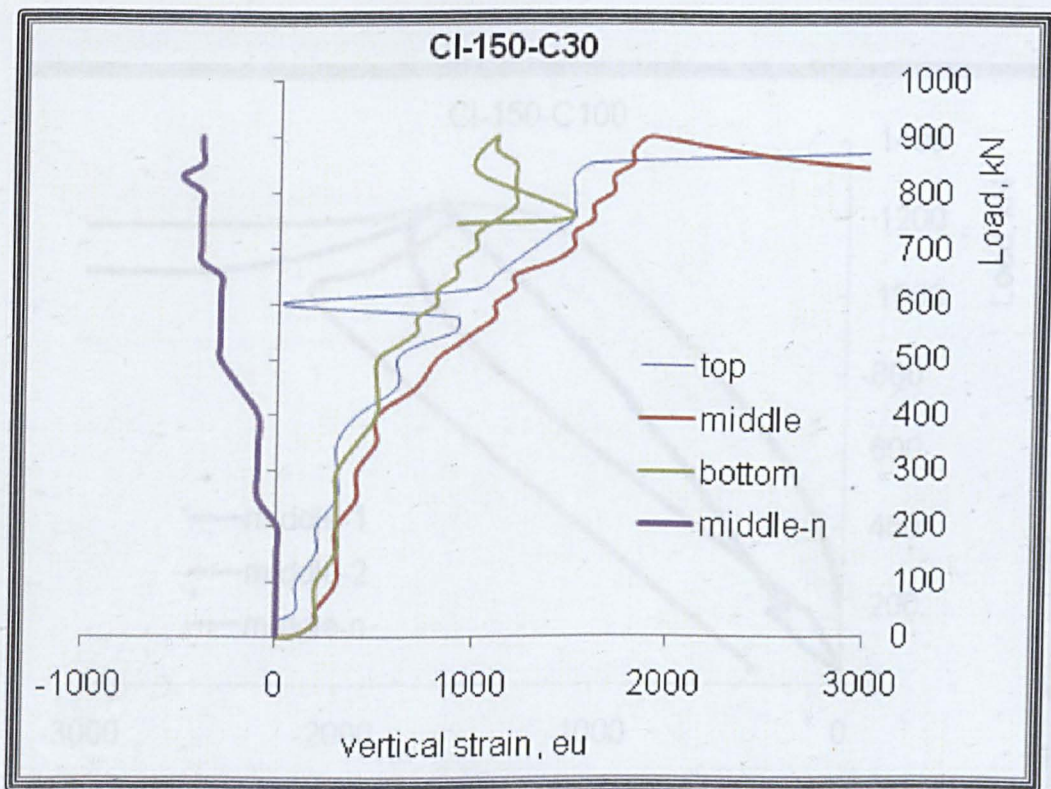
Zhu, W. and Bartos, P. J. M. (2003) Permeation properties of self-compacting concrete. *Cement and Concrete Research*, 33 (6), pp.921-926.

Zhu, Y. and Wilkinson, T. (2007) Finite Element Analysis of Structural Steel Elliptical Hollow Sections in Compression. *Research Report No.R874*, Centre of Advanced Structural Engineering, School of Civil Engineering, The University of Sydney, Australia.

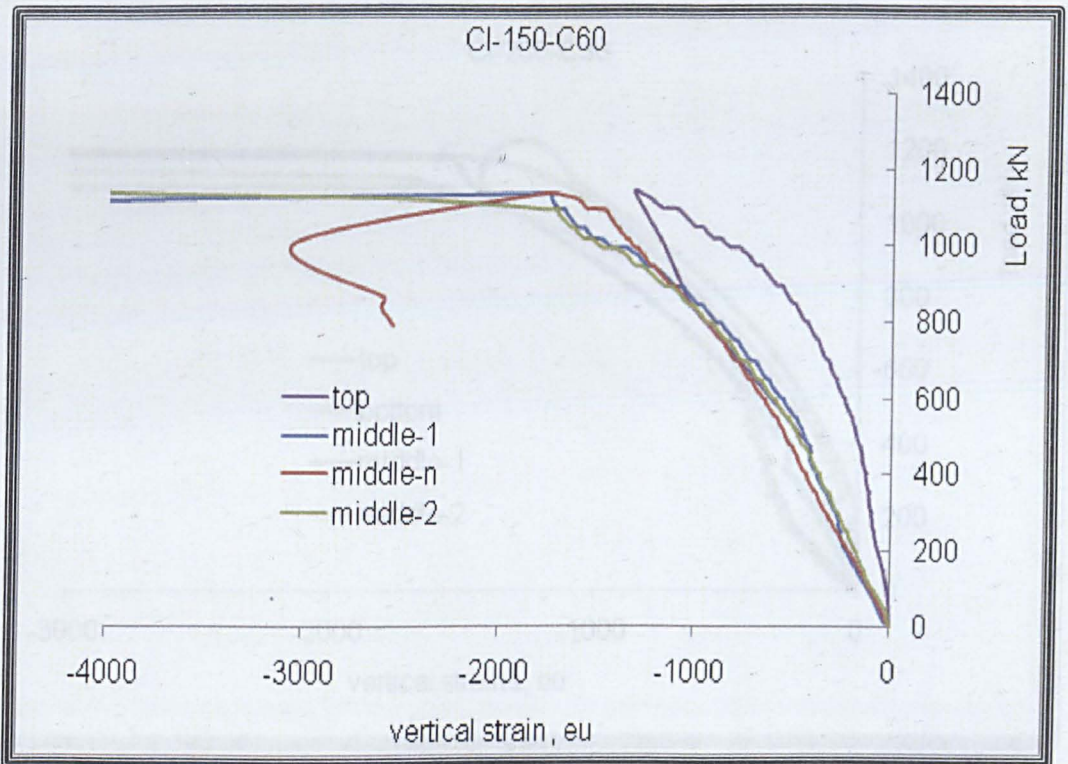
APPENDIX A



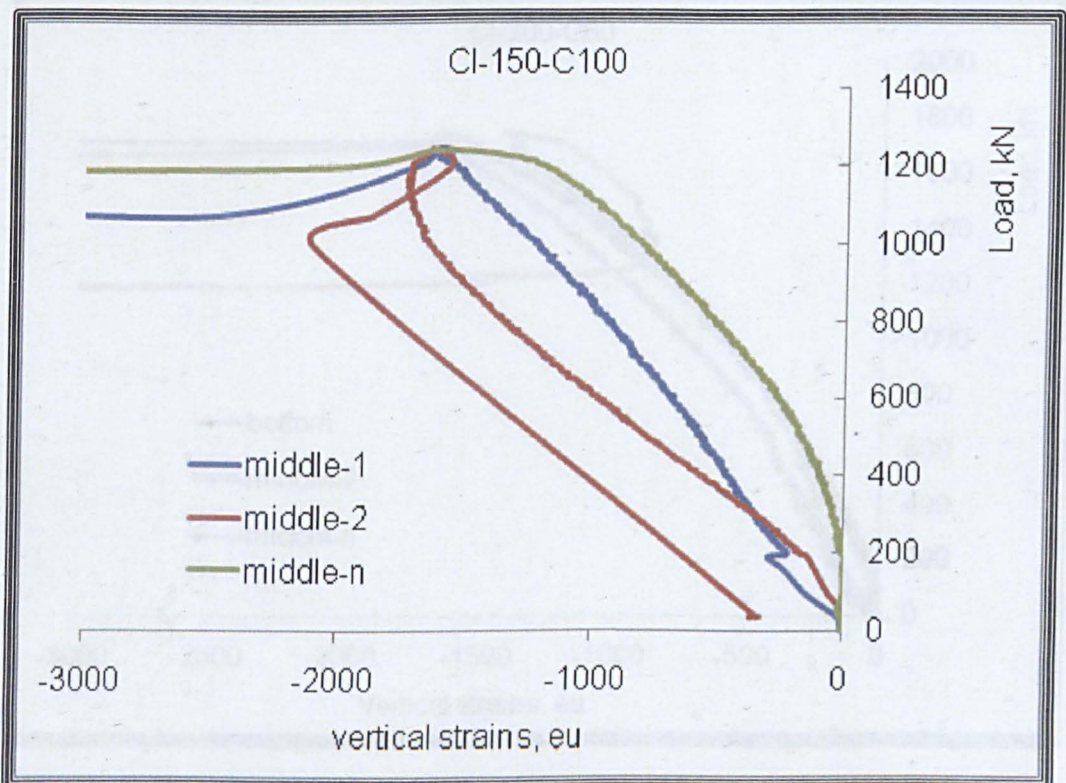
(a)



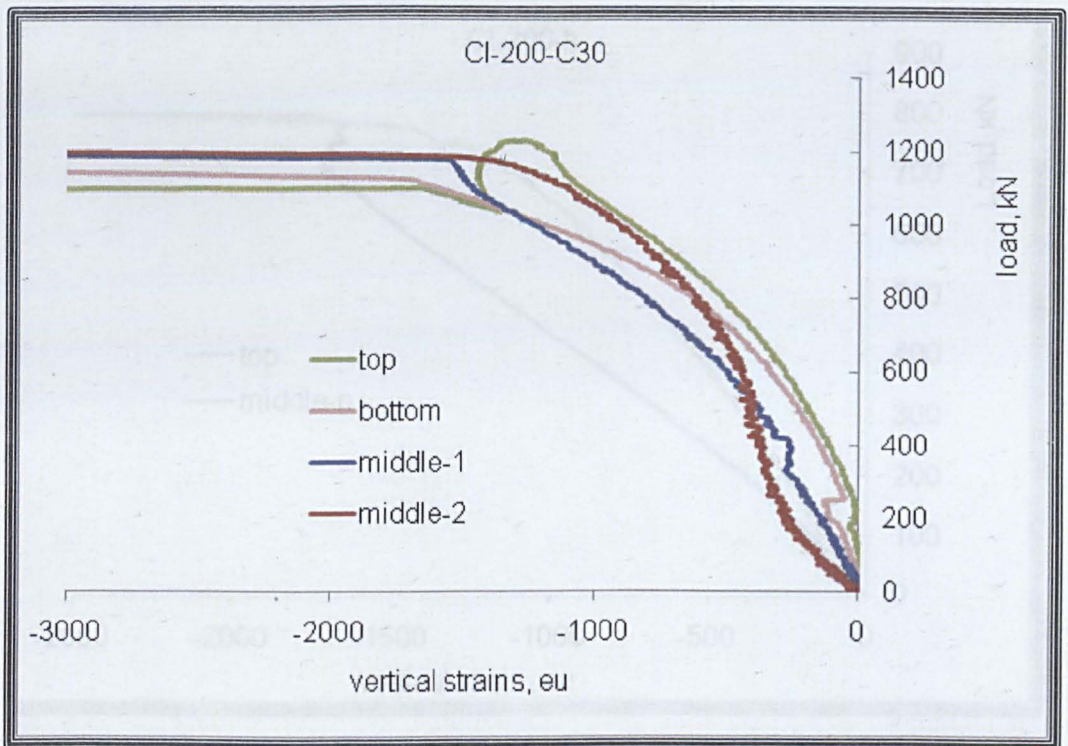
(b)



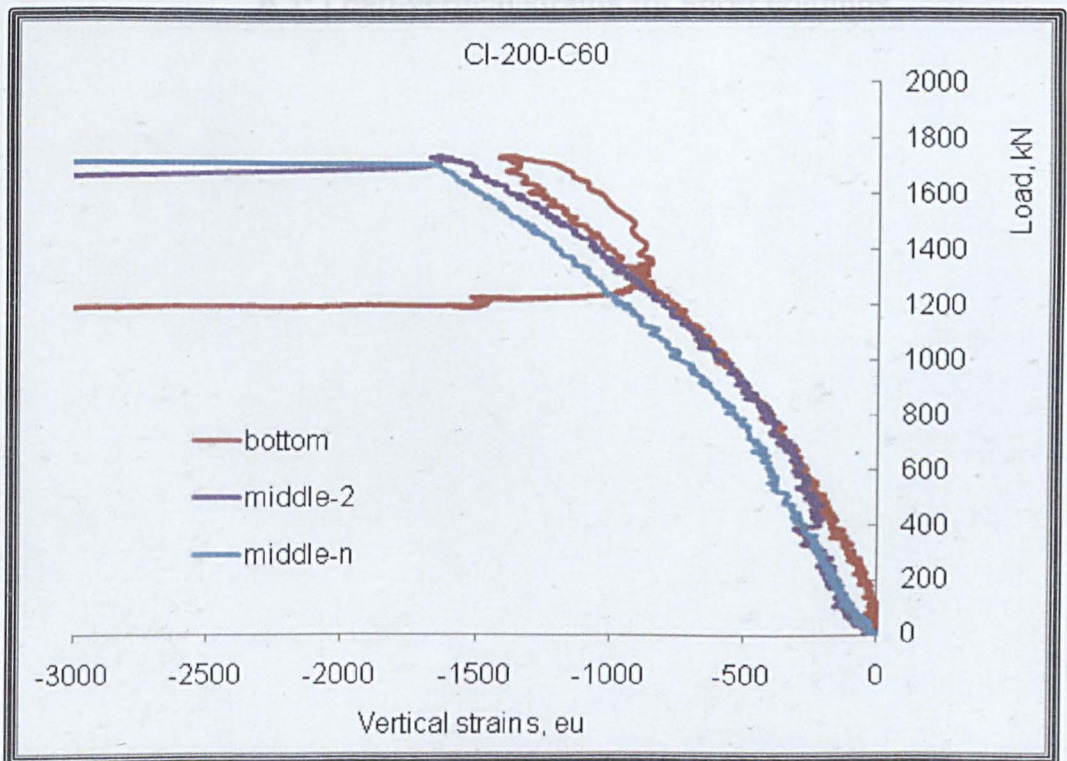
(c)



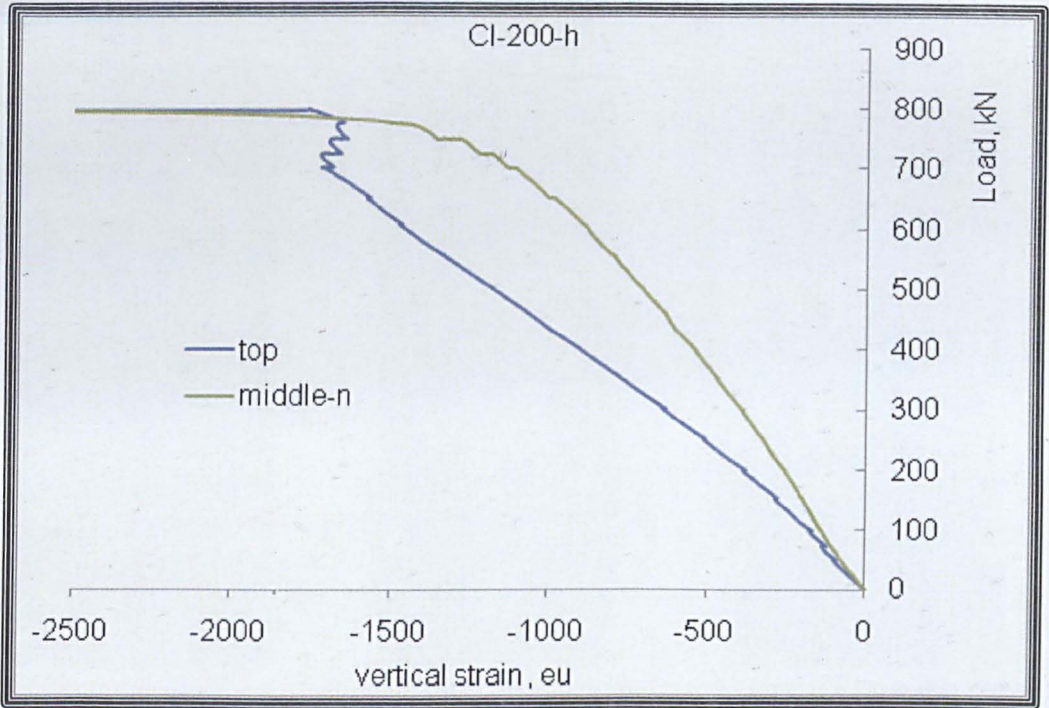
(d)



(e)



(f)



(g)

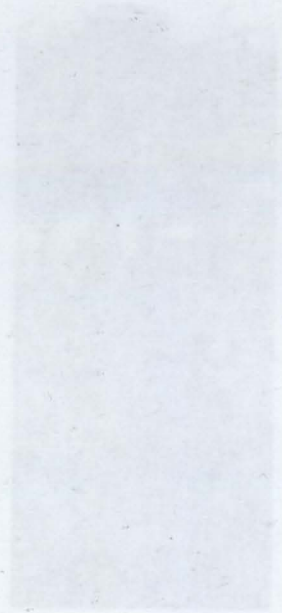
A.1: Load-vertical strains for short columns



(a) CII-150-C30

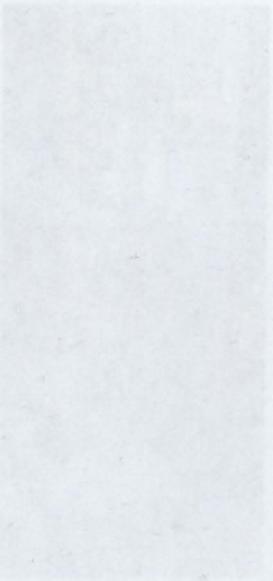


(b) CII-150-C60

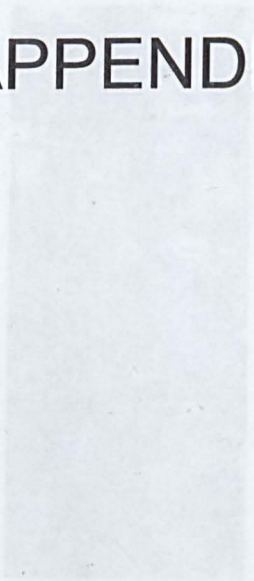


(c) CII-150-Q100

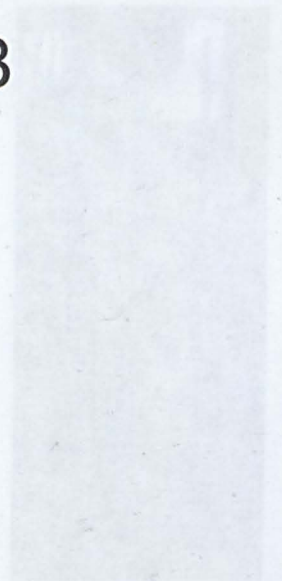
APPENDIX B



(d) CII-200-C30



(e) CII-200-C60



(f) CII-200-Q100

Figure B.1: 1.5m column length



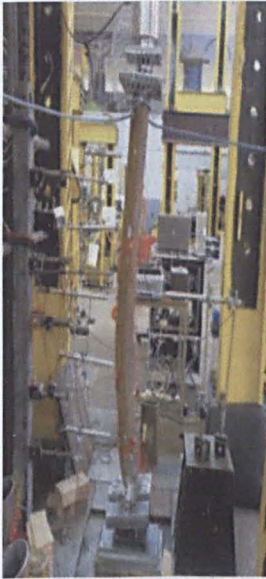
(a) CII-150-C30



(b) CII-150-C60



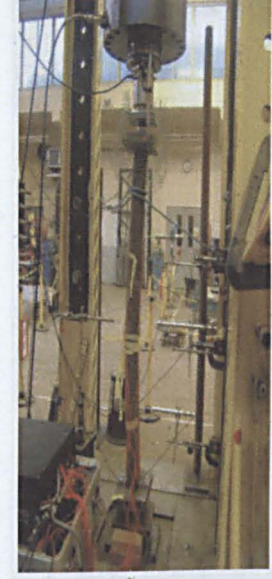
(c) CII-150-C100



(d) CII-200-C30



(e) CII-200-C60



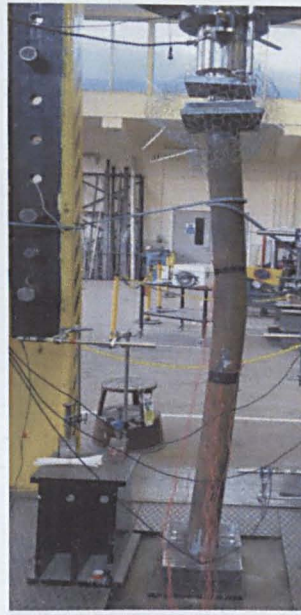
(f) CII-200-C100

Figure B.1: 1.5m columns length

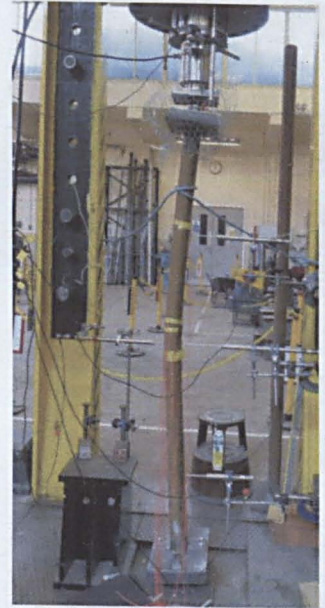
Figure B.2: 1.73m columns length



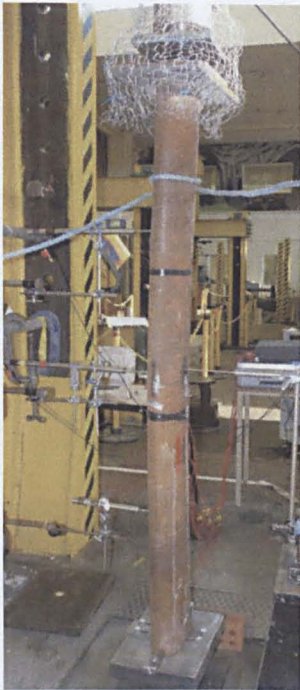
(a) CIII-150-C30



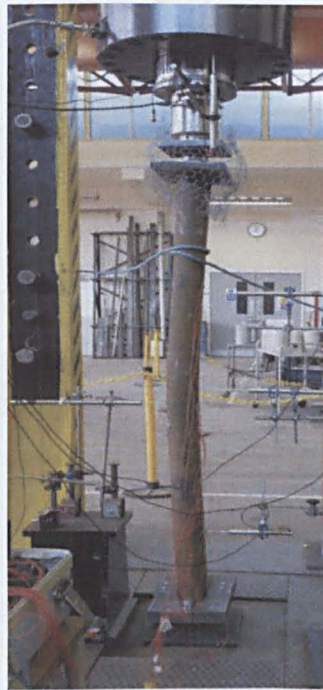
(b) CIII-150-C60



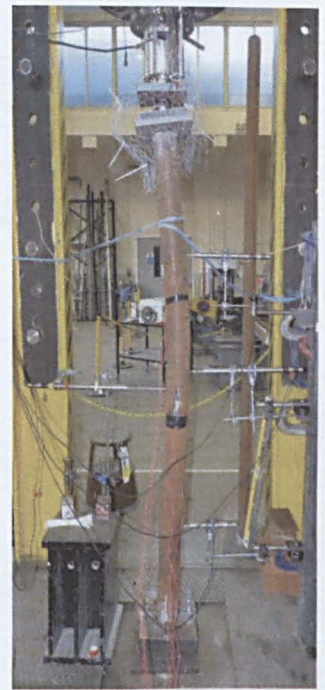
(c) CIII-150-C100



(d) CIII-200-C30

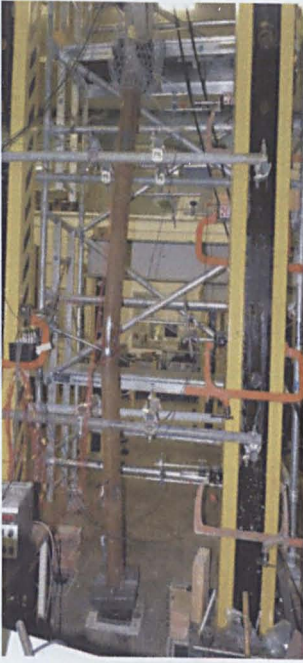


(e) CIII-200-C60

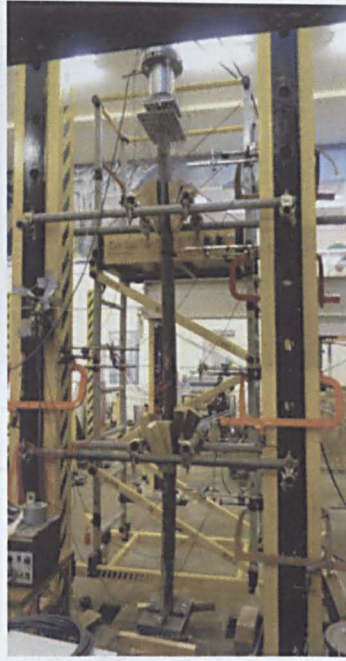


(f) CIII-200-C100

Figure B.2: 1.79m columns length



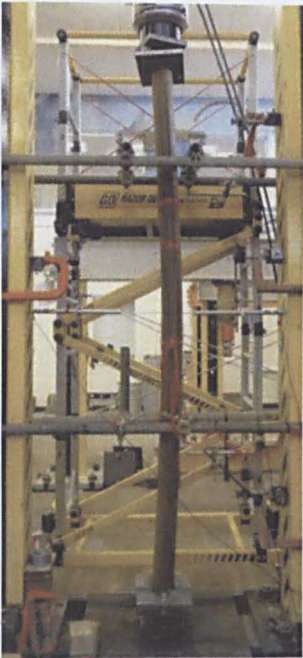
(a) CIV-150-C30



(b) CIV-150-C60



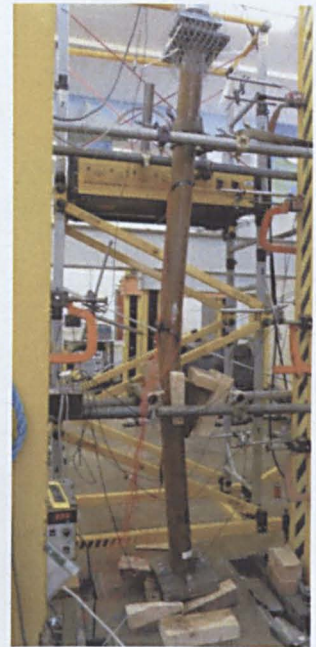
(c) CIV-150-C100



(d) CIV-200-C30



(e) CIV-200-C60



(f) CIV-200-C100

Figure B.3: 2.5m columns length